DOCTORAL THESIS

Pathways and Distribution of Microplastic in the Eastern Baltic Sea

Arun Mishra

TALLINNA TEHNIKAÜLIKOOL
TALLINN UNIVERSITY OF TECHNOLOGY
TALLINN 2025

Pathways and Distribution of Microplastic in the Eastern Baltic Sea

ARUN MISHRA

**TAL
TECH** PRESS

TALLINN UNIVERSITY OF TECHNOLOGY
School of Science
Department of Marine Systems

This dissertation was accepted for the defence of the degree of Doctor of Philosophy (Oceanography and Meteorology) 07/05/2025

Supervisor: Dr. Germo Väli
                             Department of Marine Systems,
                             School of Science
                             Tallinn University of Technology
                             Tallinn, Estonia

Co-supervisor: Dr. Taavi Liblik
                             Department of Marine Systems,
                             School of Science
                             Tallinn University of Technology
                             Tallinn, Estonia

Opponents: Dr. Jens Murawski
                             Department of Weather Research
                             Danish Meteorological Institute
                             Copenhagen, Denmark

                             Dr. Margit Heinlaan
                             National Institute of Chemical Physics and Biophysics
                             Laboratory of Environmental Toxicology
                             Tallinn, Estonia

Defence of the thesis: 13/06/2025, Tallinn

Declaration:

Hereby I declare that this doctoral thesis, my original investigation and achievement, submitted for the doctoral degree at Tallinn University of Technology has not been submitted for doctoral or equivalent academic degree.

Arun Mishra

_____
                             signature

Mikroplasti levik ja jaotused Läänemere idaosas

ARUN MISHRA

Contents

List of Publications

The present Ph.D. thesis is based on the following publications that are referred to in the text by Roman numbers:

I   Mishra A., Buhhalko N., Lind K., Lips I., Liblik T., Väli G., et al. (2022). Spatiotemporal variability of microplastics in the Eastern Baltic Sea. Front. Mar. Sci. 9. doi: 10.3389/fmars.2022.875984

II   Mishra A, Siht E, Väli G, Liblik T, Buhhalko N and Lips U (2025). Mapping microplastic pathways and accumulation zones in the Gulf of Finland, Baltic Sea – insights from modeling. Front. Mar. Sci. 11:1524585. doi: 10.3389/fmars.2024.1524585

III Siht E., Väli G., Liblik T., Mishra A., Buhhalko N., Lips U. (2025). Modeling the pathways of microplastics in the Gulf of Finland, Baltic Sea - sensitivity of parametrizations. Ocean Dynamics. Ocean Dynamics 75, 9. doi: 10.1007/s10236-024-01649-0

Author's Contribution to the Publications

I   The author contributed to conducting field experiments and performed data analysis, interpretation, and visualization of the results. The manuscript was primarily written by the author with valuable input from co-authors.

II   The author was responsible for setting up the model experiment with realistic loads and analysed, interpreted, and visualized the data. The manuscript was primarily written by the author with valuable input from co-authors.

III   The author contributed to finding the parameterizations for processes and contributed to the analysis of the data and writing the manuscript.

Abbreviations

ANOVA	Analysis of Variance
EGB	Eastern Gotland Basin
EMODnet	European Marine Observation and Data Network
EU	European Union
FABM	Framework Aquatic Biogeochemical Models
GETM	General Estuarine Transport Model
GoF	Gulf of Finland
GoR	Gulf of Riga
GOTM	General Ocean Turbulence Model
HELCOM	Helsinki Commission
MFSD	Marine Strategy Framework Directive
MP	Microplastics
NBP	Northern Baltic Proper
PE	Polyethylene
PET	Polyethylene Terephthalate
PP	Polypropylene
PVC	Polyvinyl Chloride
STD	Standard deviation
VS	Väinameri Sea
WGB	Western Gotland Basin
WWTPs	Waste Water Treatment Plants

1 Introduction

1.1 General overview of plastic pollution

Plastic pollution is a problem affecting today's marine environment. Plastics, due to their low cost and high durability are important in our lives. The significant increase in plastic production over the past five to six decades have raised numerous concerns about plastic waste in general, and about its impact in the aquatic environment. Recent studies have estimated that over 170 trillion plastic particles, weighing approximately 2.3 million tonnes, are floating in the world's oceans (Eriksen et al., 2013, 2023), and their presence is increasing in the seabed, coastlines and in marine biota (e.g Barnes et al., 2009; Suaria and Aliani, 2014; Llorca et al., 2020; Matjašič et al., 2023). Despite substantial efforts and several initiatives taken to control the use of plastics, the global annual plastic waste production is still projected to continue rising in the coming years. This has been recognized by the United Nations and their sustainable development goal 14.1 aims to reduce the marine pollution, including plastics, by 2025 (United Nations, 2015).

The Marine Strategy Framework Directive (MFSD; 2008/56/EC, European Commission, 2008) identified anthropogenic litter as a pressure on coastal habitats. The MSFD sets guidelines for the European Union (EU) member states to achieve good environmental status in their marine environments and to prevent any future deterioration including the MSFD descriptor D10 ("Properties and quantities of marine litter do not cause harm to the coastal and marine environment"). In 2021, the EU also banned single-use plastics within its associated member states (Harvey and Watts, 2018).

Microplastics (MP) are defined as plastics less than 5mm in diameter (e.g. Arthur et al., 2009; Cole et al., 2011). MPs are either manufactured as microscopic particles found in personal care products (primary MPs) or derived from fragmentation of large particles (secondary MPs). Secondary MPs are also formed by degradation of improperly disposed plastics waste, tire abrasion, and washing of synthetic textiles. The MP debris found in the aquatic environment are mainly due to inappropriate human behaviour and improper waste management. MP particles are categorized under different shape classes: fragments, films, filaments, foams, and pellets (GESAMP, 2019).

1.2 Sources of microplastics

Plastic can penetrate the marine environment via multiple entry points including riverine systems, coastal activities, shipping, and atmospheric deposition (GESAMP, 2019), so it is paramount to understand different MP's sources and pathways to prevent plastics from entering the ecosystem (He et al., 2019). Wastewater Treatment Plants (WWTPs) are considered as one of the major emission pathways to the aquatic environment (e.g. Ziajahromi et al., 2016; Mintenig et al., 2017; Kay et al., 2018; Prata, 2018; Schernewski et al., 2020). High MP concentrations were reported for untreated WWTP effluents (e.g. Sun et al., 2019; Schernewski et al., 2020). However, WWTPs, where wastewater is treated, could be efficient in removing MP (e.g. Carr et al., 2016; Talvitie et al., 2017; Gies et al., 2018). In the Baltic Sea, the MP retention (removal efficiency) was assumed to range between 85% and 98% based on different treatment stages in WWTPs (Baresel and Olshammar, 2019). Despite this good overall removal efficiency, WWTPs are still considered a significant source of MP to the Baltic Sea due to the substantial volume of water being treated (Baresel and Olshammar, 2019). The wastewater and stormwater plants are usually not interlinked in the Baltic Sea area (Schernewski et al., 2020). During

heavy precipitation, sewer overflows which consist of both stormwater and untreated wastewater can act as a critical gateway for MP into the aquatic environment (e.g. Magnusson, 2016; Dris et al., 2018). Baresel and Olshammar (2019) suggest that the annual discharge from the sewer flows is comparable in magnitude to that of treated wastewater.

Rivers also play a critical role in the transport of MP into oceans as outlined in a number of studies (e.g. Jambeck et al., 2015; Siegfried et al., 2017; Schrank et al., 2022; Veerasingam et al., 2016). It is estimated that annually, between 1.15 and 2.41 million tons of plastics enters to oceans via rivers. The high variability of MPs seen in the water column and sediments depends on the factors such as anthropogenic activities, and size of the catchment area (e.g. Matjašič et al., 2023). River retention is considered in some studies based on particle size and density (e.g. Kooi and Koelmans, 2019), but some studies do not consider the retention in rivers at all (e.g. Schernewski et al., 2020, 2021). For instance, it has been estimated that the MP retention in the Warnow River estuary ranges between 50% and 90% (Piehl et al., 2021).

1.3   Overview of the Eastern Baltic Sea

The Baltic Sea, located in the northern Europe, is a semi-enclosed brackish water sea with limited water exchange to the North Sea via the Danish Straits. With a catchment area four times bigger than surface area (372,858 km^2) and an average depth of 55 m, the Baltic Sea is one of the largest brackish water bodies in the world (HELCOM 2023). The Baltic Sea, faces significant challenges related to marine litter (HELCOM 2023). Beach litter is found in significant amounts along the coastal areas of the Baltic Sea (HELCOM 2023). Plastic materials are the most frequently found marine litter in the Baltic Sea (HELCOM 2023). Therefore, it is reasonable to assume that the Baltic Sea serves as a major hotspot for MP, mainly through river discharge and freshwater input. The HELCOM's aim to reduce the plastics waste and mitigation strategies used to counter the harmful effects on coastal and marine environment remains unfulfilled, as of 2023 (HELCOM 2023).

The average annual riverine runoff to the Baltic Sea is approximately 14,100 m^3/s (e.g. Meier and Kauker, 2003). The water renewal time of the Baltic is approximately 30 years. The long residence time, small volume of the sea in combination with large catchment area and high population density makes the Baltic Sea highly vulnerable for pollution.

The Baltic Proper (BP) is the central basin of the Baltic Sea, encompassing the Northern Baltic Proper (NBP), Western Gotland Basin (WGB), and Eastern Gotland Basin (EGB) (Figure 1A). The BP has a surface area of approximately 211,069 km^2 and a mean depth of 62 m.

The Gulf of Finland (GoF) is an estuary-type basin located in the northeastern part of the Baltic Sea with an average depth of 37 m and a maximum depth of 123 m (Leppäranta and Myrberg, 2009). The gulf is about 400 km in length, and width varies between 48 and 135 km (Alenius et al., 1998). Compared with other regions of the sea, the water exchange between GoF and NBP is not restricted at the western border and the freshwater is mostly discharged to the eastern part of the GoF.

The Gulf of Riga (GoR) covering an area of 140 km from west to east and 150 km from south to north is a semi-enclosed sub-basin (Suursaar et al., 2002) along with the other small sub-basin Väinameri Sea (VS) with a surface area of 2,243 km^2 (Suursaar et al., 2003). The average depths of GoR and VS are 23 m and 4.7 m, respectively.

Only few studies have described the MP distributions in the eastern Baltic Sea (e.g. Lips et al., 2020; Setälä et al., 2016; Uurasjärvi et al., 2021). However, the knowledge of spatiotemporal variability of MPs in the Baltic Sea is still limited due to lack of regular observations and uncertainties in simulations (She et al., 2022).

1.4   Modelling the pathways of MP

Modelling the fate and transport of MP in the marine environment has become an important tool to predict the accumulation areas of the debris (Tsiaras et al., 2021). Generally, two types of models are commonly used to estimate the MP pathways. The first type are Eulerian models which consider advection and diffusion at specific locations (e.g. Osinski et al., 2020; Schernewski et al., 2021; Frishfelds et al., 2022) and the second type are Lagrangian particle tracking models which can simulate the pathways of individual particles (e.g. Van Sebille et al., 2018). Among the two types, Lagrangian models are preferred to be more suitable for MP simulations. This is because they solve transport equations for the particles being tracked, unlike Eulerian models, which solve equations for the entire grid. In addition, Lagrangian models are also efficient, flexible and provide faster computation (Van Sebille et al., 2018; Lobelle et al., 2021). For instance, Pärn et al. (2023) used a combination of hydrodynamic and Lagrangian particle tracking model to track the fate and movement of floating litter in the Baltic Sea. Osinski et al. (2020) and Schernewski et al. (2020) have used GETM (General Estuarine Transport Model) ocean circulation model in combination with an Eulerian approach in their studies to analyze the MP transport in the Baltic Sea. In the eastern GoF, Martyanov et al. (2023) considered different fall velocities of suspended plastics to study the distribution of MP in the vicinity of Neva River using the Massachusetts Institute of Technology general circulation model (MITgcm). Schernewski et al. (2020) have utilized emission scenarios from the WWTPs and combined sewerage plants as an input to their model in the whole Baltic Sea. Biofouling as an important sink has not been considered in all the modelling studies. For instance, in the Baltic Sea only Martyanov et al. (2021), Frishfelds et al. (2022) and Murawski et al. (2022) used biofouling to increase the settling velocity of MP particles, while Osinski et al. (2020) and Schernewski et al. (2020) did not include the biofouling process. In the Mediterranean Sea, Tsiaras et al. (2021) used bacterial species concentration to parameterize biofilm growth, following the approach of Chubarenko et al. (2022), while in the North Sea, Cuttat (2018) employed the Kooi biofouling parametrization from dolly ropes.

1.5   Aim and objectives of the study

The main aim of this thesis is to investigate the spatial distribution, transport pathways and accumulation of MPs in the eastern Baltic Sea, with a specific focus on the GoF. By integrating high-resolution modelling and observational data, this research seeks to enhance our understanding of MP's behaviour in the marine environment and provide this information for future mitigation strategies to tackle the MP problem in the marine environment. This includes also examining the combined effects of key processes, such as advection, diffusion, biofouling, and resuspension on MP pathways and accumulation.

There are four main objectives covered in this thesis.

The first objective is to characterize the spatial and temporal variability of MP across the eastern Baltic Sea, with specific attention to seasonal changes, regional differences, and composition of particles in terms of type, size and colour.

The second objective is to understand the pathways and accumulation areas of MPs, including the sea surface, water column, seabed and beaches.

The third objective is to identify the influence of various physical and particle-related processes, such as advection, diffusion, resuspension, beaching and biofouling in determining the distribution, transport and fate of MPs.

The fourth objective is to investigate the contribution of wind-induced mixing and mesoscale processes, such as coastal upwelling, downwelling, surface water convergence and divergence to the short-term fluctuations in MP concentration and distribution in the GoF.

Through these objectives, the thesis aims to improve the understanding of the factors influencing the MP distribution and their accumulation in the eastern Baltic Sea.

2 Materials and Methods

2.1 Hydrodynamic model and setup

The General Estuarine Transport Model (GETM; Burchard and Bolding, 2002) has been utilized for this thesis to simulate the current, temperature, and salinity fields of the Baltic Sea and more specifically, in the GoF. GETM is a hydrostatic, three-dimensional primitive equation model that incorporates adaptive vertical coordinates (Hofmeister et al., 2010; Klingbeil et al., 2018), which have shown to significantly reduce the numerical mixing in the simulations (Gräwe et al., 2015). The vertical mixing in GETM is provided by coupling it with the General Ocean Turbulence Model (GOTM; Burchard, 2001) and more specifically, we have used a two-equation k-ε scheme (Canuto et al., 2001). Sub-grid horizontal mixing (viscosity for momentum and diffusion for tracers) is computed using the Smagorinsky parameterization (Smagorinsky, 1963).

The biogeochemical model ERGOM (e.g. Neumann et al., 2002; Neumann and Schernewski, 2008) is coupled with the hydrodynamic model via Framework Aquatic Biogeochemical Models (FABM; Brüggemann and Bolding, 2016) and was used to calculate the chlorophyll-a (CHLA) concentrations in the GoF. ERGOM has 12 state variables and describes a nitrogen and phosphorus cycle, although part of the phosphorus is considered with the N:P ratio (Redfield, 1934). The CHLA can be calculated from the simulated phytoplankton concentrations. More details about the latest version of the ERGOM model can be found from (Neumann et al., 2022).

The hydrophysical and biogeochemical part in this thesis has been calculated with a one-way nested model system. The entire Baltic Sea was simulated using a horizontal grid step of 1 nautical mile (approximately 1852 m) and 50 adaptive vertical layers (Gräwe et al., 2015). Boundary conditions in the Kattegat were derived from sea surface observations at the Gothenburg Torshamnen station, which describe the barotropic water exchange between the Baltic Sea and the North Sea. A medium resolution model, based on the settings described in Zhurbas et al. (2018) and Liblik et al. (2020, 2022) has a horizontal grid spacing of 0.5 nautical miles (approximately 1 km) and covers the central BP along with the GoF and GoR. Temperature, salinity, and current velocity components from the coarse-resolution model, with an hourly resolution, were spatially interpolated and applied at the open boundaries of the medium-resolution model.

The high-resolution model domain covers the GoF and has a horizontal grid spacing of 0.125 nautical miles (approximately 250 m), which is high enough to permit also sub-mesoscale processes (e.g. Lips et al., 2016a; Salm et al., 2025). Similar to the medium-resolution nesting, boundary conditions for the high-resolution model were provided using spatially interpolated results with hourly resolution from the medium-resolution model. Both the medium- and high-resolution simulations employed 60 adaptive vertical layers.

Atmospheric forcing at the sea surface (wind stress and heat flux) is calculated offline from the ERA5 re-analysis (Hersbach et al., 2020). Freshwater input to the models is based on the runoff data compiled for the Baltic Model Intercomparison Project (Gröger et al., 2022) by Väli et al. (2019) and Estonian rivers have been corrected by the input estimates from EstModel (https://estmodel.app/en/#/estimates, last access 13.02.2025).

Initial temperature and salinity fields for the coarse-resolution model were taken from the Copernicus Marine Service re-analysis product for 2009-12-30. The medium- and high-resolution models are using the results from the coarse- and medium-resolution

runs, respectively. The high-resolution model was used for the period from late 2018 to mid-2021. The runs are initially started from motionless state i.e. current velocity components and sea surface height set to zero. Previous studies have indicated that the adjustment of the wind-driven circulation in the numerical models of the Baltic Sea occurs within a few days (e.g. Krauss and Brügge, 1991; Lips et al., 2016b).

A more detailed description of the model setup and validation is provided in Papers II and III.

2.2   Lagrangian particle model

To track the virtual MP particles, we used the Lagrangian particle model, as presented in Paper III. The particle tracking model used 3D hydrodynamic fields from the GETM setup, which were saved at 12-hour intervals for particle transport. In addition to advection and sinking of particles, the model accounted for several additional processes important for MP tracking: 1) dispersion, 2) beaching, 3) biofouling, and 4) resuspension.

The horizontal diffusion for particle dispersion was based on the current shear velocity, following the Smagorinsky method (Smagorinsky, 1963) and the constant coefficient C_s was set to 0.2.

Beaching was modelled using a timer-based approach, where particles were classified as beached after spending a specified duration of time in the beach zone. In the realistic simulation (Paper II), a uniform beaching time of 10 days was applied to all particle types although the sensitivity was tested with various beaching times as described in Paper III. The beach zone was defined as the sea cell closest to the land (i.e., 250m). Resuspension of particles from the beach zone was excluded from the simulations, meaning that once the particle was beached, it remained still and was effectively removed from further tracking. By assuming finite beaching, the model reflects real-world observations that a significant portion of MPs, particularly lightweight particles, remain retained on beaches due to limited resuspension under normal conditions. For example, MP concentrations on Baltic Sea beaches have been reported to range from 0.31 to 11.7 particles per kilogram of dry sediment (Dimante-Deimantovica et al., 2023).

Biofouling was described as a saturated growth process that depended on the maximum biofilm thickness and the growth time scale, following the approach of Murawski et al. (2022). The biofouling process was initiated when the chlorophyll-a concentration exceeded 1.1 mg m^{-3}. In the current simulations, the maximum biofilm thickness was set to 6.7% of the initial particle radius, and the growth duration was set to 20 days. Biofouling impacts the buoyancy of particles by increasing their mass due to growth of biomass on the particles surface. For example, biofouled particles become denser, causing them to sink more rapidly than clean particles.

Negatively buoyant particles could settle and were resuspended when the critical shear velocity was exceeded. The vertical velocity gained from resuspension was set proportional to the local bottom friction velocity.

The particle tracking model was simulated for the period from 2018-02-05 to 2021-01-01. Particle coordinates were updated at a time step of 600 seconds. At each time step, the current velocity components and other hydrological parameters were interpolated in both time and space to match the precise location of the particles and advection was calculated using the second order Runge-Kutta method following Väli et al. (2018).

Approximately 146 million particles were released both from rivers and WWTPs during the simulation and the Lagrangian particle coordinates were recorded at 12-hour intervals.

A more detailed description of the Lagrangian particle model setup is provided in Paper III.

2.3   MP sampling and sample processing

Surface water samples were collected using a Manta Trawl with a 330 µm mesh, towed at the surface for 15–60 minutes at ~2knots (Paper I). The samples were rinsed, sieved (5,000 µm, 1,000 µm, and 330 µm), and stored in glass jars with formaldehyde (1:100). When organic material was present it was oxidized with hydrogen peroxide for up to 7 days before vacuum filtration onto glass fiber filter. Filters were dried at 60 °C and analyzed under a stereomicroscope. MPs were counted, partially photographed, and tested with hot needle for plastic identification (De Witte et al., 2014).

MPs were categorized as fibers or fragments (including films, foams, and pellets) and divided into two size classes: 330–999 µm and 1,000–4,999 µm (Paper I). Concentrations were calculated both as counts per cubic meter (counts/m^3; total number of MP divided by the volume of water sampled) and counts per square meter (counts/m^2; total number of MP divided by the area covered during the sampling). Colors were classified using the European Marine Observation and Data Network (EMODnet) 8-color scheme (Galgani et al., 2019), grouping similar colors into categories such as black/gray, white, blue/green, red/pink, and others.

2.4   Statistical analysis and calculations

To examine the spatial and temporal variability of MPs, a one-way analysis of variance (ANOVA) was employed. When significant differences were identified, pairwise comparisons using regression tests were conducted to assess statistical significance, with a threshold set at 5%.

Additionally, meteorological conditions were incorporated into the analysis by extracting hourly wind speed components from the ERA-5 reanalysis dataset (Hersbach et al., 2020). Linear regression analyses were performed to explore the relationship between MP abundances and wind conditions. Further details are explained in Paper I.

Hydrophysical conditions during sampling dates were evaluated using sea surface temperature and salinity data derived from long-term model simulations. More details can be seen in Paper I.

MP concentrations in the surface layer were defined from the sea surface to a geopotential height of -1m (Paper II). The water column was defined as extending from the sea surface to the seabed, with concentrations integrated over the entire column (Paper II). Meridionally integrated values represent the temporal average of concentrations integrated from south to north, effectively describing the cross-sectional profile of the model domain in the GoF (Paper II).

To reduce high-frequency variability, all mean concentration fields were spatially smoothed using a 2.5 km window, corresponding to the local baroclinic Rossby radius of 2–4 km (Alenius et al., 2003). The analysis presented in this thesis is based on two model years (2019–2020), following a one-year spin-up period.

2.5 Emission scenarios – Microplastic sources and emission calculations

The behaviour and distribution of MPs in the marine environment are influenced by their density. Density plays a crucial role in classifying plastics into two main categories: floating and sinking types. We specifically focused on polypropylene/polyethylene (PP/PE) with a density of 960 kg/m³, which falls within the floating plastic category, and polyethylene terephthalate (PET) with a density of 1380 kg/m³, classified as a sinking plastic (Schernewski et al., 2020).

In this thesis, two main MP sources were considered for modelling:

a) MP inputs from WWTPs with estimated loads based on the study by Schernewski et al. (2020). We considered maximum MP concentrations, and river retention was not taken into consideration. The MP load into the GoF catchment area was calculated using the treated wastewater discharge data and particle concentrations in raw water (Figures 1A, B). Further information can be found from Paper II.

b) Rivers were identified as another significant source of MP (Jambeck et al., 2015). The considered MP amount in rivers (excluding WWTPs contribution) was 35 particles/m³. The daily MP load from riverine sources (particles/day) was calculated by multiplying concentration of 35 particles/m³ to the river discharge to the GoF. For more information regarding MP found in European rivers, please refer to Paper II.

Besides density, the floating and sinking behaviour of MP is also influenced by their size and shape. In this thesis, we analysed MPs ranging from 20 to 500 µm, categorizing them into two size classes: 20–200 µm and 200–500 µm. Following the findings of Schernewski et al. (2021) and Kuddithamby et al. (2024), it was assumed that 90% of the MP would fall into the 20–200 µm size category.

Emissions from WWTPs and rivers were used as inputs for two main scenario runs.

Scenario 1 focused on PET and PP/PE loads from WWTPs, specifically for the 20–500 µm size fraction, further divided into small (20–200 µm) and large particles (200–500 µm) for both PET and PP/PE.

Scenario 2 focused on PET and PP/PE loads from rivers, also considering the 20–500 µm size fraction, with the same subdivisions as scenario 1.

In total, eight scenarios were simulated, covering two MP types, two size ranges, and two emission pathways. All scenarios assumed constant daily MP emissions throughout the simulation period (see Paper II, Table 1).
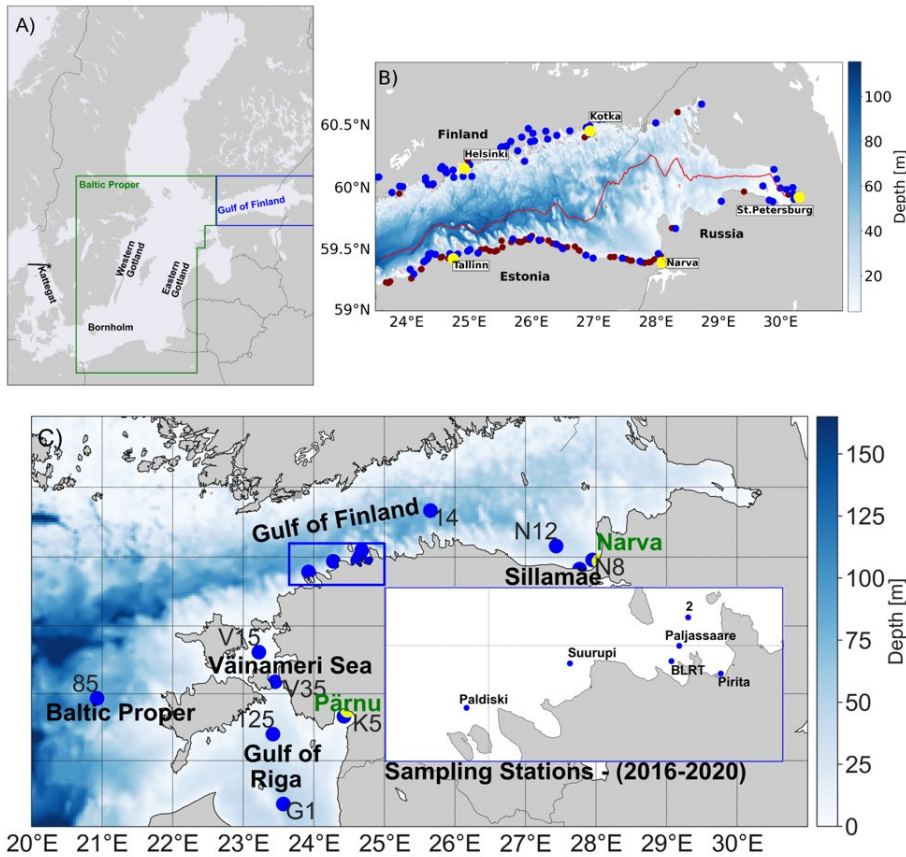
Figure 1 – Panel (A, B) represent a map of the Baltic Sea and a map of the WWTPs (blue dots) and river (red dots) emission points at the coast of the GoF. Yellow dots represent the cities mentioned in the thesis. The red line indicates the thalweg along the GoF. The black line in panel (A) is the location of the open boundary, Gothenburg station marked by the star; panel (C) display the map of the eastern Baltic Sea with 16 stations of surface water sampling in the BP region (85), VS (V15 and V35), GOFW (Paldiski, Suruti, BLRT, Paljassaare, and Pirita), GOFC (14), and GOFE (N12, Sillamäe, and N8). The locations of Narva and Pärnu river are highlighted in green. Amended from Papers I and II.

2.6   Processes governing the MP transport

The sensitivity of different parameterizations to MP transport was studied in Paper III. The summarizing illustration with the impact of processes with contrasting conditions, which either support or limit the spreading and horizontal transport of the MP, is shown in Figure 2. In the weak horizontal transport scenario, stronger removal processes, such as beaching and biofouling, combined with lower diffusion and resuspension, lead to low surface concentrations and particle accumulation near sources, either along the coast or in the bottom sediments. This limited transport prevented widespread particle spreading. Conversely, strong horizontal transport conditions were characterized by lower removal processes and higher diffusion and resuspension, resulting in a more extensive distribution of MPs throughout the water column and bottom sediments. These scenarios highlighted

the interplay between hydrodynamic conditions and removal mechanisms in shaping the MP pathways and accumulation zones.

The particle budget under weak and strong horizontal transport conditions was also summarized in Paper III (see Figure 16). In the case of weak horizontal transport, only 4% particles remained in the water column by the end of the simulation, a 92% decrease compared to the reference run, due to enhanced removal processes like beaching (49% of particles) and settling. In contrast, under strong horizontal transport conditions remained suspended longer, with 31% fewer settled particles compared to reference run and only 4% beached. Additionally, strong transport facilitated particle movement toward the domain boundary at the mouth of the GoF in west, with 11% of particles reaching the domain boundary compared to just 0.4% under weak transport. These results emphasized how transport conditions influenced particle retention, dispersion, and movement within the GoF.
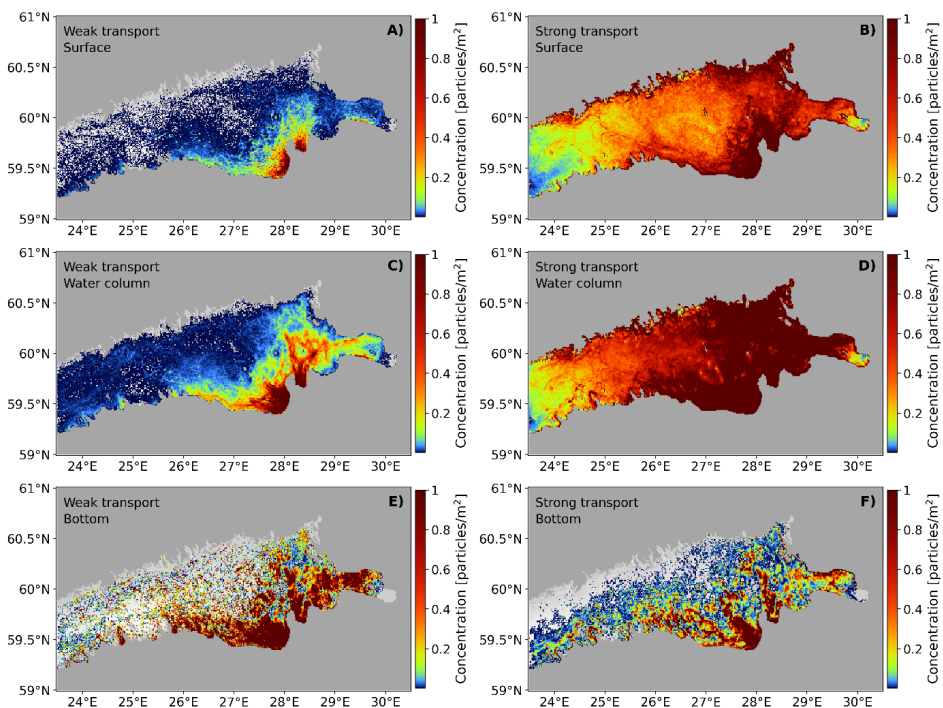

Figure 2 – Average concentration of particles at the surface (A, B), in the water column (C, D) and bottom sediments (E, F) over the period from 5 February to 31 December 2018. Left panels (A, C, E) represent weak transport conditions; right panels (B, D, F) represent strong transport conditions. The combined processes include diffusion, resuspension, biofouling and beaching. From Paper III.

3   Results & Discussion

3.1   Spatial variability of MP

3.1.1   Surface

Observational results across the eastern Baltic Sea revealed distinct spatial patterns and considerable variations in MP concentrations (Paper I). The main findings identified three distinct areas based on MP levels. The first group comprised the BP-GoF region, which included BP (0.65 counts/m³) (0.11 counts/m²), GOFW (0.65 counts/m³) (0.11 counts/m²), GOFC (0.59 counts/m³) (0.10 counts/m²) and GOFE (0.46 counts/m³) (0.08 counts/m²) (see Figure 3). The second one was the GoR, with a mean concentration of 0.33 counts/m³ (0.06 counts/m²), and the third one was the VS, which exhibited the lowest mean of 0.11 counts/m³ (0.02 counts/m²). The data revealed a high degree of variability in MP concentrations (STD ±0.46 counts/m³) and heterogeneity in their distribution patterns across the eastern Baltic Sea. The modelling studies focused on the area of highest MP concentration, i.e. the GoF. The highest mean concentrations were measured in the GOFW (Figure 4B) near Tallinn, at stations 2 and Pal, 0.74 and 0.66 counts/m³, respectively. The latter station was located near the release location of a WWTP. Complementing these observations, the modelling studies confirmed that MP from WWTPs showed elevated concentrations near major urban centres such as Tallinn, Helsinki, and St. Petersburg (Paper II). In the BP, offshore station 85 exhibited values similar to those in the GOFW, whereas offshore station 14 in GOFC had lower values than those in the GOFW and BP. Additionally, the pollution levels near the mouths of the Pärnu and Narva Rivers (station K5 and N8) were lower compared to open sea stations. The modelling study further supported the observational findings, indicating that MP concentrations from WWTPs were also lower near station N8 (Figures 4C, D), consistent with the observed lower levels in this area. In the monitoring study (Paper I), the focus was on monitoring the whole MP particles, including fibers and fragments, rather than specific polymer types like PET and PP/PE. Therefore, while the particle types are not directly comparable, the spatial patterns observed in both studies suggest a consistent regional distribution of MPs.

The mean spatial distribution of modelled MP particles in the surface layer in the GoF is shown in Paper II (Figure 4). PP/PE (light) particles had higher concentrations compared to PET (heavy) particles for both WWTP and riverine origin particles near major coastal sources (Figures 4E, F). The riverine input to the Russian part was six times greater than the combined input from Estonia and Finland, resulting in the highest concentrations of riverine-origin MPs in the eastern gulf. The overall mean concentration of riverine-origin PP/PE particles in the gulf was approximately 3.8 particles/m², with significantly higher concentrations in the eastern gulf, where maximum values exceeded 50 particles/m². The riverine PET particles did not disperse as widely as PP/PE particles from the eastern to the western part of the gulf. The PET particles from WWTPs primarily accumulated in the eastern part of the gulf and near other sources such as Helsinki (Figure 4C). PP/PE particles from WWTPs had a similar distribution to the PET, but dispersion was higher, and the impact of Tallinn and Helsinki was more pronounced. The mean concentrations in the gulf for both PET and PP/PE particles combining both the sources were 1.4 particles/m² and 4.8 particles/m², respectively.

Our observed mean MP concentrations were consistent with those reported in other studies using surface trawling in the Baltic Sea and beyond. For instance: Aigars et al.

(2021) reported MP concentrations ranging from 0.09–4.43 counts/m^3 in the GoR and EGB. Schönlau et al. (2020) found concentrations in between 0.18–0.92 counts/m^3 in the Gullmar fjord on the Swedish west coast and 0.05–0.09 counts/m^3 were observed in the South Funen Archipelago (Tamminga et al., 2018), while 0.19–7.73 counts/m^3 was measured in the Stockholm Archipelago (Gewert et al., 2017), and 0–0.8 counts/m^3 in the GoF (Setälä et al., 2016). In other regions of the world, for instance in the Arctic, concentrations have varied from 0 to 1.31 counts/m^3 Lusher et al. (2015) while in the Mediterranean Sea from 0.07–9.25 counts/m^3 (in the eastern part by Adamopoulou et al., 2021) to the overall mean value is 1.82 counts/m^3 (Zeri et al., 2018). In the eastern Indian Ocean, the observed MP concentrations lie within 0.06–25.9 counts/m^3 (e.g. Li et al., 2021).

The differences in human pressure appeared to influence regional MP distributions: the GoF region, with catchment densities of approximately 400 inhabitants per km², exhibited higher MP concentrations than the GoR region (around 150 inhabitants per km²), while the VS region, with minimal human impact and few major point sources revealed the lowest levels (HELCOM, 2004). Both, the observational and modelling results indicated that MPs tend to accumulate as localized pollution hotspots near primary emission sources rather than dispersing widely across the central gulf as suggested before by Murawski et al. (2022) and Martyanov et al. (2023). These tendencies in spatial distributions were consistent with other studies, where lower MP concentrations were attributed to a reduced anthropogenic influence (Tamminga et al., 2018) and higher MP levels to urbanization and pollution sources such as industrial activities and WWTPs (e.g. Yonkos et al., 2014; Gewert et al., 2017; Schönlau et al., 2020).
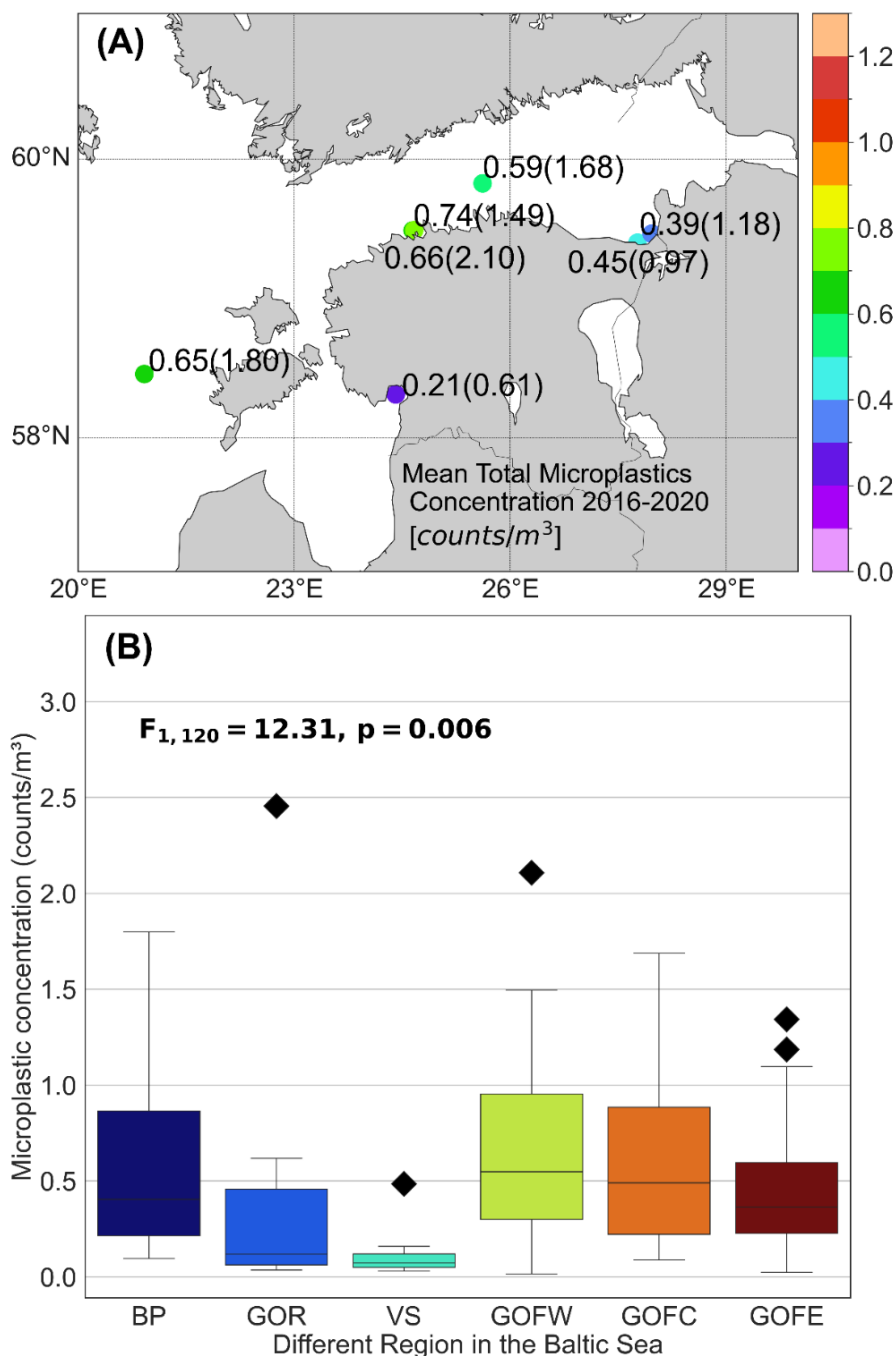
Figure 3 – Mean MP concentration in the surface layer based on observations from 2016 to 2020. In panel A the mean average concentration, calculated as an arithmetic mean at sampling locations, is presented. The highest MP concentration observed at each station is displayed in parentheses alongside the mean value. The mean MP concentration in different regions of the eastern Baltic Sea in 2016-2020 is presented in the panel B. The analysis indicated a statistically significant difference in MP concentrations across the regions ($F_{1,120}$ = 12.31, p = 0.006), highlighting variability in MP levels among the studied areas. Amended from Paper I.
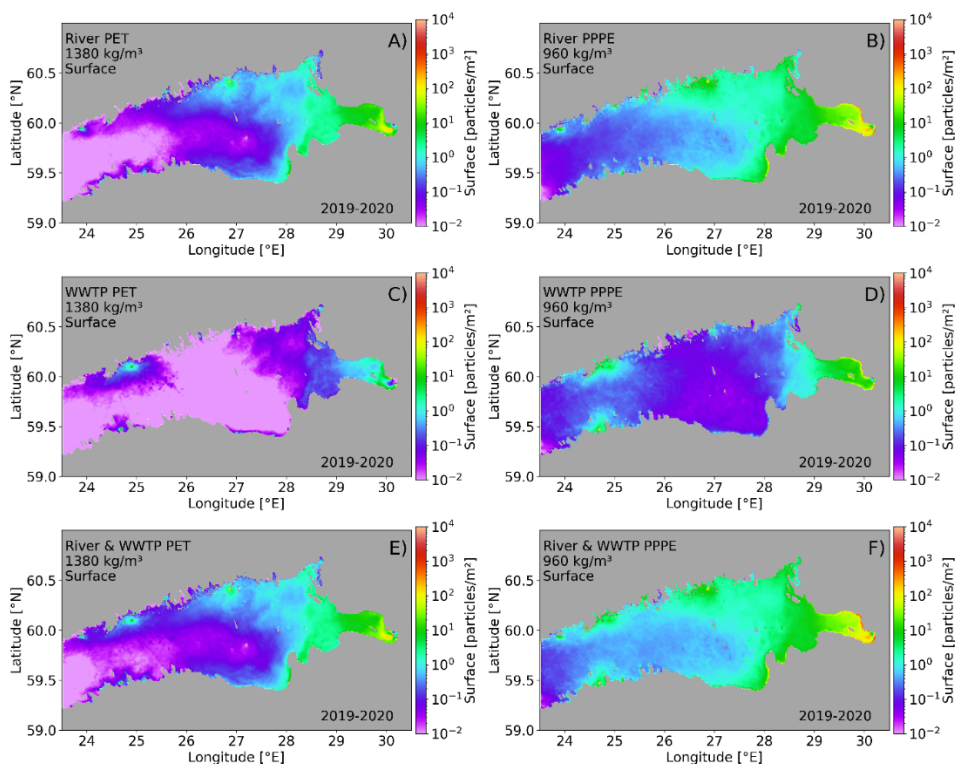
Figure 4 – Modelled mean concentrations of PET and PP/PE MP particles (20–500 μm) in the surface layer of the GoF from 2019 to 2020. Panels A and B represent the riverine origin PET and PP/PE particles; panels C and D WWTP origin PET and PP/PE particles; panels E and F display composite maps of different origin PET and PP/PE particles. From Paper II.

3.1.2 Water column and seabed

The time-series of the share of MP particles in different states in the GoF was reported in Paper II (Figure 5). The overall model spin-up was relatively fast as after initialization, the total amount of particles in the water column decreased to approximately 15%, while sedimented particles stabilized between 75–80% with 6-months of simulation. The share of particles reaching the western boundary (at the mouth of the gulf) was around 1%, and the beached particles accounted for about 10% after the spin-up period. Generally, the small, light particles were the most abundant in the water column, and the large, heavy particles were the least common (see, Figure 5A-B). Most particles that exited the GoF (reached the boundary) were from the small light class (3%), whereas the large light particles were most likely beached (28%). After three years of simulation, approximately 65% of the small and large light particles and 92% and 95% of the small and large heavy particles, respectively, had settled.
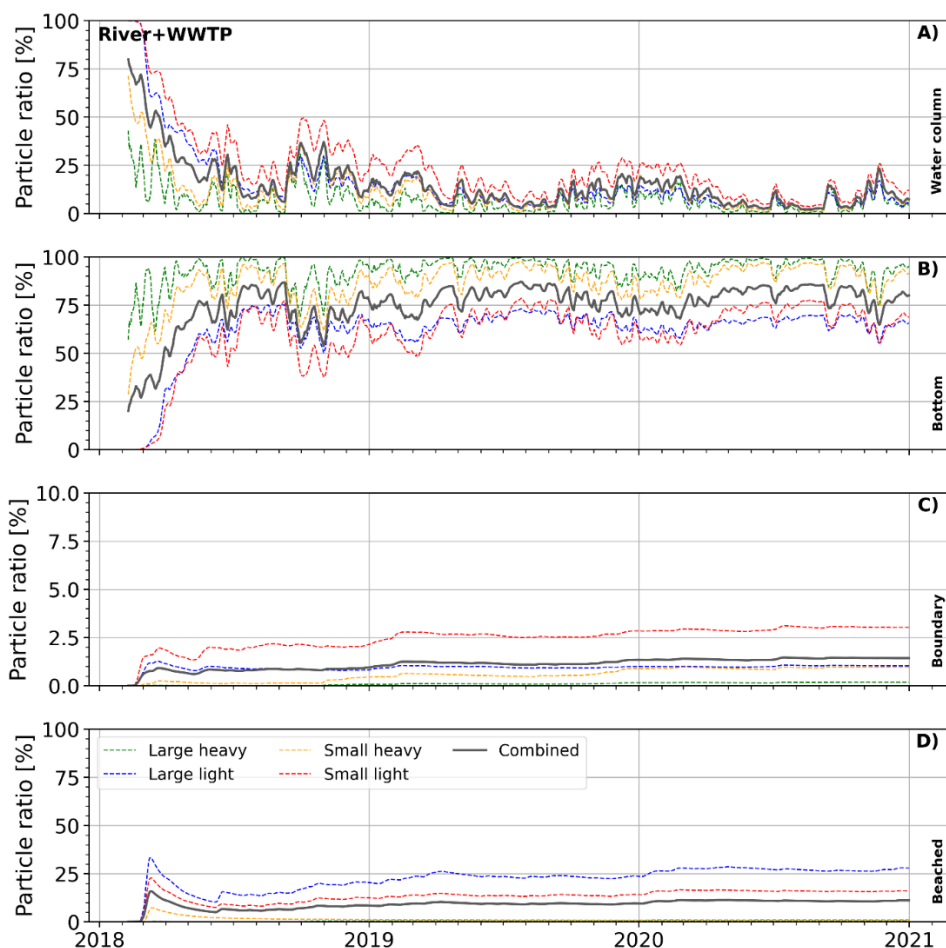
Figure 5 – Time series of particle budget in different classes for the GoF: A) water column, B) bottom, C) boundary, D) beached. The time series have been smoothed using a 7-day moving window. From Paper II.

The mean spatial distributions of vertically integrated simulated MP concentration in the water column is shown in Figure 6. The model data indicates that the gradual decrease in MP concentrations in the gulf is influenced by its configuration and distance from the main sources. Higher concentrations of riverine-origin PET and PP/PE particles were observed in shallower eastern areas beyond 28 °E, whereas lower concentrations were noted in the western regions, where the Neva River's influence diminishes. In contrast, WWTP-origin particles showed higher mean concentrations in both the eastern and western regions, with reduced levels between 26 °E and 28 °E.

Figure 7 illustrates the meridionally integrated concentrations from south to north within the water column, for the years 2019 and 2020. From the surface to the seabed, PET particles had lower concentrations as due to higher density they sink quicker, while PP/PE particles were more prevalent, likely due to the higher density of PET particles (Figures 7A–D). Both particle type exhibited a vertical distribution pattern, with concentrations peaking near the surface and seabed and reaching a lower level in the intermediate layer, particularly in the deeper regions of the GoF. This distribution pattern

aligns with findings from the study (Zhou et al., 2021), which reported that MP accumulation is notably higher at the halocline, where it acts as a trapping layer, concentrating MP, while the layer above the halocline contained fewer particles. However, this distribution is not static. Resuspension events primarily driven by bottom currents (e.g. Liblik et al., 2013; Rasmus et al., 2015; Suhhova et al., 2018) or wave-induced shear stress (Jönsson et al., 2005) can shift MPs from seabed to the water column. This dynamic interplay between accumulation and resuspension highlights the critical role of hydrodynamic forces in redistributing MPs.
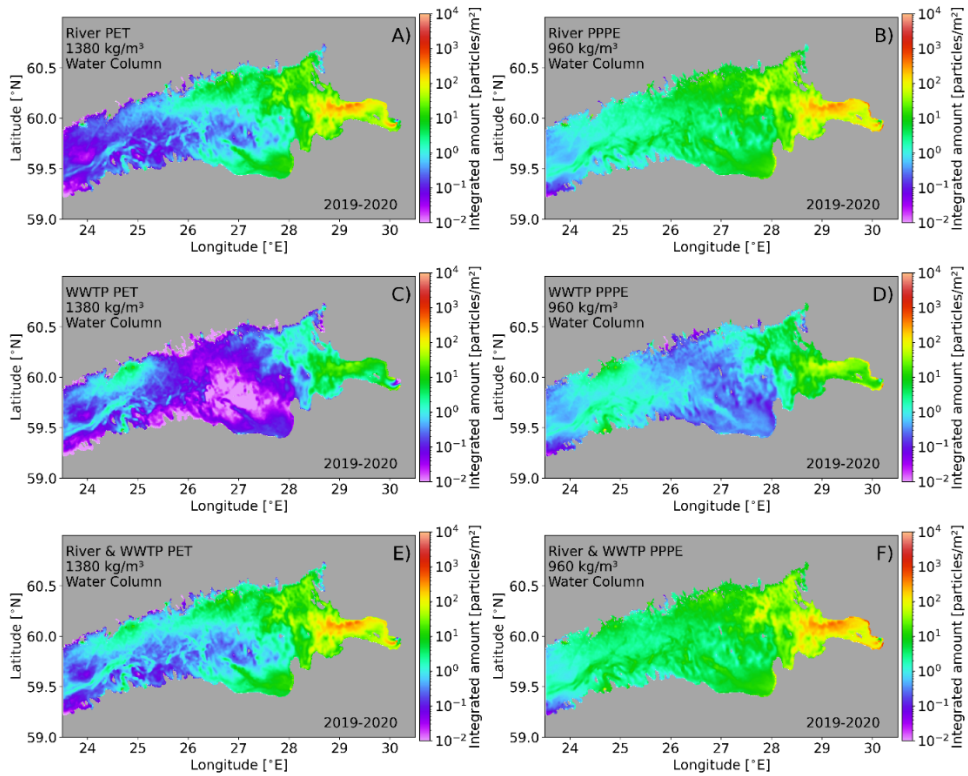

Figure 6 – Modelled mean spatial distribution of vertically integrated concentrations of PET and PP/PE particles (20–500 μm) in the GoF from 2019 to 2020. Panels A and B represent the riverine origin PET and PP/PE particles; panels C and D WWTP origin PET and PP/PE particles; panels E and F display the composite maps of different origin PET and PP/PE particles. From Paper II.
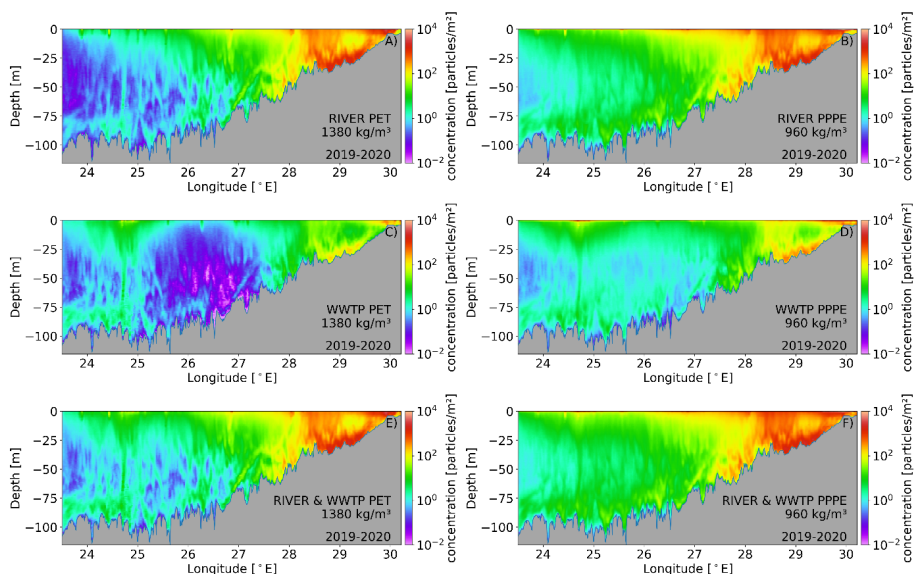
Figure 7 – Modelled mean meridionally integrated concentration of PET and PP/PE MP particles (20– 500 μm) in the water column of the GoF in 2019-2020. Panels A and B represent the riverine origin PET and PP/PE particles; panels C and D WWTP origin PET and PP/PE particles; panels E and F display composite maps of different origin PET and PP/PE particles. The bathymetry data along the latitude axis is represented as the maximum depth values for each longitude coordinate. From Paper II.

Figure 8 provides an overview of MP particles of different origin and classes found in the seabed. Sedimentation was widespread across the entire seabed of the gulf. The largest concentrations in the seabed were in the eastern part of the gulf. The heavy particles (PET) sank quickly and accumulated in the coastal areas with significant amounts in the Neva Bay, Narva Bay and near Kotka on the northern coast. Riverine-origin PET particles had higher values in the deeper areas of the gulf (Figure 8A). WWTP-origin PET particles exhibited the highest concentrations in the western and eastern regions of the gulf, with lower accumulation rates observed between 26.5 and 28 °E (Figure 8C). Regarding overall accumulation (Figures 8E, F), highest concentrations of both PET and PP/PE particles were found in the easternmost part of the gulf and Narva Bay. Along the southern coast, there was a tendency for higher concentrations near the coastline, whereas in the northern part, sedimentation appeared more homogeneous (Figure 8F).

Our findings from Paper II revealed that both PET and PP/PE particles exhibited widespread sedimentation across the Gulf, with higher accumulation near emission areas and in coastal regions. Notably, PP/PE particles showed a broader accumulation pattern that extended further offshore compared to PET particles. In coastal areas, PET particles due to their negative buoyancy consistently descended into the water column and ultimately settling on the seabed. A recent study by Schernewski et al. (2020) which used Eulerian tracers, reported accumulation of PET particles in shallow coastal waters of the Baltic Sea. This coastal accumulation was more pronounced near riverine sources, including the Neva River estuary and Narva Bay. The GoF due to their shallow depth facilitates higher deposition rates in these areas. Similarly, Kuprijanov et al. (2021) observed comparable patterns of hazardous substances accumulation in shallow areas, such as Neva Bay and Finnish coastal inlets, although MP accumulation might persist for longer periods in deeper regions.
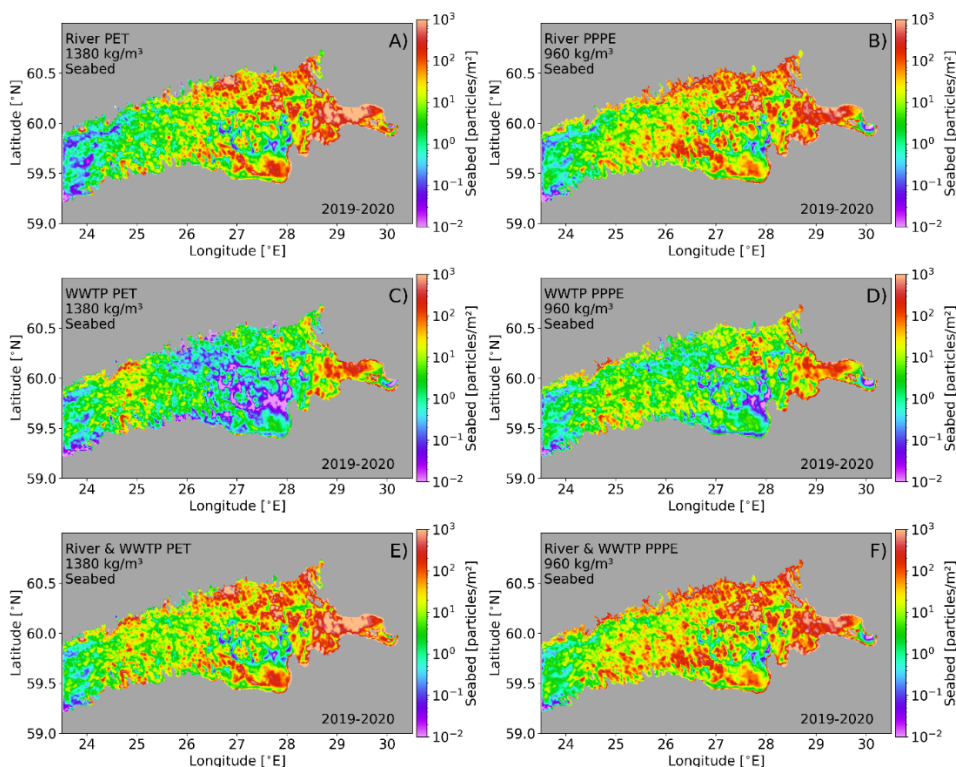
Figure 8 – Mean spatial concentrations of PET and PP/PE MP particles (20–500 μm) on the seabed of the GoF. Panels A) and B) represent the riverine origin PET and PP/PE particles; panels C) and D) WWTP origin PET and PP/PE particles; panels E) and F) display composite maps of different origin PET and PP/PE particles. From Paper II.

3.1.3 Particle distribution along coastline

The beaching of MP particles was evident along the entire coastline of the GoF (see Paper II, Figure 7). Light particles were significantly more prevalent, with an average beached concentration nearly 20 times higher than the heavy particles. Such high beaching rates is likely due to the differences in their buoyancy and settling dynamics. However, substantial numbers of heavy particles from rivers (> 10^5 particles/m) accumulated along the southern shore of Neva Bay. Light particles from rivers were abundant in Neva Bay, Narva Bay, and along the Finnish coastline. Additionally, particles from WWTPs were numerous around Neva Bay, inside Tallinn Bay, near Helsinki, and at localized spots along the northern coast. Previous studies have highlighted similar tendencies, with higher particle accumulation near the major rivers and urban areas, such as St. Petersburg (Schernewski et al., 2021). Dimante-Deimantovica et al. (2023) reported that in coastal areas of the GoR and western GoR, light particles were more prevalent than heavy particles, which aligns with the general distribution patterns observed in our study. Furthermore, Walther et al. (2024) observed a similar trend along the German coastlines, where light particles, particularly fibers, dominated the MP pollution. Additionally, a study on plastic contamination along the southern Baltic beaches found higher concentrations of light particles on beaches compared to coastal waters, reinforcing the role of beaches as key sites for accumulation (Mazurkiewicz et al., 2022).

3.2 Temporal variability of MP

3.2.1 Inter-annual variability and seasonal variability

The annual mean of MP concentrations for the study area was calculated for the years 2016 to 2020 (see Paper I, Figure 3). Mean concentrations and standard deviations (STD) are 0.90 (±0.53), 0.53 (±0.24), 0.43 (±0.4287), 0.18 (±0.30), and 0.25 (±0.21 counts/m³), respectively. This showed a general decrease in both mean concentrations and variability over the 5-year period. While this trend indicates a reduction in MP concentrations, explaining the interannual variability is challenging. Possible factors influencing the decrease include improved waste management practices and changes seasonal variations that impact MP distribution. Additionally, variations in meteorological conditions, such as changes in wind patterns could also affect the dispersion and deposition of MPs.

The model effectively replicates the seasonal variability of MP concentrations in the GoF. During summer (JJA, June-August), PET MP concentrations were lower in the surface (Figure 10A) and water column (Figure 10C), with highest concentrations found near the seabed, particularly along the northern and southern coasts, and especially in the eastern part of the gulf (Figure 10E), while winter (DJF, December-February) showed increased surface and water column concentrations due to reduced sedimentation and stronger resuspension driven by bottom currents. These results highlight how summer conditions favour seabed accumulation of PET particles, mainly due to weaker currents and biofilm formation, while winter conditions, with enhanced resuspension, lead to higher concentrations in the water column.

Observations support these model results, with higher concentrations found in spring compared to summer at 12 out of 16 sampling stations (Figure 9B). The mean concentration in spring and summer was 0.46 counts/m³ and 0.36 counts/m³, respectively. The highest seasonal mean concentration (0.81 counts/m³) was reported in autumn (Figure 9B). The only winter observation from GoF confirms the trend of increasing concentration from summer to winter (Figure 9A).

For PP/PE particles, surface concentrations peaked during the summer, particularly along Narva Bay, Tallinn, and Helsinki coasts (Figures 11A, B). Similar to PET, in winter, reduced biofilm growth likely led to lower seabed concentrations, while in summer, enhanced biofilm formation and stratification promoted particle settling (Figures 10C, F).

The seasonal variations of PET and PP/PE particles in the surface layer, water column, and sediments during summer and winter align with previous studies. Spring and summer are characterized by heightened biological activity in the Baltic Sea (Lips et al., 2014). Similarly, a recent modelling study conducted in Neva Bay, using a different modelling approach, reported a tenfold decrease in surface concentrations during summer relative to winter (Martyanov et al., 2021). This seasonal pattern highlights the combined effects of biofouling, hydrodynamics, and stratification. During summer, phytoplankton blooms enhance biofouling, increasing the sinking rates of MPs and contributing to their accumulation on the seabed. Vertical stratification, while facilitating biofouling, also acts as a barrier, trapping MPs within the thermocline (Uurasjärvi et al., 2021). By late summer, the breakdown of the thermocline and reduced primary production result in diminished biofilm formation and lower organic matter availability, potentially slowing MP sinking (Almroth-Rosell et al., 2011; Liblik and Lips, 2011).
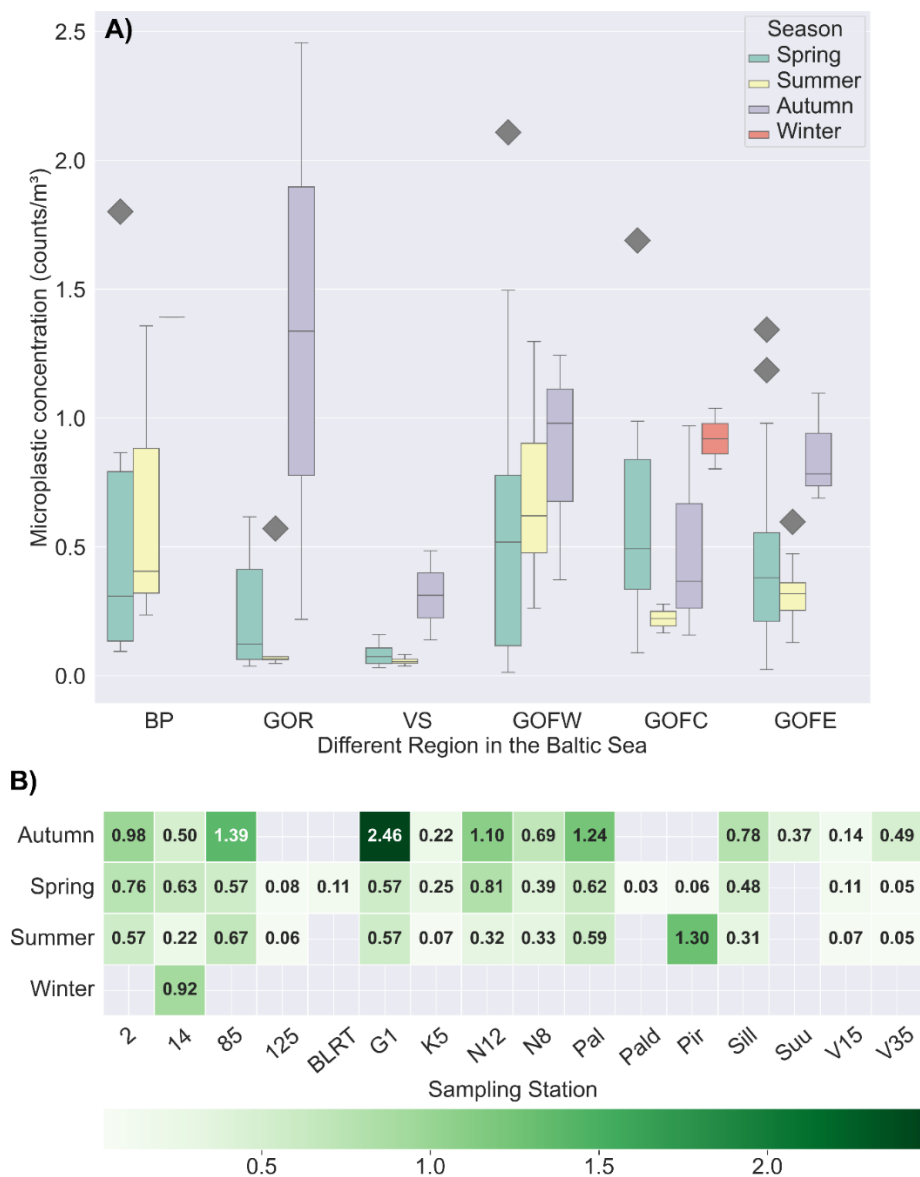
Figure 9 – Panel A) represents the seasonal variability of MP concentration across different regions in the Baltic Sea, while Panel B) illustrates the seasonal variation of mean MP concentration. Samples are categorized into 4 seasons: spring (April–June), summer (July–August), autumn (September–November), and winter (December–February). The concentration values are in counts/m³. Amended from Paper I.
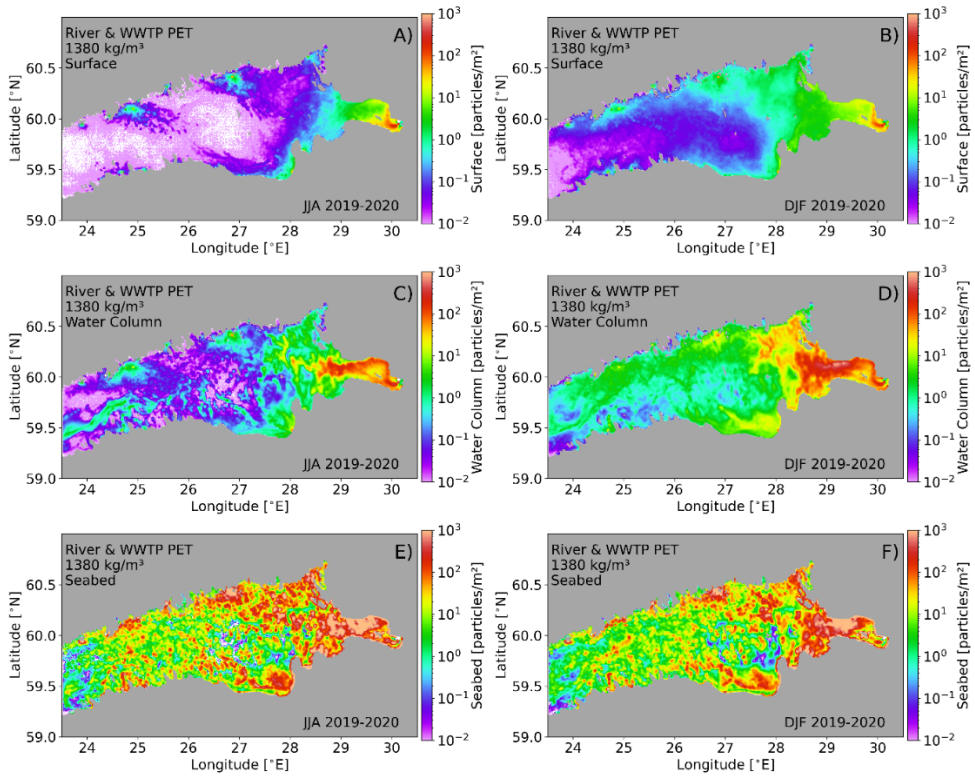
Figure 10 – Modelled mean spatial concentration of PET MP particles (20–500 mm) sourced from both rivers and WWTPs in different layers of the GoF during the summer months JJA (June, July, and August, panels (A, C, E) and winter months DJF (December, January, and February, panels (B, D, F). Panels (A, B) illustrate the concentration in the surface layer; panels (C, D) focus on concentration in the water column; panels (E, F) showcase the concentration in the bottom layer. From Paper II.
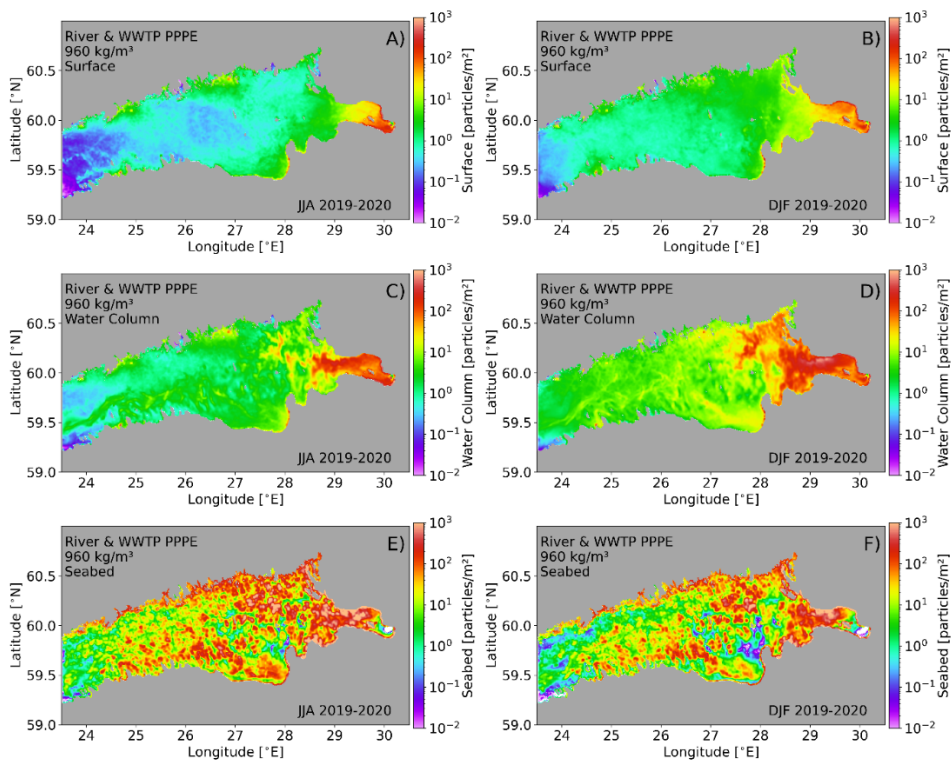
Figure 11 – Modelled mean spatial concentration of PP/PE MP particles (20–500 mm) sourced from both rivers and WWTPs in different layers of the GoF during the summer months JJA (June, July, and August) and winter months DJF (December, January, and February). Panels (A, B) illustrate the concentration in the surface layer; panels (C, D) focus on concentration in the water column; panels (E, F) showcase the concentration in the bottom layer. From Paper II.

3.2.2 Short-term variability

Short-term variability in MP concentrations along the coastal areas may be influenced by changes in hydrodynamic conditions. At coastal station N8, this variability was closely linked to local environmental factors. Prior to the highest observed MP concentration, the 3-day mean discharge from the Narva River (589 m³/s) was higher than the long-term average (440 m³/s), and westerly winds with speeds exceeding 8 m/s triggered coastal downwelling (Figure 12A). This downwelling event led to the convergence of surface waters, accumulating plastics along the coast and resulting in a peak in MP concentrations. In contrast, during the lowest concentration period, the easterly wind conditions indicated coastal upwelling and consequently, a 60-fold difference was observed between the highest and lowest case (Figure 12B). This low concentration during the upwelling would have originated from the sub-surface origin of water as the upwelled water usually originates from the cold intermediate layer in the GoF (Lips et al., 2009). The downwelling on the other hand, causes convergence of the sea surface water and the upper mixed layer in the summer could deepen over 40 m (Liblik and Lips, 2017).

Similar short-term fluctuations in MP concentration were also evident at Pir station in Tallinn Bay. There was a clear westward upwelling jet during the low concentration case (Figure 12C) and an eastward downwelling jet along the coast with relatively large current velocities during the high concentration case (Figure 12D). Such variations in coastal

circulation highlight how wind-driven upwelling and downwelling events can influence the accumulation or dispersal of MP through convergence and divergence of surface waters.

On the sea surface, wind speed is often considered an important physical parameter affecting MP concentration, as an increase in the wind speed also leads to increased vertical mixing of MP (Kukulka et al. 2012; Schönlau et al. 2020). However, our data shows weak and insignificant correlations between windspeed and observed MP concentrations for the entire dataset and with only a few stations showing significant correlations. At station 14, a significant negative correlation was found for MP fragments (r^2 = 0.35, p = 0.01, n = 15), while a significant positive correlation was only found at coastal station K5 (r^2 = 0.47, p = 0.01, n = 11). At station K5, the shallow depth (5m) allows strong winds to resuspend particles from the seabed, leading to higher surface concentrations. In contrast, weaker winds result in less resuspension and lower surface concentrations. As Xia et al., (2021) suggested, disturbance-induced vertical transport can resuspend small plastic particles to the sea surface layer, further emphasizing the role of wind in MP distribution.
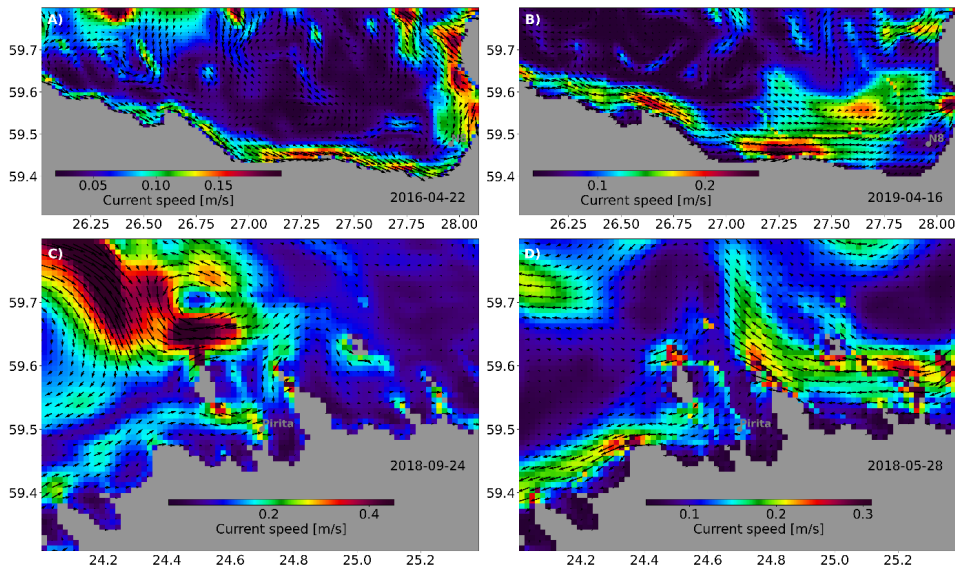

Figure 12 – Mean surface current vectors and current speed averaged 3 days before observations of (A) highest concentrations at station N8, (B) lowest concentrations at station N8, (C) highest concentrations at station Pir, and (D) lowest concentrations at station Pir. From Paper I.

To better understand the hydrodynamic condition at the offshore station 14, the simulated sea surface temperature and salinity fields in the vicinity of the stations along with the convergence and divergence based on the modelled current components during the highest and lowest MP values were checked (Figure 13). During the high concentration case at the station, strong lateral gradients and temperature fields in the vicinity of the stations were seen (Figures 13A, B). The lateral gradients were much weaker, and the variance of the fields were much smaller during the low concentration case (Figures 13D, E). Moreover, during the high concentration case, divergence was mostly negative, suggesting convergence, meaning accumulation of particles in the surface layer. The divergence was mostly positive during the lowest case.
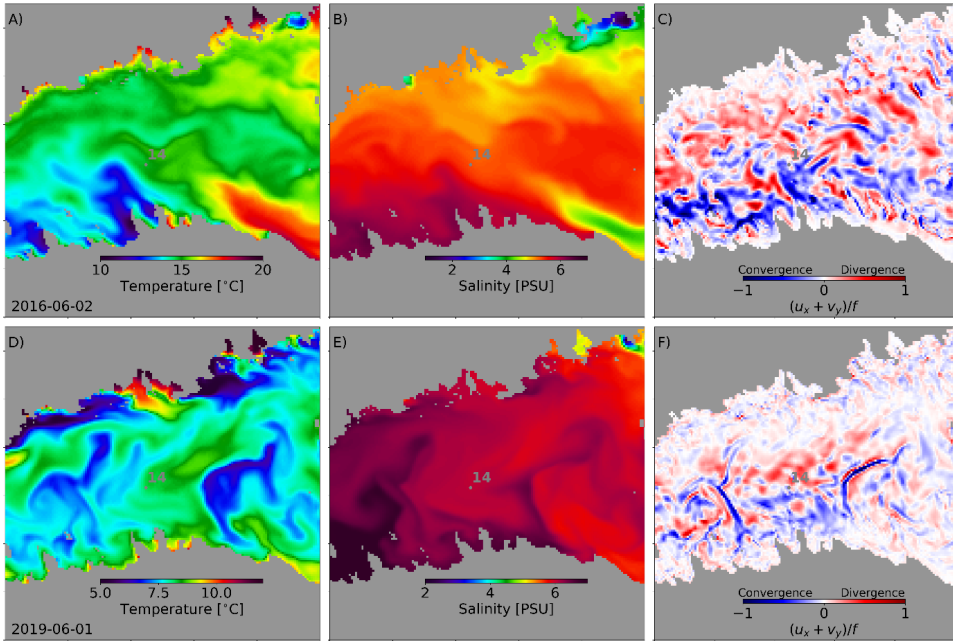
Figure 13 – Snapshots of surface temperature (A, D), surface salinity (B, E), and current field divergence, u_x+v_y/f, in the surface layer (C, F) during the highest (A, B, C) and lowest (D, E, F) measured concentration of MPs at station 14. Amended from Paper II.

Having discussed the role of wind-driven processes like upwelling and downwelling in short-term variability in MP concentrations, the modelling results were analysed to further investigate these dynamics. Specifically, an upwelling event was studied, which most effectively demonstrated the advection of particles towards the southern coast. For instance, on 18 July, initial signs of upwelling were visible, with surface concentrations displaying strong spatial variability, particularly in the easternmost areas, and patches also evident along the northern coast and central part of the Gulf (Figures 14A, D). As the upwelling intensified by 22 July, particles began to advect offshore, forming prominent patches in the central Gulf (Figure 14E). At the peak of the upwelling event on 24 July, a large patch of particles was transported southwards, aligning with colder, upwelling-affected zones (Figure 14F). During this peak upwelling phase, we also observed high Rossby numbers (Ro = ζ/f, the ratio of relative vorticity to the Coriolis parameter; Figures 14H, I), signifying enhanced cyclonic circulation linked to the event.

Prior studies have reported that coastal upwelling might lead to relatively low concentrations of MPs in coastal waters (e.g. de Lucia et al., 2014; Desforges et al., 2014). However, in another study, La Daana et al. (2017) found no significant difference in MP concentration between Benguela upwelling sites and other non-upwelling sites. Also, during upwelling events, surface layer particle concentrations were observed to converge in sub-mesoscale stripes or small eddy-like features within the upwelling frontal zones, characterized by high Rossby numbers and significant temperature gradient (Figure 14). Previous studies by Väli et al., (2017, 2018) highlighted similar particle convergence during an upwelling event in regions of elevated Rossby numbers and sub-mesoscale activity in the GoF.
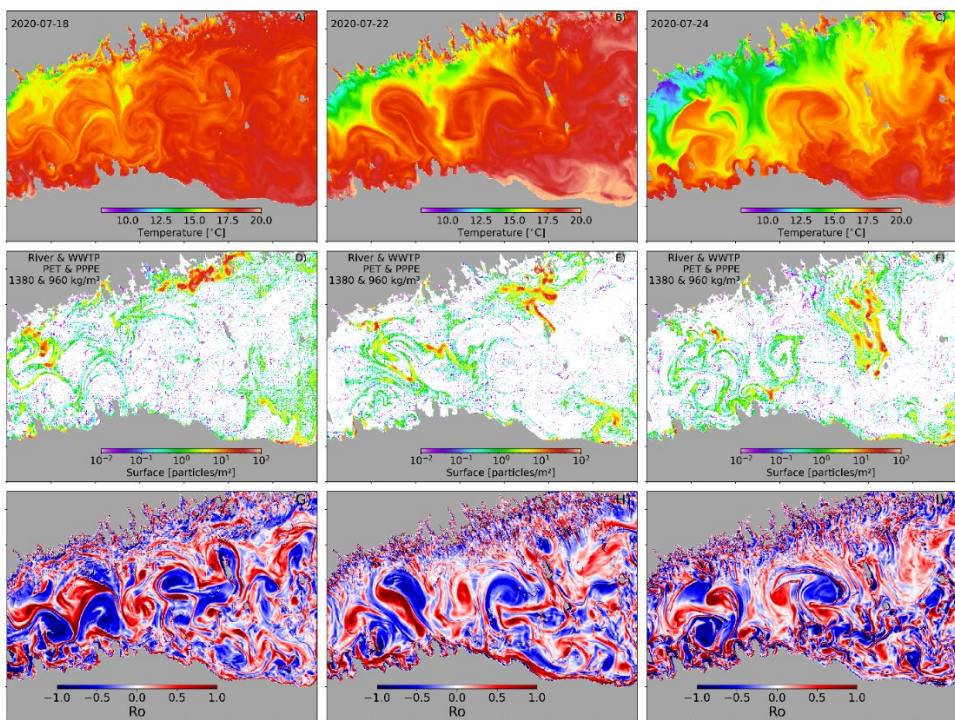
Figure 14 – Sea Surface Temperature (SST) maps (A–C), surface layers (D–F), and Rossby number (G–I), during Upwelling conditions along the Finnish coast in the GoF. Amended from Paper II.

The influence of near-bottom currents on particle concentrations in the 5-meter layer above the seabed is shown in Figure 15. On December 6, stronger near-bottom currents (Figure 15B) led to increased particle resuspension, resulting in higher concentrations in the near-bottom layer (Figure 15D) and this demonstrates that stronger currents enhance resuspension. Episodic events, such as high waves or wind-driven bottom currents that disturb sediments and resuspend particles back into the water column (Osinski et al., 2020; Zhou et al., 2021). In regions with high sedimentation rates, even short-term increases in current velocity can release accumulated MPs from the seabed into the overlying water (Kane and Clare, 2019). Similarly, our findings show a significant decrease in sedimented MP concentrations and a corresponding increase in water column particles following periods of intensified bottom currents.
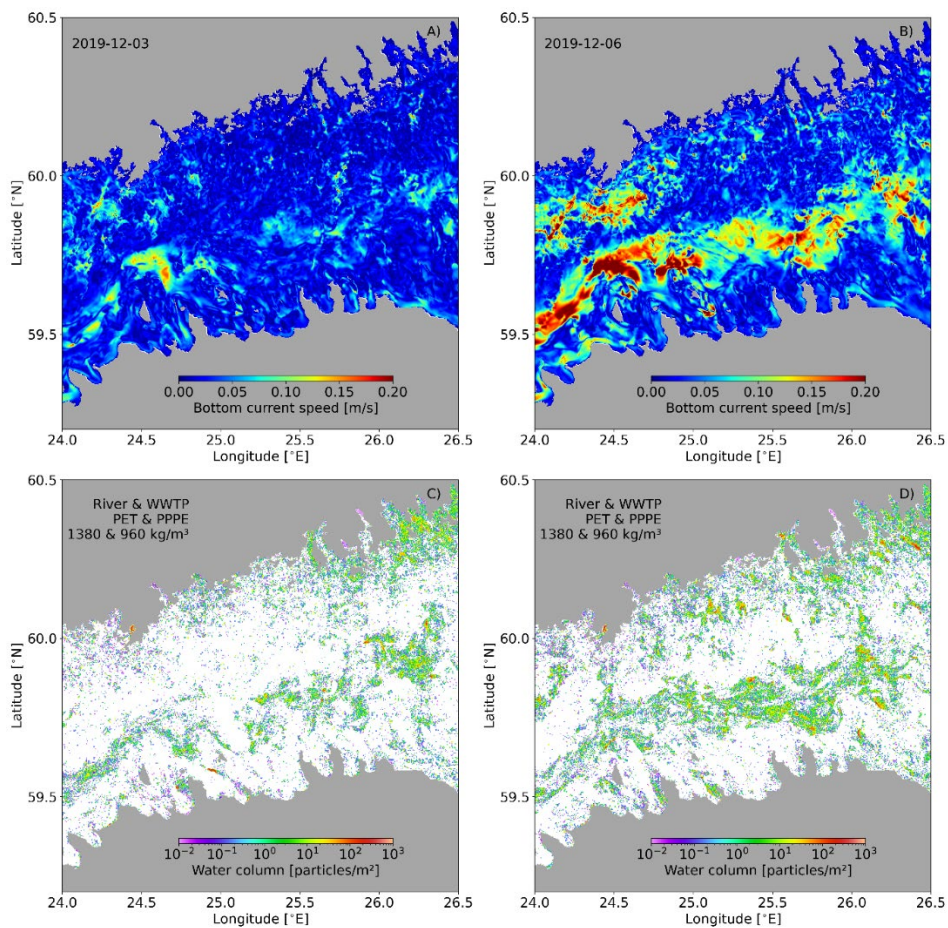
Figure 15 – Snapshots of bottom currents (A–B), and water column particles integrated within 5 meters above the seabed (C–D) in the GoF. From Paper II.

4 Conclusions

In this thesis, the first comprehensive insights into MP pollution and its spatiotemporal variability of the eastern part of the Baltic Sea is presented. MPs were detected in all 122 samples of measurements, with concentrations ranging from 0.01 to 2.45 counts/m^3 (overall mean: 0.49 counts/m^3). Regional differences in MP concentrations in the Gulf of Finland, Gulf of Riga, and Väinameri Sea likely reflect variations in human pressure from surrounding populations. Smaller concentrations were found in the Väinameri, the area of low human pressure while remarkably higher concentrations revealed in the Gulf of Finland, which is the sea area of considerable human impact from the catchment area and point sources.

The seasonal variations of MP concentrations were detected from observations. Higher concentrations were observed in autumn and winter, and lower in summer. The modelling results of PET particles suggest that during summer the accumulation of particles on the seabed was enhanced by weaker currents and biofilm formation while in autumn and winter, resuspension and lower biofilm formation resulted in higher concentration in the water column. According to the modelling in the Gulf of Finland, the seasonality for PP/PE concentrations is not that pronounced as for PET. However, these findings underscored the importance of seasonal variability of biofilm growth and hydrodynamic activity in shaping the MP distribution patterns in the eastern Baltic Sea.

The modelling provided insights into the MP distribution by using a combination of hydrodynamic, biogeochemical, and Lagrangian particle tracking models to map the MP pathways and identify potential accumulation zones in the Gulf of Finland. By using a three-year simulation in combination with sub-mesoscale permitting horizontal resolution, we estimated MP concentrations at the sea surface, within the water column, accumulation on the seabed, and accumulation to beaches. Approximately 75% of MPs accumulated on the seabed, 10% beached, 14% of particles remained suspended in the water column, and only 1% exit the gulf. The semi-enclosed nature of the Gulf of Finland, concentration of the main MP sources to the internal (eastern) part of the gulf, and hydrodynamic and morphologic conditions make the gulf a significant retention zone of MPs.

Highest MP concentrations were near the major riverine and coastal sources, specifically in the eastern Gulf of Finland, with surface concentrations of light particles exceeding those of heavy particles near WWTPs and river mouths. Meridionally integrated concentrations revealed a vertical distribution pattern of MP, with concentrations peaking near the surface and seabed and reaching lower levels in the intermediate layer, particularly in the deeper regions of the Gulf of Finland.

The short-term variability in MP concentrations along coastal areas was influenced by hydrodynamic conditions. Mesoscale processes, namely wind-driven downwelling and upwelling events caused accumulation and dispersal of particles in the surface layer through surface water convergence and divergence, respectively. Stronger near-bottom currents were shown to resuspend particles, increasing MP concentrations in the near-bottom layer. Sub-mesoscale processes, particularly the convergence in the upwelling frontal zones, were found to concentrate particles. These results illustrate the role of natural processes behind the high spatiotemporal variability of MP concentrations in the eastern Baltic Sea.

Mitigation measures should focus on addressing hotspot areas such as Neva Bay and Narva Bay, which are crucial for policymaking to regulate the MP emissions. To improve the effectiveness of mitigation, future studies should adopt multipoint sampling at various depths near emission sources and continue further development of numerical simulations. Future research should incorporate the effects of wind waves, improve the parameterizations of particle interactions with the seabed and beaching processes. These improvements will reduce uncertainties of simulations and improve applicability of MP spreading simulations.

References

Adamopoulou, A., Zeri, C., Garaventa, F., Gambardella, C., Ioakeimidis, C., and Pitta, E. (2021). Distribution patterns of floating microplastics in open and coastal waters of the eastern Mediterranean Sea (Ionian, Aegean, and Levantine seas). *Front. Mar. Sci.* 8, 699000. doi: 10.3389/fmars.2021.699000.

Aigars, J., Barone, M., Suhareva, N., Putna-Nimane, I., and Dimante-Deimantovica, I. (2021). Occurrence and spatial distribution of microplastics in the surface waters of the Baltic Sea and the Gulf of Riga. *Mar. Pollut. Bull.* 172, 112860. doi: 10.1016/j.marpolbul.2021.112860.

Alenius, P., Myrberg, K., and Nekrasov, A. (1998). The physical oceanography of the Gulf of Finland: a review. *Boreal Environ. Res* 3, 97–125.

Alenius, P., Nekrasov, A., and Myrberg, K. (2003). Variability of the baroclinic Rossby radius in the Gulf of Finland. *Cont. Shelf Res.* 23, 563–573. doi: 10.1016/S0278-4343(03)00004-9.

Almroth-Rosell, E., Eilola, K., Hordoir, R., Meier, H. E. M., and Hall, P. O. J. (2011). Transport of fresh and resuspended particulate organic material in the Baltic Sea—a model study. *J. Mar. Syst.* 87, 1–12. doi: 10.1016/j.jmarsys.2011.02.005.

Arthur, C., Baker, J. E., and Bamford, H. A. (2009). Proceedings of the International Research Workshop on the Occurrence, Effects, and Fate of Microplastic Marine Debris, September 9-11, 2008, University of Washington Tacoma, Tacoma, WA, USA.

Baresel, C., and Olshammar, M. (2019). On the importance of sanitary sewer overflow on the total discharge of microplastics from sewage water. *J. Environ. Prot. (Irvine,. Calif).* 10, 1105–1118. doi: 10.4236/jep.2019.109065.

Barnes, D. K. A., Galgani, F., Thompson, R. C., and Barlaz, M. (2009). Accumulation and fragmentation of plastic debris in global environments. *Philos. Trans. R. Soc. B Biol. Sci.* 364, 1985–1998. doi: 10.1098/rstb.2008.0205.

Burchard, H. (2001). Applied turbulence modelling in marine waters.

Burchard, H., and Bolding, K. (2002). GETM: A General Estuarine Transport Model, Scientific Documentation, European Commission, Joint Research Centre. *Inst. Environ. Sustain.* 12262, 25.

Canuto, V. M., Howard, A., Cheng, Y., and Dubovikov, M. S. (2001). Ocean turbulence. Part I: One-point closure model—Momentum and heat vertical diffusivities. *J. Phys. Oceanogr.* 31, 1413–1426. doi: 10.1175/1520-0485(2001)031<1413:OTPIOP>2.0.CO;2.

Carr, S. A., Liu, J., and Tesoro, A. G. (2016). Transport and fate of microplastic particles in wastewater treatment plants. *Water Res.* 91, 174–182. doi: 10.1016/j.watres.2016.01.002.

Chubarenko, I., Esiukova, E., Zobkov, M., and Isachenko, I. (2022). Microplastics distribution in bottom sediments of the Baltic Sea Proper. *Mar. Pollut. Bull.* 179, 113743. doi: 10.1016/j.marpolbul.2022.113743.

Cole, M., Lindeque, P., Halsband, C., and Galloway, T. S. (2011). Microplastics as contaminants in the marine environment: a review. *Mar. Pollut. Bull.* 62, 2588–2597. doi: 10.1016/j.marpolbul.2011.09.025.

Cuttat, F. M. R. (2018). Marine transport of plastic fragments from dolly ropes used in demersal fisheries in the North Sea.

de Lucia, G. A., Caliani, I., Marra, S., Camedda, A., Coppa, S., Alcaro, L., et al. (2014). Amount and distribution of neustonic micro-plastic off the western Sardinian coast (Central-Western Mediterranean Sea). *Mar. Environ. Res.* 100, 10–16. doi: 10.1016/j.marenvres.2014.03.017.

De Witte, B., Devriese, L., Bekaert, K., Hoffman, S., Vandermeersch, G., Cooreman, K., et al. (2014). Quality assessment of the blue mussel (Mytilus edulis): Comparison between commercial and wild types. *Mar. Pollut. Bull.* 85, 146–155.

Desforges, J.-P. W., Galbraith, M., Dangerfield, N., and Ross, P. S. (2014). Widespread distribution of microplastics in subsurface seawater in the NE Pacific Ocean. *Mar. Pollut. Bull.* 79, 94–99. doi: 10.1016/j.marpolbul.2013.12.035.

Dimante-Deimantovica, I., Bebrite, A., Skudra, M., Retike, I., Viška, M., Bikše, J., et al. (2023). The baseline for micro-and mesoplastic pollution in open Baltic Sea and Gulf of Riga beach. *Front. Mar. Sci.* 10, 1251068.

Dris, R., Gasperi, J., and Tassin, B. (2018). Sources and fate of microplastics in urban areas: a focus on Paris megacity. *Freshw. microplastics Emerg. Environ. Contam.*, 69–83. doi: 10.1007/978-3-319-61615-5_4.

Eriksen, M., Cowger, W., Erdle, L. M., Coffin, S., Villarrubia-Gómez, P., Moore, C. J., et al. (2023). A growing plastic smog, now estimated to be over 170 trillion plastic particles afloat in the world's oceans—Urgent solutions required. *PLoS One* 18, e0281596. doi: 10.1371/journal.pone.0281596.

Eriksen, M., Mason, S., Wilson, S., Box, C., Zellers, A., Edwards, W., et al. (2013). Microplastic pollution in the surface waters of the Laurentian Great Lakes. *Mar. Pollut. Bull.* 77, 177–182. doi: 10.1016/j.marpolbul.2013.10.007.

Frishfelds, V., Murawski, J., and She, J. (2022). Transport of microplastics from the daugava estuary to the Open Sea. *Front. Mar. Sci.* 9, 886775. doi: 10.3389/fmars.2022.886775.

Galgani, F., Giorgetti, A., Vinci, M., Le Moigne, M., Moncoiffe, G., Brosich, A., et al. (2019). Proposal for gathering and managing data sets on marine micro-litter on a European scale.[Updated version: 19/04/2019][SUPERSEDED by http://dx. doi. org/10.25607/OBP-495].

Gewert, B., Ogonowski, M., Barth, A., and MacLeod, M. (2017). Abundance and composition of near surface microplastics and plastic debris in the Stockholm Archipelago, Baltic Sea. *Mar. Pollut. Bull.* 120, 292–302. doi: 10.1016/j.marpolbul.2017.04.062.

Gies, E. A., LeNoble, J. L., Noël, M., Etemadifar, A., Bishay, F., Hall, E. R., et al. (2018). Retention of microplastics in a major secondary wastewater treatment plant in Vancouver, Canada. *Mar. Pollut. Bull.* 133, 553–561. doi: 10.1016/j.marpolbul.2018.06.006.

Gräwe, U., Naumann, M., Mohrholz, V., and Burchard, H. (2015). Anatomizing one of the largest saltwater inflows into the B altic S ea in D ecember 2014. *J. Geophys. Res. Ocean.* 120, 7676–7697. doi: 10.1002/2015JC011269.

Gröger, M., Placke, M., Meier, H. E., Börgel, F., Brunnabend, S.-E., Dutheil, C., et al. (2022). The Baltic Sea Model Intercomparison Project (BMIP)–a platform for model development, evaluation, and uncertainty assessment. *Geosci. Model Dev.* 15, 8613–8638. doi: 10.5194/gmd-15-8613-2022.

Harvey, F., and Watts, J. (2018). Microplastics found in human stools for the first time. *Guard.* 22.

He, P., Chen, L., Shao, L., Zhang, H., and Lü, F. (2019). Municipal solid waste (MSW) landfill: A source of microplastics?-Evidence of microplastics in landfill leachate. *Water Res.* 159, 38–45. doi: 10.1016/j.watres.2019.04.060.

HELCOM (2023) (2023). State of the Baltic Sea. Third HELCOM holistic assessment 2016-2021. in *Baltic Sea Environment Proceedings* Available at: https://helcom.fi/post_type_publ/holas3_sobs.

Hersbach, H., Bell, B., Berrisford, P., Hirahara, S., Horányi, A., Muñoz-Sabater, J., et al. (2020). The ERA5 global reanalysis. *Q. J. R. Meteorol. Soc.* 146, 1999–2049. doi: 10.1002/qj.3803.

Hofmeister, R., Burchard, H., and Beckers, J.-M. (2010). Non-uniform adaptive vertical grids for 3D numerical ocean models. *Ocean Model.* 33, 70–86. doi: 10.1016/j.ocemod.2009.12.003.

Jambeck, J. R., Geyer, R., Wilcox, C., Siegler, T. R., Perryman, M., Andrady, A., et al. (2015). Plastic waste inputs from land into the ocean. *Science (80-.).* 347, 768–771. doi: 10.1126/science.1260352.

Jönsson, A., Danielsson, Å., and Rahm, L. (2005). Bottom type distribution based on wave friction velocity in the Baltic Sea. *Cont. Shelf Res.* 25, 419–435. doi: 10.1016/j.csr.2004.09.011.

Kane, I. A., and Clare, M. A. (2019). Dispersion, accumulation, and the ultimate fate of microplastics in deep-marine environments: a review and future directions. *Front. earth Sci.* 7, 80. doi: 10.3389/feart.2019.00080.

Kay, P., Hiscoe, R., Moberley, I., Bajic, L., and McKenna, N. (2018). Wastewater treatment plants as a source of microplastics in river catchments. *Environ. Sci. Pollut. Res.* 25, 20264–20267. doi: 10.1007/s11356-018-2070-7.

Klingbeil, K., Lemarié, F., Debreu, L., and Burchard, H. (2018). The numerics of hydrostatic structured-grid coastal ocean models: State of the art and future perspectives. *Ocean Model.* 125, 80–105. doi: 10.1016/j.ocemod.2018.01.007.

Kooi, M., and Koelmans, A. A. (2019). Simplifying microplastic via continuous probability distributions for size, shape, and density. *Environ. Sci. Technol. Lett.* 6, 551–557. doi: 10.1021/acs.estlett.9b00379.

Krauss, W., and Brügge, B. (1991). Wind-produced water exchange between the deep basins of the Baltic Sea. *J. Phys. Oceanogr.* 21, 373–384. doi: 10.1175/1520-0485(1991)021<0373:WPWEBT>2.0.CO;2.

Kuddithamby, G., ALMEDA, R., Vianello, A., Lorenz, C., Iordachescu, L., Papacharalampos, K., et al. (n.d.). Does Water Column Stratification Influence the Vertical Distribution of Microplastics? *Available SSRN 4540469*. doi: 10.1016/j.envpol.2023.122865.

Kuprijanov, I., Väli, G., Sharov, A., Berezina, N., Liblik, T., Lips, U., et al. (2021). Hazardous substances in the sediments and their pathways from potential sources in the eastern Gulf of Finland. *Mar. Pollut. Bull.* 170, 112642. doi: 10.1016/j.marpolbul.2021.112642.

La Daana, K. K., Officer, R., Lyashevska, O., Thompson, R. C., and O'Connor, I. (2017). Microplastic abundance, distribution and composition along a latitudinal gradient in the Atlantic Ocean. *Mar. Pollut. Bull.* 115, 307–314. doi: 10.1016/j.marpolbul.2016.12.025.

Leppäranta, M., and Myrberg, K. (2009). *Physical oceanography of the Baltic Sea*. Springer Science & Business Media.

Li, C., Wang, X., Liu, K., Zhu, L., Wei, N., Zong, C., et al. (2021). Pelagic microplastics in surface water of the Eastern Indian Ocean during monsoon transition period: Abundance, distribution, and characteristics. *Sci. Total Environ.* 755, 142629. doi: 10.1016/j.scitotenv.2020.142629.

Liblik, T., Laanemets, J., Raudsepp, U., Elken, J., and Suhhova, I. (2013). Estuarine circulation reversals and related rapid changes in winter near-bottom oxygen conditions in the Gulf of Finland, Baltic Sea. *Ocean Sci.* 9, 917–930. doi: 10.5194/os-9-917-2013.

Liblik, T., and Lips, U. (2011). Characteristics and variability of the vertical thermohaline structure in the Gulf of Finland in summer.

Liblik, T., and Lips, U. (2017). Variability of pycnoclines in a three-layer, large estuary: the Gulf of Finland. *Boreal Environ. Res.* 22, 27.

Liblik, T., Väli, G., Lips, I., Lilover, M.-J., Kikas, V., and Laanemets, J. (2020). The winter stratification phenomenon and its consequences in the Gulf of Finland, Baltic Sea. *Ocean Sci.* 16, 1475–1490. doi: 10.5194/os-16-1475-2020, 2020.

Liblik, T., Väli, G., Salm, K., Laanemets, J., Lilover, M.-J., and Lips, U. (2022). Quasi-steady circulation regimes in the Baltic Sea. *Ocean Sci. Discuss.* 2022, 1–37. doi: 10.5194/os-18-857-2022, 2022.

Lips, I., Lips, U., and Liblik, T. (2009). Consequences of coastal upwelling events on physical and chemical patterns in the central Gulf of Finland (Baltic Sea). *Cont. Shelf Res.* 29, 1836–1847. doi: 10.1016/j.csr.2009.06.010.

Lips, I., Rünk, N., Kikas, V., Meerits, A., and Lips, U. (2014). High-resolution dynamics of the spring bloom in the Gulf of Finland of the Baltic Sea. *J. Mar. Syst.* 129, 135–149. doi: 10.1016/j.jmarsys.2013.06.002.

Lips, U., Kikas, V., Liblik, T., and Lips, I. (2016a). Multi-sensor in situ observations to resolve the sub-mesoscale features in the stratified Gulf of Finland, Baltic Sea. *Ocean Sci.* 12, 715–732. doi: 10.5194/os-12-715-2016.

Lips, U., Zhurbas, V., Skudra, M., and Väli, G. (2016b). A numerical study of circulation in the Gulf of Riga, Baltic Sea. Part I: Whole-basin gyres and mean currents. *Cont. Shelf Res.* 112, 1–13. doi: 10.1016/j.csr.2015.11.008.

Llorca, M., Álvarez-Muñoz, D., Ábalos, M., Rodríguez-Mozaz, S., Santos, L. H., León, V. M., et al. (2020). Microplastics in Mediterranean coastal area: Toxicity and impact for the environment and human health. *Trends Environ. Anal. Chem.* 27, e00090. doi: 10.1016/j.teac.2020.e00090.

Lobelle, D., Kooi, M., Koelmans, A. A., Laufkötter, C., Jongedijk, C. E., Kehl, C., et al. (2021). Global modeled sinking characteristics of biofouled microplastic. *J. Geophys. Res. Ocean.* 126, e2020JC017098. doi: 10.1029/2020JC017098.

Lusher, A. L., Tirelli, V., O'Connor, I., and Officer, R. (2015). Microplastics in Arctic polar waters: the first reported values of particles in surface and sub-surface samples. *Sci. Rep.* 5, 14947.

Magnusson, K. (2016). *Microlitter in sewage treatment systems: A Nordic perspective on waste water treatment plants as pathways for microscopic anthropogenic particles to marine systems*. Nordic Council of Ministers doi: 10.6027/TN2016-510.

Martyanov, S. D., Isaev, A. V, and Ryabchenko, V. A. (2021). Model estimates of microplastic potential contamination pattern of the eastern Gulf of Finland in 2018. *Oceanologia*. doi: 10.1016/j.oceano.2021.11.006.

Martyanov, S. D., Isaev, A. V, and Ryabchenko, V. A. (2023). Model estimates of microplastic potential contamination pattern of the eastern Gulf of Finland in 2018. *Oceanologia* 65, 86–99.

Matjašič, T., Mori, N., Hostnik, I., Bajt, O., and Viršek, M. K. (2023). Microplastic pollution in small rivers along rural–urban gradients: Variations across catchments and between water column and sediments. *Sci. Total Environ.* 858, 160043. doi: 10.1016/j.scitotenv.2022.160043.

Mazurkiewicz, M., Martinez, P. S., Konwent, W., Deja, K., Kotwicki, L., and Węsławski, J. M. (2022). Plastic contamination of sandy beaches along the southern Baltic–a one season field survey results. *Oceanologia* 64, 769–780.

Meier, H. E. M., and Kauker, F. (2003). Modeling decadal variability of the Baltic Sea: 2. Role of freshwater inflow and large-scale atmospheric circulation for salinity. *J. Geophys. Res. Ocean.* 108. doi: 10.1029/2003JC001799.

Mintenig, S. M., Int-Veen, I., Löder, M. G. J., Primpke, S., and Gerdts, G. (2017). Identification of microplastic in effluents of waste water treatment plants using focal plane array-based micro-Fourier-transform infrared imaging. *Water Res.* 108, 365–372. doi: 10.1016/j.watres.2016.11.015.

Mishra, A., Buhhalko, N., Lind, K., Lips, I., Liblik, T., Väli, G., et al. (2022). Spatiotemporal variability of microplastics in the Eastern Baltic Sea. *Front. Mar. Sci.* 9, 875984. doi: 10.3389/fmars.2022.875984.

Murawski, J., She, J., and Frishfelds, V. (2022). Modelling drift and fate of microplastics in the Baltic Sea. *Front. Mar. Sci.*, 1656. doi: 10.3389/fmars.2022.886295.

Neumann, T., Fennel, W., and Kremp, C. (2002). Experimental simulations with an ecosystem model of the Baltic Sea: a nutrient load reduction experiment. *Global Biogeochem. Cycles* 16, 1–7. doi: 10.1029/2001GB001450.

Neumann, T., Radtke, H., Cahill, B., Schmidt, M., and Rehder, G. (2022). Non-Redfieldian carbon model for the Baltic Sea (ERGOM version 1.2)–implementation and budget estimates. *Geosci. Model Dev.* 15, 8473–8540. doi: 10.5194/gmd-15-8473-2022, 2022.

Neumann, T., and Schernewski, G. (2008). Eutrophication in the Baltic Sea and shifts in nitrogen fixation analyzed with a 3D ecosystem model. *J. Mar. Syst.* 74, 592–602. doi: 10.1016/j.jmarsys.2008.05.003.

Osinski, R. D., Enders, K., Gräwe, U., Klingbeil, K., and Radtke, H. (2020). Model uncertainties of a storm and their influence on microplastics and sediment transport in the Baltic Sea. *Ocean Sci.* 16, 1491–1507. doi: 10.5194/os-16-1491-2020, 2020.

Pärn, O., Moy, D. M., and Stips, A. (2023). Determining the distribution and accumulation patterns of floating litter in the Baltic Sea using modelling tools. *Mar. Pollut. Bull.* 190, 114864. doi: 10.1016/j.marpolbul.2023.114864.

Piehl, S., Hauk, R., Robbe, E., Richter, B., Kachholz, F., Schilling, J., et al. (2021). Combined approaches to predict microplastic emissions within an urbanized estuary (Warnow, Southwestern Baltic Sea). *Front. Environ. Sci.* 9, 616765.

Prata, J. C. (2018). Microplastics in wastewater: State of the knowledge on sources, fate and solutions. *Mar. Pollut. Bull.* 129, 262–265. doi: 10.1016/j.marpolbul.2018.02.046.

Rasmus, K., Kiirikki, M., and Lindfors, A. (2015). Long-term field measurements of turbidity and current speed in the Gulf of Finland leading to an estimate of natural resuspension of bottom sediment. *Boreal Environ. Res.* 20, 735.

Redfield, A. C. (1934). *On the proportions of organic derivatives in sea water and their relation to the composition of plankton*. university press of liverpool Liverpool.

Salm, K., Väli, G., Liblik, T., and Lips, U. (2025). Forcing-dependent submesoscale variability and subduction in a coastal sea area (Gulf of Finland, Baltic Sea). *EGUsphere* 2025, 1–30.

Schernewski, G., Radtke, H., Hauk, R., Baresel, C., Olshammar, M., and Oberbeckmann, S. (2021). Urban microplastics emissions: effectiveness of retention measures and consequences for the Baltic Sea. *Front. Mar. Sci.* 8, 594415. doi: 10.3389/fmars.2021.594415.

Schernewski, G., Radtke, H., Hauk, R., Baresel, C., Olshammar, M., Osinski, R., et al. (2020). Transport and behavior of microplastics emissions from urban sources in the Baltic Sea. *Front. Environ. Sci.* 8, 579361. doi: 10.3389/fenvs.2020.579361.

Schönlau, C., Karlsson, T. M., Rotander, A., Nilsson, H., Engwall, M., van Bavel, B., et al. (2020). Microplastics in sea-surface waters surrounding Sweden sampled by manta trawl and in-situ pump. *Mar. Pollut. Bull.* 153, 111019. doi: 10.1016/j.marpolbul.2020.111019.

Schrank, I., Löder, M. G. J., Imhof, H. K., Moses, S. R., Heß, M., Schwaiger, J., et al. (2022). Riverine microplastic contamination in southwest Germany: A large-scale survey. *Front. Earth Sci.* 10. doi: 10.3389/feart.2022.794250.

Setälä, O., Magnusson, K., Lehtiniemi, M., and Norén, F. (2016). Distribution and abundance of surface water microlitter in the Baltic Sea: a comparison of two sampling methods. *Mar. Pollut. Bull.* 110, 177–183. doi: 10.1016/j.marpolbul.2016.06.065.

She, J., Buhhalko, N., Lind, K., Mishra, A., Kikas, V., Costa, E., et al. (2022). Uncertainty and consistency assessment in multiple microplastic observation datasets in the Baltic Sea. *Front. Mar. Sci.* 9, 886357. doi: 10.3389/fmars.2022.886357.

Siegfried, M., Koelmans, A. A., Besseling, E., and Kroeze, C. (2017). Export of microplastics from land to sea. A modelling approach. *Water Res.* 127, 249–257. doi: 10.1016/j.watres.2017.10.011.

Smagorinsky, J. (1963). General circulation experiments with the primitive equations: I. The basic experiment. *Mon. Weather Rev.* 91, 99–164. doi: 10.1175/1520-0493(1963)091<0099:GCEWTP>2.3.CO;2.

Suaria, G., and Aliani, S. (2014). Floating debris in the Mediterranean Sea. *Mar. Pollut. Bull.* 86, 494–504. doi: 10.1016/j.marpolbul.2014.06.025.

Suhhova, I., Liblik, T., Lilover, M.-J., and Lips, U. (2018). A descriptive analysis of the linkage between the vertical stratification and current oscillations in the Gulf of Finland. *Boreal Environ. Res* 23, 83–103.

Sun, J., Dai, X., Wang, Q., Van Loosdrecht, M. C. M., and Ni, B.-J. (2019). Microplastics in wastewater treatment plants: Detection, occurrence and removal. *Water Res.* 152, 21–37. doi: 10.1016/j.watres.2018.12.050.

Suursaar, Ü., Kullas, T., and Otsmann, M. (2002). Flow modelling in the Pärnu Bay and the Kihnu Strait. in *Proceedings of the Estonian Academy of Sciences. Engineering*, 189œ203.

Suursaar, Ü., Kullas, T., Otsmann, M., and Kõuts, T. (2003). Extreme sea level events in the coastal waters of western Estonia. *J. Sea Res.* 49, 295–303.

Talvitie, J., Mikola, A., Koistinen, A., and Setälä, O. (2017). Solutions to microplastic pollution–Removal of microplastics from wastewater effluent with advanced wastewater treatment technologies. *Water Res.* 123, 401–407. doi: 10.1016/j.watres.2017.07.005.

Tamminga, M., Hengstmann, E., and Fischer, E. K. (2018). Microplastic analysis in the South Funen Archipelago, Baltic Sea, implementing manta trawling and bulk sampling. *Mar. Pollut. Bull.* 128, 601–608. doi: 10.1016/j.marpolbul.2018.01.066.

Tsiaras, K., Hatzonikolakis, Y., Kalaroni, S., Pollani, A., and Triantafyllou, G. (2021). Modeling the pathways and accumulation patterns of micro-and macro-plastics in the Mediterranean. *Front. Mar. Sci.* 8, 743117. doi: 10.3389/fmars.2021.743117.

Uurasjärvi, E., Pääkkönen, M., Setälä, O., Koistinen, A., and Lehtiniemi, M. (2021). Microplastics accumulate to thin layers in the stratified Baltic Sea. *Environ. Pollut.* 268, 115700. doi: 10.1016/j.envpol.2020.115700.

Väli, G., Meier, H. E. M., Liblik, T., Radtke, H., Klingbeil, K., Gräwe, U., et al. (2024). Submesoscale processes in the surface layer of the central Baltic Sea: A high-resolution modelling study. *Oceanologia* 66, 78–90.

Väli, G., Meier, M., Dieterich, C., and Placke, M. (2019). River runoff forcing for ocean modeling withinthe Baltic Sea Model Intercomparison Project. doi: 10.12754/msr-2019-0113.

Väli, G., Zhurbas, V., Lips, U., and Laanemets, J. (2017). Submesoscale structures related to upwelling events in the Gulf of Finland, Baltic Sea (numerical experiments). *J. Mar. Syst.* 171, 31–42. doi: 10.1016/j.jmarsys.2016.06.010.

Vali, G., Zhurbas, V. M., Laanemets, J., and Lips, U. (2018). Clustering of floating particles due to submesoscale dynamics: a simulation study for the Gulf of Finland, Baltic Sea. *Фундаментальная и прикладная гидрофизика* 11, 21–35. doi: 10.7868/s2073667318020028.

Van Sebille, E., Griffies, S. M., Abernathey, R., Adams, T. P., Berloff, P., Biastoch, A., et al. (2018). Lagrangian ocean analysis: Fundamentals and practices. *Ocean Model.* 121, 49–75.

Veerasingam, S., Saha, M., Suneel, V., Vethamony, P., Rodrigues, A. C., Bhattacharyya, S., et al. (2016). Characteristics, seasonal distribution and surface degradation features of microplastic pellets along the Goa coast, India. *Chemosphere* 159, 496–505. doi: 10.1016/j.chemosphere.2016.06.056.

Walther, B. A., Pasolini, F., Korez Lupše, Š., and Bergmann, M. (2024). Microplastic detectives: a citizen-science project reveals large variation in meso-and microplastic pollution along German coastlines. *Front. Environ. Sci.* 12, 1458565.

Xia, F., Yao, Q., Zhang, J., and Wang, D. (2021). Effects of seasonal variation and resuspension on microplastics in river sediments. *Environ. Pollut.* 286, 117403.

Yonkos, L. T., Friedel, E. A., Perez-Reyes, A. C., Ghosal, S., and Arthur, C. D. (2014). Microplastics in four estuarine rivers in the Chesapeake Bay, USA. *Environ. Sci. Technol.* 48, 14195–14202. doi: 10.1021/es5036317.

Zeri, C., Adamopoulou, A., Varezić, D. B., Fortibuoni, T., Viršek, M. K., Kržan, A., et al. (2018). Floating plastics in Adriatic waters (Mediterranean Sea): From the macro- to the micro-scale. *Mar. Pollut. Bull.* 136, 341–350. doi: 10.1016/j.marpolbul.2018.09.016.

Zhou, Q., Tu, C., Yang, J., Fu, C., Li, Y., and Waniek, J. J. (2021). Trapping of microplastics in halocline and turbidity layers of the semi-enclosed Baltic Sea. *Front. Mar. Sci.* 8, 761566. doi: 10.3389/fmars.2021.761566.

Zhurbas, V., Väli, G., Golenko, M., and Paka, V. (2018). Variability of bottom friction velocity along the inflow water pathway in the Baltic Sea. *J. Mar. Syst.* 184, 50–58. doi: 10.1016/j.jmarsys.2018.04.008.

Ziajahromi, S., Neale, P. A., and Leusch, F. D. L. (2016). Wastewater treatment plant effluent as a source of microplastics: review of the fate, chemical interactions and potential risks to aquatic organisms. *Water Sci. Technol.* 74, 2253–2269. doi: 10.2166/wst.2016.414.

Acknowledgements

I am deeply indebted to my supervisors, Ph.D. Germo Väli and Ph.D. Taavi Liblik, for their invaluable guidance, encouragement, and continuous support throughout my PhD journey. Their expertise, patience, and insightful feedback have been instrumental in shaping both my research and personal growth.

I am profoundly grateful to Prof. Urmas Lips, who involved me in his projects, which were essential for this thesis.

I am also thankful to my supervisors and Prof. Jüri Elken for reviewing my thesis and insightful feedback.

A special thanks go to the co-authors of the publications of the current thesis: Ph.D. Germo Väli, Ph.D. Taavi Liblik, Prof. Urmas Lips, Ph.D. Inga Lips, Ph.D. Natalja Buhhalko, Enriko Siht and Kati Lind. Your help and insights were essential.

My deepest gratitude goes to my family and my wife, Pallavi, whose unwavering belief in me has been a constant source of strength throughout this journey. I am especially indebted to my wife for her understanding and patience during the most demanding phase of my work. Their unconditional love and support have been the foundation of my achievements.

And finally, I want to thank my colleagues in the Department of Marine Systems at TalTech for their advice along the way.

Abstract

Pathways and Distribution of Microplastic in the Eastern Baltic Sea

Microplastic (MP) pollution is a burgeoning issue in aquatic environments, including the Baltic Sea, where its distribution and pathways remain critical concerns. This thesis integrates observational and modelling approaches to investigate the spatiotemporal variability, fate, transport and accumulation of MPs in the eastern Baltic Sea and the Gulf of Finland (GoF). Observations of the MP concentrations in the surface layer from a research vessel were conducted by a Mantra trawl at 16 stations during 2016–2020. In order to simulate the MP distributions in the Gulf of Finland during 2018–2020 an offline coupled Lagrangian particle model, and hydrodynamic and biogeochemical models were used, focusing on polypropylene/polyethylene (PP/PE) and polyethylene terephthalate (PET) particles. The coupled model system also permitted (sub)mesoscale processes and allowed to study the possible impact of these processes to the MP concentrations in the sea. Sensitivity analysis for the selected implemented processes was performed by analysing the effect to the spatiotemporal variability at the sea surface and by comparing the simulation results with observations. As a result, optimal setup of parameters describing horizontal diffusion, beaching, biofouling and resuspension were determined and applied in simulations with realistic MP loads in the Gulf of Finland.

The dissertation is a summary of three papers, of which the first analysed the spatio-temporal variability of MP concentration based on observations, and the other two focused on modelling the MP concentrations. Observations revealed MP concentrations in the region ranging from 0.01 to 2.45 counts/m^3 (overall mean: 0.49 counts/m^3), with MP-Fibers and MP-Fragments contributing equally to the overall concentration. Spatial distributions indicated higher MP concentrations in the Baltic Proper (BP) and GoF, while lower values were observed in the Gulf of Riga (GoR) and Väinameri Sea (VS). This spatial pattern corresponds to the magnitude of human pressure to the respective basins from the catchment areas. Seasonally, the concentrations in the surface layer and water column were higher in autumn and winter compared to summer. Weaker currents and biofilm formation supported the MP accumulation to seabed in summer while in autumn and winter, resuspension and lower biofilm formation resulted in higher concentration in the water column.

According to the simulations, the Gulf of Finland is significant retention zone of the MP. Approximately 75% of MPs that entered to the gulf from riverine and WWTP sources accumulated on the seabed, 10% beached, 14% of particles remained suspended in the water column, and only 1% exit the gulf. The highest MP concentrations could be likely found near the major riverine and coastal sources, specifically in the eastern Gulf of Finland. There is heterogeneous vertical distribution pattern of the MP, with concentrations peaking near the surface and seabed while lower levels are in the intermediate layer, particularly in the deeper regions of the Gulf of Finland.

The short-term variability in MP concentrations was influenced by hydrodynamic variability in synoptic timescales. Both, simulations and observations suggest that wind-driven downwelling and upwelling events cause accumulation and dispersal of particles in the surface layer through surface water convergence and divergence, respectively, in the coastal areas. Stronger near-bottom currents were shown to resuspend particles, increasing MP concentrations in the near-bottom layer. Sub-mesoscale

processes, particularly the convergence in the upwelling frontal zones, were found to concentrate particles.

This combined analysis provides critical insights into MP pathways, spatial variability, and accumulation dynamics in the eastern Baltic Sea. These findings underscore the need for future studies addressing sub-mesoscale processes and land-sea fluxes of MP while highlighting the importance of targeted mitigation efforts to reduce MP pollution.

Kokkuvõte

Mikroplasti levik ja jaotused Läänemere idaosas

Mikroplasti (MP) reostus on tõsine ja kasvav probleem veekeskkondades, sealhulgas Läänemeres, kus selle jaotumine ja levikuteed on jätkuvalt olulised uurimisküsimused. Käesolev doktoritöö ühendab vaatlus- ja modelleerimismeetodid, et uurida MP ruumilist ja ajalist varieeruvust, levikut ja akumulatsiooni Läänemere idaosas, sealhulgas Soome lahes. Vaatlused viidi läbi Eesti merealade seire raames uurimislaevalt Salme Manta traali abil 16 jaamas aastatel 2016–2020. MP jaotuse modelleerimiseks Soome lahes kasutati hüdrodünaamika, biogeokeemia ja Lagrange'i osakeste jälgimise mudelsüsteemi perioodi 2018–2020 vältel keskendudes polüpropüleeni/polüetüleeni (PP/PE) ja polüetüleentereftalaadi (PET) osakestele. Modelleeriti jõgedest ja veepuhastusjaamadest merre saabuvate osakeste levikut. Mudelsüsteem võimaldas lahutada ka (sub)mesomastaapseid protsesse ning uurida nende võimalikku mõju MP kontsentratsioonidele meres. Osakeste mudelis tehti valitud protsessidele tundlikkuse analüüs varieerides erinevaid parameetreid ning uurides nende mõju osakeste üldisele levikule. Tundlikkuse analüüsis käsitleti protsessidena randumist, osakeste tiheduse suurenemist biokile tekke tõttu, horisontaalset segunemist ning resuspensiooni. Analüüsi tulemusena leiti mudelile seadistus, millega modelleeriti MP levikut Soome lahes realistlike koormustega.

Väitekiri on koostatud kolme artikli põhjal, milledest esimeses käsitleti mõõdetud MP kontsentratsioonide ajalis-ruumilist varieeruvust ning ülejäänud kahes keskenduti modelleerimistulemustele. Mõõdetud MP kontsentratsioonid pinnakihis olid vahemikus 0,01 kuni 2,45 tk/m³ (keskmine: 0,49 tk/m³). Mõõdetud MP kontsentratsioonid olid suuremad Läänemere avaosas ja Soome lahes; madalamad väärtused esinesid Liivi lahes ja Väinameres. Sesoonselt olid kontsentratsioonid pinnakihis ja veesambas kõrgemad sügisel ja talvel ning madalamad suvel. Suvel soodustas settimist biokile kasv ja osakeste ujuvuse vähenemine. Talvel põhjustas sagedasem resuspensioon osakeste tõusmist veesambasse.

Simulatsiooni tulemused viitavad, et enamus maismaalt pärit MP akumuleerub Soome lahes. Ligikaudu 75% MP settis merepõhja, 10% randus, 14% oli veesambas ja vaid 1% väljus Soome lahest Läänemere avaossa. Kõrgeimad kontsentratsioonid esinesid küll allikate lähedal, kuid MP vertikaalne jaotus veesambas ei ole ühtlane. Kõrgemad väärtused esinesid pinnakihis ja põhjalähedases kihis; vahekihis esinesid madalamad väärtused.

MP sisalduses esines märkimisväärne lühiajaline muutlikkus, mis oli seotud hüdrodünaamiliste protsessidega. Rannikutsoonis tuvastati nii mõõtmiste kui simulatsiooniga väga madalad MP kontsentratsioonid apvellingu vältel ja kõrged kontsentratsioonid daunvellingu ajal. Daunvellinguga tekib ranna lähedal konvergents ja MP kogunemine. Apvellingu käigus tõuseb pinnale vahekihi vesi, kus MP kontsentratsioonid on madalad. Tugevad hoovused põhjustavad MP resuspensiooni ja kontsentratsiooni tõusu veesambas.

Käesolev dissertatsioon annab teadmisi MP levikuteedest, ruumilisest varieeruvusest ja akumulatsioonist Läänemere idaosas. Tulemused näitavad vajadust edasiste uuringute järele, mis keskenduksid muuhulgas submesomastaapsete protsesside mõjule ning maismaalt tuleva MP reostuse levikule rannikutsoonis.

Appendix

Publication I

Mishra A., Buhhalko N., Lind K., Lips I., Liblik T., Väli G., et al. (2022). Spatiotemporal variability of microplastics in the Eastern Baltic Sea. Front. Mar. Sci. 9. doi: 10.3389/fmars.2022.875984

Spatiotemporal Variability of Microplastics in the Eastern Baltic Sea

Arun Mishra[1]*, Natalja Buhhalko[1], Kati Lind[1], Inga Lips[2], Taavi Liblik[1],
Germo Väli[1] and Urmas Lips[1]

[1] Department of Marine Systems, Tallinn University of Technology, Tallinn, Estonia, [2] European Global Ocean Observing
System (EuroGOOS) AISBL, Brussels, Belgium

Microplastic (MP) pollution is present in all aquatic environments and is gaining critical concern. We have conducted sea surface MP monitoring with a Manta trawl at 16 sampling stations in the eastern Baltic Sea in 2016–2020. The concentrations varied from 0.01 to 2.45 counts/m^3 (0.002–0.43 counts/m^2), and the mean was 0.49 counts/m^3 (0.08 counts/m^2). The fibers and fragments had, on average, an approximately equal share in the samples. Correlation between the concentration of fibers and fragments was higher near the land and weaker further offshore. The following spatial patterns were revealed: higher mean values were detected in the Baltic Proper (0.65 counts/m^3) (0.11 counts/m^2) and the Gulf of Finland (0.46–0.65) (0.08–0.11) and lower values were detected in the Gulf of Riga (0.33) (0.06) and Väinameri Archipelago Sea (0.11) (0.02). The difference between the latter three sub-basins and the meridional gradient in the Gulf of Riga can likely be explained by the degree of human pressure in the catchment areas. The MP concentration was higher in autumn than in summer in all regions and stations, probably due to the seasonality of the biofouling and consequent sinking rate of particles. A weak negative correlation between the wind speed and the MP concentration was detected only in the central Gulf of Finland, and positive correlation in the shallow area near river mouth. We observed a 60-fold difference in MP concentrations during coastal downwelling/upwelling. Divergence/convergence driven by the (sub)mesoscale processes should be one of the subjects in future studies to enhance the knowledge on the MP pathways in the Baltic Sea.

Keywords: microplastics, Manta trawl, Baltic Sea, spatiotemporal variability, physical factors

INTRODUCTION

Plastic pollution is ubiquitous in the marine environment. Plastics, due to their durability, low cost, and lightweight, are important in our lives and have been shed to the environment in the last few decades like never. Since the beginning of plastic production in the early 20th century, it has continuously increased and reached 368 million tons globally in 2019 (Plastics Europe, 2020). Microplastics (MPs) are frequently defined as particles with lengths of less than 5 mm (Arthur et al., 2009; Cole et al., 2011).

MPs' sources and pathways are of utmost importance to control and prevent plastics from entering the ecosystem (He et al., 2019). The exuberance of MPs in the aquatic environment is due to inappropriate human behavior and improper waste management (Jambeck et al., 2015). There is limited information on the amount of plastic waste entering the oceans, but it is widely cited that land sources contribute approximately 80% of the marine plastic debris (Jambeck et al., 2015). Rivers, surface water runoff, sewage treatment, and wind-induced air transport are the major gateways of plastic debris in the aquatic ecosystem (He et al., 2019). In addition, the plastic manufacturing industries release plastics in the form of pellets and resin powders that, *via* air-blasting, can contaminate the aquatic environment (Eriksen et al., 2013). Plastic pellets are also released from marine accidents during handling and transportation (Veerasingam et al., 2016). Coastal activities, including fisheries, aqua tourism, and marine industries, are also the sources of MP pollution in the marine environment (Eriksen et al., 2013).

MPs can be of two types, primary and secondary MPs. Primary MPs are produced as microscopic particles present before entering the environment and exist as microbeads found in personal care products and plastic pellets (or nurdles). Secondary MPs are formed by physical, biological, and chemical degradation of macroscopic plastic parts and are the main source of microparticles released into the environment (Boucher and Friot, 2017; Zhu et al., 2020). They are formed by the degradation of improperly disposed plastic waste, tire abrasion, and washing of synthetic textiles (Boucher and Friot, 2017; Zhu et al., 2020).

MP particles have different shape classes: fragments, films, filaments, foams, and pellets (GESAMP, 2019). In this study, we divided all MP particles into fibers and fragments. The fragments category includes all non-filament particles like films, foams, and pellets, and the fibers category includes both filaments and fibers. Some polymers, such as PVC, polyester, polyamide, and acrylic, are denser than seawater and, thus, sink to the bottom of the sea (Hidalgo-Ruz et al., 2012). Polymers with a lower density than seawater usually float on the surface, including polyethylene, polypropylene, and expanded polystyrene (Hidalgo-Ruz et al., 2012). Low-density MP accumulates especially within a layer of a few cm below the air–water interface (Andrady, 2011). Thus, most studies target MP abundance and distribution confined to the surface layer (Collignon et al., 2014). Plastic products, traditionally made of monomers, are linked to the form of the polymer structure. During plastic production, several additives are added for promoting specific properties towards its use (Lithner, 2011). As the plastics degrade over time, these chemicals tend to leach out, including coloring agents, and accumulate in animals' stomachs, resulting in bioaccumulation and biological effects (Mato et al., 2001; Teuten et al., 2009). Worldwide, individuals are accustomed to seafood consumption, which makes it possible for people to be exposed to MPs (Wright and Kelly, 2017). Chemical additives or remaining monomers can pose a potential danger to human health and the ecosystem (Lusher et al., 2017).

Colored plastics impose a high threat to aquatic species (Li et al., 2021). From one side, marine species have difficulty distinguishing between transparent and colored plastics, which increases the risk of MPs ingestion. Moreover, colored MPs may be accidentally ingested by fishes, turtles, and birds (Zhao et al., 2016; Gago et al., 2019). On the other hand, the impact of color affects the selection of food made by aquatic species.

As demonstrated by studies from different Baltic Sea basins, the occurrence of MPs in the Baltic Sea is evident (Setälä et al., 2016; Tamminga et al., 2019; Uurasjärvi et al., 2021). However, the knowledge about the spatial distribution and temporal variability of MPs in the Baltic Sea is limited (Aigars et al., 2021). Also, the methodology used to collect MPs varies by instruments, mesh size, sampling depth, and sampling area.

The main objective of the present paper is to assess the spatiotemporal variability of MPs in the eastern Baltic Sea and analyze environmental drivers affecting it. We report and analyze 5-year measurements of MPs in the surface layer in the eastern Baltic Sea. Specifically, we address the following main questions in this study: What is the mean spatial distribution of MPs in the eastern Baltic Sea? Is there seasonality in the MP concentrations? What is the share of fibers/fragments, different particle sizes, and colors in the MP pool? What processes cause the short-term variability in the MP concentration?
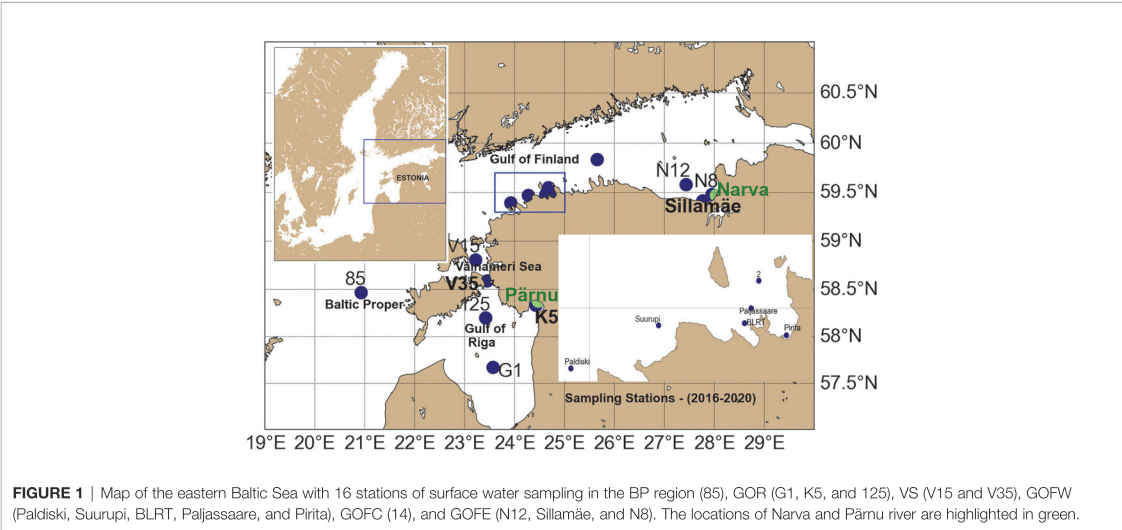
MATERIALS AND METHODS

Study Area

MP sampling was performed during monitoring cruises from 2016 to 2020 onboard the research vessel Salme in the four sub-basins of the Eastern Baltic Sea (**Figure 1**): the Gulf of Finland (GOF), the Gulf of Riga (GOR), the northern Baltic Proper (BP), and the Väinameri Sea (VS).

The GOF is an elongated estuarine basin located in the northeastern part of the Baltic Sea with an average depth of 37 m and a maximum depth of 123 m (Leppäranta and Myreberg, 2009). The gulf is about 400 km long, and its width varies between 48 and 135 km (Alenius et al., 1998). There is a free water exchange between the GOF and BP at the western border, and fresh water is discharged mostly to the eastern part of the GOF. The western Estonian coast has two semi-enclosed sub-basins. The GOR covers an area of 140 km from west to east and 150 km from south to north. The surface area of the VS is 2,243 km^2. The average depth of GOR and VS is 23 m and 4.7 m, respectively. These sub-basins are interconnected and connected with the BP *via* five straits.

In total, 16 sampling stations were visited in the western Gulf of Finland (GOFW), eastern Gulf of Finland (GOFE), central Gulf of Finland (GOFC), GOR, VS, and northern BP (**Figure 1**). Stations in the GOFW and GOFE were quite close to shore, while stations in the BP, GOFC, and GOR (excluding Station K5) were offshore. The station network was not the same each year. Visited stations in different years are shown in **Table 1**. Sampling stations N8 (visited 15 times), 14 (15), Sillamäe (Sill) (14), Paljassaare (Pal) (13), 2 (12), and K5 (11) were sampled more

FIGURE 1 | Map of the eastern Baltic Sea with 16 stations of surface water sampling in the BP region (85), GOR (G1, K5, and 125), VS (V15 and V35), GOFW (Paldiski, Suurupi, BLRT, Paljassaare, and Pirita), GOFC (14), and GOFE (N12, Sillamäe, and N8). The locations of Narva and Pärnu river are highlighted in green.

than ten times during the 5-year period. The frequency of sampling times in other stations is as follows: V15 (6), V35 (6), 125 (5), N12 (4), G1 (3), Pirita (Pir) (2), Paldiski (Pald) (1), Suurupi (Suu) (1), and BLRT (1). Please note that station Pal is located close to the largest city wastewater treatment plant outfall in the study area, station N8 close to the Narva river mouth, and station K5 close to the Pärnu river mouth. The detailed observational periods at each sampling site are mentioned in **Supplementary Table 1**.

MP Sampling and Sample Processing

Surface water samples were collected with a Manta trawl (mesh size 330 μm). The net was deployed 5 m from the side of the ship using a crane and towed at the water surface (not totally submerged) for 15 to 60 min at a speed of approximately 2 knots. The samples were collected in the cod end of the net. The content of the cod end was rinsed with tap water to a metal bucket and sieved through a set of stainless-steel sieves (5,000 μm, 1,000 μm, and 330 μm). Thereafter, particles from each sieve were flushed into a separate glass jar with ultrapure water. Formaldehyde (37%) was added in the proportion of 1 to 100 ml of sample. Samples were kept at room temperature until analysis in the lab.

If the samples contained a lot of organic material, they were left to settle. The solution on top of the settled organic material was pipetted and vacuum filtered onto a 1.6-μm pore size (VWR)

glass fiber filter (47 mm diameter). Hydrogen peroxide (34.5%–36.5%) was added to the settled organic material in a proportion of 1:1 and left for oxidation under the ventilation cabinet for up to 7 days. After oxidation, the samples were diluted with ultrapure water and vacuum filtered as described above. The filters were dried in glass Petri dishes in a drying oven (SANYO MOV-212F) at 60°C for 15 min, and the particles remaining on the filters were analyzed using a stereomicroscope (Leica M205 C or Olympus SZX16). All MP particles were counted, partially photographed, and tested with a hot needle to distinguish plastics from other microliter particles (Devriese et al., 2014). The results were calculated by summing the number of MP particles in the analyzed water sample.

In this study, we divided all MP particles into fibers and fragments. The fragments category includes all non-fiber MPs: films, foam, and pellets, and in general, we have identified fibrous plastics. As the MPs monitoring was carried out by the Manta trawl with a mesh size of 330 μm, we categorized them into two size classes (330–999 μm and 1,000–4,999 μm) according to their longest dimension. The water volume was calculated by multiplying the whole area of the trawl mouth with the ship speed and towing time. MP concentration is presented as the number of MP counts per cubic meter (counts/m^3). In addition, concentration per square meter (counts/m^2) is given in brackets throughout the text.

The 8-color classification scheme by the European Marine Observation and Data Network (EMODnet) was used for color identification that combines similar colors into one group (Galgani et al., 2020). Black/gray, white, blue/green, red/pink/orange/purple, yellow, brown, transparent, and others (golden/silver/multicolor) distinguished from colors.

Reduction of Cross-Contamination

Reduction and monitoring of potential airborne cross-contamination are crucial during sampling, sample processing,

TABLE 1 | MP sampling sites for each year.

Year	Stations visited
2016	85, G1, 14, N8, Sil, N12, Pal, 2
2017	85, 14, N8, Sil, Pal, 2, K5
2018	85, 14, N8, Sil, Pal, 2, K5, Suu, Pir, BLRT, V15, V35, 125
2019	85, 14, N8, Sil, Pal, 2, K5, V15, V35, 125, Pald
2020	85, 14, N8, Sil, Pal, 2, K5, V15, V35, 125

and analysis in the laboratory. To detect MP airborne contamination during sampling, samples of plastic-free water were kept in glass jars open on the deck near the sample collection area and later analyzed in the laboratory.

Non-synthetic clothing and cotton lab coats were worn, and glass or metal laboratory supplies were used as much as possible throughout the laboratory analysis. All labware was thoroughly rinsed with ultrapure water before use. Sample processing was done in a ventilation cabinet, except for the filtering through the sieves. Samples were covered with aluminum foil or glass lids from Petri dishes whenever possible.

For the contamination assessment during sample processing in the lab, 100 ml of ultrapure water was filtered through a clean glass fiber filter before each sample processing and analyzed as real samples. Also, one dry blank filter was placed under a ventilation cabinet during filtration and on the table near the stereomicroscope during microscopic analysis. Both blanks were analyzed as samples. In the blank samples, only fibers were found, and blank filter contamination was only a few percentages. Blank samples were used only as a reference. Hence, the overall contamination was less than one plastic fiber per sample on average. The fibers found in the blank samples could be related to airborne contamination from textiles.

Paint flakes were often observed in the samples. All paint flakes data were removed from the dataset for the analysis as their potential sources could not be confirmed.

Statistical Analysis

One-way analysis of variance (ANOVA) was performed to analyze MPs' spatial and temporal variability. When a substantial difference was discovered, a pairwise comparison using regression test was applied to determine whether the difference was statistically significant. The significance level was set to 5%.

The hourly wind speed components were extracted from ERA-5 (Hersbach, 2020) for seven monitoring stations and bi-linearly interpolated to the exact coordinates using CDO (climate data operators) software (Schulzweida, 2021). Linear regression analysis was used to relate the observed MP abundances to prevailing meteorological conditions (e.g., wind speed). Since the data series were relatively short, as an alternative to linear regression, the conditions during the sampling of lowest and highest MP concentrations were compared.

The sea surface temperature and salinity are taken from the long-term model simulations to understand the hydrophysical conditions during sampling dates. From the model output, two diagnostic parameters are calculated:

a. the lateral gradients of temperature and salinity as $|\nabla_H T|$ and $|\nabla_H S|$
b. the divergence of the current field as $u_x + v_y$ normalized with Coriolis parameter f

Numerical Modeling

The General Estuarine Transport Model (GETM) (Burchard and Bolding, 2002) has been applied to estimate temperature and salinity distributions. GETM is a three-dimensional primitive-equation hydrostatic model with a free surface and built-in vertically adaptive coordinate scheme (Hofmeister et al., 2010), which can significantly reduce numerical mixing in the simulations (Gräwe et al., 2015).

Vertical mixing is calculated using the General Ocean Turbulence Model (GOTM) (Umlauf and Burchard, 2005) using a two-equation k–ε model coupled with an algebraic second-moment closure (Canuto et al., 2001; Burchard and Bolding, 2002) to obtain the eddy viscosity and diffusivity. Sub-grid horizontal mixing is parameterized using the Smagorinsky approximation (Smagorinsky, 1963).

The model domain consists of the whole Baltic Sea (**Figure 1**), and horizontal grid spacing of 0.5 nm (approximately 926 m) is used with 60 vertically adaptive layers. The vertical resolution of the model during simulations is controlled by using the same parameters as in Hofmeister et al. (2010) and Gräwe et al. (2015). Baltic Sea Bathymetry Database (http://data.bshc.pro/, last access: 18 January 2022) with additional data for the GOF from Andrejev et al. (2010) has been used to construct the model bathymetry. The atmospheric forcing (wind stress and surface heat flux components) was calculated from the operational forecast model HIRLAM (High-Resolution Limited Area Model) maintained by the Estonian Weather Service with a spatial resolution of 11 km and a daily forecast interval of 1 h (Männik and Merilain, 2007). The model simulation was performed from April 1, 2010, to December 31, 2020, but the results for 2016 to 2020 have been used in this study.

An open boundary is located at the Danish Straits. Inflow and outflow from the model are calculated using the sea surface height measurements from Gothenburg Station with Flather (1994) radiation. Temperature and salinity at the boundary are relaxed towards climatological profiles by Janssen et al. (1999). Freshwater input from the 54 largest Baltic Sea rivers with basin-wide interannual variability corrected towards values as reported in HELCOM (Johansson and Jalkanen, 2016) has been used. Constant salinity of 0.5 g kg^{-1} and target cell sea surface temperatures are used for the riverine values.

Initial temperature and salinity fields were taken from the Copernicus reanalysis of the Baltic Sea for the period 1989–2014 (https://doi.org/10.48670/moi-00013, last accessed February 14, 2022). As the product used lower resolutions both in the horizontal and vertical, the thermohaline fields were interpolated to the model grid. The simulation started with sea surface height and current velocities set to zero, i.e., the motionless state, but as previous studies (Lips et al., 2016) have shown, the wind-driven circulation of the Baltic Sea adjusts to forcing within 5 days. More information about the model setup and validation is available from Zhurbas et al. (2018) and Liblik et al. (2020).

RESULTS

MPs were found at all 16 sampling stations. In total, 9,414 MP particles were extracted from 23,199 m^3 water of 122 surface water samples. When total MP particles were divided by the total water volume, the mean was 0.41 counts/m^3. However, the

arithmetic mean of MP concentrations in samples was 0.49 counts/m^3 (0.08 counts/m^2), and in the regions of BP, GOFC, GOFW, GOFE, GOR, and VS, the mean concentrations were 0.65, 0.59, 0.65, 0.46, 0.33, and 0.11 counts/m^3 (0.11, 0.10, 0.11, 0.08, 0.06, and 0.02 counts/m^2), respectively. The results show high variability in concentrations (STD ±0.46 counts/m^3) and heterogeneity in distribution patterns of MPs in the eastern Baltic Sea. The relative abundance of MP fibers and MP fragments at different sampling sites is presented in **Figure 2**. The average concentration of MP fibers and MP fragments across the dataset was almost the same: 0.25 and 0.24 counts/m^3 (0.04 and 0.04 counts/m^2), respectively. The annual mean of the share of fibers is higher in 2016, 2019, and 2020 (**Figure 2**).

Spatiotemporal Distribution of Microplastics

Relatively high annual mean MP concentrations (**Figure 3**; concentrations are shown if the station was visited more than once) were observed in 2016 (**Figure 3A**). The highest mean concentrations (>1.0 counts/m^3) were observed in the GOR (station G1) and the BP (station 85) and at station Pal. Lower values were observed at the GOFE stations. Mean concentrations were in a quite narrow range (0.39–0.58 counts/m^3) (0.07–0.1 counts/m^2) in the whole area in 2017; only in the GOFC was the value higher (**Figure 3B**). The highest mean concentration (>1.0 counts/m^3) was observed in the BP, while concentrations were 20-fold lower in the GOR and VS in 2018 (**Figure 3C**). Spatial distribution of the MP concentrations in the GOF had a large range, varying from 0.11 to 0.76 counts/m^3 (0.02–0.13 counts/m^2) (**Figure 3C**). Very low mean values (<0.08 counts/m^3) were observed in the GOR and VS in 2019 (**Figure 3D**). Quite low values, except at station 2, were observed in the GOF and BP as well (**Figure 3D**). A similar pattern was observed in the study area in 2020 (**Figure 3E**).

Despite high temporal variability, tendencies in the mean 5-year period spatial pattern can be found (**Figure 3F**). Significantly higher mean MP, MP fiber, and MP fragment concentrations occurred in the BP and the three areas of GOF compared to the GOR and VS (**Figures 4A–C**). It is noteworthy that the annual mean concentration in the VS was lower than in the BP in all 3 years (2018–2020) when the VS was sampled (**Figures 3C–E**). The 5-year mean concentration in the vicinity of Pärnu and Narva river mouths [stations K5 and N8, 0.21 and 0.39 counts/m^3 (0.04 and 0.06 counts/m^2), respectively] was lower than at the open sea stations (0.59–0.74 counts/m^3) (0.10–0.13 counts/m^2).

The maximum concentrations >1.6 counts/m^3 were registered at offshore stations in the BP, GOF, GOR, and at station Pal. The highest MP concentration (2.45 counts/m^3) (0.43 counts/m^2) for the entire study period was recorded at station G1 in the GOR. Maxima were lower (0.6–1.2 counts/m^3) at the GOFE stations and near the Pärnu river mouth (station K5). The maximum was only 0.15 counts/m^3 (0.03 counts/m^2) in the central VS (station V15). However, the latter station was visited only three times.

The mean share of fibers and fragments for the whole area in the 5 years was almost equal (**Figure 2**). The latter also roughly

holds when considering the means of the regions (**Figure 5**). Thus, the mean spatial distribution of fibers and fragments taken separately (**Figures 5A–F** and **Figures 5G–L**) is similar to the total MP concentration (**Figure 3F**). This means 5-year mean concentrations of fibers and fragments in the vicinity of Pärnu and Narva river mouths are lower than at the open sea stations.

The correlation between the concentrations of fibers and fragments in the whole dataset was significant, but rather low (r^2 = 0.21, p < 0.01, n = 122). Thus, often the spatiotemporal changes of fibers and fragments were not related. However, some of the stations separately revealed quite a strong correlation. High correlation was found at station K5 (r^2 = 0.87, p < 0.01, n = 11) and Pal (r^2 = 0.60, p < 0.01, n = 13). Weak but significant correlations were observed at stations 14, Sil, and N8. No correlation was found at stations 2 and 85. For instance, fibers (0.81 counts/m^3) (0.14 counts/m^2) had the major share at station 85 in the BP in 2016 (**Figure 5A**). Next year, the concentration of fragments was similar (approximately 0.2–0.3 counts/m^3), but the fiber concentration was 0.20 counts/m^3 (0.04 counts/m^2) (**Figure 5B**). The share was reversed (compared to 2016) in 2018 when fragments (0.87 counts/m^3) (0.15 counts/m^2) had the major contribution (**Figure 5I**). Thus, the highest annual mean concentration of fragments and fibers in the study area was measured in the BP, but in different years. The annual share of fragments higher than 70% occurred only at the coastal stations in the GOF (five occasions) and once at station 85 in the BP. Other stations had a fiber share approximately 50% or higher. The annual mean shares of fragments were lowest in the VS. Note that the total MP concentrations were low there as well.

Microplastics Morphology

The MPs were assorted into eight colors. The most occurred MP color was gray/black (29.7%), followed by white (22.6%) and blue/green (22.4%). Other colors such as red/pink/purple (9.9%), transparent (9.8%), yellow (3.6%), and brown (1.5%) had a lower proportion. Gold-stained plastic was the rarest out of the eight colors, having a percentage share of less than 1%. The maximum share came from white particles when the highest concentrations were detected at stations Pal, 2, 85, and 14. The dominant color for the MP fragments was white and blue/green, and for MP fibers, it was gray/black and blue/green.

Seasonal Variability of Microplastics

The mean concentration in spring and summer was 0.46 counts/m^3 (0.08 counts/m^2) and 0.36 counts/m^3 (0.06 counts/m^2), respectively. This tendency of higher concentration in spring compared to summer was revealed at most of the stations (**Supplementary Figure 1**) except at stations 85, G1, Pir, and V35. The highest seasonal mean concentration (0.81 counts/m^3) (0.14 counts/m^2) in the study area occurred in the autumn. The mean concentration was higher in autumn than summer at all stations (**Supplementary Figure 1**). This is reflected in the seasonal pattern across all regions as well (**Figure 6**). Moreover, the only observations from winter in the GOFC confirm the increasing concentration trend from summer to the cold season. However, due to high variability within each season, the differences between the
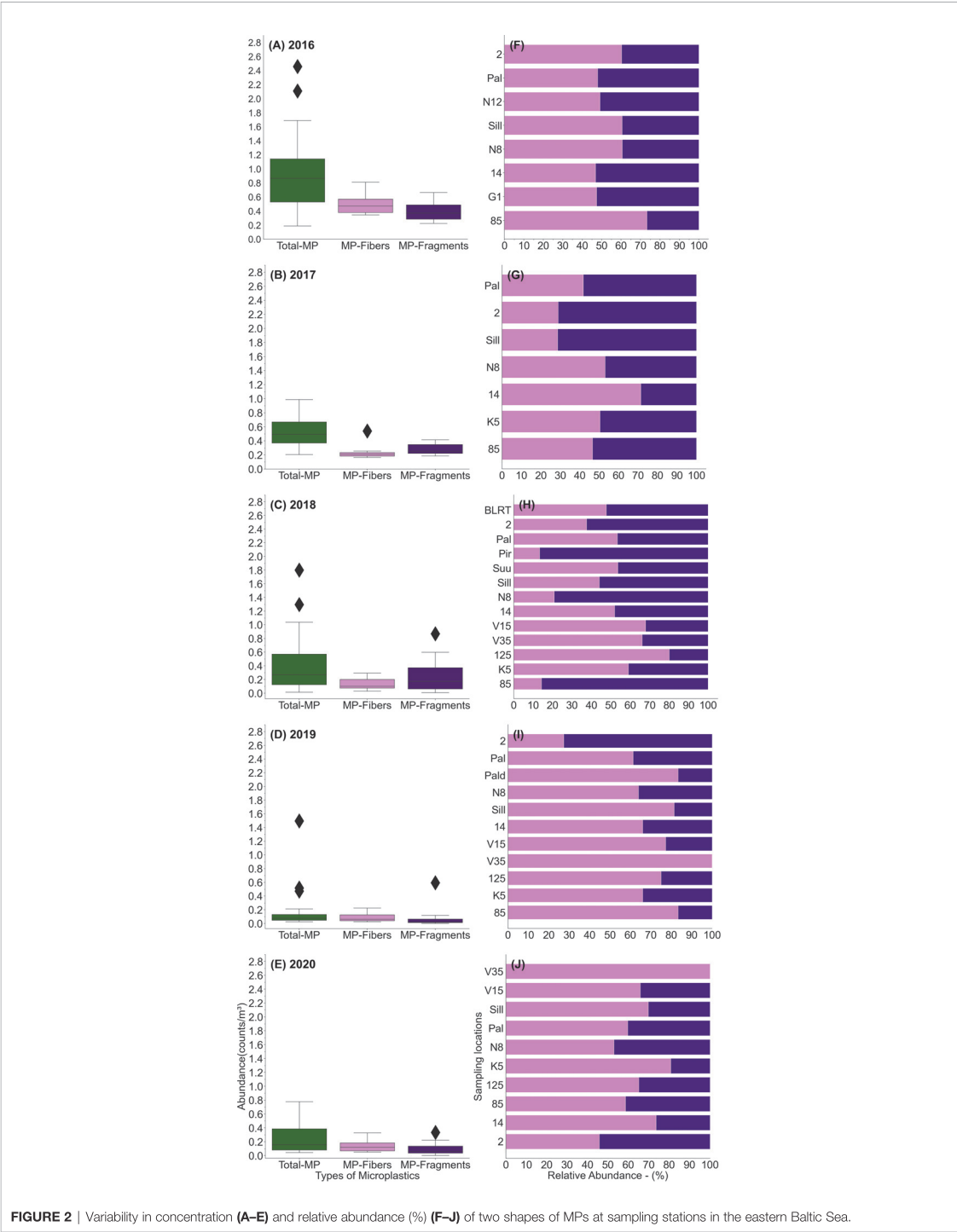
FIGURE 2 | Variability in concentration (A–E) and relative abundance (%) (F–J) of two shapes of MPs at sampling stations in the eastern Baltic Sea.
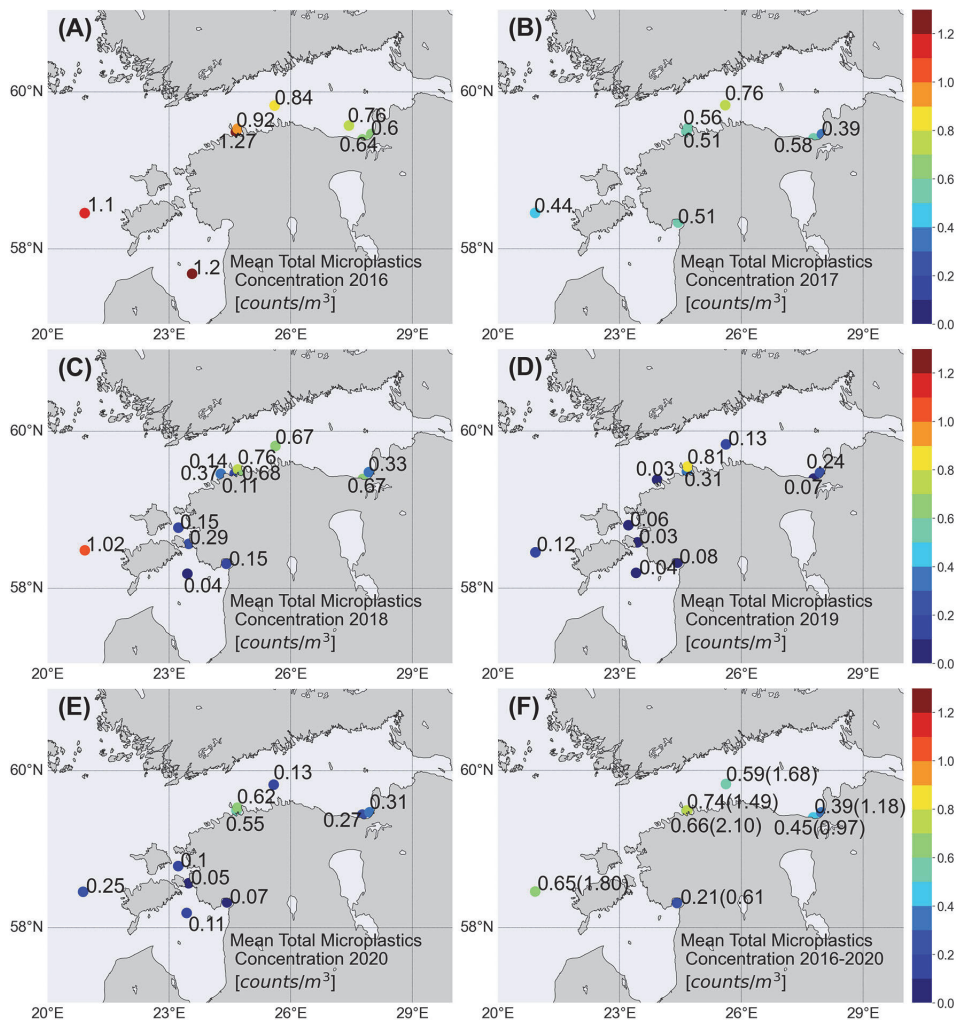
FIGURE 3 | Average MP counts/m^3 at each sampling station **(A–E)**. The overall average for 2016–2020 was calculated as an arithmetic mean of all individual concentrations in the sampling location **(F)**. The highest MP concentration (counts/m^3) at sampling station is shown in parenthesis **(F)**.

seasons were statistically not significant. MP fiber concentration differed significantly across all seasons; however, no significant difference was detected for MP fragments. Seasonally, no significant difference was observed between the two size classes—MP (330–999 µm) and MP (1,000–4,999 µm).

Impact of Physical Processes on the MP concentration

The impact of physical processes on the MP concentration was studied using the stations with the most consistent observations. Over the 5 years, seven stations had a higher number of samples.

We selected two coastal (N8 and K5) and two offshore (14 and 85) stations for further analysis.

The wind is the most obvious physical parameter to affect concentrations on the sea surface, as with increasing wind speed, the particles are mixed deeper. Significant negative correlation between the wind speed and MP concentration was found only at station 14 for MP fragments ($r^2 = 0.35$, $p = 0.01$, $n = 15$). For the whole dataset and most individual stations, the correlation was low and insignificant. A significant positive relationship between the wind speed and MP abundance was found at the coastal station K5 ($r^2 = 0.47$, $p = 0.01$, $n = 11$).
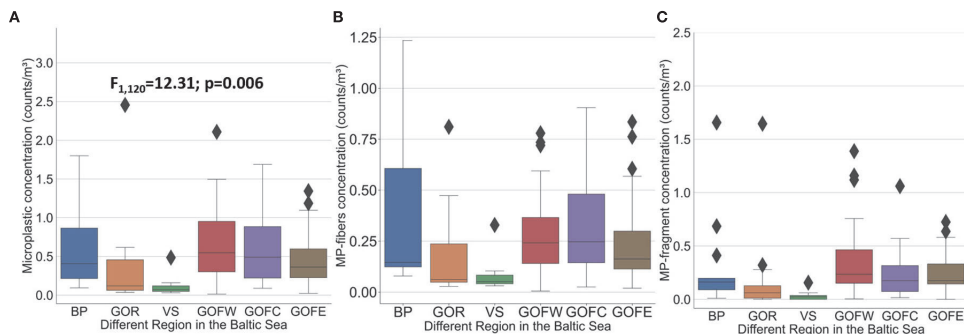
FIGURE 4 | **(A)** The variability of MP concentrations in different regions of the eastern Baltic Sea in 2016–2020. **(B)** The variability of MP fiber concentrations in different regions of the eastern Baltic Sea in 2016–2020. **(C)** The variability of MP fragment concentrations in different regions of the eastern Baltic Sea in 2016-2020.

At coastal stations K5 and N8, one can assume some effects of freshwater discharge and related MP input due to the vicinity of large rivers. Furthermore, not only the wind speed but also its direction could be critical *via* influencing convergence/divergence of surface waters. We selected the highest and lowest concentration cases for both stations to compare the effect of the river discharge and wind direction.

At coastal station N8, the highest MP concentrations were detected (1.18 counts/m^3) (0.2 counts/m^2) when the 3-day mean discharge (589 m^3/s) from the Narva river prior to the sampling date was greater than the long-term mean discharge (440 m^3/s). Moreover, before the observation of the highest MP concentration, the wind speed and direction at station N8 were favorable for the coastal downwelling (westerly winds with a maximum speed over 8 m/s), which supports the accumulation of MPs along the coast, thus resulting in a high MP concentration (**Figure 7A**).

In contrast, when the MP concentration was the lowest (0.02 counts/m^3) (0.004 counts/m^2), the wind conditions before observation indicated the occurrence of coastal upwelling in the area (north easterly winds) (**Figure 7B**). This water mostly originated from the subsurface, which explains the low MP concentration. Thus, we suggest that variation in coastal mesoscale processes, leading to convergence and divergence of surface waters, could cause both extremely high and low MP.

The impact of coastal upwelling and downwelling events was also visible at the coastal stations in the Tallinn Bay. The highest concentrations at station Pir were measured under the coastal downwelling and the lowest concentrations were measured under the coastal upwelling conditions at the southern coast of the GOF (**Figures 7C, D**). There is a clear downwelling jet along the coast directed to the east with relatively large current velocities during the high-concentration case (**Figure 7C**) and an upwelling jet in the opposite direction to the west during the low-concentration case (**Figure 7D**). Obviously, the large-scale coastal divergence and convergence have a significant impact on the distribution of MPs in the coastal sea.

When comparing the conditions for the lowest and highest MP concentrations at coastal station K5 (depth 5m), strong winds prevailed before the highest MP concentrations were observed. Strong winds cause resuspension of bottom sediments and force MPs to migrate from sediments to the surface, thereby resulting in high MP concentrations at the sea surface. On the other hand, weakened wind-induced resuspension leads to lower MP concentrations at the sea surface in shallow areas.

In order to better understand the hydrodynamic conditions in the offshore stations 85 and 14, we looked at the simulated sea surface temperature and salinity fields in the vicinity of the stations along with the convergence and divergence based on the modeled current components during dates with the observed highest and lowest MP values (**Figure 8**). The statistical parameters of different fields are summarized in **Table 2**.

In the high-concentration cases at both stations, strong lateral gradients in the salinity and temperature fields in the vicinity of the stations are seen (**Figures 8G, H**). During low-concentration cases, the lateral gradients are much weaker, and the variance of the fields is much smaller. In addition, the divergence during the high-concentration case was mostly negative, suggesting convergence, i.e., accumulation of the matter in the surface layer. During the low-concentration case, the divergence was mostly positive in the vicinity of the station.

Although the mean temperature and range during the high-concentration case was smaller than during the low-concentration case at 85, the range and variability of salinity was at least two times larger (**Table 2**). The variability of the salinity gradient around the station was almost 6 times larger. At station 14, the variance (shown as standard deviation in **Table 2**) of all parameters are greater during the high-concentration case.

DISCUSSION

We have reported results from the 5-year MP observations in the eastern Baltic Sea. Next, we compare our findings with previous
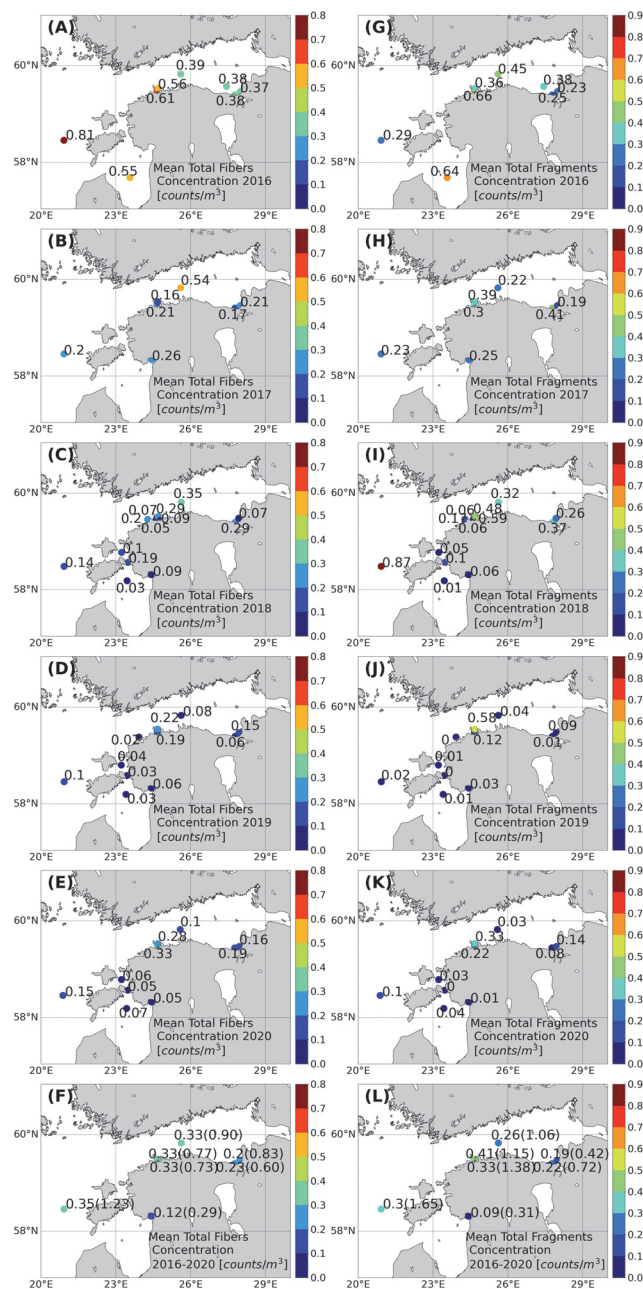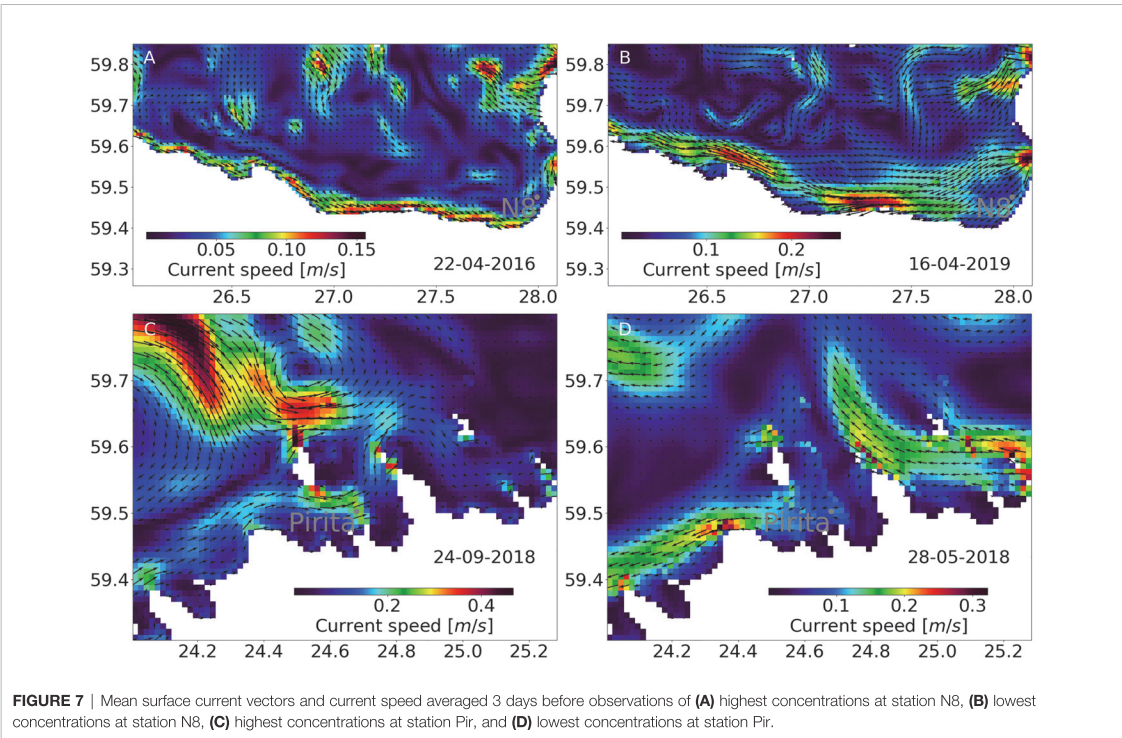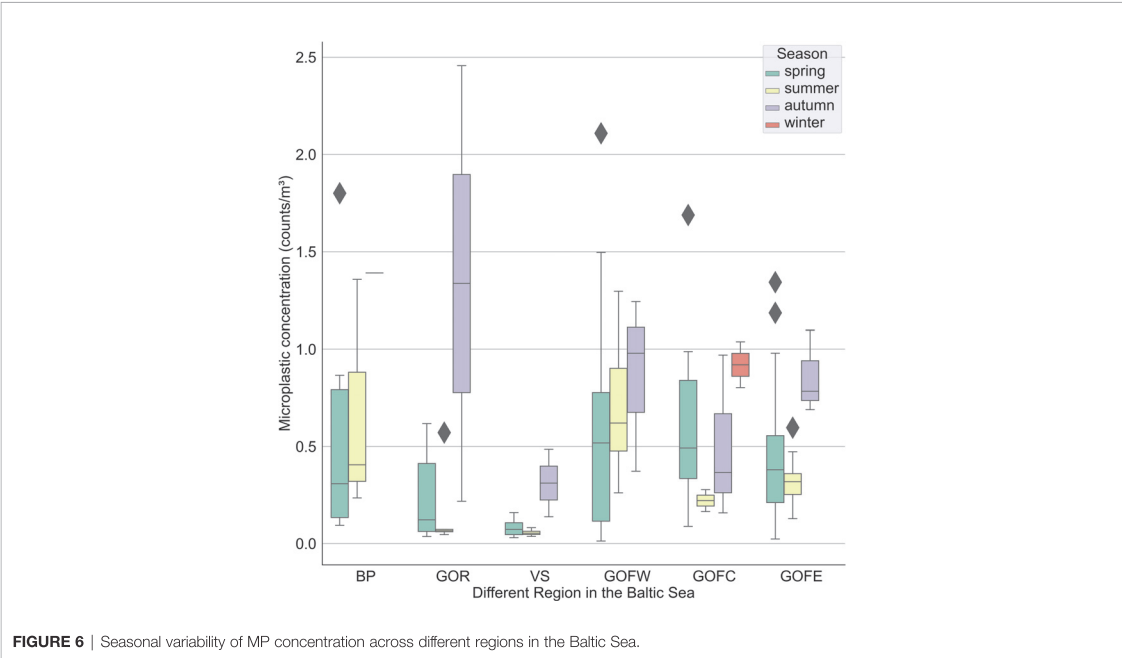
FIGURE 5 | Average MP fiber counts/m^3 (A–F) and average MP fragment counts/m^3 (G–L) at each sampling station. The overall average for 2016–2020 was calculated as an arithmetic mean of all individual concentrations in the sampling location (F, L). The highest MP fiber and MP fragment concentration (counts/m^3) at the sampling station is shown in parentheses (F, L).
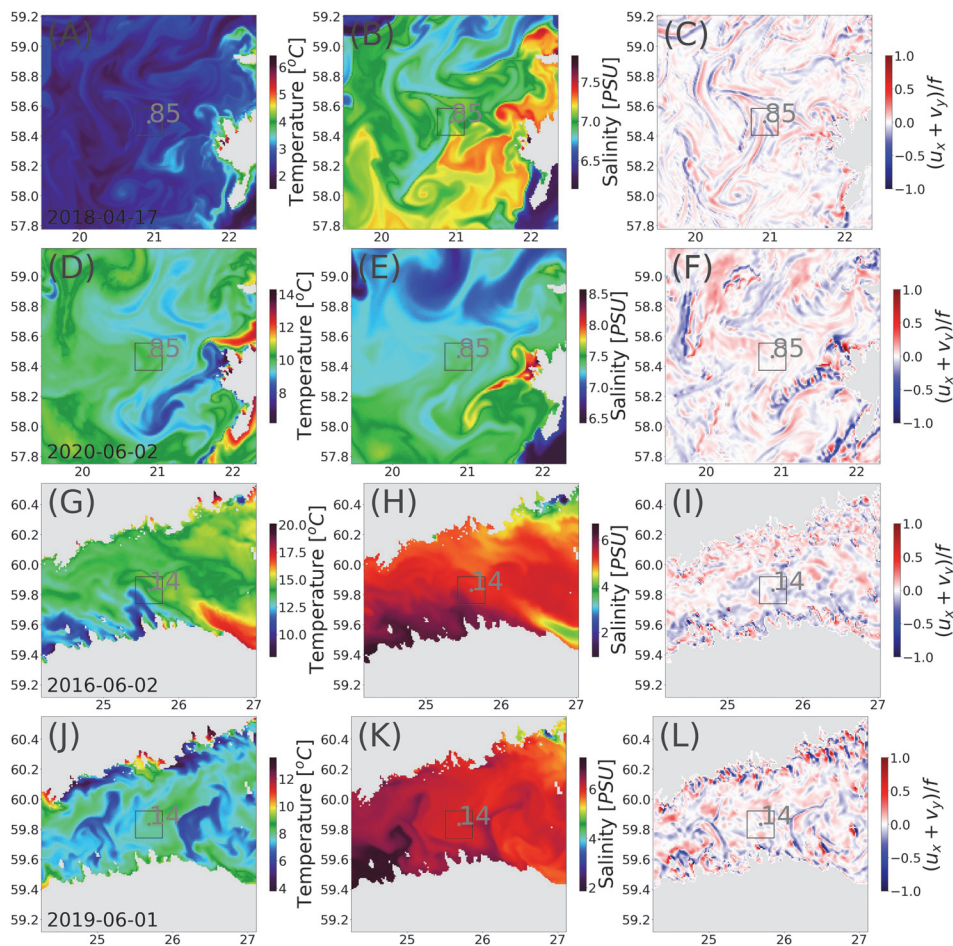
FIGURE 6 | Seasonal variability of MP concentration across different regions in the Baltic Sea.

FIGURE 7 | Mean surface current vectors and current speed averaged 3 days before observations of **(A)** highest concentrations at station N8, **(B)** lowest concentrations at station N8, **(C)** highest concentrations at station Pir, and **(D)** lowest concentrations at station Pir.

FIGURE 8 | Snapshots of surface temperature **(A, D, G, J)**, surface salinity **(B, E, H, K)**, and current field divergence, u_x+v_y/f, in the surface layers **(C, F, I, L)** during the highest and lowest measured concentration of MPs at selected stations. The gray box indicates the location around measurement location with 10-km distance.

studies that collected data using surface trawling (Manta trawl) like us in the Baltic and global oceans. In the sea surface layer of the Baltic Sea, Aigars et al. (2021) detected an MP concentration of 0.09–4.43 counts/m^3, Karlsson et al. (2020) found 0.18–0.92 counts/m^3 in the Gullmar fjord at the Swedish west coast, 0.05–0.09 counts/m^3 were observed in the South Funen Archipelago (Tamminga et al., 2018), Gewert et al. (2017) measured 0.19–7.73 counts/m^3 in the Stockholm Archipelago, and 0–0.8 counts/m^3 were found in the GOF (Setälä et al., 2016). In the Arctic waters, Lusher et al. (2015) revealed MP concentrations of 0–1.31 counts/m^3, 0.07–9.25 counts/m^3 were measured in the Eastern Mediterranean Sea (Adamopoulou et al., 2021), 1.82 counts/m^3 were observed in the Mediterranean Sea (Zeri et al., 2018), and 0.06–25.9 counts/m^3 were found in the Eastern Indian Ocean (Li et al., 2021).

Although Aigars et al. (2021) collected samples at numerous stations during 1 year, while we conducted measurements at three stations, during 5 years, the mean concentrations in the central GOR were roughly in the same order. Our observations revealed lower concentrations in the northern GOR and the Pärnu Bay; however. Setälä et al. (2016) identified an average MP concentration of 0.3 counts/m^3 in the GOFC region, and our investigation revealed 0.59 counts/m^3. We can conclude that the concentrations registered in our study—in the range of 0.01 to 2.45 counts/m^3 (0.002–0.43 counts/m^2) with a mean concentration of 0.49 counts/m^3 (0.08 counts/m^2)—are in the same order as previous studies in the Baltic Sea.

The mean concentrations in the three subregions in the GOF were in the range of 0.46–0.65 counts/m^3, while it was 0.33 counts/m^3 in the GOR. The difference between concentrations in

TABLE 2 | Statistical values of different surface parameters around the monitoring stations during the observed highest and lowest value of MPs.

Station 85 (Highest concentration)

Variable	T [°C]	S [PSU]	D	$|\nabla_H T|$ [°C km^{-1}]	$|\nabla_H S|$ [PSU km^{-1}]
Mean	2.38	6.98	−0.010	0.054	0.028
Min	2.19	6.80	−0.248	0.001	0.001
Max	2.70	7.22	0.211	0.262	0.141k
σ	0.10	0.09	0.083	0.041	0.028
Station 85 (Lowest concentration)					
Variable	T [°C]	S [PSU]	D	$|\nabla_H T|$ [°C km^{-1}]	$|\nabla_H S|$ [PSU km^{-1}]
Mean	9.83	7.35	0.020	0.060	0.011
Min	9.48	7.29	−0.063	0.001	0
Max	10.05	7.42	0.130	0.174	0.036
σ	0.13	0.03	0.032	0.039	0.007
Station 14 (Highest concentration)					
Variable	T [°C]	S [PSU]	D	$|\nabla_H T|$ [°C km^{-1}]	$|\nabla_H S|$
Mean	13.69	5.39	−0.028	0.194	0.036
Min	10.98	5.01	−0.183	0.006	0
Max	14.70	5.93	0.111	0.716	0.149
σ	1.01	0.21	0.060	0.164	0.028
Station 14 (Lowest concentration)					
Variable	T [°C]	S [PSU]	D	$|\nabla_H T|$ [°C km^{-1}]	$|\nabla_H S|$ [PSU km^{-1}]
Mean	7.90	6.08	0.015	0.050	0.012
Min	7.31	6.03	−0.105	0.002	0
Max	8.39	6.25	0.152	0.231	0.070
σ	0.21	0.04	0.051	0.043	0.011

T is temperature, S is salinity, D is current field divergence normalized with Coriolis parameter f, $|\nabla_H T|$ is lateral gradient of temperature, and $|\nabla_H S|$ is lateral gradient of salinity.

the GOR and GOF could be explained by human pressure. Population in the catchment area per surface area of the GOF is ca. 400 inhabitants km^{-2} while it is 150 inhabitants km^{-2} in the GOR catchment (HELCOM, 2004). Note that in the easternmost part of the GOF, in the area we did not cover, the MP concentrations are probably higher than we observed due to the impact of river Neva (Martyanov et al., 2021). If we combine our results with Aigars et al. (2021), a meridional pattern is revealed in the GOR: higher MP concentrations in the south and lower MP concentrations in the north. This could be related to the population in the catchment areas as well. The water entering the southern part of the GOR is impacted by ca. 2.4 million inhabitants while the total population in the catchment area of the GOR is ca. 2.7 million.

The low human pressure is a likely reason behind the small mean concentration in the VS. The catchment area of the VS has an extremely low population, and there are no larger towns or other considerable point sources at the coast of the VS. Low MP concentrations in a similar area, in the South Funen Archipelago in Denmark, were explained by the sheltered position of the study area, low human pressure on adjacent islands, and the absence of any major potential point sources (Tamminga et al., 2018).

We registered considerable amounts of MPs at stations Pal (2.10 counts/m^3) and 2 (1.49 counts/m^3) in proximity to the city of Tallinn. Our observations follow previous studies that reported that the MP particle concentrations are frequently greater near densely populated urban areas with pollution sources such as industry and wastewater treatment plants (Yonkos et al., 2014; Gewert et al., 2017; Schönlau et al., 2020).

High mean MP concentration was detected at offshore station 85. This is a somewhat controversial result as earlier studies have reported higher values near coasts and rather low values offshore in the BP (e.g., Aigars et al., 2021). No major rivers enter the area, or remarkable point sources (cities and towns) are nearby. On the one hand, a possible explanation could be that the northern BP is the accumulation zone, where the discharge and buoyant particles from different basins (the GOF, GOR, Bothnian region, and south- and eastern BP) are concentrated. Secondly, the mean cyclonic current structure of the BP (Placke et al., 2018; Liblik et al., 2022) recirculates/traps the surface water in the basin for a longer period. In addition, MPs exhibit different buoyancy characteristics based on their density, shape, size, and biofouling rate (Adamopoulou et al., 2021). Convergence and downwelling act as a sorting mechanism, with relatively larger particles staying in the surface layers and smaller particles getting transported deeper in the water column (van Sebille et al., 2020). The biofilm growth is generally faster for smaller particles due to their high surface-to-volume ratios (Tsiaras et al., 2021). Thus, the buoyancy patterns described above and the fact that nearly 81% of MPs detected were smaller than 1 mm allow us to justify the high mean MP concentration at station 85. Recently, it has been shown that the region is prone to be affected by the submeso- and mesoscale activity (Väli and Zhurbas, 2021; Zhurbas et al., 2022), which can contribute to the convergence and divergence of MPs in the surface layers. We showed that high variability and convergence at the (sub)mesoscale could be a factor leading to high MP concentrations, but further investigations are needed to understand the pathways and reasons behind the phenomenon.

We considered two shapes of the MP particles in the current study: fibers and fragments, which accounted for 96% of the encountered particles in the eastern Baltic according to the

recent study (Aigars et al., 2021). MP fragments are more likely to break up into smaller pieces and are caught in the Manta trawl than other MPs (Li et al., 2021). Synthetic fibers derived from textile materials could enter the aquatic ecosystem through sewage systems, surface runoff, or atmospheric transport and deposition (Bai et al., 2018; Liu et al., 2019; Wang et al., 2020).

The share of fibers (51%) and fragments (49%) was approximately equal in the current study. The latter is valid for the whole dataset, as well as the subregions. However, the share of shapes and concentrations might be influenced by the sampling method: Manta trawling with the mesh size of 330 μm. Many studies reported more fibers on the sea surface (Setälä et al., 2016; Bagaev et al., 2017; Gewert et al., 2017; Tamminga et al., 2018; Aigars et al., 2021), compared with fragments. On the other hand, some studies showed a lower proportion of fibers (Zhang et al., 2017; Pan et al., 2019; Karlsson et al., 2020). When samples are collected using the Manta trawl, MP fibers might leak in high numbers through the 330-μm mesh but could be more efficiently trapped when the mesh size is smaller (<100 μm; Setälä et al., 2016). However, even when a smaller mesh size (100 μm) is used, the number of fibers does not appear to rise, as fiber size, particularly from clothes, is less than 20 μm (Setälä et al., 2016).

Despite the equal share of fibers and fragments, the correlation between the concentration of the two shapes in the whole dataset was weak, although significant. However, high correlations were found near the Pärnu river mouth at station K5 (r^2 = 0.87) and near the outlet of the Paljassaare wastewater treatment plant, at station Pal (r^2 = 0.60). In the rest of the stations, there was a significant weak correlation, except at station 2 in the GOF and offshore station 85 in the BP, where the correlation was not found. Due to disturbance-induced vertical transport, small size MPs get resuspended to the surface layer (Xia et al., 2021). As K5 is a shallow station (depth, 5 m), and nearly three-fourths of MP detected are small, we suggest that the high correlation is related to the resuspension of MP to the sea surface layer. Correlation further off the sources was weaker due to the impact of marine processes, e.g., biofouling and vertical mixing, which could have a different effect on the fibers and fragments.

The MP fragments were mostly white, blue/green, and gray/black, whereas MP fibers were mostly gray/black and blue/green in the current study. This result is consistent with other studies where MP fragments and MP fibers were reported (Zhang et al., 2017; Karlsson et al., 2020; Aigars et al., 2021). The share between the two size classes 330–999 μm and 1,000–4,999 μm was 75% and 25%, respectively. The higher number of particles with decreasing size has been documented earlier in the eastern Baltic Sea (Setälä et al., 2016; Aigars et al., 2021).

The mean concentration was higher in autumn than in summer in all regions and stations. This seasonal signal is likely related to the biofouling and consequent sinking of the MP (Kaiser et al., 2017). Spring and summer are biologically active seasons in the Baltic Sea (Lips et al., 2014; Kahru et al., 2016; Purina et al., 2018). Decay and deepening of the seasonal thermocline and cooling of the upper mixed layer water start in

the second half of August in the eastern Baltic Sea (Liblik and Lips, 2011; Skudra and Lips, 2017), which leads to the decrease of organic matter production (e.g., Gasiūnaitė et al., 2005), reduced biofouling, and consequently declined sinking rate of the MP. Moreover, the density of the upper mixed layer increases in autumn, which increases the buoyancy of the MP and reduces the sinking probability as well.

The shorter-term and smaller-scale spatial variability of the MP concentration in the sea surface is shaped by various processes such as advection, divergence, convergence, and vertical mixing (Auta et al., 2017; Lebreton et al., 2018; Zhang et al., 2020). The wind mixing distributes the MP vertically (Kukulka et al., 2012); thus, the MP concentration in the surface layer and wind speed can be negatively correlated (e.g., Schönlau et al., 2020). We found a significant negative, but weak correlation between the wind speed and the MP concentration only at offshore station 14.

The highest concentrations of the MP at the coast of Narva Bay were observed during the downwelling event while the lowest value was detected during the coastal upwelling event. There was a 60-fold difference between the highest and lowest case. The low values during upwelling can be explained by the subsurface origin of the water. The upwelling water originates from the cold intermediate layer in the GOF (Lips et al., 2009). The downwelling causes convergence of the upper layer water and the upper mixed layer in summer could deepen over 40 m (Liblik et al., 2017). Despite the downward movement, the buoyant-enough particles tend to stay at the surface and accumulate (Kooi et al., 2016; Waldschläger and Schüttrumpf, 2019). Thus, in the enclosed sea, where wind from any direction causes downwelling/upwelling along some coastal sections (Myrberg and Andrejev, 2003), the coastal mesoscale processes can potentially cause remarkable variability in the MP concentrations. Moreover, mesoscale eddies could redistribute the MP. The anticyclonic eddies converge the debris, and thus, concentrations there can be much higher compared to cyclonic eddies as shown in other areas (Brach et al., 2018). It is probable that the submesoscale processes, which are evident in the observations (e.g., Lips et al., 2016) and which converge and diverge tracers according to simulations (e.g., Zhurbas et al., 2022) in the smaller spatiotemporal scale, affect the MP concentrations and pathways as well in the Baltic Sea. Our samples were collected along a 1- to 4-km long line; thus, to study the MP in the submesoscale in more detail, other measurement methods, e.g., in situ pumping (Karlsson et al., 2020), should be implemented.

CONCLUSIONS

The dataset analyzed in the present study provides the first view on MP pollution and its spatiotemporal variability in the surface water of the eastern Baltic Sea. MPs were found in all 122 samples, and their concentration varied from 0.01 to 2.45 counts/m³ with a mean concentration of 0.49 counts/m³. The obtained concentration ranges, the share of the MP fragments

and fibers, and the color composition of MPs generally agree with previous studies in the neighboring areas. The regional differences in the mean MP concentrations in the GOF, GOR, and Väinameri Archipelago Sea are likely related to the human pressure (population) in the catchment areas. The seasonal increase in the concentration from summer to autumn can likely be explained by the decline in the biofouling in autumn and related decrease in the sinking rate of particles.

The high variability in the observations was probably the result of multiple processes, which could not be fully captured by the design of the monitoring program. However, we managed to show that upwellings and downwellings, and wind mixing play a role in the variability of the sea surface MP concentration. It is likely that other (sub)mesoscale processes alter the MP concentrations in the surface layer as well. To improve the knowledge on the pathways of the MPs, the processes in the (sub)mesoscale from the sources to offshore should be addressed by further dedicated observational and modeling studies. Likewise, the measurement and modeling effort to estimate the land–sea and water column–sediment fluxes of MPs should be sought.

DATA AVAILABILITY STATEMENT

The raw data supporting the conclusions of this article will be made available by the authors, without undue reservation. The whole dataset is available *via* EMODnet Chemistry and Estonian Environmental Database (KESE).

AUTHOR CONTRIBUTIONS

AM: Conceptualization, Data curation, Formal analysis, Methodology, Validation, Software, Visualization, and Writing—original draft. NB and KL: Methodology, Data curation, Writing—original draft, and Resources. IL: Conceptualization, Resources, Validation, Writing—review and editing. TL: Conceptualization, Data curation, Visualization, Validation, and Writing—review and editing. GV: Conceptualization, Data curation, Validation, Software, Visualization, and Writing—review and editing. UL: Conceptualization, Methodology, Formal analysis, Visualization, Validation, and Writing—review and editing. All authors contributed to the article and approved the submitted version.

FUNDING

ACKNOWLEDGMENTS

SUPPLEMENTARY MATERIAL

The Supplementary Material for this article can be found online at: https://www.frontiersin.org/articles/10.3389/fmars.2022.875984/full#supplementary-material

REFERENCES

Adamopoulou, A., Zeri, C., Garaventa, F., Gambardella, C., Loakeimidis, C., and Pitta, E. (2021). Distribution Patterns of Floating Microplastics in Open and Coastal Waters of the Eastern Mediterranean Sea (Ionian, Aegean, and Levantine Seas). *Front. Mar. Sci.* 8. doi: 10.3389/fmars.2021.699000. ISSN 2296-7445.

Aigars, J., Barone, M., Suhareva, N., Putna-Nimane, I., and Dimante-Deimantovica, I. (2021). Occurrence and Spatial Distribution of Microplastics in the Surface Waters of the Baltic Sea and the Gulf of Riga. *Mar. Pollut. Bull.* 172, 1–10. doi: 10.1016/j.marpolbul.2021.112860

Alenius, P., Myrberg, K., and Nekrasov, A. (1998). The Physical Oceanography of the Gulf of Finland: A Review. *Boreal Environ. Res.* 3, 97–125.

Andrady, A. L. (2011). Microplastics in the Marine Environment. *Mar. Pollut. Bull.* 62, 1596–1605. doi: 10.1016/j.marpolbul.2011.05.030. ISSN 0025-326X.

Andrejev, O., Sokolov, A., Soomere, T., Värv, R., and Viikmäe, B. (2010). The Use of High-Resolution Bathymetry for Circulation Modelling in the Gulf of Finland. *Est. J. Eng.* 16 (3), 187. doi: 10.3176/eng.2010.3.01

Arthur, C., Baker, J., and Bamford, H. (2009). *Proceedings of the International Research Workshop on the Occurrence, Effects, and Fate of Microplastic Marine Debris. National Oceanic and Atmospheric Administration Technical Memorandum Nos-or&R-30.* Silver Spring, MD, USA: NOAA Marine Debris Division.

Auta, H. S., Emenike, C. U., and Fauziah, S. H. (2017). Distribution and Importance of Microplastics in the Marine Environment: A Review of the Sources, Fate, Effects, and Potential Solutions. *Environ. Int.* 102, 165–176. doi: 10.1016/j.envint.2017.02.013

Bagaev, A., Mizyuk, A., Khatmullina, L., Isachenko, I., and Chubarenko, I. (2017). Anthropogenic Fibers in the Baltic Sea Water Column: Field Data, Laboratory and Numerical Testing of Their Motion. *Sci. Total Environ.* 599–600, 560–571. doi: 10.1016/j.scitotenv.2017.04.185. ISSN 0048-9697.

Bai, M., Zhu, L., An, L., Peng, G., and Li, D. (2018). Estimation and Prediction of Plastic Waste Annual Input Into the Sea From China. *Acta Oceanol. Sin.* 37, 26–39. doi: 10.1007/s13131-018-1279-0

Boucher, J., and Friot, D. (2017). *Primary Microplastics in the Oceans: A Global Evaluation of Sources.* Gland, Switzerland: IUCN. doi: 10.2305/IUCN.CH.2017.01.en

Brach, L., Deixonne, P., Bernard, M. F., Durand, E., Desjean, M. C., Perez, E., et al. (2018). Anticyclonic Eddies Increase Accumulation of Microplastic in the North Atlantic Subtropical Gyre. *Mar. Pollut. Bull.* 126, 191–196. doi: 10.1016/j.marpolbul.2017.10.077

Burchard, H., and Bolding, K. (2002). *Getm – A General Estuarine Transport Model. Scientific Documentation. Tech Rep EUR 20253 En* (Ispra: press. Copernicus Marine Service). Available at: https://resources.marine.copernicus.eu/products.

Canuto, V. M., Howard, A., Cheng, Y., and Dubovikov, M. S. (2001). Ocean Turbulence. Part I: One-point Closure Model—Momentum and Heat Vertical Diffusivities. *J. Phys. Oceanography* 31 (6), 1413–1426. doi: 10.1175/1520-0485 (2001)031<1413:OTPIOP>2.0.CO;2

Cole, M., Lindeque, P., Halsband, C., and Galloway, T. S. (2011). Microplastics as Contaminants in the Marine Environment: A Review. *Mar. Pollution Bull.* 62 (12), 2588–2597. doi: 10.1016/j.marpolbul.2011.09.025. ISSN 0025-326X.

Collignon, A., Hecq, J. H., Galgani, F., Collard, F., and Goffart, A. (2014). Annual Variation in Neustonic Micro- and Meso-Plastic Particles and Zooplankton in the Bay of Calvi (Mediterranean-Corsica). *Mar. Pollut. Bull.* 79 (1-2), 293–298. doi: 10.1016/j.marpolbul.2013.11.023

Devriese, L., De Witte, B., Bekaert, K., Hoffman, S., Vandermeersch, G., Cooreman, K., et al. (2014). Quality Assessment of the Blue Mussel (Mytilusedulis): Comparison Between Commercial and Wild Types. *Mar. Pollut. Bull.* 85 (1), 146–155. doi: 10.1016/j.marpolbul.2014.06.006

Eriksen, M., Mason, S., Wilson, S., Box, C., Zellers, A., Edwards, W., et al. (2013). Microplastic Pollution in the Surface Waters of the Laurentian Great Lakes. *Mar. Pollut. Bull.* 77 (1-2), 177–182. doi: 10.1016/j.marpolbul.2013.10.007

Flather, R. A. (1994). A Storm Surge Prediction Model for the Northern Bay of Bengal With Application to the Cyclone Disaster in April 1991. *J. Phys. Oceanography* 24 (1), 172–190. doi: 10.1175/1520-0485(1994)024<0172: ASSPMF>2.0.CO;2

Gago, J., Portela, S., Filgueiras, A. V., Salinas, M. P., and Macías, D. (2019). Ingestion of Plastic Debris (Macro and Micro) by Longnose Lancetfish (Alepisaurus Ferox) in the North Atlantic Ocean Reg. *Stud. Mar. Sci.* 33, 100977. doi: 10.1016/j.rsma.2019.100977

Galgani, F., Giorgetti, A., Vinci, M., Moigne, M., Moncoiffe, G., Brosich, A., et al. (2020). *Proposal for Gathering and Managing Data Sets on Marine Micro-Litter on a European Scale.* (Belgium: EMODnet Oostende). 34 pp. doi: 10.6092/8ce4e8b7-f42c-4683-9ece-c32559606dbd

Gasiūnaitė, Z. R., Cardoso, A., Heiskanen, A., Henriksen, P., Kauppila, P., Olenina, I., et al. (2005). Seasonality of Coastal Phytoplankton in the Baltic Sea: Influence of Salinity and Eutrophication. *Estuarine Coastal Shelf Sci.* 65, 239–252. doi: 10.1016/j.ecss.2005.05.018

GESAMP (2019). Guidelines on the Monitoring and Assessment of Plastic Litter and Microplastics in the Ocean. *GESAMP Rep. Stud. Ser.* 99, 130.

Gewert, B., Ogonowskia, M., Barth, A., and MacLeoda, M. (2017). Abundance and Composition of Near Surface Microplastics and Plastic Debris in the Stockholm Archipelago, Baltic Sea. *Mar. Pollut. Bull.* 120, 292–302. doi: 10.1016/j.marpolbul.2017.04.062

Gräwe, U., Naumann, M., Mohrholz, V., and Burchard, H. (2015). Anatomizing One of the Largest Saltwater Inflows Into the Baltic Sea in December 2014. *J. Geophys Res. Ocean* 120 (11), 7676–7697. doi: 10.1002/2015JC011269

He, P., Chen, L., Shao, L., Zhang, H., and Lü, F. (2019). *Municipal Solid Waste (MSW) Landfill: A Source of Microplastics? -Evidence of Microplastics in Landfill Leachate, Water Research*, Vol. Volume 159. Pages 38–45 ELSEVIER. doi: 10.1016/j.watres.2019.04.060

HELCOM (2004). The Fourth Baltic Sea Pollution Load Compilation (Plc-4). *Baltic Sea Environ. Proc. No* 93, 1–189.

Hersbach, H. (2020). The ERA5 Global Reanalysis. *Q. J. R. Meteorol. Soc.* 146.730, 1999–2049. doi: 10.1002/qj.3803

Hidalgo-Ruz, V., Gutow, L., Thompson, R. C., and Thiel, M. (2012). Microplastics in the Marine Environment: A Review of the Methods Used for Identification and Quantification. *Environ. Sci. Technol. 46 (2012)* pp, 3060–3075. doi: 10.1021/es2031505

Hofmeister, R., Burchard, H., and Beckers, J. M. (2010). *Non-Uniform Adaptive Vertical Grids for 3D Numerical Ocean Models, Ocean Modelling*, Vol. Volume 33. ELSEVIER. doi: 10.1016/j.ocemod.2009.12.003

Jambeck, J. R., Geyer, R., Wilcox, C., Siegler, T. R., Perryman, M., Andrady, A., et al. (2015). Marine Pollution. *Plast. Waste Inputs Land. Into Ocean Sci.* 347, 768–771. doi: 10.1126/science.1260352

Janssen, F., Schrum, C., and Backhaus, J. O. (1999). A Climatological Data Set of Temperature and Salinity for the Baltic Sea and the North Sea. *Dtsch. Hydrogr. Z.* 51 (S9), 5–245. doi: 10.1007/BF02933676

Johansson, L., and Jalkanen, J. P. (2016). *Emissions From Baltic Sea Shipping in 2015* (HELCOM: Baltic Sea Environment Fact Sheets).

Kahru, M., Elmgren, R., and Savchuk, O. P. (2016). Changing Seasonality of the Baltic Sea. *Biogeosciences* 13, 1009–1018. doi: 10.5194/bg-13-1009-2016

Kaiser, D., Kowalski, N., and Waniek, J. J. (2017). Effects of Biofouling on the Sinking Behavior of Microplastics. *Environ. Res. Lett.* 12, 1–12. doi: 10.1088/1748-9326/aa8e8b

Karlsson, T. M., Kärrman, A., Rotander, A., and Hasselöv, M. (2020). Comparison Between Manta Trawl and *In Situ* Pump Filtration Methods, and Guidance for Visual Identification of Microplastics in Surface Waters. *Environ. Sci. Pollut. Res.* 27, 5559–5571. doi: 10.1007/s11356-019-07274-5

Kooi, M., Reisser, J., Slat, B., Ferrari, F., Schmid, M., Cunsolo, S., et al. (2016). The Effect of Particle Properties on the Depth Profile of Buoyant Plastics in the Ocean. *Sci. Rep.* 6, 1–10. doi: 10.1038/srep33882

Kukulka, T., Proskurowski, G., Morét, S., Meyer, D., and Law, K. (2012). The Effect of Wind Mixing on the Vertical Distribution of Buoyant Plastic Debris. *Geophysical Res. Lett.* 39, L07601. doi: 10.1029/2012GL051116

Lebreton, L., Slat, B., and Ferrari, F. (2018). Evidence That the Great Pacific Garbage Patch Is Rapidly Accumulating Plastic. *Sci. Rep.* 8, 4666. doi: 10.1038/s41598-018-22939-w

Leppäranta, M., and Myreberg, K. (2009). *Physical Oceanography of the Baltic Sea* (Berlin, Heidelberg: Springer Berlin Heidelberg). doi: 10.1007/978-3-540-79703-6

Liblik, T., and Lips, U. (2011). Characteristics and Variability of the Vertical Thermohaline Structure in the Gulf of Finland in Summer. *Boreal Environ. Res.* 16, 73–83.

Liblik,, Taavi,, Lips,, and Urmas, (2017). Variability of Pycnoclines in a Three-Layer, Large Estuary: The Gulf of Finland. *Boreal Environ. Res.* 22, 27–47.

Liblik, T., Väli, G., Lips, I., Lilover, M. J., Kikas, V., and Laanemets, J. (2020). The Winter Stratification Phenomenon and Its Consequences in the Gulf of Finland, Baltic Sea. *Ocean Sci.* 16, 1475–1490. doi: 10.5194/os-16-1475-2020

Liblik, T., Väli, G., Salm, K., Laanemets, J., Lilover, M.-J., and Lips, U. (2022). Quasi-Steady Circulation Regimes in the Baltic Sea. *Ocean Sci. Discuss*. doi: 10.5194/os-2021-123

Lips, U., Kikas, V., Liblik, T., and Lips, I. (2016). Multi-Sensor in Situ Observations to Resolve the Sub-Mesoscale Features in the Stratified Gulf of Finland, Baltic Sea. *Ocean Sci.* 12, 715–732. doi: 10.5194/os-12-715-2016

Lips, I., Lips, U., and Liblik, T. (2009). Consequences of Coastal Upwelling Events on Physical and Chemical Patterns in the Central Gulf of Finland (Baltic Sea). *Continental Shelf Res.* 29, 1836–1847. doi: 10.1016/j.csr.2009.06.010

Lips, I., Rünk, N., Kikas, V., Meerits, A., and Lips, U. (2014). High-Resolution Dynamics of the Spring Bloom in the Gulf of Finland of the Baltic Sea. *J. Mar. Syst.* 129, 135–149, 129. doi: 10.1016/j.jmarsys.2013.06.002. ISSN 0924-7963.

Lips, U., Zhurbas, V., Skudra, M., and Väli, G. (2016). A Numerical Study of Circulation in the Gulf of Riga, Baltic Sea. Part I: Whole-Basin Gyres and Mean Currents. *Cont Shelf Res.* 112, 1–13. doi: 10.1016/j.csr.2015.11.008

Lithner, D. (2011). *Environmental and Health Hazards of Chemicals in Plastic Polymers and Products* (Gothenburg: University of Gothenburg).

Liu, K., Wang, X., Wei, N., Song, Z., and Li, D. (2019). Accurate Quantification and Transport Estimation of Suspended Atmospheric Microplastics in Megacities: Implications for Human Health. *Environ. Int.* 132, 105127. doi: 10.1016/j.envint.2019.105127. ISSN 0160-4120.

Li, C., Wang, X., Liu, K., Zhu, L., Wei, N., Zong, C., et al. (2021). Pelagic Microplastics in Surface Water of the Eastern Indian Ocean During Monsoon Transition Period: Abundance, Distribution, and Characteristics. *Sci. Total Environ.* 755, 755. doi: 10.1016/j.scitotenv.2020.142629

Lusher, A., Hollman, P., and Mendoza-Hill, J. (2017). *Microplastics in Fisheries and Aquaculture: Status of Knowledge on Their Occurrence and Implications for Aquatic Organisms and Food Safety* (Rome, Italy: FAO Fisheries and Aquaculture Technical Paper).

Lusher, A., Tirelli, V., O'Connor, I., and Officer, R. (2015). Microplastics in Arctic Polar Waters: The First Reported Values of Particles in Surface and Sub-Surface Samples. *Sci. Rep.* 5, 14947. doi: 10.1038/srep14947

Männik, A., and Merilain, M. (2007). Verification of Different Precipitation Forecasts During Extended Winter-Season in Estonia. *HIRLAM Newslett.* 52, 65–70. doi: 10.1126/science.1260352

Martyanov, S., Isaev, A., and Ryabchenko, V. (2021). Model Estimates of Microplastic Potential Contamination Pattern of the Eastern Gulf of Finland in 2018. *Oceanologia*, in press. doi: 10.1016/j.oceano.2021.11.006. ISSN 0078-3234.

Mato, Y., Isobe, T., Takada, H., Kanehiro, H., Ohtake, C., and Kaminuma, T. (2001). Plastic Resin Pellets as a Transport Medium for Toxic Chemicals in the Marine Environment. *Environ. Sci. Technol* 35, 318–324. doi: 10.1021/es0010498

Myrberg, K., and Andrejev, O. (2003). Main Upwelling Regions in the Baltic Sea – a Statistical Analysis Based on Three-Dimensional Modelling. *Boreal Environ. Res.* 8, 97–112. ISSN 1239-6095.

Pan, Z., Guo, H., Chen, H., Wang, S., Sun, X., Zou, Q., et al. (2019). Microplastics in the Northwestern Pacific: Abundance, Distribution, and Characteristics. *Sci. Total Environ.* 650, 1913–1922. doi: 10.1016/j.scitotenv.2018.09.244

Placke, M., Meier, M., Gräwe, U., Neumann, T., Frauen, C., and Liu, Y. (2018). Long-Term Mean Circulation of the Baltic Sea as Represented by Various Ocean Circulation Models. *Front. Mar. Sci.* 5. doi: 10.3389/fmars.2018.00287. ISSN- 2296-7745.

Plastics Europe (2020) *Plastics-the Facts 2020. An Analysis of European Plastics Production, Demand and Waste Data*. Available at: https://www.plasticseurope.org/en/resources/publications/4312-plastics-facts-2020.

Purina, I., Labucis, A., Barda, I., Jurgensone, I., and Aigars, J. (2018). Primary Productivity in the Gulf of Riga (Baltic Sea) in Relation to Phytoplankton Species and Nutrient Variability. *Oceanologia* 60, 544–552. doi: 10.1016/j.oceano.2018.04.005

Schönlau, C., Karlsson, T., Rotander, A., Nilsson, H., Engwall, M., Bavel, B., et al. (2020). Microplastics in Sea-Surface Waters Surrounding Sweden Sampled by Manta Trawl and in-Situ Pump. *Mar. Pollut. Bull.* 153, 1–8. doi: 10.1016/j.marpolbul.2020.111019

Schulzweida, U. (2021). *Cdo User Guide (Version 2.0.0)* (Hamburg: Zenodo). doi: 10.5281/zenodo.5614769

Setälä, O., Magnusson, K., Lehtiniemi, M., and Norén, F. (2016). Distribution and Abundance of Surface Water Microlitter in the Baltic Sea: A Comparison of Two Sampling Methods. *Mar. Pollut. Bull.* 110, 177–183. doi: 10.1016/j.marpolbul.2016.06.065

Skudra, M., and Lips, U. (2017). Characteristics and Inter-Annual Changes in Temperature, Salinity and Density Distribution in the Gulf of Riga. *Oceanologia* 59, 37–48. doi: 10.1016/j.oceano.2016.07.001. ISSN 0078-3234.

Smagorinsky, J. (1963). General Circulation Experiments With the Primitive Equation I the Basic Experiment. *Monthly Weather Rev.* 91, 99–164. doi: 10.1175/1520-0493(1963)091<0099:GCEWTP>2.3.CO;2

Tamminga, M., Hengstmann, E., and Fischer, E. K. (2018). Microplastic Analysis in the South Funen Archipelago, Baltic Sea, Implementing Manta Trawling and Bulk Sampling. *Mar. Pollut. Bulletin* 128, 601–608. doi: 10.1016/j.marpolbul.2018.01.066

Tamminga, M., Stoewer, S. C., and Fischer, E. K. (2019). On the Representativeness of Pump Water Samples Versus Manta Sampling in Microplastic Analysis. *Environ. Pollut.* 254 (Pt A), 112970. doi: 10.1016/j.envpol.2019.112970

Teuten, E. L., Saquing, J. M., Knappe, D. R., Barlaz, M. A., Jonsson, S., Björn, A., et al. (2009). Transport and Release of Chemicals From Plastics to the Environment and to WildlifePhilosophical Transactions of the Royal Society B. *Biol. Sci.* 364 (1526), 2027–2045. doi: 10.1098/rstb.2008.0284

Tsiaras, K., Hatzonikolakis, Y., Kalaroni, S., Pollani, A., and Triantafyllou, G. (2021). Modeling the Pathways and Accumulation Patterns of Micro- and Macro-Plastics in the Mediterranean. *Front. Mar. Sci.* 8. doi: 10.3389/fmars.2021.743117. ISSN 2296-7745.

Umlauf, L., and Burchard, H. (2005). Second-Order Turbulence Closure Models for Geophysical Boundary Layers. A Review of Recent Work. *Cont Shelf Res.* 25 (7–8), 795–827. doi: 10.1016/j.csr.2004.08.004

Uurasjärvi, E., Pääkkönen, M., Setälä, O., Koistinen, A., and Lehtiniemi, M. (2021). Microplastics Accumulate to Thin Layers in the Stratified Baltic Sea. *Environ. Pollut.* 268, 1–9. doi: 10.1016/j.envpol.2020.115700

Väli, G., and Zhurbas, V. (2021). Seasonality of Submesoscale Coherent Vortices in the Northern Baltic Proper: A Model Study. *Fundamentalnaya I Prikladnaya Gidrofizika* 14, 122—129. doi: 10.7868/S2073667321030114

van Sebille, E., Aliani, S., Law, K., Maximenko, N., Alsina, J. M., Bagaev, V., et al. (2020). The Physical Oceanography of the Transport of Floating Marine Debris. *Environ. Res. Lett.* 15, 023003. doi: 10.1088/1748-9326/ab6d7d

Veerasingam, S., Saha, M., Suneel, V., Vethamony, P., Rodrigues, A., Bhattacharyya, S., et al. (2016). *Characteristics, Seasonal Distribution and Surface Degradation Features of Microplastic Pellets Along the Goa Coast* Vol. Volume 159 (India: Chemosphere), Pages 496–505. ISSN 0045-6535. doi: 10.1016/j.chemosphere.2016.06.056

Waldschläger, K., and Schüttrumpf, H. (2019). Effects of Particle Properties on the Settling and Rise Velocities of Microplastics in Freshwater Under Laboratory Conditions. *Environ. Sci. Technol.* 53, 1958–1966. doi: 10.1021/acs.est.8b06794

Wang, X., Li, C., Liu, K., Zhu, L., Song, Z., and Li, D. (2020). Atmospheric Microplastic Over the South China Sea and East Indian Ocean: Abundance, Distribution and Source. *J. Hazard Mater.* 389, 1–9. doi: 10.1016/j.jhazmat.2019.121846

Wright, S., and Kelly, F. (2017). Plastic and Human Health: A Micro Issue? *Environ. Sci. Technol.* 51 (12), 6634–6647. doi: 10.1021/acs.est.7b00423

Xia, F., Yao, Q., Zhang, J., and Wang, D. (2021). Effects of Seasonal Variation and Resuspension on Microplastics in River Sediments. *Environ. Pollut.* 286, 117403. doi: 10.1016/j.envpol.2021.117403. ISSN 0269-7491.

Yonkos, L., Friedel, E., Perez-Reyes, A., Ghosal, S., and Arthur, C. (2014). Microplastics in Four Estuarine Rivers in the Chesapeake Bay, U.S.A. *Environ. Sci. Tech.* 48 (2014), 14,195–14,202. doi: 10.1021/es5036317

Zeri, C., Adamopoulou, A., Varezić, D. B., Fortibuoni, T., Viršek, M. K., Kržan, A., et al. (2018). Floating Plastics in Adriatic Waters (Mediterranean Sea): From the Macro- to the Micro-Scale. *Mar. Pollution Bull.* 136, 341–350. doi: 10.1016/j.marpolbul.2018.09.016

Zhang, Z., Wu, H., Peng, G., Xu, P., and Li, D. (2020). Coastal Ocean Dynamics Reduce the Export of Microplastics to the Open Ocean. *Sci. Total Environ.* 713, 136634. doi: 10.1016/j.scitotenv.2020.136634. ISSN 0048-9697.

Zhang, W., Zhang, S., Wang, J., Wang, Y., Mu, J., Wang, P., et al. (2017). Microplastic Pollut. in the Surface Waters of the Bohai Sea, China. *Environ. Pollut.* 231, 541–548. doi: 10.1016/j.envpol.2017.08.058

Zhao, S., Zhu, L., and Li, D. (2016). Microscopic Anthropogenic Litter in Terrestrial Birds From Shanghai, China: Not Only Plastics But Also Natural Fibers. *Sci. Total Environ.* 550, 1110–1115. doi: 10.1016/j.scitotenv.2016.01.112

Zhurbas, V., Väli, G., Golenko, M., and Paka, V. (2018). Variability of Bottom Friction Velocity Along the Inflow Water Pathway in the Baltic Sea. *J. Mar. Syst.* 184, 50–58. doi: 10.1016/j.jmarsys.2018.04.008

Zhurbas, V., Väli, G., and Kuzmina, N. (2022). Striped Texture of Submesoscale Fields in the Northeastern Baltic Proper: Results of Very High-Resolution Modelling for Summer Season. *Oceanologia* 64, 1–21. doi: 10.1016/j.oceano.2021.08.003. ISSN 0078-323.

Zhu, L., Zhao, S., Bittar, T. B., Stubbins, A., and Li, D. (2020). Photochemical Dissolution of Buoyant Microplastics to Dissolved Organic Carbon: Rates and Microbial Impacts. *J. Hazardous Mater.* 383, 121065. doi: 10.1016/j.jhazmat.2019.121065

Publication II

Mishra A, Siht E, Väli G, Liblik T, Buhhalko N and Lips U (2025). Mapping microplastic pathways and accumulation zones in the Gulf of Finland, Baltic Sea – insights from modeling. Front. Mar. Sci. 11:1524585. doi: 10.3389/fmars.2024.1524585

Mapping microplastic pathways and accumulation zones in the Gulf of Finland, Baltic Sea – insights from modeling

Arun Mishra*, Enriko Siht, Germo Väli, Taavi Liblik,
Natalja Buhhalko and Urmas Lips

Department of Marine Systems, Tallinn University of Technology, Tallinn, Estonia

A hydrodynamic model coupled with a particle tracking model was used to identify the pathways and accumulation areas of microplastics (MP) in the Gulf of Finland (GoF) over a three-year period (2018-2020). Two key sources, wastewater treatment plants (WWTPs) and rivers, were considered, focusing on polypropylene (PP)/polyethylene (PE) and polyethylene terephthalate (PET) particles sized 20-500 μm. Rivers contribute 76% of total MP entering the gulf, while WWTPs account for the remaining 24%. Most of the MP accumulates inside the gulf and does not drift to the Baltic Proper. The eastern part of the gulf exhibits the highest surface concentrations of particles influenced by the Neva River. In the water column, MP concentrations were notably high in shallow coastal areas, decreasing gradually offshore. Potential MP accumulation zones were identified primarily between longitudes 28°E and 30°E, particularly near the major rivers Narva and Kymi and in the easternmost gulf related to the Neva River discharge. The MP concentrations in the surface layer and water column were higher in winter while settling was more intense in summer. Short-term variability in the surface layer was caused by (sub)mesoscale advection and divergence/convergence, while in the near-bottom layer, strong bottom currents and consequent resuspension elevated the concentrations.

1 Introduction

Microplastics (MP), which are particles smaller than 5 mm, can be found in various aquatic environments, including the oceans, seas, estuaries and rivers (Cole et al., 2011; Jambeck et al., 2015; Setälä et al., 2016; Mishra et al., 2022; Matjašič et al., 2023). The significant increase in plastic production since the early 1970s has raised numerous

concerns about plastic pollution in aquatic systems. It has been estimated that over 170 trillion plastic particles are floating in the world's oceans (Eriksen et al., 2023), and their presence is also increasing in the seabed, coastlines, and marine biota (Barnes et al., 2009; Suaria and Aliani, 2014; Llorca et al., 2020; Matjašič et al., 2023). Despite substantial efforts and initiatives to reduce plastic usage, global annual plastic waste production is projected to continue rising in the coming years. By 2025, the United Nations Sustainable Development Goal 14.1 aims to reduce marine pollution, including plastics.

In Europe, The Marine Strategy Framework Directive (2008/56/EC, European Commission, 2008) (MFSD) identified anthropogenic litter as a dominant pressure and a main source of impact on coastal habitats. The MSFD establishes requirements for the EU (European Union) member states to achieve and maintain a good environmental status in their marine environments, as well as to prevent any future deterioration including the MSFD descriptor D10. In addition, the European Chemical Agency (EGCHA) has proposed restriction of MP in many products within the EU/EEA (European Economic Area) region, with the goal of preventing or minimizing their discharge into the environment (European Chemicals Agency, 2019). In 2021, the European Union also banned single-use plastics within its member states (Harvey and Watts, 2018).

According to GESAMP (2019), the marine environment can be infiltrated by plastic through multiple entry points, including riverine systems, shoreline activities, shipping, and atmospheric deposition. Various studies (Ziajahromi et al., 2016; Mintenig et al., 2017; Kay et al., 2018; Prata, 2018; Schernewski et al., 2020) have highlighted the significant influence of human activities on MP deposition. Among these activities, Wastewater Treatment Plants (WWTPs) are recognized as a significant emission pathway. For example, Municipal WWTPs have shown high efficiency in removing MP (Carr et al., 2016; Talvitie et al., 2017; Gies et al., 2018); however, untreated WWTP effluents exhibit elevated MP concentrations (Sun et al., 2019; Schernewski et al., 2020). Baresel and Olshammar (2019) proposed that MP retention in WWTPs based on their respective treatment stages ranges from 85% to 98% in the Baltic Sea region. Despite this relatively high overall removal efficiency, WWTPs are still considered a significant MP emission pathway in the Baltic Sea region due to the substantial volumes of wastewater they process (Baresel and Olshammar, 2019). In the Baltic Sea, wastewater and stormwater plants are typically separated (Schernewski et al., 2020). Sewer overflows, comprising stormwater and untreated wastewater can substantially contribute to the MP load in the environment (Magnusson, 2016; Dris et al., 2018). During periods of heavy precipitation, stormwater serves as a critical entry point for MP into the aquatic environment. Baresel and Olshammar (2019) suggest that the yearly discharge from sewer overflows is comparable in magnitude to that of treated wastewater.

Several studies have indicated that rivers are a primary source of MP and play a crucial role in transporting plastic waste into oceans (Jambeck et al., 2015; Siegfried et al., 2017; Schrank et al., 2022). Rivers flowing through highly populated cities with significant industrial activity along their banks may serve as an important source of MP in the estuarine bays such as the Gulf of Finland (GoF) in the Baltic Sea (Martyanov et al., 2021). It has been estimated that between 1.15 and 2.41 million tons or more of plastics are deposited annually into oceans via rivers (Lebreton et al., 2017; Schmidt et al., 2017). Numerous studies have discussed the pollution patterns of large rivers and provided insights into the regional and global factors responsible for MP pollution in the water column and sediments (Matjašič et al., 2023). High variability in MP concentration can be seen in both the water column and sediments depending on factors such as sampling methodology, anthropogenic activities and the size of the catchment area (She et al., 2022; Matjašič et al., 2023). Additionally, a significant proportion of marine beach litter is attributed to the input of plastic waste into rivers (Veerasingam et al., 2016). However, it is important to note that this study does not consider river retention in its analysis.

The Baltic Sea, located in northern Europe, is known as one of the largest brackish water bodies in the world (HELCOM, 2023). With a catchment area four time larger than its surface area (372,858 km^2) (Marko and Urs, 2013) and an average depth of 55m, the Baltic Sea faces significant challenges related to marine litter (HELCOM, 2023). Coastal areas along the Baltic Sea exhibit significant concentration of beach litter (HELCOM, 2023). Plastic materials make up the most frequently encountered marine litter in the Baltic Sea (HELCOM, 2023). As of 2023, HELCOM's aim to substantially decrease plastic waste and mitigate its harmful effects on coastal and marine ecosystems remains unfulfilled (HELCOM, 2023). The Baltic Sea receives a substantial volume of water from various rivers, with an average combined flow rate of approximately 14,085 m^3/s (Meier and Kauker, 2003). Due to the extended residence time of pollutants in the Baltic Sea during the water renewal period, which can last up to 30 years (Leppäranta and Myrberg, 2009), the pollutants present in the Baltic Sea have a significant impact on the aquatic environment. Consequently, it is reasonable to assume that the Baltic Sea serves as a major hotspot for plastics, primarily through river discharge. Large impacts of riverine inputs as critical pathways for plastics into marine environments has also been identified in other parts of the world (Vianello et al., 2018; Uaciquete et al., 2024).

The GoF is an elongated estuarine basin situated in the northeastern region of the Baltic Sea with an average depth of 37 m and a maximum depth of 123 m (Leppäranta and Myrberg, 2009). The gulf stretches approximately 400 km in length, with a width that varies between 48 and 135 km (Alenius et al., 1998). There is a free water exchange between the GoF and BP at the western border, and fresh water is discharged mostly to the eastern part of the GoF. Several studies have reported the presence of MP in the GoF (Lips et al., 2020; Setälä et al., 2016; Uurasjärvi et al., 2021; Mishra et al., 2022). However, the knowledge about the spatial and temporal variation of MPs in the Baltic Sea is limited (Aigars et al., 2021). In addition, the methodology for acquiring information about MPs can vary based on the instruments utilized, mesh size, sampling depth, and the extent of the sampling area (Mishra et al., 2022; She et al., 2022).

Modeling the movement and fate of MP is particularly relevant in semi-enclosed systems like the Gof, where limited exchange and localized inputs contribute to accumulation of marine debris (Tsiaras et al., 2021). Eulerian and Lagrangian models are

commonly used in such simulations (Bigdeli et al., 2022). Lagrangian modeling, also known as particle tracking modeling, tracks individual particles (Siht et al., 2025, in press), while an Eulerian approach considers advection and diffusion at specific locations (Bigdeli et al., 2022). Pärn et al. (2023) employed a combination of a hydrodynamic model and a particle tracking model to understand the transport and fate of marine litter including accumulation areas in the Baltic Sea. Martyanov et al. (2023) considered different initial fall velocities of suspended MP to study their distribution in the eastern GoF. Schernewski et al. (2021) incorporated emission scenarios from WWTPs and combined sewerage plants into their model to estimate the fate of plastics in the Baltic Sea environment. The GETM (General Estuarine Transport Model) ocean circulation model has been utilized in several studies, including those conducted by Schernewski et al. (2021) and Osinski et al. (2020), to analyze the transportation of MP in the Baltic Sea. However, these studies did not include the impact of biofouling on the buoyancy of floating MP and their removal process through sinking and sedimentation (Osinski et al., 2020; Schernewski et al., 2021). Modeling studies in the Baltic Sea (Martyanov et al., 2021; Frishfelds et al., 2022; Murawski et al., 2022), North Sea (Cuttat, 2018), and Mediterranean Sea (Tsiaras et al., 2021) have incorporated biofouling of MP particles that is important to simulate their fate in the marine environment accurately (Murawski et al., 2022).

The objective of this study is to provide an overview of the pathways and accumulation areas of MP in the GoF using a multi-year high-resolution model simulation and realistic loads from the rivers and WWTPs. We chose Lagrangian particle tracking model approach, describing MP as Super-Individuals (SI; (Scheffer et al., 1995) to improve computational efficiency, with each SI representing a group of particles. We have also conducted a series of sensitivity experiments aimed at gaining a deeper insight into the impact of various processes, such as mixing, beaching, resuspension, and biofouling (Siht et al., 2025, in press). In the present study, a 3-year model simulation was conducted to identify potential MP accumulation patterns in the surface layer, water column and sediments.

The paper is organized as follows: it begins with a description of the hydrodynamic model, biogeochemistry model, and Lagrangian particle tracking model, along with MP input data sets. It is followed by an analysis of the model results, aiming to uncover the MP pathways and accumulation areas in the GoF. Finally, the results are discussed, and conclusions are derived.

2 Materials and methods

2.1 Hydrodynamic model and setup

General Estuarine Transport Model (GETM) (Burchard and Bolding, 2002) has been used to simulate the circulation and density fields of the Baltic Sea and GoF in this study. GETM is a hydrostatic, three-dimensional primitive equation model that has embedded adaptive vertical coordinates (Hofmeister et al., 2010; Klingbeil et al., 2018), which significantly reduces the numerical mixing in the

simulations (Gräwe et al., 2015). The vertical mixing (viscosity and diffusion) in the GETM is calculated with two equation k-ε model via coupling with General Ocean Turbulence Model (GOTM) (Burchard, 2001; Canuto et al., 2001) and the sub-grid horizontal mixing with Smagorinsky parameterization (Smagorinsky, 1963).

The biogeochemistry model ERGOM (Neumann et al., 2002; Neumann and Schernewski, 2008) is coupled with the hydrodynamic model via Framework Aquatic Biogeochemical Models (FABM; Bruggeman and Bolding, 2014) and has been used to calculate the chlorophyll-a concentration for biofouling of MP in the Gulf of Finland. In short, ERGOM has 12 state variables and describes a nitrogen and phosphorus cycle, although part of the phosphorus is considered with the N:P ratio (Redfield, 1934). More details about the ERGOM model can be found from in (Radtke et al., 2019; Neumann et al., 2022) and references therein.

We are using a three-level nested modelling system. The whole Baltic Sea has been simulated with a horizontal grid step of 1 nautical mile (approximately 1852 m) and 50 adaptive vertical layers (Gräwe et al., 2015). Medium-resolution model based on the settings described in Zhurbas et al. (2018) and Liblik et al. (2020, 2022) has a horizontal grid spacing of 0.5 nautical miles and covers the central Baltic Proper along with the Gulf of Finland and the Gulf of Riga. The high-resolution model covers the Gulf of Finland and has a horizontal grid spacing of 0.125 nautical miles. The number of adaptive layers in medium- and high-resolution runs is 60. Spatially interpolated results with hourly resolution from the coarse-resolution model are used for the boundary conditions in the medium-resolution model and from the medium-resolution model are used for the boundary conditions in the high-resolution model.

Atmospheric forcing at the sea surface (wind stress and heat flux) is calculated offline from the ERA5 re-analysis (Hersbach et al., 2020). Freshwater input to the models is based on the runoff data compiled for the Baltic Model Intercomparison Project (Gröger et al., 2022) by Väli et al. (2019) and Estonian rivers have been corrected by the input estimates from EstModel (https://estmodel.app/en/#/estimates, last access 10.09.2023).

The simulation period for the high-resolution model was from 2018 to mid-2021. The runs were initially started from a motionless state, i.e. current velocity components and sea surface height were set to zero. Previous studies have shown that the adjustment of the wind-driven circulation in the Baltic Sea takes only a few days (e.g. Krauss and Brügge, 1991; Lips et al., 2016).

For more details of the model setup and validation, the reader is referred to (Siht et al 2025, in press).

2.2 Lagrangian particle model

We employed the Lagrangian particle tracking model described by (Siht et al 2025, in review) to track virtual MP particles. The particle tracking model used the 12-hour 3-dimensional output of the high-resolution GETM setup for particle transport. Beyond advection, our model accounted for several additional processes: 1) dispersion, 2) beaching, 3) biofouling, and 4) resuspension.

Our model computed the horizontal diffusion coefficient for particle dispersion based on the current shear velocity, following the Smagorinsky method (Smagorinsky, 1963). Here, we set the Smagorinsky coefficient C_s to 0.2.

Beaching was implemented through a timer-based approach, where particles became beached after a specified duration in the beach zone. In our simulations, all particle types shared a uniform beaching time of 10 days. The beaching zone was defined as the sea cell nearest to the shoreline (i.e., 250m). Resuspension from beaches was not implemented, i.e., once beached, the particle remained still and was effectively removed from the simulation.

Following Murawski et al. (2022), biofouling is described as a saturated growth process that depends on the maximum biofilm thickness and the growth time scale. The biofouling process was initiated when chlorophyll-a concentration exceeded 1.1 mg m^{-3}. In the current simulations, the maximum biofilm thickness was set to 6.7% of the initial particle radius, and the growth time scale was set to 20 days.

Negatively buoyant particles could settle and be resuspended when the critical shear velocity was exceeded. The vertical velocity gained from resuspension was proportional to the local bottom friction velocity.

The simulation period for the particle tracking model was from 2018-02-05 to 2021-01-01. New particle coordinates were calculated with a time step of 600 seconds. At each time step, the current velocity components (and other hydrological parameters) were interpolated in time and space to the exact particle locations. The particle coordinates were saved at 12-hour intervals. A total of approximately 146 million particles were released during the simulation.

2.2.1 Calculations

The concentrations of MP particles in the surface layer were defined for the water layer from the sea surface to the geopotential height of -1 m. The water column was defined as extending from the sea surface to the uppermost layer of the seabed, and the concentrations were integrated over the entire column. The meridionally integrated values refer to the temporal average of integrated values from south to north, which essentially describes the cross-sectional profile of the entire model domain. All mean concentration fields were spatially smoothed with a 2.5 km window to reduce the high-frequency variability. The size of the window aligns with the local baroclinic Rossby radius of approximately 2-4 km (Alenius et al., 2003). The results presented in the current study are based on two model years (2019-2020) after a spin-up period of one year.

2.3 Emission scenarios

2.3.1 Microplastics sources and emission calculations

The fate of MP in the marine environment relies heavily on the density of plastics. Density serves as a determining factor in classifying plastics into two main categories: floating and sinking types. Floating plastics consist of high- and low-density polyethylene (PE) with a density range of 915–970 kg/m^3, as well

as polypropylene (PP) with a density range of 890–920 kg/m^3 (Schernewski et al., 2020). Sinking plastics include rigid polyvinyl chloride (PVC) with a density range of 1300–1450 kg/m^3 and polyethylene terephthalate (PET) with a density of 1380 kg/m^3 (Schernewski et al., 2020). PP, PE, and PET are the most prevalent plastics observed in aquatic environments (Kooi and Koelmans, 2019). In this study, two main sources of plastics were considered:

a. MP inputs from WWTPs were estimated based on the study by Schernewski et al. (2020). The MP load into the GoF catchment (Figures 1A, B) was calculated using treated wastewater discharge data and particle concentrations in raw water. The average minimum and maximum MP concentrations in raw wastewater were based on literature (Schernewski et al., 2020), and we considered maximum MP concentrations (Figure 1C), and river retention was not taken into consideration.

b. MP inputs from rivers were selected as another major source of marine plastic pollution because they are responsible for a high level of land-based sources, such as mismanaged waste (Jambeck et al., 2015). The variability in observed MP concentrations in rivers is notable (Constant et al., 2020) partly caused by the choice of sampling method, the type of instrument used, the lower size limit of MPs being sampled, the season during which sampling takes place, and the specific processing and analysis methods employed. According to Schrank et al. (2022), surface water samples from the Danube River had an average concentration of 48.7 particles/m^3. The average concentration of plastic in the Têt River was 42 particles/m^3 (Constant et al., 2020), while the Narva River had an average of 47 particles/m^3 (Lips et al., 2020). Based on the above literature and assuming that only a quarter comes from WWTPs (Schernewski et al., 2020), in this study, we considered the MP amount in the rivers (without contribution of WWTPs) to be 35 particles/m^3. We calculated the daily load of MP from river sources (particles/day) by multiplying the concentration of 35 particles/m^3 by the river discharge in the GoF (Figure 1D).

The floating and sinking behavior of MP is not only determined by their density but is also influenced by their size and shape. In our study, we focused on MP with a size range of 20–500 μm, which we divided into two classes: 20-200 and 200-500 μm. Based on Schernewski et al. (2021) and Kuddithamby et al. (2024), we assumed that 90% of the MP would fall into the 20-200 μm size class. Additionally, we assumed that the MP had a spherical shape.

2.3.2 Emission scenarios for PP/PE and PET

Calculated emissions from WWTPs and rivers serve as the inputs for the two main scenario runs.

In Scenario 1, the focus was on evaluating the loads of PET and PP/PE from WWTP sources, specifically considering the 20-500 μm MP size fraction. To gain a deeper understanding, this size fraction was further divided into two sub-ranges: small particles (20-200 μm) and large particles (200-500 μm) for both PET and PP/PE.

In Scenario 2, the analysis encompassed PET and PP/PE loads from riverine sources, taking into account the 20-500 μm MP size
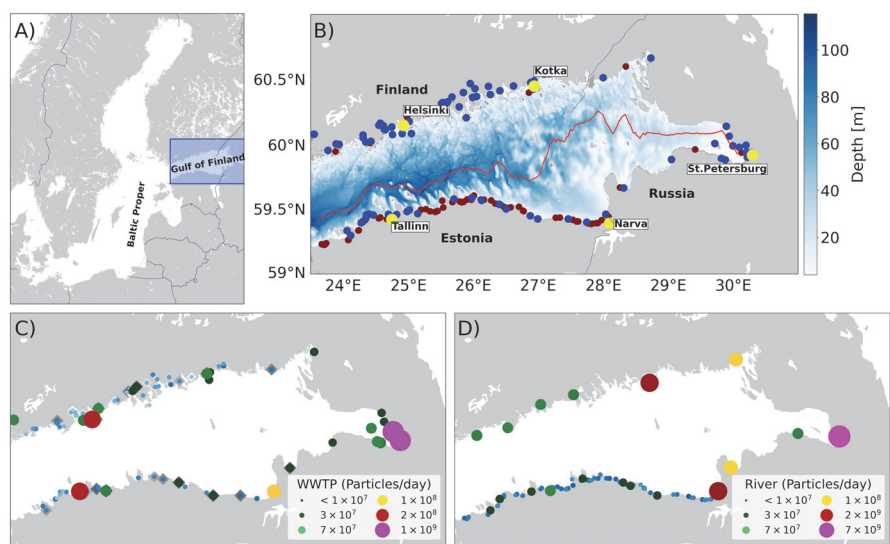
FIGURE 1
Panel **(A, B)** represent a map of the Baltic Sea and a map of the WWTPs (blue dots) and river (red dots) emissions points at the coast of the GoF. Yellow dots represent the cities mentioned in the study. The red line indicates the thalweg along the GoF; panels **(C, D)** display the emissions of PET and PP/PE MP particles (20-500 um) from WWTPs and riverine sources entering the GoF. The diamond markers in panel (1C) represent emissions from inland WWTPs.

fractions. Like Scenario 1, this size fraction was divided into two sub-ranges: small particles (20-200 μm) and large particles (200-500 μm) for both PET and PP/PE.

Thus, eight scenario runs were simulated in total, representing two types of MP, two size fractions, and two emission pathways. It is important to note that all scenarios assume a constant daily MP emission throughout the entire simulation period (Table 1), facilitating a thorough evaluation of MP pollution. Thus, eight scenario runs were simulated in total, representing two types of MP, two size fractions, and two emission pathways.

3 Results

3.1 Overall variability of microplastic distribution

The time series of the share of particles in different states is shown in Figure 2. The overall spin-up of the model was relatively

fast – after initialization, the share of particles in the water column dropped quickly to approximately 15%, while the share of sedimented particles stabilized between 75 – 80%. Meanwhile, the share of particles at the boundary reached approximately 1%, and the share of beached particles reached 10% during the spin-up period. The small light particles were the most abundant in the water column, and the large heavy particles were the least common (see Figures 2A, B). Most particles that left the GoF (reached the boundary) also belonged to the small light class (3%), whereas the large light particles beached the most (28%). Approximately 65% of the small light and large light particles and 92% and 95% of the small heavy and large heavy particles, respectively, settled after 3 years of simulation.

3.1.1 Variability of surface concentrations

The average concentration of MP particles in the surface layer is shown in Figure 3. The concentrations were larger for the light particles (PP/PE) compared to heavy particles (PET) but high for both types near major coastal sources (Figures 3E, F). Since the

TABLE 1 Distribution of total emissions of PET and PP/PE particles from WWTPs and rivers per day.

Emissions to the GoF catchment				
Sources	20-500 μm	20-200 μm	200-500 μm	% share
WWTP - (PET)	1.55E+09	1.40E+09	1.55E+08	24.3
WWTP - (PP/PE)	1.95E+09	1.76E+09	1.95E+08	
River - (PET + PP/PE)	1.09E+10	9.86E+09	1.09E+09	75.7

riverine input to the Russian part was six-fold greater than the combined input to the Estonian and Finland parts, the highest concentrations of riverine-origin MP were in the eastern part of the gulf (Figures 3A, B). The WWTP-origin particle concentrations were high in the vicinity of larger cities (St. Petersburg, Helsinki and Tallinn, Figures 3C, D). The overall mean riverine origin particle concentrations for PP/PE within the model domain were about 3.8 particles/m^2, but the maximum values exceeded 50 particles/m^2 in the eastern part of the gulf (Figure 3B). The PET particles did not disperse as extensively as PP/PE particles from the eastern part of the gulf towards the west. PET particles from WWTPs were primarily gathered near Helsinki and in the eastern part of the gulf (Figure 3C). PP/PE particles from WWTPs had a similar distribution to the PET, but dispersion was higher, and the impact of Tallinn was more pronounced. On average, the PET and PP/PE particles released from WWTPs had concentrations of 0.1 and 1.0 particles/m^2 within the model domain, respectively. When considering particles from both rivers and WWTPs, the average surface concentrations for PET and PP/PE particles were 1.4 particles/m^2 and 4.8 particles/m^2, respectively. The findings indicate that most of the MP particles in the central gulf are predominantly retained near their source areas, with limited long-distance transport.

3.1.2 Water column

Figure 4 provides an overview of the mean spatial distributions of vertically integrated MP amounts in the water column during 2019 and 2020. The occurrence of particles in the water column was larger in the eastern part than in the western part of the gulf, where concentrations were much smaller for both the riverine and WWTP-origin particles. Heavy particles tended to remain closer to sources (rivers and WWTPs) in the eastern part, but high integrated concentrations can also be seen along the thalweg of the gulf in the western part.

The model data suggests that a gradual decrease in MP concentration was likely influenced by both the configuration of the gulf and the distance from the main sources (Figure 4). Particularly in shallower areas, to the east from 28°E, there was an elevated presence of riverine PET and PP/PE particles (Figures 4A, B). Conversely, in the region to the west from 28°E, where the Neva River has less influence, lower concentrations of riverine-origin PET and PP/PE particles were observed. The mean concentrations of WWTP-origin particles were higher in both the eastern and western regions, with lower concentrations between 26°E and 28°E (Figures 4C, D). This variation in WWTP-origin PET and PP/PE particles is likely due to the locations of the main input sources. The region between 26°E and 28°E receives less pollution from WWTPs, resulting in lower concentrations of WWTP-origin particles in this area.
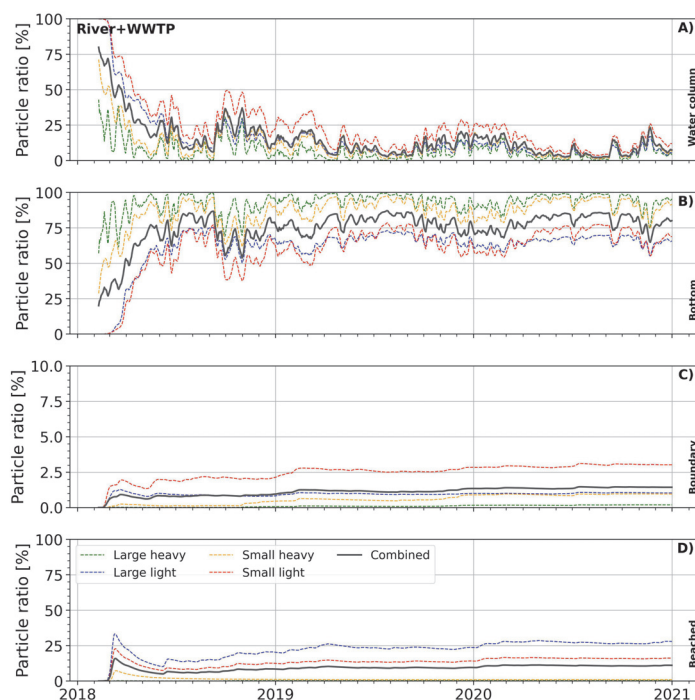

FIGURE 2
Time series of the particle budget in different classes for the Gulf of Finland. **(A)** water column, **(B)** bottom, **(C)** boundary, and **(D)** beached. All time series have been smoothed using a 7-day moving window.
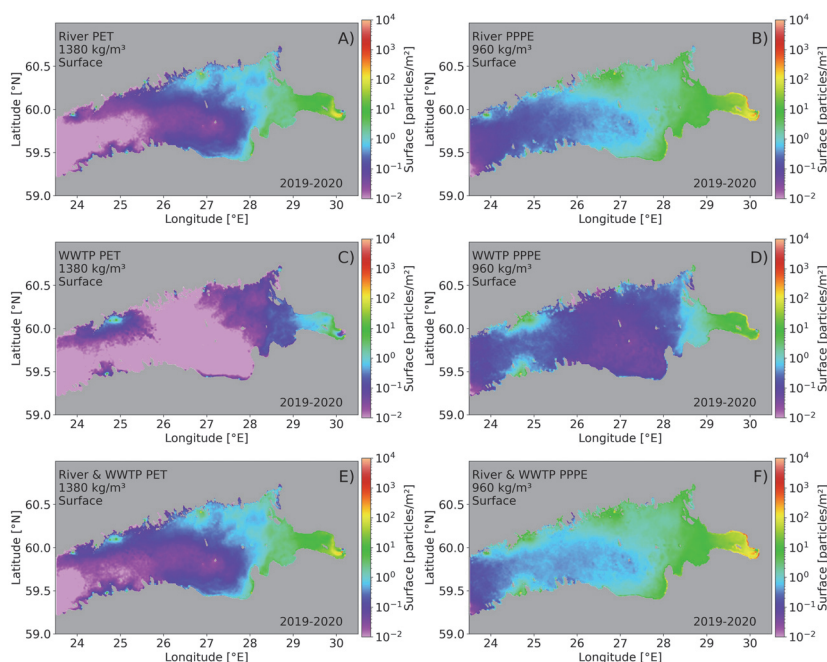
FIGURE 3
Mean concentrations of PET and PP/PE MP particles (20 - 500 µm) in the surface layer of the GoF in 2019-2020. Panels **(A, B)** represent the riverine origin PET and PP/PE particles; panels **(C, D)** WWTP origin PET and PP/PE particles; panels **(E, F)** display composite maps of different origin PET and PP/PE particles.

Figure 5 represents the meridionally integrated concentrations from south to north in the water column during 2019 and 2020. From the surface to the seabed, PET particles had lower concentrations, while PP/PE particles were more prevalent, likely due to the higher density of PET particles, causing them to sink more quickly (Figures 5A–D). A characteristic vertical distribution of particles with high concentrations near the sea surface and the seabed and a minimum in the intermediate water layer is revealed for both particle types in the deeper areas of the gulf.

3.1.3 Accumulation of particles

Sedimentation of particles of different origins and classes is shown in Figure 6. Sedimentation of the MP has occurred almost on the whole seabed of the gulf. The largest concentrations in the seabed are in the eastern part of the gulf, similar to those in the water column. The heavy particles (PET) tend to sink quickly and accumulate in the coastal areas, with notable amounts observed in Neva Bay, Narva Bay and near Kotka on the northern coast. Relatively high values were also in deeper areas of the central part of the gulf (Figure 6A). WWTP-origin PET particles had the highest values in the western and eastern parts of the gulf, while lower accumulation rates were revealed between 26.5 and 28°E (Figure 6C).

The composite maps indicate the overall accumulation (Figures 6E, F). In principle, the highest concentrations of both heavy and light particles were in the easternmost part of the gulf and

Narva Bay. There is a tendency for higher concentrations near the coastline along the southern coast, while in the northern part, the sedimentation is more homogenous (Figure 6F).

3.1.4 Beaching of particles

The accumulation of particles on beaches around the GoF is shown in Figure 7. The whole coastline of the gulf has been impacted by the MP, although the load varied in space. Overall, more light particles beached compared to the heavy particles – the average number of beached particles was nearly 20 times higher for the light particles. Nevertheless, a relatively high number of heavy particles from rivers ($> 10^5$ particles/m) have beached on the southern shore of Neva Bay. A high number of light particles from rivers have beached in Neva Bay and Narva Bay, and along the Finnish coastline; particles from WWTPs are also numerous around Neva Bay, inside Tallinn Bay, in the vicinity of Helsinki, and at some spots along the northern coast.

3.2 Seasonal variability

3.2.1 Seasonal dynamics

Figures 8 and 9 illustrate the seasonal variations of PET and PP/PE particles in the surface layer, water column and sediments during the summer and winter months in the GoF.
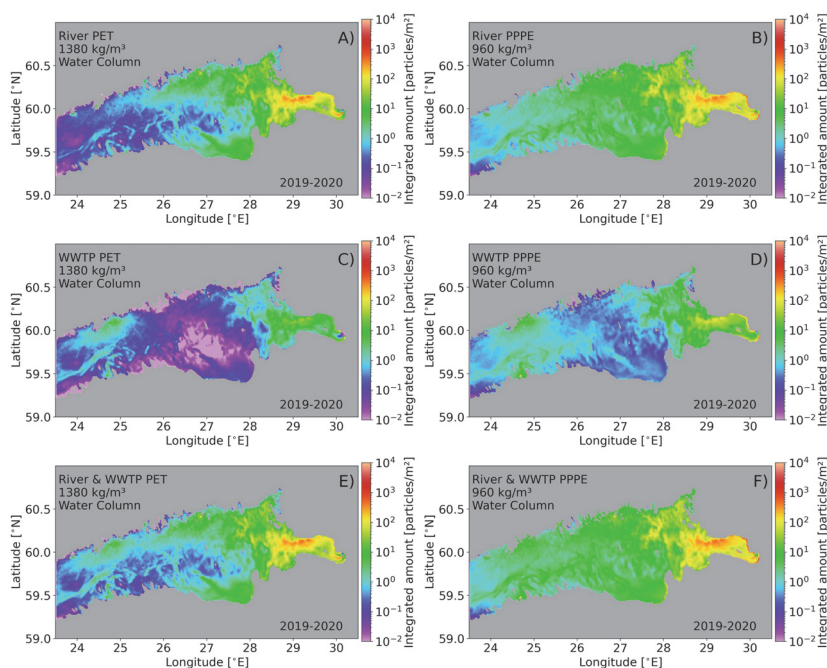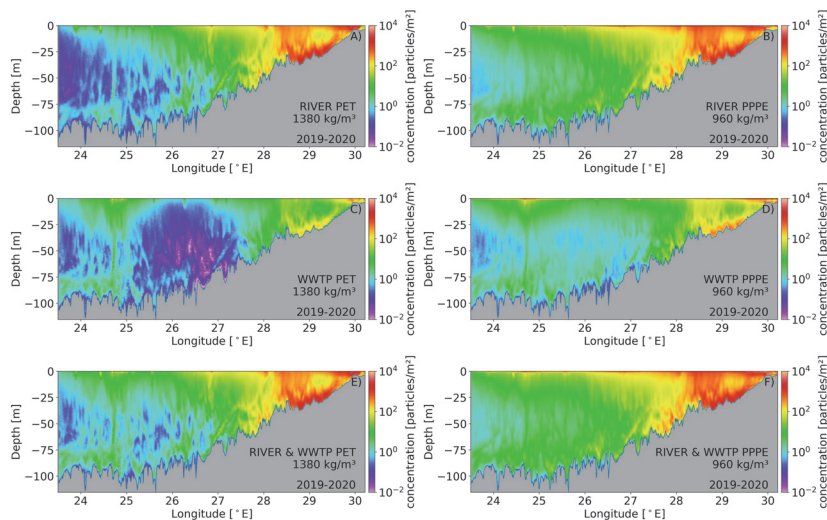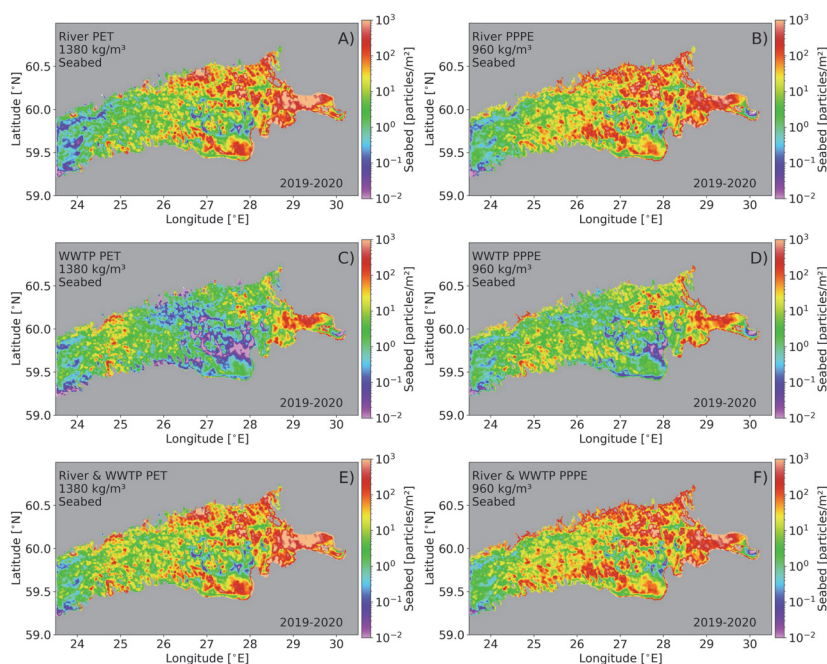
FIGURE 4
Mean spatial distribution of vertically integrated concentrations of PET and PP/PE (20-500 mm) in the GoF in 2019-2020. Panels **(A, B)** represent the riverine origin PET and PP/PE particles; panels **(C, D)** WWTP origin PET and PP/PE particles; panels **(E, F)** display composite maps of different origin PET and PP/PE particles.

FIGURE 5
Mean meridionally integrated concentration of PET and PP/PE MP particles (20 - 500 μm) in the water column of the GoF in 2019-2020. Panels **(A, B)** represent the riverine origin PET and PP/PE particles; panels **(C, D)** WWTP origin PET and PP/PE particles; panels **(E, F)** display composite maps of different origin PET and PP/PE particles. The bathymetry data along the latitude axis is represented as the maximum depth values for each longitude coordinate.

FIGURE 6
Mean spatial concentrations of PET and PP/PE MP particles (20 – 500 µm) on the seabed of the GoF in 2019-2020. Panels **(A, B)** represent the riverine origin PET and PP/PE particles; panels **(C, D)** WWTP origin PET and PP/PE particles; panels **(E, F)** display composite maps of different origin PET and PP/PE particles.

During the summer months (JJA, June-August), PET MP concentrations near the surface were elevated along the northern and southern coasts, with the highest concentrations near St. Petersburg (Figure 8A). Despite lower river runoff and MP loads in winter (DJF, December-February), surface PET concentrations were higher in winter compared to summer (Figure 8B). A similar tendency was observed in the water column, where vertically integrated PET concentrations were higher in winter, likely due to reduced sedimentation and stronger resuspension driven by winter currents. In contrast, the settled particle concentrations were higher in summer, driven by enhanced biofilm formation and stratification (Figures 8E, F).

The mean surface concentration of PP/PE particles was higher in summer than in winter (Figures 9A, B), with higher levels observed in Narva Bay and along the Tallinn and Helsinki coasts. This winter increase likely reflects reduced sedimentation due to weaker biofilm growth. In contrast, summer concentrations were lower near the surface but higher on the seabed, primarily driven by enhanced biofilm formation and stratification, which promote particle settling (Figures 9C–F).

3.3 Short-term variability

The impact of an upwelling event along the northern coast is shown in Figure 10. There was already a small upwelling visible along the

northern coast on 18 July (Figure 10A), the surface concentrations (Figure 10D) were strongly inhomogeneous, with the highest values in the easternmost areas of the gulf and patches also appearing along the northern coast and central part of the gulf. As the upwelling intensified on 22 July (Figure 10B), particles began to advect offshore, forming significant surface patches of MP concentrations in the central gulf (Figure 10E). During the upwelling peak (24th of July), a large patch of particles was advected southwards, particularly in the areas with colder temperatures, i.e. in the upwelling zone (Figure 10F).

The impact of near-bottom currents on particle concentrations in the 5 m thick layer above the seabed is shown in Figure 11. Stronger near-bottom currents observed on December 6 (Figure 11B) caused increased resuspension of particles from the seabed, as evidenced by higher concentrations in the near-bottom layer (Figure 11E). On December 7, as the bottom currents relaxed (Figure 11C), resuspension levels decreased moderately (Figure 11F). This suggests that while stronger currents lead to particle resuspension, the eventual relaxation of currents allows particles to settle back onto the seabed over time.

4 Discussion

In this study, results from a multi-year (2018-2020) high-resolution model experiment were employed. This model system
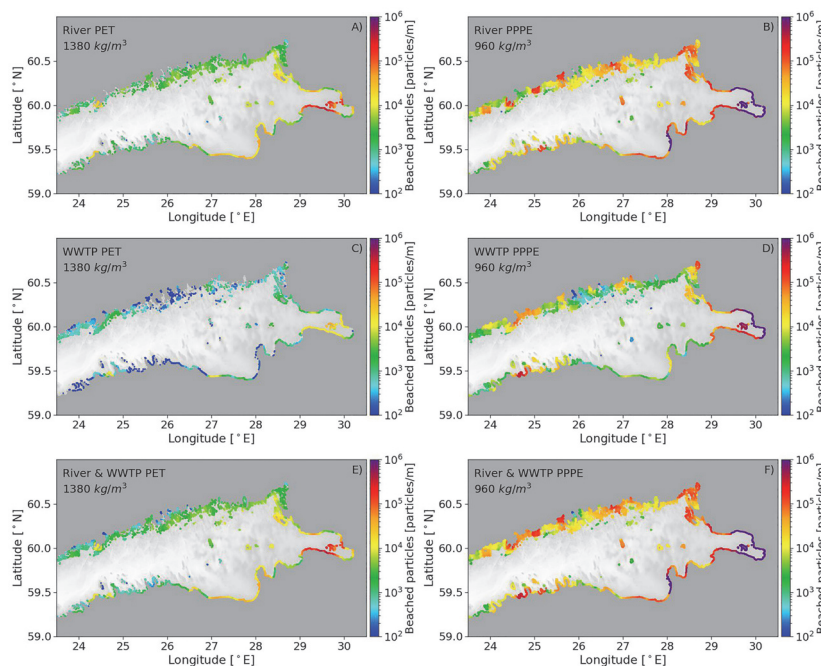
FIGURE 7
Distribution of particle accumulation on beaches over the period 2019–2020. Panels **(A, B)** represent the PET and PP/PE particles, respectively, from rivers; panels **(C, D)** focus on PET and PP/PE particles sourced from WWTPs; panels **(E, F)** display PET and PP/PE particles sourced from both rivers and WWTPs. The values have been spatially smoothed with a window length of 10 km.

incorporated hydrodynamic, biogeochemical and Lagrangian particle tracking models to identify the MP pollution's pathways and accumulation zones within the GoF in the surface layer, water column, coastline and bottom layer. Our research utilized the existing datasets for MP distribution estimates and employed advanced modeling techniques.

We considered two distinct particle types: (1) PET particles with density greater than sea water and (2) PP/PE particles with density less than sea water. In addition, particles within a size range of 20 to 500 um were considered and further categorized into small (20 - 200) and large (200 - 500) particles. Generally, this is well supported by literature. PP, PE, PET, PVC, and PS are the most common polymers found worldwide (Vermeiren et al., 2016; Geyer et al., 2017; Kooi and Koelmans, 2019). In China, Lv et al. (2019) found the following polymer shares: PP (15%), PE (18%), PET (47%) and PS (20%) in the raw wastewater. In the Mediterranean, out of the total MP observed, Pedrotti et al. (2016) reported that around 86-97% share accounted for the following polymers: PP, PE and polyamides. In our study, we used PP, PE and PET due to their abundance in the environment and as they cover a wide range of densities from 900 to 1300 kg/m^3. We used the previous load estimates from Schernewski et al. (2020), which included WWTP locations and emissions exclusively used within the GoF catchment area. Based on the available literature (Schrank et al., 2022; Constant et al., 2020), we have considered mean MP particles

found in the rivers. Nevertheless, substantial uncertainties still exist regarding emissions from the WWTPs and MP presence in rivers.

The Baltic Sea receives land-based MPs from rivers and coastal catchment areas (Murawski et al., 2022). The GoF is under considerable anthropogenic pressure, and as a result, the levels of pollutants, including the MP in water and biota are higher compared to the neighboring basins such as the Gulf of Riga or Baltic Proper (Mishra et al., 2022; Kuprijanov et al., 2024). In addition, our results indicate that most of the MP particles entering the GoF do not spread to the Baltic Proper, but instead accumulate within the GoF.

Due to prevailing cyclonic surface circulation in the GoF, floating litter tends, in general, to drift towards the Baltic Proper in higher abundances along the northern coast (Pärn et al., 2023). Our study reveals that the easternmost part of the GoF exhibits the highest levels of MP pollution in the surface layer. Similar tendencies for the GoF have been shown by other modelling studies (e.g. Murawski et al., 2022; Pärn et al., 2023) due to the large freshwater input from the Neva River. Pollution levels were notably reduced in the central gulf, with concentrations at least an order of magnitude smaller. Rivers discharge freshwater and substances in amounts not typically found in seawater (e.g. Hetland and Hsu, 2013) and, as a result, river plumes, small or large, with high concentrations of tracers and plume fronts in the vicinity of sources are formed. Five river plume fronts were
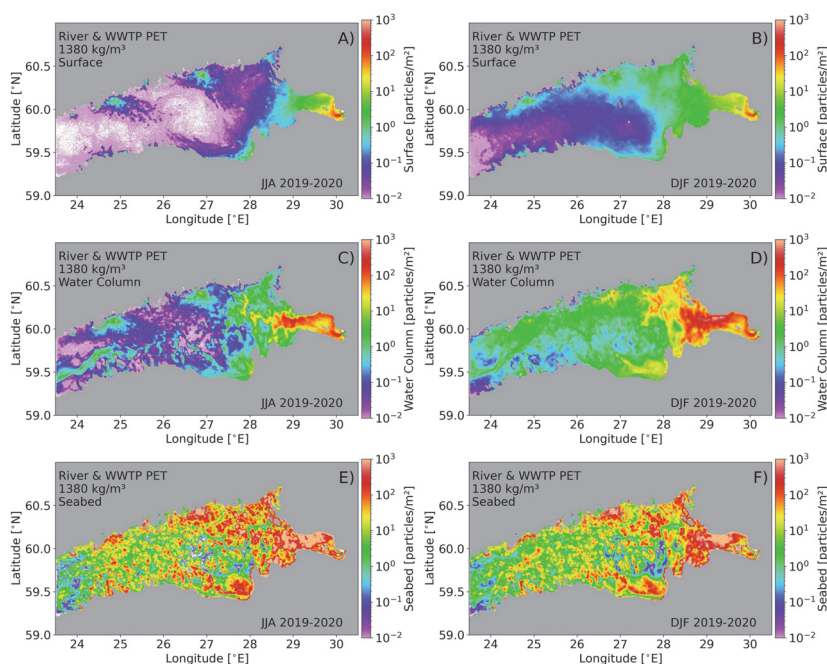
FIGURE 8
Mean spatial concentration of PET MP particles (20 – 500 µm) sourced from both rivers and WWTPs in different layers of the GoF during the summer months JJA (June, July, and August, panels **(A, C, E)** and winter months DJF (December, January, and February, panels **(B, D, F)**. Panels **(A, B)** illustrate the concentration in the surface layer; panels **(C, D)** focus on concentration in the water column; panels **(E, F)** showcase the concentration in the bottom layer.

noticeable in the study area associated with the Neva River, Luga River, Narva River and Kymi River (Suursaar et al., 2021). Nevertheless, none of these fronts are stationary as they undergo spatial excursions and other dynamic transformations (Suursaar et al., 2021), and consequently, we could not detect regions with persistently high MP concentrations at these frontal regions. However, such convergent density fronts are characterized by relatively large vertical velocities (D'Asaro et al., 2020) that likely restrict MP transport over long horizontal distances. Additionally, quasi-persistent eddy activity may contribute to such a high number of plastics near the emission areas (Andrejev et al., 2004; Pärn et al., 2023).

Our simulations revealed that both the PET and PP/PE particles predominantly accumulated in the seabed in close proximity to coastal regions and emission points. The accumulation areas of lighter PP/PE particles extended further offshore. Due to their negative buoyancy, PET particles consistently descend into the water column, ultimately settling on the seabed, particularly near coastal areas. Recent research, using an Eulerian modeling approach, also reported the accumulation of PET particles in shallow coastal waters of the Baltic Sea (Schernewski et al., 2020). In contrast, PP/PE particles, initially buoyant, remained suspended longer before sinking. This coastal accumulation was particularly evident near riverine sources such as the Neva River estuary and the Narva Bay. The shallow nature of the GoF, with an average depth of 37 m (Leppäranta and Myrberg, 2009), contributes to higher

deposition rates in these areas. Kuprijanov et al. (2021) reported similar patterns of hazardous substance accumulation in shallow areas, such as Neva Bay and Finnish coastal inlets, though MP accumulation may persist longer in deeper areas.

Resuspension events, driven by near-bottom currents > 30 cm s^{-1}, occasionally > 50 cm s^{-1} (Liblik et al., 2013; Rasmus et al., 2015; Suhhova et al., 2018), or wave-induced shear stress (Jönsson et al., 2005), can remobilize MPs from sediments back into the water column gulf. This dynamic interplay of deposition and resuspension highlights the importance of hydrodynamic forces in redistributing MPs in the current study.

The beaching of particles occurred almost throughout the entire GoF. The hotspots were mostly in bays with limited access to the open sea, e.g. Neva Bay, Tallinn Bay, and multiple locations on the northern coast. Previous studies have highlighted similar trends, with higher particle accumulation near the major rivers and urban areas, such as St. Petersburg and the Gulf of Riga (Schernewski et al., 2021). Our results show that light particles had substantially higher beaching rates compared to heavy particles, likely due to differences in their buoyancy and settling dynamics. Likely, a lot of the heavy PET particles settled in the shallow areas quicker than in 10 days required for a particle to be considered beached as defined in the simulations in the present study. Therefore, a significantly smaller amount of PET was found on beaches compared to light particles. These findings underline the importance of focused monitoring and sampling near key pollution
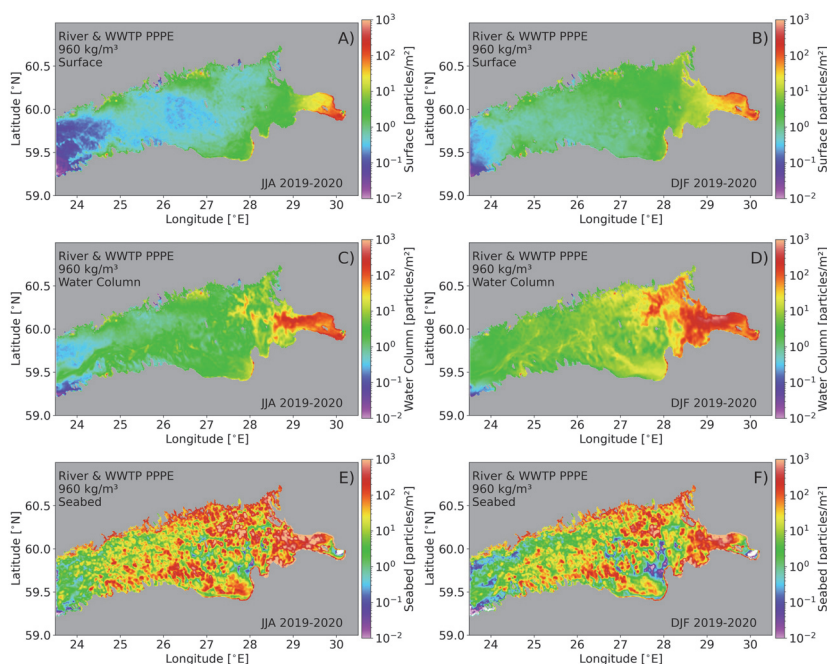
FIGURE 9
Mean spatial concentration of PP/PE MP particles (20 – 500 µm) sourced from both rivers and WWTPs in different layers of the GoF during the summer months JJA (June, July, and August) and winter months DJF (December, January, and February). Panels **(A, B)** illustrate the concentration in the surface layer; panels **(C, D)** focus on concentration in the water column; panels **(E, F)** showcase the concentration in the bottom layer.

sources, such as the Bay of Tallinn, to validate the simulation results and improve understanding of beaching dynamics.

The model effectively replicates the seasonal variability of MP concentrations observed in the GoF. Spring and summer are periods of heightened biological activity in the Baltic Sea (e.g. Lips et al., 2014). MP concentrations in the surface layer are lower in summer than winter were consistent with observations in the northern Baltic Proper and the GoF (Mishra et al., 2022).
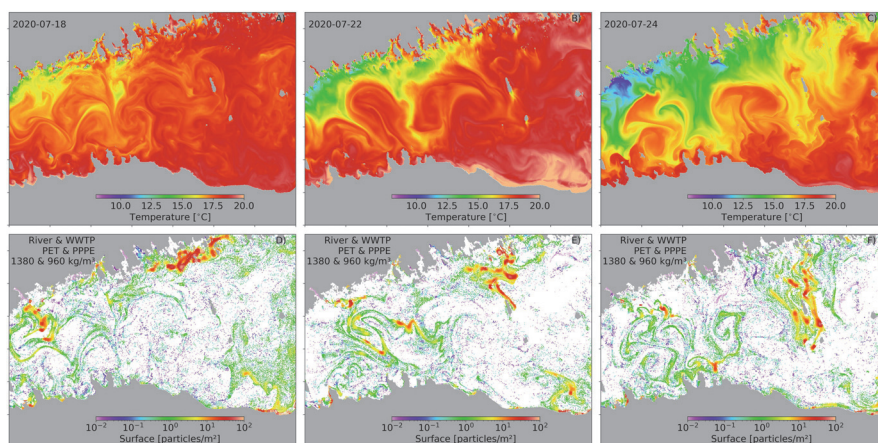
FIGURE 10
Sea Surface Temperature (SST) maps **(A–C)** and surface layers **(D–F)** during Upwelling conditions along the Finnish coast in the GoF.
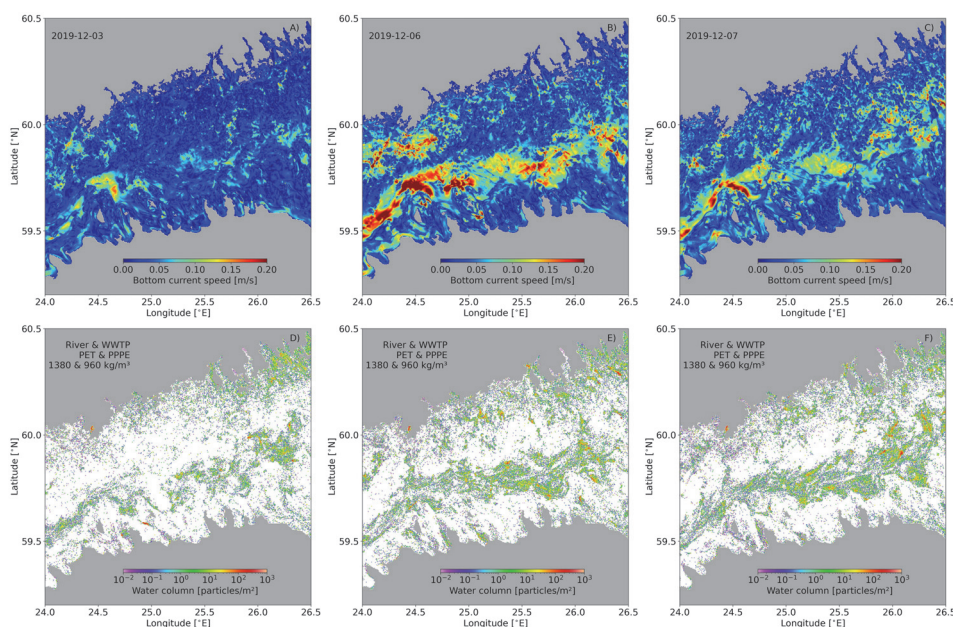
FIGURE 11
Snapshots of bottom currents (A−C), and water column particles integrated within 5 meters above the seabed (D−F) in the GoF.

Furthermore, a recent modeling study conducted in Neva Bay, which used a different modeling approach compared to our study, reported a 10-fold decrease in the surface concentration during the summer months compared to the winter (Martyanov et al., 2021). This seasonal pattern reflects the combined influence of biofouling, hydrodynamics and stratification. In summer, phytoplankton blooms promote biofouling, enhancing the sinking rates of MPs and further leading to their accumulation on the seabed. Vertical stratification, while necessary for biofouling, also acts as a barrier, potentially trapping MPs withing the thermocline (Uurasjärvi et al., 2021). By late summer, the decay of thermocline and reduced primary production lead to less biofilm formation and reduced organic matter (Almroth-Rosell et al., 2011; Liblik and Lips, 2011) which may slow MP sinking.

In contrast, during winter, reduced biofouling, weaker stratification and stronger hydrodynamic activity contribute to higher MP concentrations at the surface. Stronger near-bottom currents can also resuspend particles from the seabed, maintaining elevated MP levels in the water column.

A wind-induced coupled coastal upwelling-downwelling event, which is frequent in the GoF (e.g. Lips et al., 2009; Uiboupin and Laanemets, 2009; Laanemets et al., 2011; Väli et al., 2011; Liblik and Lips, 2017) was selected as a case study. Previous studies have proposed that coastal upwelling may result in relatively low concentrations of MPs in coastal waters (de Lucia et al., 2014; Desforges et al., 2014; Mishra et al.,

2022) while high concentration patches can form in the convergence zone of coastal downwelling (Mishra et al., 2022). In contrast, La Daana et al. (2017) found no significant difference in MP concentrations between Benguela upwelling sites and other non-upwelling sites.

During the upwelling events, the distribution in the surface layers indicated large particle concentrations converged in the sub-mesoscale stripes or small eddy-like features in the upwelling frontal zone, where the Rossby numbers (not shown) and temperature gradients were high (Figure 10). Previously, Väli et al. (2017, 2018) showed the convergence of particles in the GoF at the locations of the high Rossby number and sub-mesoscale activity. A recent modelling study (Väli et al., 2024) indicated the frequent occurrence of sub-mesoscale activity in the GoF. Observations of the temporal changes of MP concentrations are very challenging in such estuarine systems, where, on the one hand, the MP input from land is high, and, on the other hand, strong thermohaline gradients exist.

Previous studies have shown that episodic events, such as storms or wind-driven upwelling, can generate bottom currents, which can disturb bottom sediments, resuspending MPs into the overlying water column (Osinski et al., 2020; Zhou et al., 2021). In areas with high sedimentation rates, where MPs accumulate on the seabed, even short-term increases in current velocity have been shown to result in the release of particles back into the water column (Kane and Clare, 2019). Our results mirror this process, where we observed a marked

decrease in sedimented MP concentrations and an increase in water column particles following periods of intensified bottom currents.

5 Conclusions and summary

We applied a combination of hydrodynamic, biogeochemical, and Lagrangian particle tracking models to trace MP pathways and identify potential accumulation zones in the GOF. This three-year simulation, with sub-mesoscale permitting horizontal resolution, revealed MP concentrations at the surface, within the water column, and accumulation on the seabed. The results provide critical insights into MP distribution pathways, spatial heterogeneity and the influence of hydrodynamics on MP transport and accumulation.

The study revealed that approximately 75% of MP particles settle on the seabed, making it the primary accumulation area in the GoF. Around 10% of particles were beached, with notable accumulation in Neva Bay, Narva Bay, and parts of the Finnish coastline. Only 1% of MP particles exited the gulf through the western boundary, while 14% remained suspended in the water column, influenced by episodic resuspension events. These findings highlight the GoF's role as a significant retention zone for MPs due to its semi-enclosed geography and hydrodynamic conditions.

MP concentrations were highest near major coastal and riverine sources, particularly in the eastern part of the gulf. Surface concentrations of light particles exceeded those of heavy particles, especially in proximity to WWTPs and river mouths. The zonally integrated concentrations demonstrated higher values in the shallower eastern areas and a marked decrease west of 28°E. This spatial variability underscores the influence of anthropogenic inputs and local hydrodynamics on MP distribution.

Hydrodynamic processes played a key role in shaping MP transport and redistribution in the GoF. Upwelling and downwelling events, as well as episodic intensification of bottom currents, significantly influenced the redistribution of MPs. Strong bottom currents resuspended settled MPs into the water column, temporarily increasing their concentrations. These dynamic processes emphasize the importance of monitoring MPs across all layers of the marine environment – not just the surface layer but also the water column and seabed, to fully understand their transport and fate.

This study provides a scientific basis for policymakers to regulate MP emissions from WWTPs, manage riverine inputs, and address urban coastal pollution. By identifying hotspot areas, such as Neva Bay and Narva Bay, the findings can help prioritize resources for pollution control. Future monitoring efforts in the GoF and Baltic Sea should extend beyond the surface layer to include the water column and seabed, incorporating multipoint sampling at various depths, especially near emission sources. Additionally, mitigation measures should focus on the eastern gulf, where MP concentrations are consistently elevated.

Data availability statement

The raw data supporting the conclusions of this article will be made available by the authors, without undue reservation.

Conflict of interest

The authors declare that the research was conducted in the absence of any commercial or financial relationships that could be construed as a potential conflict of interest.

Generative AI statement

The author(s) declare that no Generative AI was used in the creation of this manuscript.

Publisher's note

References

Aigars, J., Barone, M., Suhareva, N., Putna-Nimane, I., and Dimante-Deimantovica, I. (2021). Occurrence and spatial distribution of microplastics in the surface waters of the Baltic Sea and the Gulf of Riga. *Mar. pollut. Bull.* 172, 112860. doi: 10.1016/j.marpolbul.2021.112860

Alenius, P., Myrberg, K., and Nekrasov, A. (1998). The physical oceanography of the Gulf of Finland: a review. *Boreal Environ. Res.* 3, 97–125.

Alenius, P., Nekrasov, A., and Myrberg, K. (2003). Variability of the baroclinic Rossby radius in the Gulf of Finland. *Cont. Shelf Res.* 23, 563–573. doi: 10.1016/S0278-4343(03)00004-9

Almroth-Rosell, E., Eilola, K., Hordoir, R., Meier, H. E. M., and Hall, P. O. J. (2011). Transport of fresh and resuspended particulate organic material in the Baltic Sea—a model study. *J. Mar. Syst.* 87, 1–12. doi: 10.1016/j.jmarsys.2011.02.005

Andrejev, O., Myrberg, K., Alenius, P., and Lundberg, P. A. (2004). Mean circulation and water exchange in the Gulf of Finland—a study based on three-dimensional modelling. *Boreal Environ. Res.* 9, 1.

Baresel, C., and Olshammar, M. (2019). On the importance of sanitary sewer overflow on the total discharge of microplastics from sewage water. *J. Environ. Prot. (Irvine,. Calif).* 10, 1105–1118. doi: 10.4236/jep.2019.109065

Barnes, D. K. A., Galgani, F., Thompson, R. C., and Barlaz, M. (2009). Accumulation and fragmentation of plastic debris in global environments. *Philos. Trans. R. Soc B Biol. Sci.* 364, 1985–1998. doi: 10.1098/rstb.2008.0205

Bigdeli, M., Mohammadian, A., Pilechi, A., and Taheri, M. (2022). Lagrangian modeling of marine microplastics fate and transport: the state of the science. *J. Mar. Sci. Eng.* 10, 481. doi: 10.3390/jmse10040481

Bruggeman, J., and Bolding, K. (2014). A general framework for aquatic biogeochemical models. *Environ. Model. Software* 61, 249–265. doi: 10.1016/j.envsoft.2014.04.002

Burchard, H. (2001). *Applied turbulence modelling in marine waters.* Springer. doi: 10.5194/gmd-15-8613-2022

Burchard, H., and Bolding, K. (2002). GETM: A general estuarine transport model, scientific documentation, european commission, joint research centre. *Inst. Environ. Sustain.* 12262, 25.

Canuto, V. M., Howard, A., Cheng, Y., and Dubovikov, M. S. (2001). Ocean turbulence. Part I: One-point closure model—Momentum and heat vertical diffusivities. *J. Phys. Oceanogr.* 31, 1413–1426. doi: 10.1175/1520-0485(2001) 031<1413:OTPIOP>2.0.CO;2

Carr, S. A., Liu, J., and Tesoro, A. G. (2016). Transport and fate of microplastic particles in wastewater treatment plants. *Water Res.* 91, 174–182. doi: 10.1016/j.watres.2016.01.002

Cole, M., Lindeque, P., Halsband, C., and Galloway, T. S. (2011). Microplastics as contaminants in the marine environment: a review. *Mar. pollut. Bull.* 62, 2588–2597. doi: 10.1016/j.marpolbul.2011.09.025

Constant, M., Ludwig, W., Kerhervé, P., Sola, J., Charrière, B., Sanchez-Vidal, A., et al. (2020). Microplastic fluxes in a large and a small Mediterranean river catchments: The Têt and the Rhône, Northwestern Mediterranean Sea. *Sci. Total Environ.* 716, 136984. doi: 10.1016/j.scitotenv.2020.136984

Cuttat, F. M. R. (2018). Marine transport of plastic fragments from dolly ropes used in demersal fisheries in the North Sea. (Denmark: DTU Aqua)

D'Asaro, E. A., Carlson, D. F., Chamecki, M., Harcourt, R. R., Haus, B. K., Fox-Kemper, B., et al. (2020). Advances in observing and understanding small-scale open ocean circulation during the Gulf of Mexico Research Initiative Era. *Front. Mar. Sci.* 7. doi: 10.3389/fmars.2020.00349

de Lucia, G. A., Caliani, I., Marra, S., Camedda, A., Coppa, S., Alcaro, L., et al. (2014). Amount and distribution of neustonic micro-plastic off the western Sardinian coast (Central-Western Mediterranean Sea). *Mar. Environ. Res.* 100, 10–16. doi: 10.1016/j.marenvres.2014.03.017

Desforges, J.-P. W., Galbraith, M., Dangerfield, N., and Ross, P. S. (2014). Widespread distribution of microplastics in subsurface seawater in the NE Pacific Ocean. *Mar. pollut. Bull.* 79, 94–99. doi: 10.1016/j.marpolbul.2013.12.035

Dris, R., Gasperi, J., and Tassin, B. (2018). Sources and fate of microplastics in urban areas: a focus on Paris megacity. *Freshw. microplastics Emerg. Environ. Contam.* 69–83. doi: 10.1007/978-3-319-61615-5_4

Eriksen, M., Cowger, W., Erdle, L. M., Coffin, S., Villarrubia-Gómez, P., Moore, C. J., et al. (2023). A growing plastic smog, now estimated to be over 170 trillion plastic particles afloat in the world's oceans—Urgent solutions required. *PloS One* 18, e0281596. doi: 10.1371/journal.pone.0281596

European Chemicals Agency. (2019). Annex XV Restriction Report: Proposal for a Restriction – Intentionally Added Microplastics.

Frishfelds, V., Murawski, J., and She, J. (2022). Transport of microplastics from the daugava estuary to the Open Sea. *Front. Mar. Sci.* 9. doi: 10.3389/fmars.2022.886775

GESAMP (2019). Guidelines on the monitoring and assessment of plastic litter and microplastics in the 632 ocean. *GESAMP Rep. Stud. Ser.* 99, 130.

Geyer, R., Jambeck, J. R., and Law, K. L. (2017). Production, use, and fate of all plastics ever made. *Sci. Adv.* 3, e1700782. doi: 10.1126/sciadv.1700782

Gies, E. A., LeNoble, J. L., Noël, M., Etemadifar, A., Bishay, F., Hall, E. R., et al. (2018). Retention of microplastics in a major secondary wastewater treatment plant in Vancouver, Canada. *Mar. pollut. Bull.* 133, 553–561. doi: 10.1016/j.marpolbul.2018.06.006

Gräwe, U., Naumann, M., Mohrholz, V., and Burchard, H. (2015). Anatomizing one of the largest saltwater inflows into the B altic S ea in D ecember 2014. *J. Geophys. Res. Ocean.* 120, 7676–7697. doi: 10.1002/2015JC011269

Gröger, M., Placke, M., Meier, H. E., Börgel, F., Brunnabend, S.-E., Dutheil, C., et al. (2022). The Baltic Sea Model Intercomparison Project (BMIP)–a platform for model development, evaluation, and uncertainty assessment. *Geosci. Model. Dev.* 15, 8613–8638. doi: 10.5194/gmd-15-8613-2022

Harvey, F., and Watts, J. (2018). Microplastics found in human stools for the first time. *Guard* 22.

HELCOM (2023). "State of the Baltic Sea. Third HELCOM holistic assessment 2016-2021," in *Baltic sea environment proceedings.* Helsinki, Finland: HELCOM. Available at: https://helcom.fi/post_type_publ/holas3_sobs.

Hersbach, H., Bell, B., Berrisford, P., Hirahara, S., Horányi, A., Muñoz-Sabater, J., et al. (2020). The ERA5 global reanalysis. *Q. J. R. Meteorol. Soc* 146, 1999–2049. doi: 10.1002/qj.3803

Hetland, R. D., and Hsu, T. J. (2013). "Freshwater and sediment dispersal in large river plumes," in *Biogeochem. Dyn. Large river-coastal interfaces linkages with glob. Clim. Chang.* Eds. T. S. Bianchi, M. A. Allison and „ W.-J. Cai (Springer, New York, USA), 55–85.

Hofmeister, R., Burchard, H., and Beckers, J.-M. (2010). Non-uniform adaptive vertical grids for 3D numerical ocean models. *Ocean Model.* 33, 70–86. doi: 10.1016/j.ocemod.2009.12.003

Jambeck, J. R., Geyer, R., Wilcox, C., Siegler, T. R., Perryman, M., Andrady, A., et al. (2015). Plastic waste inputs from land into the ocean. *Sci. (80-.).* 347, 768–771. doi: 10.1126/science.1260352

Jönsson, A., Danielsson, Å., and Rahm, L. (2005). Bottom type distribution based on wave friction velocity in the Baltic Sea. *Cont. Shelf Res.* 25, 419–435. doi: 10.1016/j.csr.2004.09.011

Kane, I. A., and Clare, M. A. (2019). Dispersion, accumulation, and the ultimate fate of microplastics in deep-marine environments: a review and future directions. *Front. Earth Sci.* 7. doi: 10.3389/feart.2019.00080

Kay, P., Hiscoe, R., Moberley, I., Bajic, L., and McKenna, N. (2018). Wastewater treatment plants as a source of microplastics in river catchments. *Environ. Sci. pollut. Res.* 25, 20264–20267. doi: 10.1007/s11356-018-2070-7

Klingbeil, K., Lemarié, F., Debreu, L., and Burchard, H. (2018). The numerics of hydrostatic structured-grid coastal ocean models: State of the art and future perspectives. *Ocean Model.* 125, 80–105. doi: 10.1016/j.ocemod.2018.01.007

Kooi, M., and Koelmans, A. A. (2019). Simplifying microplastic via continuous probability distributions for size, shape, and density. *Environ. Sci. Technol. Lett.* 6, 551–557. doi: 10.1021/acs.estlett.9b00379

Krauss, W., and Brügge, B. (1991). Wind-produced water exchange between the deep basins of the Baltic Sea. *J. Phys. Oceanogr.* 21, 373–384. doi: 10.1175/1520-0485(1991) 021<0373:WPWEBT>2.0.CO;2

Kuddithamby, G., ALMEDA, R., Vianello, A., Lorenz, C., Iordachescu, L., Papacharalampos, K., et al. (2024). Does water column stratification influence the vertical distribution of microplastics? *Environ Pollut.* 340, 122865. doi: 10.1016/j.envpol.2023.122865

Kuprianov, I., Buhhalko, N., Eriksson, U., Sjöberg, V., Rotander, A., Kolesova, N., et al. (2024). A case study on microlitter and chemical contaminants: assessing biological effects in the southern coast of the Gulf of Finland (Baltic Sea) using the mussel Mytilus trossulus as a bioindicator. *Mar. Environ. Res.*, 106628. doi: 10.1016/j.marenvres.2024.106628

Kuprianov, I., Väli, G., Sharov, A., Berezina, N., Liblik, T., Lips, U., et al. (2021). Hazardous substances in the sediments and their pathways from potential sources in the eastern Gulf of Finland. *Mar. pollut. Bull.* 170, 112642. doi: 10.1016/j.marpolbul.2021.112642

Laanemets, J., Väli, G., Zhurbas, V., Elken, J., Lips, I., and Lips, U. (2011). Simulation of mesoscale structures and nutrient transport during summer upwelling events in the Gulf of Finland in 2006. *Boreal Environ. Res.* 16, 15.

La Daana, K. K., Officer, R., Lyashevska, O., Thompson, R. C., and O'Connor, I. (2017). Microplastic abundance, distribution and composition along a latitudinal gradient in the Atlantic Ocean. *Mar. pollut. Bull.* 115, 307–314. doi: 10.1016/j.marpolbul.2016.12.025

Lebreton, L. C. M., van der Zwet, J., Damsteeg, J.-W., Slat, B., Andrady, A., and Reisser, J. (2017). River plastic emissions to the world's oceans. *Nat. Commun.* 8, 15611. doi: 10.1038/ncomms15611

Leppäranta, M., and Myrberg, K. (2009). *Physical oceanography of the baltic sea.* (Berlin, Germany: Springer Science & Business Media). doi: 10.1007/978-3-540-79703-6

Liblik, T., Laanemets, J., Raudsepp, U., Elken, J., and Suhhova, I. (2013). Estuarine circulation reversals and related rapid changes in winter near-bottom oxygen conditions in the Gulf of Finland, Baltic Sea. *Ocean Sci.* 9, 917–930. doi: 10.5194/os-9-917-2013

Liblik, T., and Lips, U. (2011). Characteristics and variability of the vertical thermohaline structure in the Gulf of Finland in summer. *Boreal Environ. Res.* 16. 73-83.

Liblik, T., and Lips, U. (2017). Variability of pycnoclines in a three-layer, large estuary: the Gulf of Finland. *Boreal Environ. Res.* 22, 27.

Liblik, T., Väli, G., Lips, I., Lilover, M.-J., Kikas, V., and Laanemets, J. (2020). The winter stratification phenomenon and its consequences in the Gulf of Finland, Baltic Sea. *Ocean Sci.* 16, 1475–1490. doi: 10.5194/os-16-1475-2020

Liblik, T., Väli, G., Salm, K., Laanemets, J., Lilover, M.-J., and Lips, U. (2022). Quasi-steady circulation regimes in the Baltic Sea. *Ocean Sci. Discuss.* 2022, 1–37. doi: 10.5194/os-18-857-2022

Lips, I., Lips, U., and Liblik, T. (2009). Consequences of coastal upwelling events on physical and chemical patterns in the central Gulf of Finland (Baltic Sea). *Cont. Shelf Res.* 29, 1836–1847. doi: 10.1016/j.csr.2009.06.010

Lips, I., Rünk, N., Kikas, V., Meerits, A., and Lips, U. (2014). High-resolution dynamics of the spring bloom in the Gulf of Finland of the Baltic Sea. *J. Mar. Syst.* 129, 135–149. doi: 10.1016/j.jmarsys.2013.06.002

Lips, I., Turov, P., Lind, K., Buhhalko, N., and Thennakoon, H. (2020). Mikroplasti allikad ja levikuteed Eesti rannikumerre, potentsiaalne mõju pelaagilistele ja bentilistele organismidele. *Report 4-1/18/30*. Tallinn: Tallinn University of Technology, Department of Marine Systems; p. 1–46.

Lips, U., Zhurbas, V., Skudra, M., and Väli, G. (2016). A numerical study of circulation in the Gulf of Riga, Baltic Sea. Part I: Whole-basin gyres and mean currents. *Cont. Shelf Res.* 112, 1–13. doi: 10.1016/j.csr.2015.11.008

Lips, I., Turov, P., Lind, K., Buhhalko, N., and Thennakoon, H. (2020). Mikroplasti allikad ja levikuteed Eesti rannikumerre, potentsiaalne mõju pelaagilistele ja bentilistele organismidele. Report 4-1/18/30. Tallinn: Tallinn University of Technology, Department of Marine Systems; p. 1–46.

Llorca, M., Álvarez-Muñoz, D., Ábalos, M., Rodríguez-Mozaz, S., Santos, L. H., León, V. M., et al. (2020). Microplastics in Mediterranean coastal area: Toxicity and impact for the environment and human health. *Trends Environ. Anal. Chem.* 27, e00090. doi: 10.1016/j.teac.2020.e00090

Lv, X., Dong, Q., Zuo, Z., Liu, Y., Huang, X., and Wu, W.-M. (2019). Microplastics in a municipal wastewater treatment plant: Fate, dynamic distribution, removal efficiencies, and control strategies. *J. Clean. Prod.* 225, 579–586. doi: 10.1016/j.jclepro.2019.03.321

Magnusson, K. (2016). Microlitter in sewage treatment systems: A Nordic perspective on waste water treatment plants as pathways for microscopic anthropogenic particles to marine systems. *Nordic Council Ministers*. doi: 10.6027/TN2016-510

Marko, F., and Urs, B. (2013). Mass balance of perfluoroalkyl acids in the baltic sea. *Environmental Science & Technology*. 47, 4088–4095. doi: 10.1021/es400174y

Martyanov, S. D., Isaev, A. V., and Ryabchenko, V. A. (2021). Model estimates of microplastic potential contamination pattern of the eastern Gulf of Finland in 2018. *Oceanologia* 65, 86–99. doi: 10.1016/j.oceano.2021.11.006

Martyanov, S. D., Ryabchenko, V. A., Ershova, A. A., Eremina, T. R., and Martin, G. (2023). On the assessment of microplastic distribution in the eastern part of the Gulf of Finland. *Fundamental and Applied Hydrophysics*, 16(1), 5–14. doi: 10.7868/S2073667323010020

Matjašič, T., Mori, N., Hostnik, I., Bajt, O., and Viršek, M. K. (2023). Microplastic pollution in small rivers along rural–urban gradients: Variations across catchments and between water column and sediments. *Sci. Total Environ.* 858, 160043. doi: 10.1016/j.scitotenv.2022.160043

Meier, H. E. M., and Kauker, F. (2003). Modeling decadal variability of the Baltic Sea: 2. Role of freshwater inflow and large-scale atmospheric circulation for salinity. *J. Geophys. Res. Ocean.* 108. doi: 10.1029/2003JC001799

Mintenig, S. M., Int-Veen, I., Löder, M. G. J., Primpke, S., and Gerdts, G. (2017). Identification of microplastic in effluents of waste water treatment plants using focal plane array-based micro-Fourier-transform infrared imaging. *Water Res.* 108, 365–372. doi: 10.1016/j.watres.2016.11.015

Mishra, A., Buhhalko, N., Lind, K., Lips, I., Liblik, T., Väli, G., et al. (2022). Spatiotemporal variability of microplastics in the Eastern Baltic Sea. *Front. Mar. Sci.* 9. doi: 10.3389/fmars.2022.875494

Murawski, J., She, J., and Frishfelds, V. (2022). Modelling drift and fate of microplastics in the Baltic Sea. *Front. Mar. Sci.* 1656. doi: 10.3389/fmars.2022.886295

Neumann, T., Fennel, W., and Kremp, C. (2002). Experimental simulations with an ecosystem model of the Baltic Sea: a nutrient load reduction experiment. *Global Biogeochem. Cycles* 16, 1–7. doi: 10.1029/2001GB001450

Neumann, T., Radtke, H., Cahill, B., Schmidt, M., and Rehder, G. (2022). Non-Redfieldian carbon model for the Baltic Sea (ERGOM version 1.2)–implementation and budget estimates. *Geosci. Model. Dev.* 15, 8473–8540. doi: 10.5194/gmd-15-8473-2022

Neumann, T., and Schernewski, G. (2008). Eutrophication in the Baltic Sea and shifts in nitrogen fixation analyzed with a 3D ecosystem model. *J. Mar. Syst.* 74, 592–602. doi: 10.1016/j.jmarsys.2008.05.003

Osinski, R. D., Enders, K., Gräwe, U., Klingbeil, K., and Radtke, H. (2020). Model uncertainties of a storm and their influence on microplastics and sediment transport in the Baltic Sea. *Ocean Sci.* 16, 1491–1507. doi: 10.5194/os-16-1491-2020

Pärn, O., Moy, D. M., and Stips, A. (2023). Determining the distribution and accumulation patterns of floating litter in the Baltic Sea using modelling tools. *Mar. pollut. Bull.* 190, 114864. doi: 10.1016/j.marpolbul.2023.114864

Pedrotti, M. L., Petit, S., Elineau, A., Bruzaud, S., Crebassa, J.-C., Dumontet, B., et al. (2016). Changes in the floating plastic pollution of the Mediterranean Sea in relation to the distance to land. *PloS One* 11, e0161581. doi: 10.1371/journal.pone.0161581

Prata, J. C. (2018). Microplastics in wastewater: State of the knowledge on sources, fate and solutions. *Mar. pollut. Bull.* 129, 262–265. doi: 10.1016/j.marpolbul.2018.02.046

Radtke, H., Lipka, M., Bunke, D., Morys, C., Woelfel, J., Cahill, B., et al. (2019). Ecological ReGional Ocean Model with vertically resolved sediments (ERGOM SED 1.0): coupling benthic and pelagic biogeochemistry of the south-western Baltic Sea. *Geosci. Model. Dev.* 12, 275–320. doi: 10.5194/feart.2021.594415

Rasmus, K., Kiirikki, M., and Lindfors, A. (2015). Long-term field measurements of turbidity and current speed in the Gulf of Finland leading to an estimate of natural resuspension of bottom sediment. *Boreal Environ. Res.* 20, 735.

Redfield, A. C. (1934). *On the proportions of organic derivatives in sea water and their relation to the composition of plankton.* (Liverpool, United Kingdom: University Press of Liverpool).

Scheffer, M., Baveco, J. M., DeAngelis, D. L., Rose, K. A., and van Nes, Eh. (1995). Super-individuals a simple solution for modelling large populations on an individual basis. *Ecol. Modell.* 80, 161–170. doi: 10.1016/0304-3800(94)00055-M

Schernewski, G., Radtke, H., Hauk, R., Baresel, C., Olshammar, M., and Oberbeckmann, S. (2021). Urban microplastics emissions: effectiveness of retention measures and consequences for the Baltic Sea. *Front. Mar. Sci.* 8. doi: 10.3389/fmars.2021.594415

Schernewski, G., Radtke, H., Hauk, R., Baresel, C., Olshammar, M., Osinski, R., et al. (2020). Transport and behavior of microplastics emissions from urban sources in the Baltic Sea. *Front. Environ. Sci.* 8. doi: 10.3389/fenvs.2020.579361

Schmidt, C., Krauth, T., and Wagner, S. (2017). Export of plastic debris by rivers into the sea. *Environ. Sci. Technol.* 51, 12246–12253. doi: 10.1021/acs.est.7b02368

Schrank, I., Löder, M. G. J., Imhof, H. K., Moses, S. R., Heß, M., Schwaiger, J., et al. (2022). Riverine microplastic contamination in southwest Germany: A large-scale survey. *Front. Earth Sci.* 10. doi: 10.3389/feart.2022.794250

Setälä, O., Magnusson, K., Lehtiniemi, M., and Norén, F. (2016). Distribution and abundance of surface water microlitter in the Baltic Sea: a comparison of two sampling methods. *Mar. Pollut. Bull.* 110, 177–183. doi: 10.1016/j.marpolbul.2016.06.065

She, J., Buhhalko, N., Lind, K., Mishra, A., Kikas, V., Costa, E., et al. (2022). Uncertainty and consistency assessment in multiple microplastic observation datasets in the Baltic Sea. *Front. Mar. Sci.* 9. doi: 10.3389/fmars.2022.886357

Siegfried, M., Koelmans, A. A., Besseling, E., and Kroeze, C. (2017). Export of microplastics from land to sea. A modelling approach. *Water Res.* 127, 249–257. doi: 10.1016/j.watres.2017.10.011

Siht, E., Väli, G., Liblik, T., Mishra, A., Buhhalko, N., and Lips, U. (2025). Modeling the pathways of microplastics 797 in the Gulf of Finland, Baltic Sea - sensitivity of parametrizations. Ocean Dynamics. *Ocean Dynamics* 75, 9. doi: 10.1007/s10236-024-01649-0

Smagorinsky, J. (1963). General circulation experiments with the primitive equations: I. The basic experiment. *Mon. Weather Rev.* 91, 99–164. doi: 10.1175/1520-0493(1963)091<0099:GCEWTP>2.3.CO;2

Suaria, G., and Aliani, S. (2014). Floating debris in the mediterranean sea. *Mar. pollut. Bull.* 86, 494–504. doi: 10.1016/j.marpolbul.2014.06.025

Suhhova, I., Liblik, T., Lilover, M.-J., and Lips, U. (2018). A descriptive analysis of the linkage between the vertical stratification and current oscillations in the Gulf of Finland. *Boreal Environ. Res.* 23, 83–103.

Sun, J., Dai, X., Wang, Q., Van Loosdrecht, M. C. M., and Ni, B.-J. (2019). Microplastics in wastewater treatment plants: Detection, occurrence and removal. *Water Res.* 152, 21–37. doi: 10.1016/j.watres.2018.12.050

Suursaar, Ü., Elken, J., and Belkin, I. M. (2021). Fronts in the Baltic Sea: A review with a focus on its north-eastern part. *Chem. Oceanogr. Front. Zo.*, 143–181. doi: 10.1007/698_2021_813

Talvitie, J., Mikola, A., Koistinen, A., and Setälä, O. (2017). Solutions to microplastic pollution–Removal of microplastics from wastewater effluent with advanced wastewater treatment technologies. *Water Res.* 123, 401–407. doi: 10.1016/j.watres.2017.07.005

Tsiaras, K., Hatzonikolakis, Y., Kalaroni, S., Pollani, A., and Triantafyllou, G. (2021). Modeling the pathways and accumulation patterns of micro-and macro-plastics in the Mediterranean. *Front. Mar. Sci.* 8. doi: 10.3389/fmars.2021.743117

Uaciquete, D., Mitsunaga, K., Aoyama, K., Kitajima, K., Chiba, T., Jamal, D. L., et al. (2024). Microplastic abundance in the semi-enclosed Osaka Bay, Japan. *Environ. Sci. pollut. Res.* 31, 49455–49467. doi: 10.1007/s11356-024-34444-x

Uiboupin, R., and Laanemets, J. (2009). Upwelling characteristics derived from satellite sea surface temperature data in the Gulf of Finland, Baltic Sea. *Boreal Environ. Res.* 14, 297–304.

Uurasjärvi, E., Pääkkönen, M., Setälä, O., Koistinen, A., and Lehtiniemi, M. (2021). Microplastics accumulate to thin layers in the stratified Baltic Sea. *Environ. pollut.* 268, 115700. doi: 10.1016/j.envpol.2020.115700

Väli, G., Meier, H. E. M., Liblik, T., Radtke, H., Klingbeil, K., Gräwe, U., et al. (2024). Submesoscale processes in the surface layer of the central Baltic Sea: a high-resolution modelling study. *Oceanologia*. 66, 78-90. doi: 10.1016/j.oceano.2023.11.002

Väli, G., Meier, M., Dieterich, C., and Placke, M. (2019). River runoff forcing for ocean modeling withinthe Baltic Sea Model Intercomparison Project. *Meereswiss*. 113, 1–26. doi: 10.12754/msr-2019-0113

Väli, G., Zhurbas, V., Laanemets, J., and Elken, J. (2011). Simulation of nutrient transport from different depths during an upwelling event in the Gulf of Finland. *Oceanologia* 53, 431–448. doi: 10.5697/oc.53-1-TI.431

Vali, G., Zhurbas, V. M., Laanemets, J., and Lips, U. (2018). Clustering of floating particles due to submesoscale dynamics: a simulation study for the Gulf of Finland, Baltic Sea. *Фундаментальная и прикладная гидрофизика* 11, 21–35. doi: 10.7868/s2073667318020028

Väli, G., Zhurbas, V., Lips, U., and Laanemets, J. (2017). Submesoscale structures related to upwelling events in the Gulf of Finland, Baltic Sea (numerical experiments). *J. Mar. Syst.* 171, 31–42. doi: 10.1016/j.jmarsys.2016.06.010

Veerasingam, S., Saha, M., Suneel, V., Vethamony, P., Rodrigues, A. C., Bhattacharyya, S., et al. (2016). Characteristics, seasonal distribution and surface degradation features of microplastic pellets along the Goa coast, India. *Chemosphere* 159, 496–505. doi: 10.1016/j.chemosphere.2016.06.056

Vermeiren, P., Muñoz, C. C., and Ikejima, K. (2016). Sources and sinks of plastic debris in estuaries: a conceptual model integrating biological, physical and chemical distribution mechanisms. *Mar. pollut. Bull.* 113, 7–16. doi: 10.1016/j.marpolbul.2016.10.002

Vianello, A., Da Ros, L., Boldrin, A., Marceta, T., and Moschino, V. (2018). First evaluation of floating microplastics in the Northwestern Adriatic Sea. *Environ. Sci. pollut. Res.* 25, 28546–28561. doi: 10.1007/s11356-018-2812-6

Zhou, Q., Tu, C., Yang, J., Fu, C., Li, Y., and Waniek, J. J. (2021). Trapping of microplastics in halocline and turbidity layers of the semi-enclosed Baltic Sea. *Front. Mar. Sci.* 8. doi: 10.3389/fmars.2021.761566

Zhurbas, V., Väli, G., Golenko, M., and Paka, V. (2018). Variability of bottom friction velocity along the inflow water pathway in the Baltic Sea. *J. Mar. Syst.* 184, 50–58. doi: 10.1016/j.jmarsys.2018.04.008

Ziajahromi, S., Neale, P. A., and Leusch, F. D. L. (2016). Wastewater treatment plant effluent as a source of microplastics: review of the fate, chemical interactions and potential risks to aquatic organisms. *Water Sci. Technol.* 74, 2253–2269. doi: 10.2166/wst.2016.414

Publication III

Siht E., Väli G., Liblik T., Mishra A., Buhhalko N., Lips U. (2025). Modeling the pathways of microplastics in the Gulf of Finland, Baltic Sea - sensitivity of parametrizations. Ocean Dynamics. Ocean Dynamics 75, 9. doi: 10.1007/s10236-024-01649-0

Check for
updates

Modeling the pathways of microplastics in the Gulf of Finland, Baltic Sea – sensitivity of parametrizations

Enriko Siht[1] · Germo Väli[1] · Taavi Liblik[1] · Arun Mishra[1] · Natalja Buhhalko[1] · Urmas Lips[1]

Abstract

This study introduces an open software Lagrangian particle tracking model designed for simulating the transport of microplastics (MPs), which incorporates crucial processes such as horizontal diffusion, beaching, resuspension, and biofouling. A sensitivity analysis for the parametrization of these processes was conducted on a regional scale – in the Gulf of Finland (GoF), the eastern Baltic Sea – employing very high-resolution hydrodynamic model output to drive the particle model. The sensitivity analysis underscores the impact of each process on the number of particles in the water column, sediments, beach areas, and at the domain boundary. The results indicate a significant impact of including or excluding a process and relatively high sensitivity of the parametrization on the simulated MP pathways. Stronger diffusion dispersed particles widely throughout the gulf and enhanced the export of the MPs out from the gulf. Beaching and biofouling were the major contributing factors to particle removal from the water column, while resuspension promoted settling in offshore areas. The number of beached particles rapidly increased during the wind-induced downwelling process. Scenario simulations, including parametrizations favoring or hindering MP transport, showed that a coincidence of several factors could lead to very diverse MP pathways. The analysis offers valuable insights, providing a foundation for tuning the model parameters to improve simulations with realistic loads in the future.

1 Introduction

Microplastics (MPs), defined as plastic particles with dimensions of 5 mm or smaller, pervade the marine ecosystem due to the degradation of larger plastic items and the direct release of MPs into the environment (Andrady 2011; GESAMP 2015). MPs enter the marine environment through various sources, including maritime activities, wear and tear of textiles and tires, and inadequate waste management (Andrady 2011). Its ingestion by marine organisms can yield harmful consequences, potentially affecting human health through the aquatic food chain (Caruso 2019; GESAMP 2015; Möhlenkamp et al. 2018; Wright et al. 2013).

Modeling the fate and transport of MPs in the marine environment is an important step in understanding the impact of MPs and in developing effective management strategies,

especially as field measurements are too sparse to estimate their dynamics efficiently (Khatmullina and Chubarenko 2019; Lindeque et al. 2020). Typically, models for estimating pathways fall into two broad categories. The first category comprises Eulerian models, which employ tracers carried by ocean currents directly within their native grid. The other category of models is the Lagrangian models (a.k.a. particle tracking models), which track individual particles in the Lagrangian framework. Particle tracking models do not compute the hydrodynamics themselves; instead, they are coupled with or use the output of Eulerian models to acquire the ambient hydrological parameters. The Lagrangian approach is particularly well-suited for applications involving MPs, primarily due to the inherent efficiency of integration algorithms within the Lagrangian framework. In this context, the transport equations are only solved for active particles, unlike to Eulerian models, which solve transport equations for tracers in all computational cells, even when no particles are present. Despite relying on Eulerian model outputs for forcing data, the offline-coupling Lagrangian approach allows this data to be reused. For instance, it is possible to simulate various scenarios with particles of differing characteristics without recalculating hydrodynamics. Lagrangian algorithms

---

Responsible Editor: Sandro Carniel

✉ Enriko Siht
enriko.siht@taltech.ee

[1] Department of Marine Systems, Tallinn University of Technology, Tallinn 12618, Estonia

are also naturally parallelizable, offering the potential to enhance computational speed significantly. Furthermore, particle tracking models usually record the history of each particle, thus allowing to analyze and describe their behavior easily (Bigdeli et al. 2022; Pilechi et al. 2022; van Sebille et al. 2018).

Several particle tracking models are available, each with its distinct set of strengths and limitations. These include OpenDrift (Dagestad et al. 2018), Parcels (Lange and van Sebille 2017), TRACMASS (Döös et al. 2017), and MOHID Lagrangian (Cloux et al. 2022). A comprehensive overview of such models is presented by van Sebille et al. (2018). These models have been applied across various global marine environments and have contributed to our understanding of MP transport (Berglund et al. 2021; Cloux et al. 2022; Fischer et al. 2022; Jonsson et al. 2020; Lobelle et al. 2021; Rosas et al. 2022).

MPs suspended in water are influenced by various processes that dictate their trajectories and eventual destinations. These processes comprise physical transport mechanisms such as advection and diffusion, drift caused by wind and waves, buoyancy, beaching, deposition, and resuspension (Bigdeli et al. 2022; Cole et al. 2011). In addition, MPs undergo transformational processes such as degradation (Cole et al. 2011) and biofouling (Kooi et al. 2017), which may change their physical and chemical properties. Advection and diffusion have been fundamental in all models. Most models have also considered the buoyancy of MPs (e.g., Kooi et al. 2017; Onink et al. 2022; Pilechi et al. 2022). For instance, a variation of the Stokes law is used to calculate the settling velocity of particles based on the density difference and the dimensionless particle diameter (Dietrich 1982). The resuspension process is frequently integrated, employing the Shields parametrization method (Shields 1936) and tailoring it to account for sediment material characteristics (Waldschläger and Schüttrumpf 2019; Wilcock 1988). Alternatively, models may define a critical shear velocity threshold, as in Zhurbas et al. (2018). Beaching, another critical factor, can be parameterized diversely, incorporating elements such as coastal morphology or uniform beaching times across the model domain (Daily et al. 2021; Liubartseva et al. 2018; Onink et al. 2022). Among the most intricate processes, biofouling has given rise to various model approaches. Complex models rely on variables like algae concentrations, temperature, light availability, and grazing, sourced from biogeochemical models or computed dynamically (Fischer et al. 2022; Kooi et al. 2017; Tsiaras et al. 2021). Simpler models employ biological proxies and parametrizations (e.g., Murawski et al. 2022). Given this complexity, it becomes essential to test these process parametrizations thoroughly. Analyzing their sensitivity within the model framework becomes imperative and aids in refining model parameters and assumptions, thus increasing the accuracy and reliability of MPs simulations.

The Baltic Sea encompasses approximately 21,700 km^3 of semi-enclosed brackish water, with an average depth of 55 m and notable variations in salinity (Lehmann et al. 2022). This unique ecosystem balances freshwater inflow from rivers with saltwater from the North Sea (Markus Meier et al., 2023), resulting in a vulnerable environment susceptible to pollution and eutrophication. Furthermore, the Baltic Sea catchment area has a population of about 85 million people (HELCOM 2018). Despite its environmental challenges, the Baltic Sea remains a historically significant trade route and is important for regional commerce, tourism, and the conservation of its biodiversity.

Previous investigations have documented the presence of MPs in all Baltic Sea basins (Aigars et al. 2021; Gewert et al. 2017; Schönlau et al. 2020). Additionally, reports of washed-up MP particles have emerged from various Baltic Sea regions (Graca et al. 2017). MPs have also been found in fish samples (e.g., Sainio et al. 2021). Furthermore, high variability in MPs concentrations related to the coastal mesoscale processes has been noted (e.g., Mishra et al. 2022).

In the realm of MPs simulations within the Baltic Sea, numerous modeling studies have contributed to our understanding of the distribution, transport, and fate of MPs. Several studies have adopted the Eulerian modeling approach (Frishfelds et al. 2022; Murawski et al. 2022; Osinski et al. 2020; Schernewski et al. 2021), which encompasses processes such as settling, deposition, erosion, wind and wave interactions, as well as beaching. Notably, Martyanov et al. (2023) presented a parameterization of MP particle fall velocity as a function of temperature, effectively capturing seasonal variations. Furthermore, Murawski et al. (2022) integrated a biofilm growth model, leveraging chlorophyll-a concentrations in seawater to introduce seasonality to biofilm development. In contrast, using the Lagrangian approach for MP modeling has seen fewer applications in the Baltic Sea. Pärn et al. (2023) employed a particle tracking model to estimate macro-litter pathways and accumulation in the Baltic Sea. Previous applications of Lagrangian trajectories in the region have predominantly focused on topics such as circulation (Döös et al. 2004; Engqvist et al. 2006; Miettunen et al. 2020), submesoscale features (Väli et al. 2018; Zhurbas et al. 2019), and marine transport risk assessment (Andrejev et al. 2011; Delpeche–Ellmann and Soomere 2013; Viikmäe and Soomere 2018).

This paper introduces the new Lagrangian particle tracking model, which was specifically developed for simulating the movement and accumulation of MP particles within the GoF. A sensitivity analysis is conducted to gather insights into the model's behavior across varying parameter values, which is crucial for fine-tuning the model for realistic simulations in the future. The model incorporates several key processes that significantly influence MPs transport within the marine environment. It was developed to efficiently handle

very high-resolution data, including the output from models with vertically adaptive coordinates, and has also been tested for compatibility with thehydrodynamic model outputs from the Copernicus Marine Service (Atlantic - European North West Shelf - Ocean Physics Reanalysis. E.U. Copernicus Marine Service Information (CMEMS). Marine Data Store (MDS). DOI: https://doi.org/10.48670/moi-00059, Accessed on 01-Oct-2023). See Appendix A for the CMEMS test. The particle tracking model is licensed under the GNU General Public License v3.0 and is publicly available on GitHub (https://github.com/TalTech-MFO/ParticleModel). This paper is structured as follows: the Section 2 describes the particle tracking model and provides an overview of the setup for the sensitivity analysis. The section 3 includes the validation information of the hydrodynamic and particle tracking models and presents findings from sensitivity analyses. The section 4 explores the implications of our findings, and conclusions are summarized in the Summary and Conclusions section.

2 Materials and methods

2.1 Hydrodynamic model

General Estuarine Transport Model (GETM; Burchard and Bolding 2002) has been used in this study to simulate the current, temperature, and salinity fields of the Baltic Sea and GoF. GETM is a hydrostatic, three-dimensional primitive equation model that has embedded adaptive vertical coordinates (Hofmeister et al. 2010; Klingbeil et al. 2018), which significantly reduces numerical mixing in the simulations (Gräwe et al. 2015).

The vertical mixing (vertical viscosity and diffusion) in the GETM is calculated with the General Ocean Turbulence Model (GOTM; Burchard and Bolding 2001), and more precisely, two equation k-e scheme with a second moment algebraic closure (Canuto et al. 2001) is selected. The horizontal mixing (viscosity and diffusion) is calculated using the Smagorinsky parameterization (Smagorinsky 1963).

2.2 Biogeochemistry model

The biogeochemistry model ERGOM (Neumann et al. 2002; Neumann and Schernewski 2008) is coupled with the hydrodynamic model via the Framework for Aquatic Biogeochemical Models (FABM; Bruggeman and Bolding 2014). ERGOM has 12 state variables and describes a nitrogen cycle. Phosphorus is considered with the N: P ratio (Redfield 1934). Nutrients are described with three state variables – ammonium, nitrate, and phosphate- taken up by three phytoplankton groups: diatoms, flagellates, and nitrogen-fixing cyanobacteria. The grazing pressure

on the phytoplankton is described with zooplankton. Oxygen conditions are prescribed with two state variables: dissolved oxygen and H_2S, while the consumption and production of oxygen are linked to biogeochemical processes via stoichiometric ratios. Additional variables in the model are for the dead phytoplankton and zooplankton (detritus), which is either in the water column or sedimented in the bottom. Nutrients are released from the detritus during the mineralization, although part of the nitrogen is released from the system as molecular nitrogen, and part is buried permanently in the sediments. For more details about the ERGOM model, the reader is referred to (Neumann et al. 2022).

2.3 Lagrangian particle tracking model

2.3.1 Model description

An offline coupled Lagrangian particle tracking model was developed and used to simulate the particle transport using the hydrodynamic data from the high-resolution GETM model simulation. The particle tracking model is written in Fortran and requires a compiler that supports the Fortran 2003 standard. The compilation and execution of the model have only been tested in a Linux environment and with GCC compiler versions 10.3.0 and 13.1.0. There are no external dependencies except the NetCDF Fortran library (https://docs.unidata.ucar.edu/netcdf-fortran/current/, last checked 30.09.2024). The model can be run on a single or multiple threads using OpenMP. However, since OpenMP uses a shared-memory parallelism model, the number of threads is limited to the number of cores available on a single node on large HPC clusters. The memory requirements largely depend on the size of the forcing data and the number of particles used in the simulation. For our use case, with high-resolution hydrodynamic fields ($890 \times 1557 \times 60$ cells), approximately 15GB was sufficient. The model can efficiently handle large forcing datasets (multiple terabytes) and works with two types of vertical coordinates: (1) z-level coordinates and (2) adaptive depth coordinates. The advantage of the latter is that it saves the time and storage needed to preprocess the raw output of the hydrodynamic models with adaptive coordinates.

The particles are advected using a second-order Runge-Kutta scheme, which offers greater numerical stability than the explicit Euler scheme. The particles undergo additional processes described in Sect. 2.3.2 at each time step. The Lagrangian model incorporates various parameters from the hydrodynamic model's data, including temperature, salinity, density, eddy viscosity, and sea-surface elevation. Small and large cell phytoplankton and cyanobacteria fields are used from ERGOM model output to calculate the chlorophyll-a (chl-a) concentrations.

2.3.2 Implemented processes

The following describes the implemented processes: mixing, buoyancy, beaching, resuspension, and biofouling.

The particle's displacement due to advection in all three dimensions was calculated using the second-order Runge-Kutta scheme:

$$\vec{x}(t + \Delta t) = \vec{x}(t) + 0.5 \left(\vec{u}(x, t) + \vec{u}\left(\tilde{x}, t + \Delta t \right) \right) \Delta t,$$

where

$$\tilde{x} = \vec{x}(t) + \vec{u}(x, t)\Delta t$$

is the predictor for the position at the time $t + \Delta t$.

The horizontal displacement of particles due to horizontal mixing was calculated as

$$x_{t+1} = x_t + N\sqrt{2 A_h dt},$$

where N is normally distributed with a mean value of 0 and a standard deviation of 1 random number. A_h is the eddy

viscosity calculated according to the Smagorinsky sub-grid scale parametrization (1963):

$$A_h = C_s \Delta x \Delta y \sqrt{\left(\frac{\partial u}{\partial x} \right)^2 + \left(\frac{\partial v}{\partial y} \right)^2 + \frac{1}{2} \left(\frac{\partial u}{\partial y} + \frac{\partial v}{\partial x} \right)^2},$$

where Δx and Δy are the width and length of the hydrodynamic model grid cells, u and v are current velocities, and C_s is a varying constant (see Sect. 2.4.3).

The vertical velocity of the plastic particle due to buoyancy was calculated using a modified Stokes equation (Dietrich 1982):

$$\frac{dz}{dt} = V_s(z, t) = -\left(\frac{\rho_{tot} - \rho_{sw,z}}{\rho_{sw,z}} g\omega_* v_{sw,z} \right)^{1/3},$$

where ρ_{tot} is the total density of the plastic particle, including biofilm; $\rho_{sw,z}$ is the density of seawater at depth z; g is the gravitational acceleration, and $v_{sw,z}$ is the kinematic viscosity of seawater at depth z. The dimensionless settling velocity ω_* was calculated using the empirical expression:

$$\omega_* = \begin{cases} 10^{-3.76715 + 1.92944\log D_* - 0.09815\log D_*^2 - 0.00575\log D_*^3 + 0.00056\log D_*^4}, & 0.05 \leq D_* \leq 5 \times 10^9 \\ 1.74 \times 10^{-4} D_*^2, & D_* < 0.05 \end{cases}$$

The latter is a function of the dimensionless particle diameter D_*, which was calculated as:

$$D_* = \frac{\left(\rho_{tot} - \rho_{sw,z} \right) g D_s^3}{\rho_{sw,z} v_{sw,z}^2},$$

where D_s is the equivalent spherical diameter of the particle.

In our implementation of resuspension, the particle's vertical velocity is proportional to the bottom friction velocity u_* if the particle was previously settled and u_* exceeds a predefined threshold. The bottom friction velocity, u_*, was calculated as:

$$u_* = \left(\frac{\tau_{Bx}^2}{\rho} + \frac{\tau_{By}^2}{\rho} \right)^{0.25},$$

where τ_{Bx} and τ_{By} are the bottom shear stress components in the x and y direction, respectively. The bottom stress was calculated as (Blumberg and Mellor 1983):

$$\tau_{Bx}/\rho = -C\sqrt{u_B^2 + v_B^2} \cdot u;$$

$$\tau_{By}/\rho = -C\sqrt{u_B^2 + v_B^2} \cdot v.$$

Here, u_B and v_B are the x- and y-velocity components near the bottom, respectively. The drag coefficient C was defined as:

$$C = \max \left\{ \left(\frac{\kappa^2}{(\log \frac{z}{z_0})^2} \right), C_{min} \right\},$$

where κ is the von Karman constant ($\kappa = 0.4$), z is the height from the bottom, z_0 is the roughness height, and $C_{min} = 0.0025$ is the minimum drag coefficient.

The biofilm growth on the particle was determined using the equation:

$$\frac{dh_{bf}}{dt} = \frac{\left(h_{bf,max} - h_{bf} \right)}{T_s},$$

where h_{bf} is the current thickness of the biofilm, $h_{bf,max}$ is the maximum biofilm thickness defined as a fraction of the particle's radius, and T_s represents the biofilm growth time scale (Murawski et al. 2022). The growth of the biofilm occurs only if the chl-a concentration in the surrounding water exceeds a specified threshold (1.1 mg m^{-3}). This threshold accounts for seasonal variations in biofilm growth.

Fig. 1 Upper panel: Setup of the nested grids of the hydrodynamic model. Lower panel: Domain of the particle tracking model with particle release locations (red dots) and hydrodynamic model validation stations (orange dots), offshore station LL7 (orange square), and ADCP station (orange triangle)
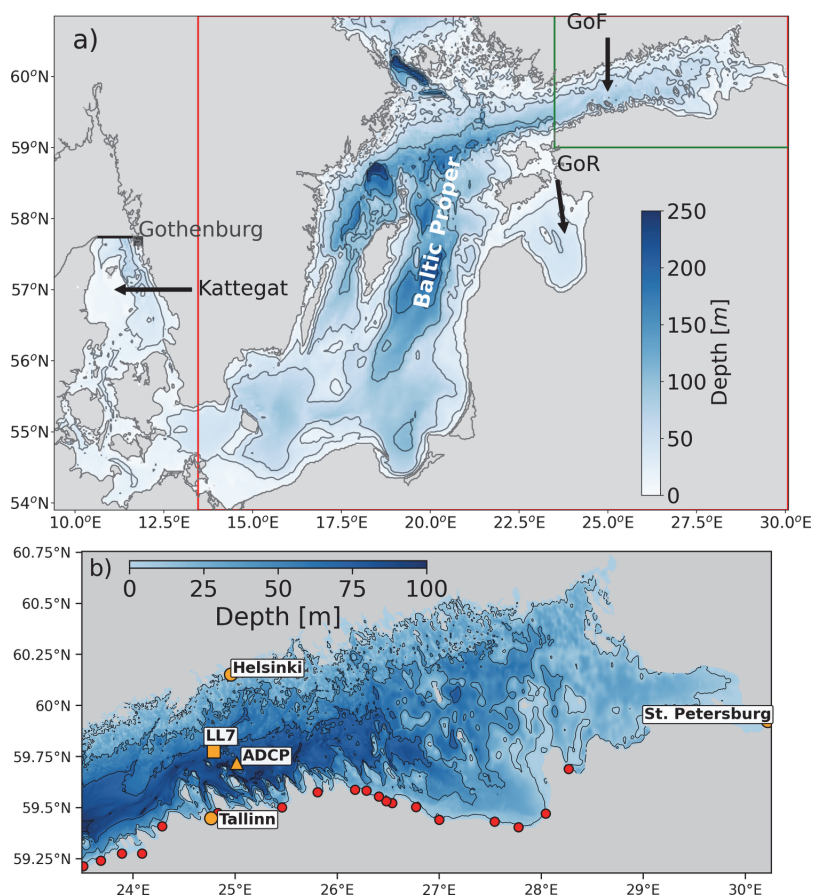
The ambient chl-a concentrations were obtained from the biogeochemical model output. As the biofilm grows, it increases the particle's radius and density. The total radius and density of the particle, including the attached biofilm, were calculated using the following formulas:

$$R_{tot} = R_{pl} + h_{bf};$$
$$\rho_{tot} = \frac{R_{pl}^3 \rho_{pl} + \left(R_{tot}^3 - R_{pl}^3\right)\rho_{bf}}{R_{tot}^3}.$$

Beaching in the model is determined by the length of time a particle spends in a beach cell. A beach cell is defined as a cell with at least one neighboring cell classified as a land cell. When a particle remains consecutively in a beach cell for a specified duration, it is considered "beached" until the end of the simulation. If the particle exits the beach cell, its timer is reset to zero, and the counting restarts when the particle re-enters a beach cell. An alternative to the timer-based beaching mechanism would be a probabilistic approach, as

implemented, e.g., by Alosairi et al. (2020) and Pilechi et al. (2022). In the studies conducted by Daily et al. (2021) and Liubartseva et al. (2018), a hybrid approach was adopted, incorporating the probability of beaching as a function of the characteristic beaching time. Their approach also allowed for particle resuspension from beached areas, while our model omitted resuspension from beaches. The timer-based beaching mechanism was selected for its simplicity and a straightforward criterion based on the duration a particle spends in a beach cell.

2.4 Model setup description

2.4.1 Hydrodynamic model

A nested GETM-ERGOM model system is used to simulate the circulation in the GoF in this study (see Fig. 1a). The lowest resolution model has a horizontal grid spacing of 1 nautical mile (approximately 1852 m) and covers the whole

Fig. 2 Timeseries of total released particles

Baltic Sea with 50 vertically adaptive layers (e.g., Gräwe et al. 2015). Sea surface observations from Gothenburg Torshamnen station describing the barotropic water exchange between the Baltic and North Sea are used for boundary conditions.

The medium resolution model has a horizontal grid spacing of 0.5 nautical miles (approximately 1 km) and covers the central Baltic Proper along with the GoF and Gulf of Riga (GoR). Settings for the medium resolution model are the same as in Zhurbas et al. (2018) and Liblik et al. (2020, 2022), but the model uses spatially interpolated values of temperature and salinity along with the current components from the coarse resolution model with hourly resolution at open boundaries.

The high-resolution model domain has a horizontal grid spacing of 0.125 nautical miles (approximately 250 m) and covers the GoF. Similarly, with the previous level nesting, spatially interpolated results with hourly resolution from medium resolution model are used for the boundary conditions. The number of adaptive layers in medium and high-resolution runs is 60.

Atmospheric forcing at the sea surface (wind stress and heat flux) is calculated offline from the ERA5 re-analysis (Hersbach et al. 2020). The ERA5 is a homogenous extensive dataset, which can be used in further studies addressing long-term pollution of the MP. Validation of hydrodynamic model results for the Baltic Sea with ERA5 forcing against current measurements has revealed good performance of the setup (e.g. Liblik et al. 2022). Freshwater input to the models is based on the runoff data compiled for the Baltic Model Intercomparison Project (BMIP; Gröger et al. 2022) by Väli et al. (2019). Runoff and N/P loads from Estonian rivers have been replaced with the values from EstModel (https://estmodel.app/en/#/, last accessed 10.09.2023).

The initial temperature and salinity fields for the coarse resolution model were taken from the Copernicus Marine Service re-analysis product for 2009-12-30. The medium and high-resolution models use the daily mean for 2017-12-03 from the coarse and medium-resolution runs, respectively. In this paper, we use the results from the high-resolution run for 2018.

2.4.2 Lagrangian particle tracking model

The simulation period ranged from February 5 to December 31, 2018. The year 2018 was chosen because of the good coverage of observational data, which allowed us to validate the hydrodynamic model. Daily particle releases originated only from rivers along the southern coast, with the particle load proportional to the river discharge. The dataset contained particles from 19 of the largest rivers which enter the GoF along the southern coast. The discharge from the rest of the rivers, including the largest river Neva, was not included. We used a limited number of rivers in the simulations to keep the number of particles smaller for computational reasons. The latter allowed us to conduct numerous sensitivity runs in a reasonable time. The number of particles released at each time step varied seasonally, mirroring the changes in river discharge (Fig. 2). The peak particle release occurred in April-May, gradually decreasing thereafter. Throughout the entire simulation period, a total of 145,146 particles were released. The released particles had an initial radius of 0.1 mm and initial densities of 920 kg m^{-3} (hereafter named light particles) and 1380 kg m^{-3} (hereafter named heavy particles). Light particles, being buoyant, initially floated, while the heavy particles were denser than seawater and prone to settle. The light to heavy particles ratio remained constant at 60:40 (60% light, 40% heavy). This choice, which does not mirror actual conditions, was made because most of the processes examined in this paper predominantly affect floating particles, apart from resuspension, which affects settled particles.

The particle positions were calculated with a time step of 200 seconds. Particle information, including position, velocity, age (the time from the moment a particle entered the sea), biofilm thickness, and state, was recorded at 12-hour intervals. The state parameter represents the current condition of the particle, which can be categorized as "suspended", "beached", "on boundary" (i.e., particles that have exited the model domain), or "settled." Using the output from the Lagrangian model, concentration maps for the surface (defined as the uppermost 1-meter layer) and water column were generated, and the particle budget was calculated

Table 1 Set of sensitivity tests performed in the study

Process (parameter)	Low	Moderate	Strong	Very strong	Weak transport	Strong transport
Beaching (beaching time [d])	30	20	10	1	1	30
Mixing (C_s)	0.01	0.3	1.0	2.0	Fixed at 0.157 m^2 s^{-1}	0.5
Resuspension (near-bottom current velocity threshold [m s^{-1}])	0.191	0.148	0.075	0.0375	0.191	0.0375
Biofouling (T_s [d])	20	10	1	0.5	20/30%	20/5%

for each state, enabling an analysis of the distribution and fate of the particles.

2.4.3 Sensitivity scenarios

A series of experiments were conducted to assess the sensitivity of the implemented processes to the distribution of MPs in the simulation. Each process was individually tested by modifying a specific parameter, while the remaining processes were switched off. The initial reference run was carried out without incorporating beaching, resuspension, or biofouling processes. A small constant background horizontal diffusion (0.157 m^2 s^{-1}) was applied in each experiment (including the reference run). The parameter adjustments were categorized as "low," "moderate," "strong," or "very strong," with the latter being twice (or half) the value of the "strong" setting. For beaching experiments, we reduced the beaching time, leading to a quicker removal of particles near the coast and a reduced likelihood of transportation them towards the open sea. For the diffusion tests, we modified the constant C_s, which subsequently affected the eddy viscosity A_h. Lowering the minimum bottom friction velocity to initiate resuspension was tested in the resuspension experiments. In the biofouling tests, we altered the biofilm growth time scale parameter T_s and the maximum biofilm thickness h_{max} was fixed. The former controlled the rate of biofouling, while the latter determined its maximum severity. To simulate and understand extreme scenarios of the MP pathways, we conducted two simulations involving all processes – one with parameter values that suppress the particle transport (referred to as "weak transport") and another with values that stimulate it (referred to as "strong transport").

A summary of the processes and their corresponding parameters can be found in Table 1. Firstly, it is important to note that the "very strong" scenarios were executed as an addition to the initial three scenarios, and the values for the experiments were selected based on the values of the "strong" experiments – either doubled (diffusion) or reduced to half (resuspension, biofouling). For beaching, the highest value, representing the longest beaching time ("low scenario"), was set to approximate the best estimate obtained by Kaandorp et al. (2020) (24 days) in the Mediterranean Sea, while the

values for the "moderate", "strong" and "very strong" scenarios were chosen from those used in Onink et al. (2021). As for diffusion, the Smagorinsky parameter C_s was initially configured at 0.3 ("moderate scenario"), resulting in a mean horizontal diffusion coefficient (A_h) of 0.93 m^2 s^{-1}. This value was computed using the 12-hour GETM surface current data from 2018. However, diffusivity exhibits significant spatial and temporal variability (Zhurbas et al. 2008). Therefore, we established the lower and upper bounds for this parameter to cover a wide range of values. For the resuspension threshold, we computed values based on near-bottom current speed data, setting them at the 99th, 90th, and 50th percentiles for the "low", "moderate", and "strong" scenarios, respectively. The maximum biofilm thickness (h_{max}) was fixed at 6.7% of the particle radius. This limit corresponds to approximately the minimum thickness necessary for the particle to initiate sinking, assuming an average seawater density of 1003 kg m^{-3} in the surface layer of the GoF during summer (Liblik and Lips 2017). Following the findings of Fischer et al. (2014), the lowest saturation timescale (T_s) parameter was established at 20 days, with subsequent decrements, albeit potentially exceeding the realistic range of values.

We applied all processes in the weak transport scenario at very strong settings except for diffusion and resuspension. Diffusion was set to constant background diffusion (0.157 m^2 s^{-1}), and resuspension was set to low settings. This scenario also featured very strong biofouling, characterized by $h_{max} = 30\%$ and $T_s = 20$ days. Conversely, the strong transport scenario involved the opposite approach, with resuspension set to very strong. The Smagorinsky parameter for diffusion was set to 0.5, as this was the value used in the GETM simulations for calculating horizontal viscosity. The other processes were configured at their low settings. The biofouling in this scenario was defined by $h_{max} = 5\%$ and $T_s = 20$ days.

2.5 Validation datasets

Sea surface height measurements were obtained from the following Copernicus Marine Service product: Baltic Sea - In Situ Near Real Time Observations. E.U. Copernicus Marine Service Information (CMEMS). Marine Data Store

(MDS). DOI: https://doi.org/10.48670/moi-00032 (Accessed on 16-Mar-2023).

The temperature and salinity observations at coastal offshore station were taken from the ICES dataset (https://www.ices.dk/data/data-portals/Pages/ocean.aspx, last accessed on 11-Oct-2024).

Current velocity data were used for validation from a bottom-mounted current profiler (ADCP – acoustic Doppler current profiler, 300 kHz; Teledyne RDI) that was deployed to the central Gulf of Finland (Fig. 1) from 27.07.2018 to 30.09.2018. Velocities were measured as an average of 5 min with a vertical depth interval of 2 m in the depth range of 12–106 m.

3 Results

3.1 Model evaluation

3.1.1 Physical parameters

High-resolution simulation is validated against the sea surface height (SSH) measurements at different coastal stations of the GoF, temperature and salinity observations at the monitoring station LL7 in the middle of the gulf, and current measurements at a deep station in the southern GoF. Variations in SSH describe barotropic water exchange between the gulf and Baltic Proper. If the circulation is not simulated correctly, the bias and root mean square difference (RMSD) between the model and observations will be high. A comparison of the bottom and surface temperatures and salinities between the model and observations shows whether the baroclinic flow component and vertical mixing are simulated correctly in the model.

In principle, the model reproduces SSH variability reasonably well. The difference between the observed and simulated standard deviations was less than 3 cm, the correlation between the model and observations was more than 0.9, and the maximum root mean square difference was 12 cm (Fig. 3). The biases between the model and observations were largest at Helsinki station (3 cm, not shown), where also the number of missing observations was the largest. In other stations, the mean bias was less than 2.2 cm. The mean absolute bias was slightly smaller than RMSD reaching 9.3 cm at St. Petersburg station.

The simulated temperature and salinity are validated in the surface and bottom layer of LL7 (see Fig. 4). In principle, the model captures the salinity variability in the GoF relatively well. The surface salinity tends to be only slightly lower than the observations, while the bottom salinities ranging from 7 to 10 PSU in the observations are captured extremely well. In addition, there are likely several estuarine circulation reversals (Elken et al. 2003; Liblik et al. 2013)

seen as drops in the bottom salinity and high surface salinity captured both by the observations and simulation.

A comparison of simulated and observed currents is shown in Fig. 5. The model relatively well simulated the currents during a 2-month measurement period. The high eastward velocities in the water column (depths below 20 m to 65 m) in the beginning and at the end of the measurement period are well reproduced. The three observed strong eastward flow events in the upper layer (depths from 12 to 30 m) in August are also present in simulation results, although the model seems to slightly overestimate the westward flow in the surface layers.

3.1.2 Particle model performance

We performed two experiments in the Gulf of Finland and the European North-West shelf to ensure our particle model produces trustworthy results. We compared the outputs with the established OpenDrift Lagrangian trajectory model. See Appendix A for details of the experiments. In both cases, the models showed similar final distributions. The particles were concentrated along similar pathways with minor differences in the number of particles. One notable difference in Figure A.2 (panels b and c) is that there is a filament near the shelf boundary in our model but not in OpenDrift.

We also explored six distinct values for the horizontal diffusion coefficient, A_h. The diffusion coefficient A_h was set to a constant value in each case. While keeping all processes except diffusion inactive, particles were released from a single point, ensuring any shift in position was solely attributed to diffusion. The particle distributions after one month for the lowest and highest values of A_h are presented in Fig. 6. The greatest extent reached by particles with $A_h = 1.0\ m^2\ s^{-1}$ (Fig. 6b) was about 9 km, and 98% of the particles were found within a radius of 7 km. In contrast, those with $A_h = 10.0\ m^2\ s^{-1}$ reached up to 30 km (98% within 23 km). These distances correspond to "areas of influence" of approximately 156 km^2 and 1670 km^2, respectively. Consequently, increasing the diffusion coefficient from 1.0 to 10.0 expanded the area by roughly 10.7 times. As observed in Fig. 6a, particles exhibited greater dispersion as A_h increased.

3.2 Impact of different processes

Next, we describe the scenario runs and the impact of different processes, starting with the reference run. Spatial maps of the particle distribution in the high-resolution domain and time-series of the particle budget are presented as a percentage, relative to the cumulative number of particles released up to the respective date, encompassing the water column, bottom sediment, and boundary (i.e., particles that have exited the domain). In addition, the beach region is
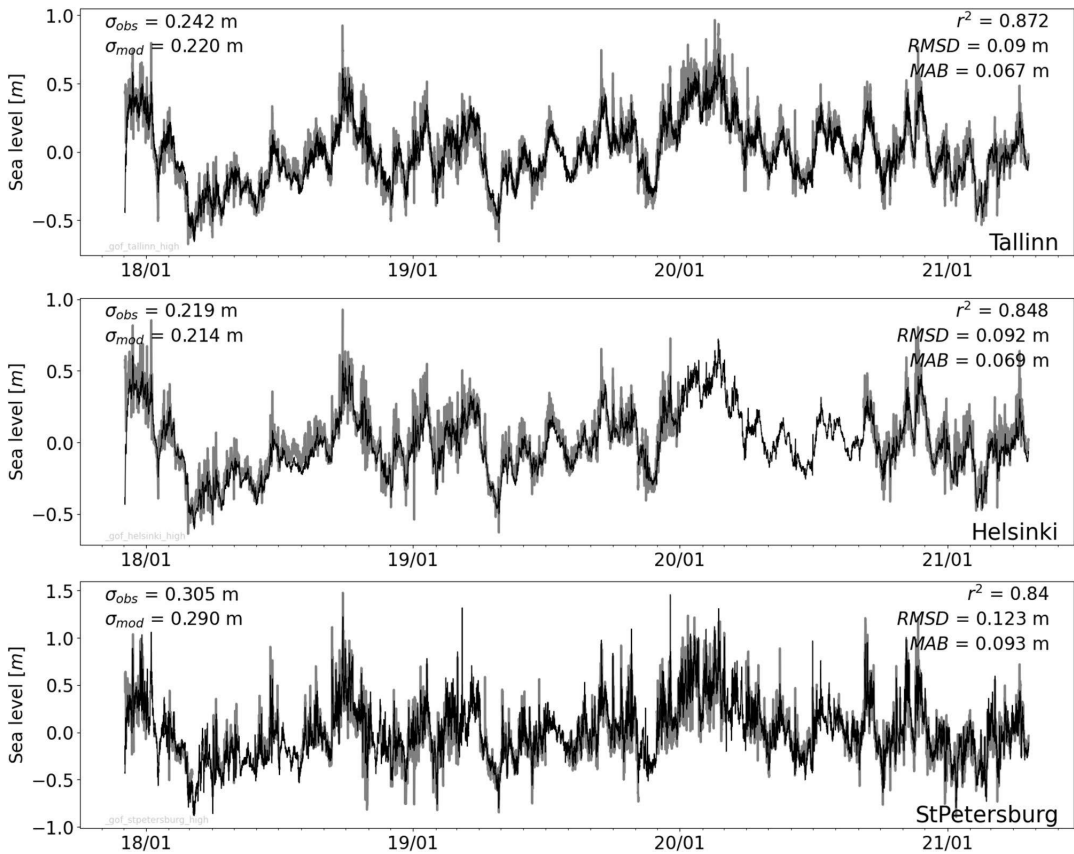
Fig. 3 Simulated (thin black line) and observed (grey bold line) sea surface height at different coastal stations (Fig. 1) of the GoF
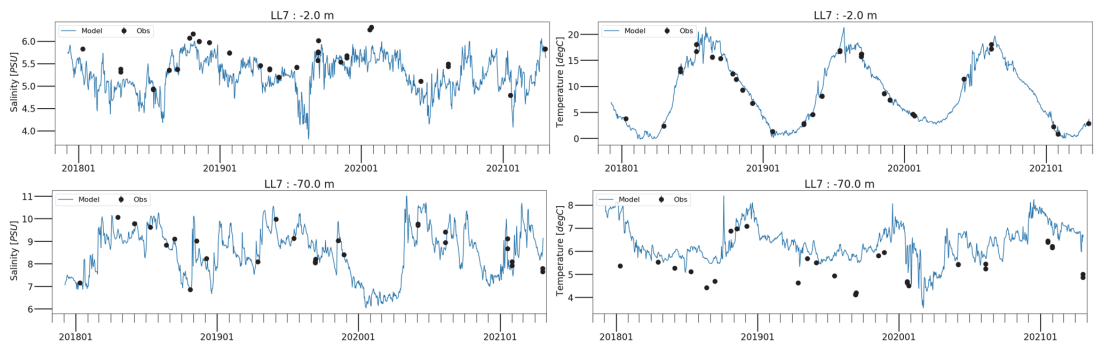

Fig. 4 Observed (black dots) and simulated (blue line) surface (top) and bottom (bottom) salinity and temperature time series at the offshore monitoring station LL7 (Fig. 1) from November 2017 to April 2021
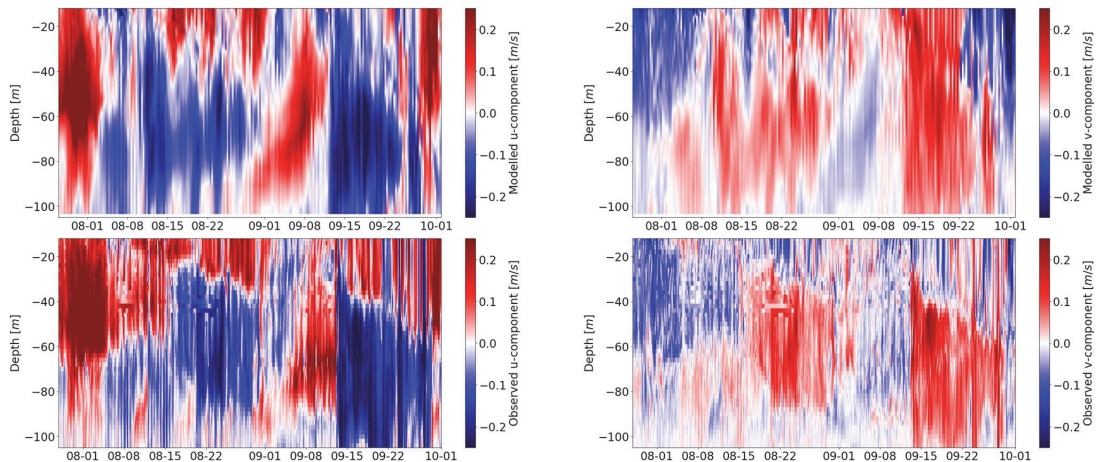
Fig. 5 Modelled (top panels) and observed (bottom panels) current velocity components in the ADCP station (Fig. 1) from 1 Aug 2018 to 1 Oct 2018

shown for scenarios where beaching was activated. The spatial maps are primarily intended to offer a qualitative description of the particle distribution. The time-series were smoothed using a 7-day window.

In the reference run, where the selected processes (beaching, resuspension, and biofouling) were deactivated, the number of particles at the bottom stabilized at around 40% after a few days, representing the share of heavy particles, which settled quickly. By the end of the simulation period, approximately 51% of the cumulative total particles were present within the water column. The remaining 9% of particles exited the domain. The temporal developments in the particle budget in the reference run are shown as grey lines in the time-series plots below.

3.2.1 Lateral diffusion

Figure 7 illustrates the average surface concentration of particles in simulations with varying values of C_s for lateral mixing. In the case of low mixing (Fig. 7a), particles exhibited distinct and sharper structures on the sea surface and remained closer to the shore. In contrast, very strong mixing (Fig. 7d) resulted in a smoother particle distribution with particles drifting further offshore. The overall mean particle concentration was reduced two times (from approximately 0.04 particles/m^2 to 0.02 particles/m^2) in the sea surface by switching from low mixing to very strong mixing, indicating a decrease in the number of particles in the surface layer with increasing mixing strength.

Analyzing the particle budget in Fig. 8, we observe that diffusion slightly enhances particle transport out of the domain, thereby reducing the number of particles in the

water column within the domain. By the end of the simulation period, around 48% of the total released particles remained in the water column in the domain under very strong diffusion conditions, representing a reduction of approximately 5% compared to the reference run. The final share of particles in the water column was 51% for low diffusion and 49% for moderate and strong diffusion. The number of settled particles remained the same as in the reference run.

The highest number of particles transported out of the domain occurred in July - early August for all diffusion scenarios, with a slight subsequent decrease, indicating that more particles were released from rivers than exited the domain in autumn (Fig. 8). By the end of the simulation period, 8.3%, 10.4%, 10.6%, and 11.2% of the total particles had crossed the domain boundary corresponding to the diffusion strength from low to very strong, respectively.

3.2.2 Beaching

The impact of beaching on particle distribution is depicted in Fig. 9. Longer beaching times (low beaching) increased the likelihood of particles being transported toward the center of the GoF. Conversely, shorter beaching times resulted in a higher probability of particles exceeding the beaching time limit and becoming beached. Consequently, the offshore concentrations were higher with low beaching and decreased as the beaching intensity increased.

With respect to all particles, 6% of the particles had become beached by the end of the simulation period under low beaching conditions, 21% under moderate beaching, 42% under strong beaching, and 56% under very strong beaching (Fig. 10). However, the heavy particles sink

Fig. 6 Upper panel: Particle distributions at the end of the simulation with diffusion coefficients of $1\,m^2\,s^{-1}$ (E1) and $10\,m^2\,s^{-1}$ (E6). Circles depict regions with radii corresponding to the 98th percentile distance. The black cross marks the release location. Lower panel: The frequency distributions of final distances from the release location, calculated with 250 m bin size and diffusion coefficients of $1\,m^2\,s^{-1}$ and $10\,m^2\,s^{-1}$. Vertical lines denote mean, maximum, and 98th percentile distances reached in each experiment (refer to figure legend)
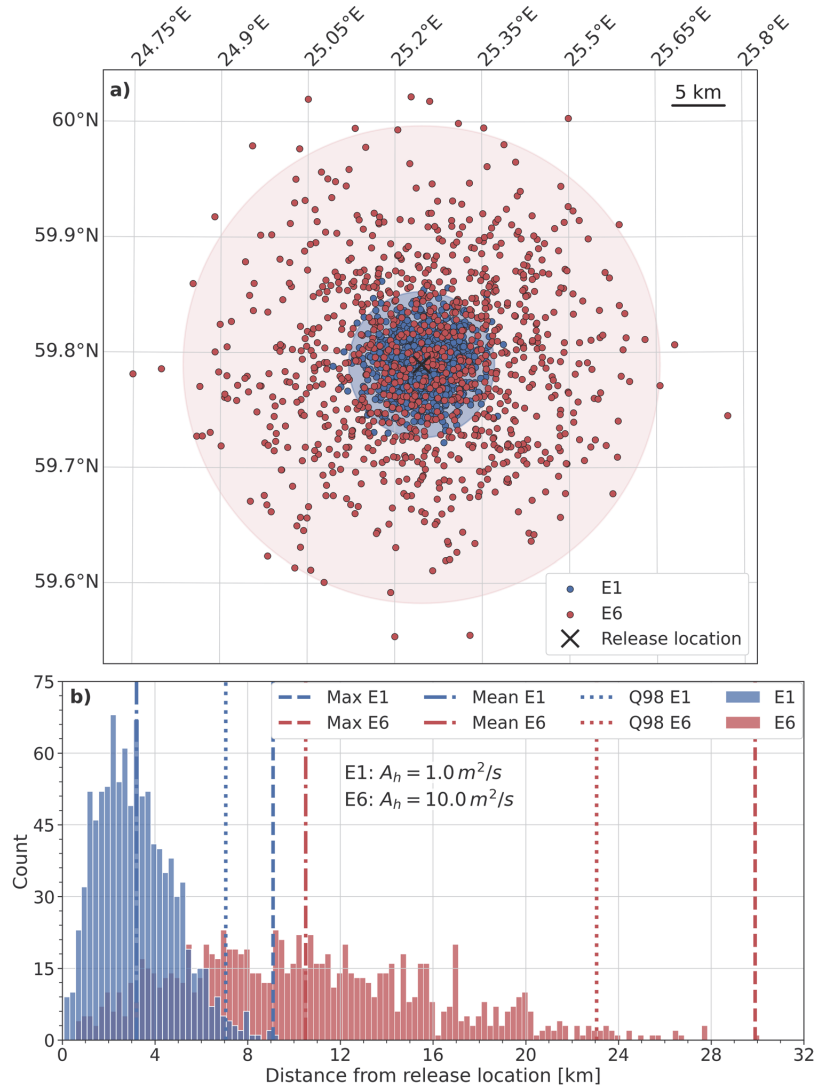
quickly, and beaching does not affect them in our model. The share of beached particles with respect to only the light, floating particles was approximately 10%, 35%, 71%, and 93% by the end of the simulation period under low, moderate, strong, and very strong beaching conditions, respectively.

Compared to the reference run, the number of particles in the water column decreased by the end of the simulation period by approximately 11% with low beaching and over 93% with very strong beaching (Fig. 10). The share of beached particles was very low until the end of July in case of low beaching, while it increased relatively fast during

the first two months in case of very strong beaching. The time series of the beached particles was more variable in the moderate and strong scenarios, where two intense beaching events, one in June and the other in July, were detected.

The difference in the number of settled particles was insignificant because the heavy particles tended to settle closer to the shore regardless of the beaching time.

3.2.3 Resuspension

The impact of resuspension was revealed as a greater proportion of particles settled in sediments further away
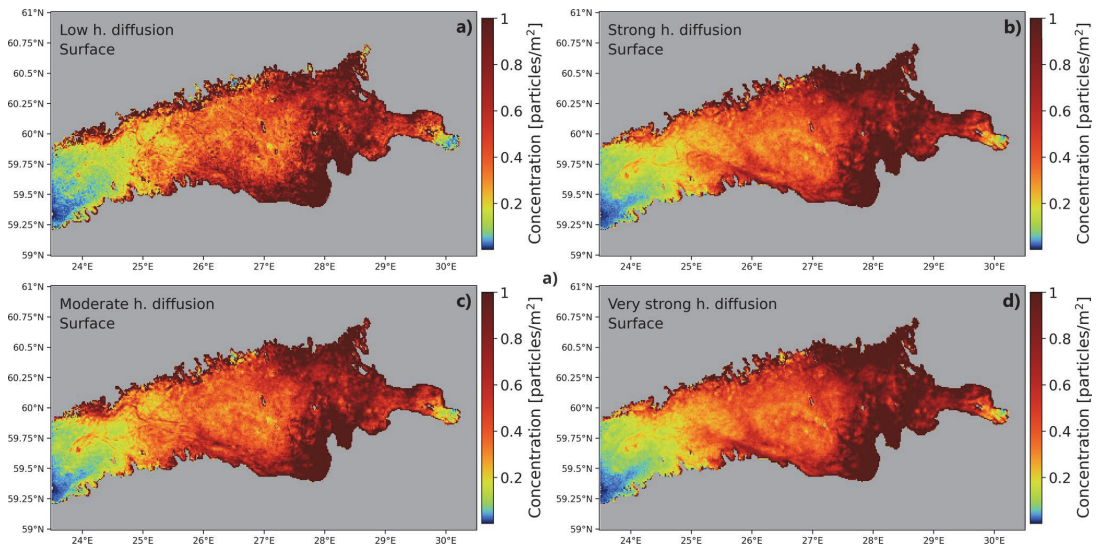
Fig. 7 Average concentration of particles at the surface over the period from 5 February to 31 December 2018 with different settings of lateral diffusion. The surface is defined as the uppermost 1-meter-thick layer

Fig. 8 Time series of particle budget in the diffusion experiments. The panels present the percentage representation of particles in the water column (**a**), bottom sediment (**b**), and open boundary (**c**) of the domain with respect to the cumulative number of particles released
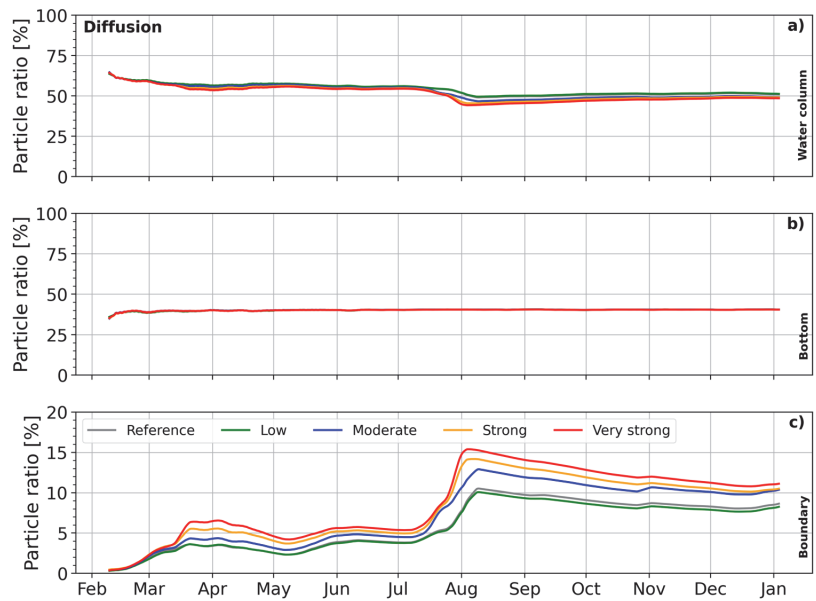
from the coast if stronger resuspension was applied (Fig. 11). Increased resuspension intensity led to a rise in the number of particles in the water column, while concurrently decreasing their abundance in the bottom sediments. On average, the particles in the bottom sediments demonstrated a 5% decrease with low

resuspension, with a further decrease with moderate, strong, and very strong resuspension. Over the entire simulation period, the average number of particles in the bottom sediments was 28% with very strong resuspension, while in the reference run, it was 40% (refer to Fig. 12). Correspondingly, the number of particles in the water
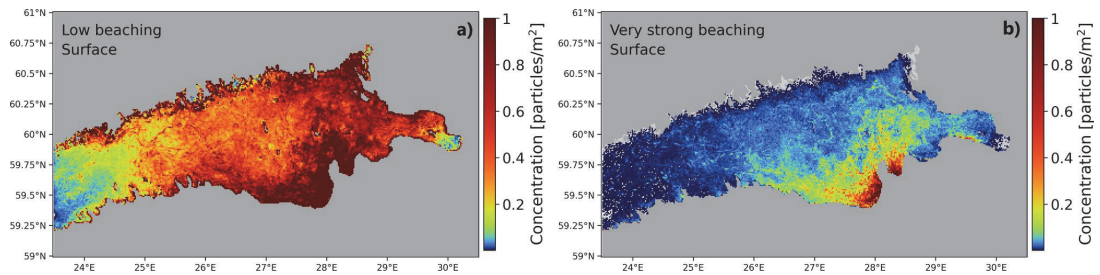
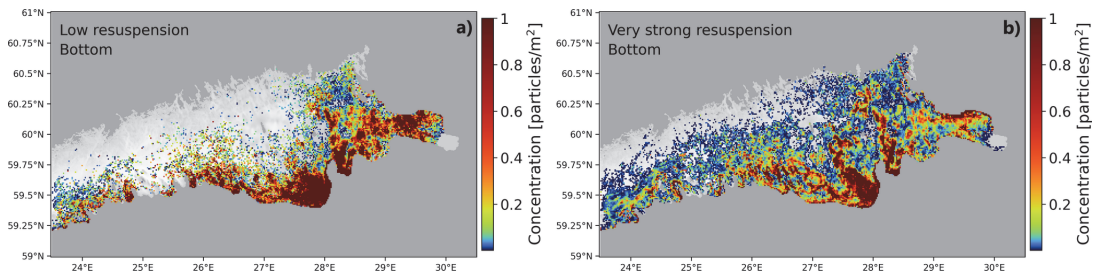**Fig. 9** Average concentration of particles at the surface over the period from 5 February to 31 December 2018 with different settings of beaching. The surface is defined as the uppermost 1-meter-thick layer

Fig. 10 Time series of particle budget in the beaching experiments. The panels present the percentage representation of particles in the water column (**a**), bottom sediment (**b**), open boundary (**c**), and beach region (**d**) of the domain with respect to the cumulative number of particles released. The solid lines are the percentage with respect to all particles (light and heavy) and the dashed lines are with respect to only the light particles
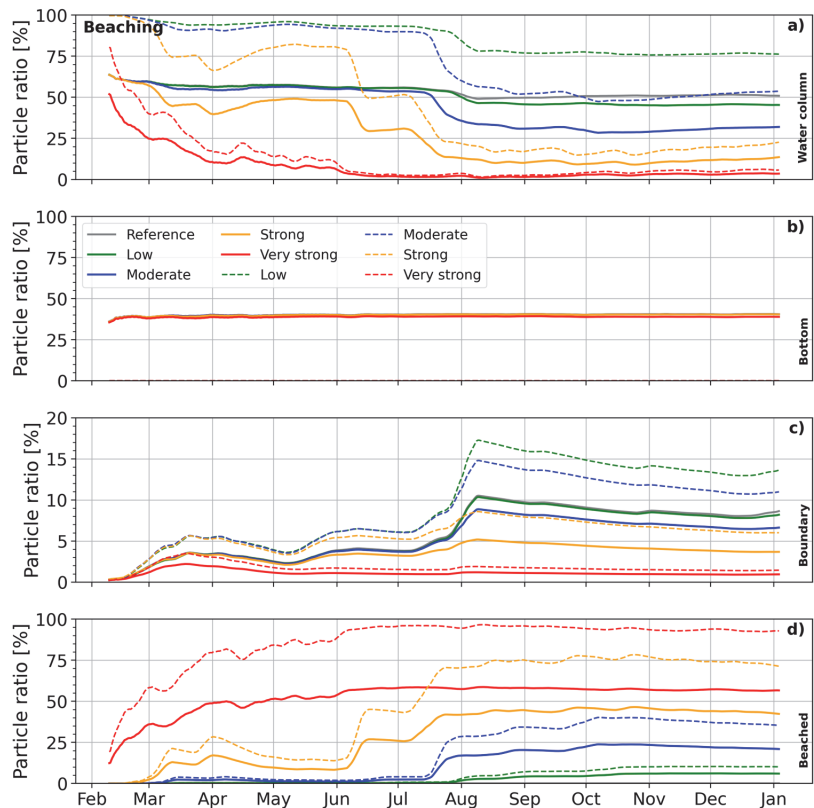
column increased with resuspension. There were no significant changes in the particle distribution in the surface layer.

Increasing the strength of resuspension did not significantly affect particle departure from the domain. The final number of particles at the boundary was approximately 9% for all scenarios.

3.2.4 Biofouling

Figure 13 illustrates the average distribution of particles at the surface in simulations with active biofouling. Increasing the intensity of biofouling resulted in a transition of particles from the surface layer to the deeper layers in the water column, eventually settling at the bottom.

Fig. 11 Average concentration of particles in the bottom sediments over the period from 5 February to 31 December 2018 with different settings of resuspension

Fig. 12 Time series of particle budget in the resuspension experiments. The panels present the percentage representation of particles in the water column (**a**), bottom sediment (**b**), and open boundary (**c**) of the domain with respect to the cumulative number of particles released
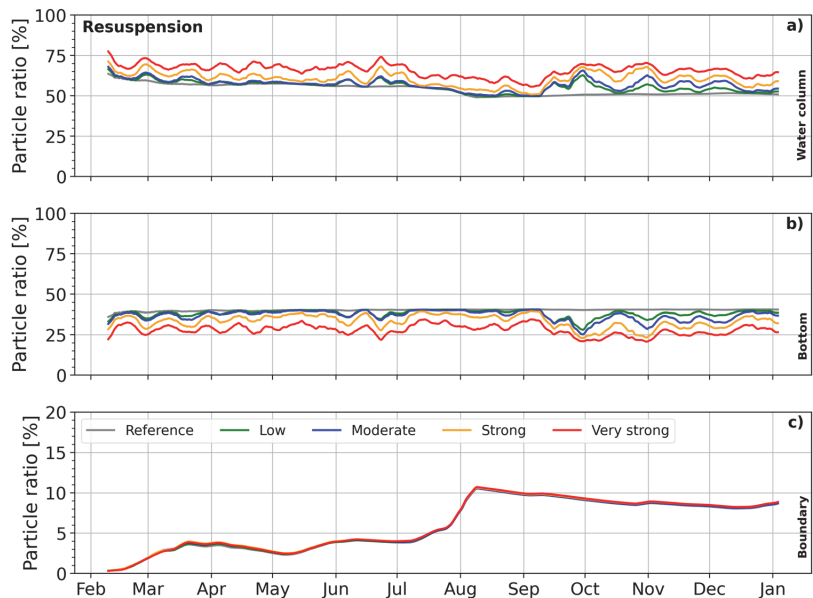
The particle budget with different values of the biofilm growth timescale parameter T_s is shown in Fig. 14. With low biofouling, the final share of particles left in the water column was 19%. The floating particles started sinking on average 37 days after their release (median 41 days). A notable decrease in the proportion of particles in the water column became visible in early May, roughly three months after the start of the simulation. This timing shifted to mid-March with moderate biofouling, with sinking beginning at about 25 days (median 28 days). By the end of the simulation period, 14% of the particles were still in the water column. Strong and very strong biofouling had similar effects on the particles. The final share of particles in the water column was approximately 8% for both scenarios and sinking started in 5 (6) days in case of (very) strong biofouling (median 5 and 7 days, respectively).

In the strong and very strong biofouling conditions, the proportion of particles departing the model domain was reduced compared to the reference scenario. This diminished outflow is mainly a consequence of increased particle settlement. Nevertheless, during the low biofouling scenario, the particle count at the domain boundary was temporarily higher than in the reference simulation, while in a similar order with the reference run at the end of the experiment.

3.2.5 Combination of processes

Figure 15 illustrates particle distributions in simulations characterized by suppressed (weak) and stimulated (strong) transport conditions. Suppressed transport refers to stronger removal processes (beaching and biofouling) and lower diffusion and resuspension, which encourage particle dispersion.
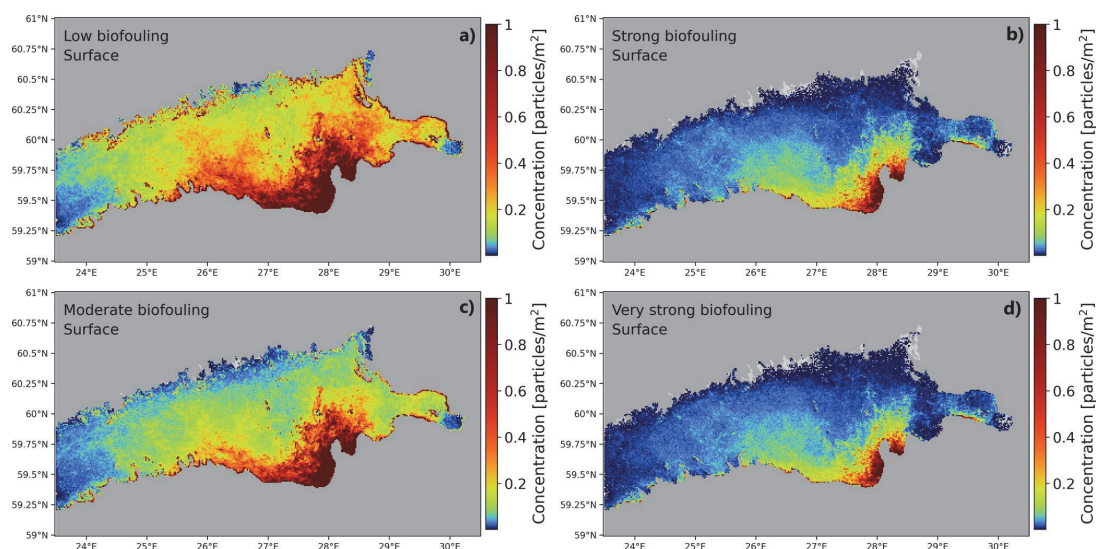
Fig. 13 Average concentration of particles at the surface over the period from 5 February to 31 December 2018 with different settings of biofouling. The surface is defined as the uppermost 1-meter-thick layer

Fig. 14 Time series of particle budget in the biofouling experiments. The panels present the percentage representation of particles in the water column (**a**), bottom sediment (**b**), and open boundary (**c**) of the domain, with respect to the cumulative number of particles released
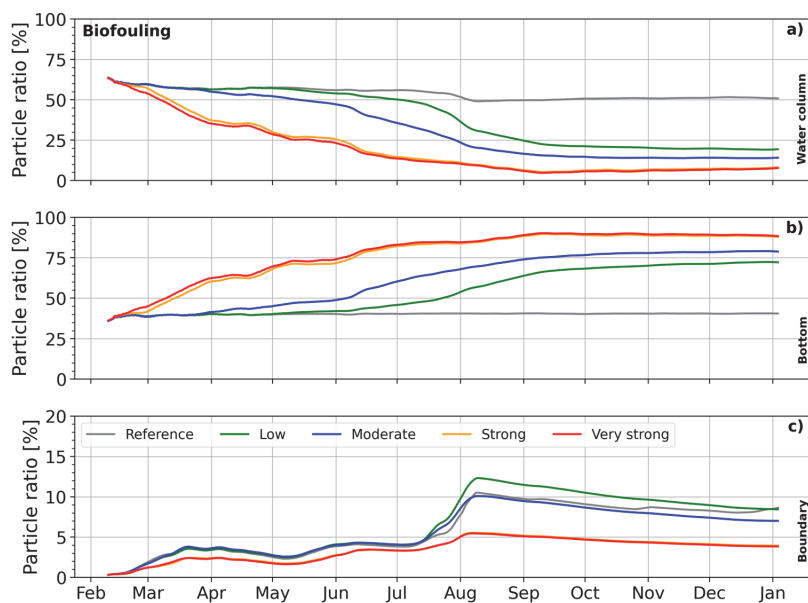
Stimulated transport refers to the opposite situation – processes that encourage dispersion are higher and removal processes are lower. In the case of weak transport, the average surface concentration remains notably low, with a significant portion of the central and northern regions of the GoF exhibiting no particles at the surface throughout the entire simulation period

(Fig. 15a). This outcome is attributed to the combination of processes employed in this scenario, which act to remove particles, leading to the accumulation of particles near their sources at the bottom (biofouling) and coast (beaching) (Fig. 15e). Furthermore, weak resuspension in this scenario prevents particles from being transported away from the coastal areas. In contrast,
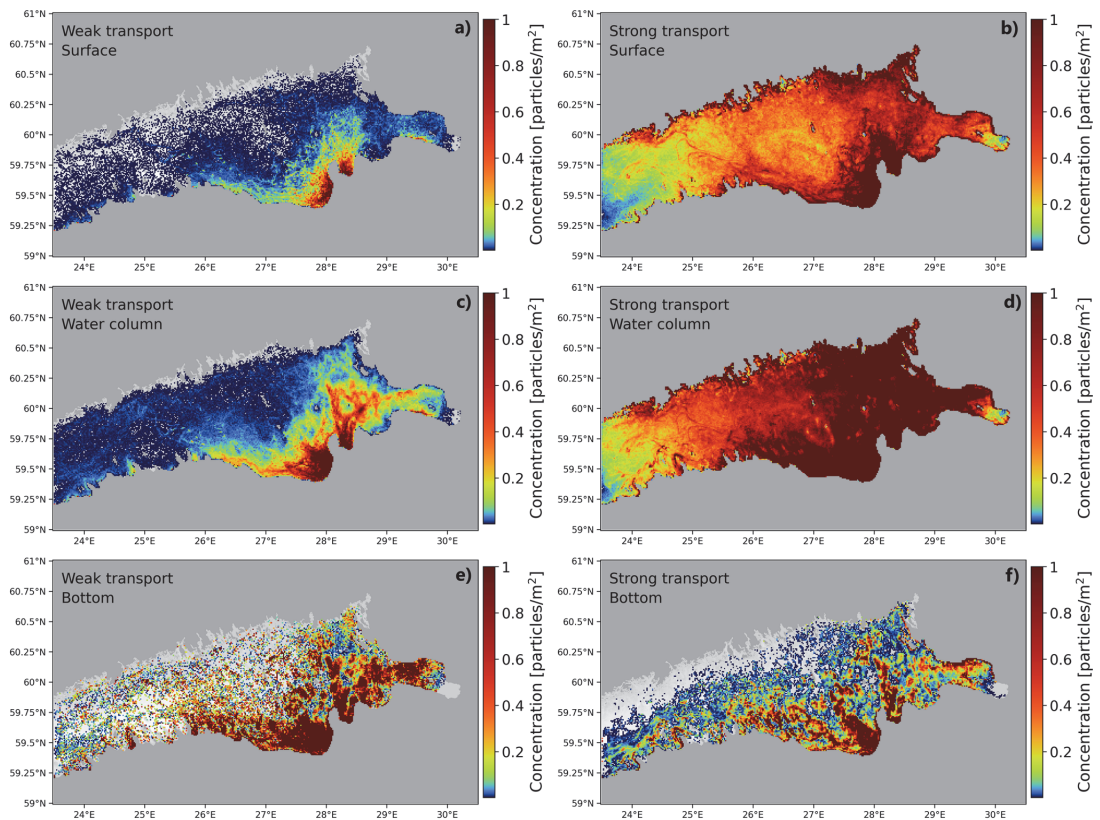
Fig. 15 Average concentration of particles at the surface, in the water column and bottom sediments over the period from 5 February to 31 December 2018 with combined processes. Left column: weak trans- port, right column strong transport. The surface is defined as the uppermost 1-meter-thick layer

the strong transport scenario results in a more widespread dis- tribution of particles throughout the GoF, primarily within the water column (Fig. 15d). Due to lower biofouling and higher resuspension, the particles have spread over a larger area within the bottom sediments (Fig. 15f).

When analyzing the particle budget (Fig. 16), a sig- nificant reduction in the percentage of particles within the water column with suppressed transport is evident compared to the reference run. By the end of the simulation period, approximately 4% of the total particles remained in the water column, corresponding to a 92% decrease compared to the reference run. However, under strong transport conditions, particles remained in the water column for extended periods. Compared to the reference run, there were approximately 31% less settled particles by the end of the simulation period.

Under suppressed transport conditions, approximately 49% of particles beached during the simulation period. In contrast, under strong transport conditions, only a marginal

4% of the total particles beached, and notable beach- ing events did not start until the end of August, roughly 6 months from the beginning of the simulation.

Concerning the domain boundary, 0.4% of the total parti- cles reached it under suppressed transport conditions, while 11% did so under strong transport conditions.

4 Discussion

A sensitivity analysis was conducted to explore the impact of the key processes—diffusion, beaching, resuspension, and biofouling on the MP transport in the GoF.

In our model, we implemented the Smagorinsky (1963) parameterization for calculating the horizontal diffusion coefficient, using high-resolution hydrodynamic model data for current velocities. This approach, distinct from certain other studies (Lacerda et al. 2019; Liubartseva et al. 2018;

Fig. 16 Time series of particle budget in the combined experiments. The panels present the percentage representation of particles in the water column (**a**), bottom sediment (**b**), open boundary (**c**), and beach region (**d**) of the domain with respect to the cumulative number of particles released
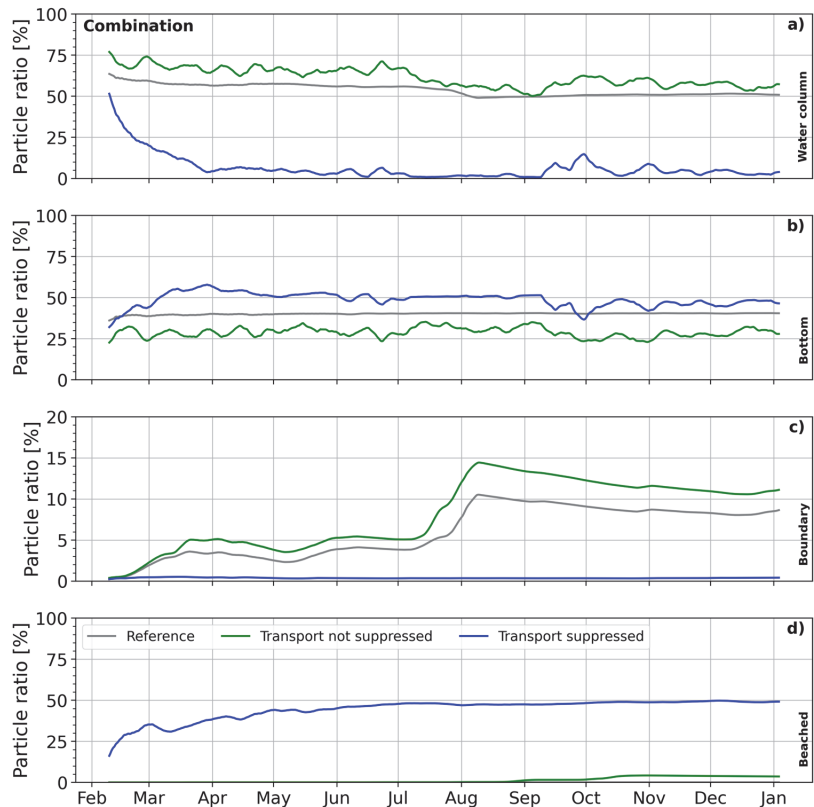
Onink et al. 2021), which employed a constant horizontal diffusion coefficient for sub-grid dispersion, enabled us to account for temporal and spatial variations in lateral mixing driven by current fluctuations. Previous studies (Salm et al. 2023; Väli et al. 2017, 2018, 2023) have indicated strong submesoscale variability within the gulf, which is also permitted in the present simulation. We determined that, with a Smagorinsky coefficient of $C_s = 0.3$, denoting moderate diffusion in our experiments, the average horizontal diffusion coefficient in the GoF for the year 2018 reached approximately 0.93 m^2 s^{-1}, with high spatial and temporal variability and a peak value of roughly 40 m^2 s^{-1}. It has also been previously shown that, during certain events, the diffusivity can temporarily grow significantly higher (e.g., Zhurbas et al. 2008). Furthermore, with $C_s = 0.3$ and $C_s = 0.5$ (unsuppressed transport scenario), the maximum velocity fluctuations due to lateral turbulent diffusion remained slightly lower than the horizontal advective velocities. Under background diffusion conditions, velocity fluctuations remained below 4 cm s^{-1}. In contrast, $C_s = 2.0$ led to excessively high velocity fluctuations, with the maxima exceeding 80 cm s^{-1}. Although such a high lateral diffusivity has

been shown in the simulation by Zhurbas et al. (2008), these velocities due to diffusion are unrealistically high compared to the observed current velocities in the gulf (Suhhova et al. 2018). Consequently, our experiments suggest that the Smagorinsky coefficient on the order of 0.5 would provide more reasonable results, avoiding the extreme velocities associated with $C_s = 2.0$.

The beaching process substantially impacted on the number of active particles within the water column. The primary influence of beaching was observed on the lighter particles, which would have been transported freely by advection had beaching not been in effect. Recently, Onink et al. (2021) reported a beached plastic fraction ranging from 31 to 95% in a global simulation, depending on their specific parameter values. Our simulations showed lower percentages for comparable beaching time values (1, 10, and 26 days). However, their definition of the beaching zone extended to 10 km from the coast, while our beaching zone was confined to the 250 m grid cell closest to the coast. The two intense beaching periods in June and July in moderate and strong beaching scenarios were likely associated with downwelling events. Downwelling events are coupled with the upwellings in the

gulf (e.g., Laanemets et al. 2011; Liblik and Lips 2012; Lips et al. 2009; Väli et al. 2017). Mishra et al. (2022) have shown a 60-fold difference in observed MP concentration near the southern coast of the gulf during the downwelling and upwelling events. MP accumulates in the convergence zone during downwelling, while the surface water is largely replaced by the intermediate layer water with low MP concentration along the coast during upwelling. Several downwelling-upwelling events were detected in the summer of 2018 (based on the model results; not shown), which likely enhanced beaching.

Note that, in the model, the particles can hold only one unique state at any given moment, and beaching is only controlled by the time parameter. Consequently, a particle might be categorized as "beached" even if only a few timesteps away from settling on the seabed (and vice versa). Furthermore, once a particle has been beached, it is effectively removed from the simulation, remaining stationary until the end of the simulation. Additionally, the beaching time depends on the particle characteristics and local geomorphology specifics (Daily et al. 2021; Onink et al. 2022), which this study did not address in detail.

Resuspension exhibited a distinctive behavior compared to other processes primarily responsible for particle removal. A significant increase in the number of active particles within the water column was observed upon lowering the threshold for resuspension initiation, a parameter determined by the bottom friction velocity. This adjustment to the threshold resulted in greater transport of particles away from coastal regions, facilitating their settlement in the offshore areas of the GoF. According to Kuhrts et al. (2004), the critical shear velocity for resuspending suspended particulate matter is as low as 2 cm s^{-1}, while our simulations employed a minimum threshold of 3.75 cm s^{-1}. However, under certain conditions, e.g., in the case of biofilm formation, critical shear velocity could be much higher (Niemistö and Lund-Hansen 2019). Mean current velocities in the GoF are on the order of 10 cm s^{-1} (Suhhova et al. 2018). Tides do not have a considerable role, but wind impulses impact velocity in the whole water column in the GoF. Velocities > 80 cm s^{-1} and 50 cm s^{-1} have been observed in the upper layer and deeper layers, respectively (Liblik et al. 2013; Rasmus et al. 2015; Suhhova et al. 2018). Thus, resuspension could occur at all depths in the GoF. In shallow areas, wind waves also cause the resuspension of particles (Martyanov and Ryabchenko 2016). Since our model did not consider wind waves, resuspension (settling) is likely underestimated (overestimated) in shallower areas.

Furthermore, our resuspension model did not consider particle properties, although studies like Xia et al. (2021) have shown that particles similar in size to natural sediment particles are more likely to be lifted into the water column. Robust resuspension models consider particle size and the type of natural sediment and parameterize the "hiding-exposure effect". In such models, MP particles of different sizes have different reasons for becoming resuspended. On one hand, larger particles are moved because they are more exposed. On the other hand, smaller particles, although shielded by larger grains, have a lower critical shear stress (Guingo and Minier 2008; Waldschläger and Schüttrumpf 2019; Wilcock 1988).

In a modeling study by Lobelle et al. (2021), the global median sinking timescale of light particles (with a density of 920 kg m^{-3} and a radius of 0.1 mm) subject to biofouling was found to be 40–43 days. This suggests that the scenario with low biofouling values - $T_s = 20$ days – in our simulations may correspond most closely to these estimates (mean 37, median 41 days). However, it is essential to recognize that the actual sinking times of biofouled particles depend on numerous variables, including particle size, hydrodynamic conditions, and biological factors. Specifically, smaller particles require less biofilm to initiate sinking compared to larger particles with equivalent densities (Lobelle et al. 2021; Murawski et al. 2022).

In more complex models, exemplified by the works of Kooi et al. (2017) and Tsiaras et al. (2021), the consideration of algal growth hinges on factors such as light intensity and temperature, and algae mortality rates. These models, in theory, allowed for the restoration of particle buoyancy under certain conditions. Subsequently, in a follow-up research by Fischer et al. (2022), the Kooi model underwent further refinement, integrating a non-linear loss term (such as diseases).

It is noteworthy that while the biofilm growth formulation employed in our study is empirical, relying on chlorophyll-a concentrations as a proxy for primary production, it offers a relatively straightforward approach. Notably, incorporating just two parameters provides flexibility in tuning to yield results that align with those obtained from more intricate models.

An unexpected result of the increase of MPs at the domain open boundary in July-early August can be explained by the distinct forcing during this period and the low sinking rate associated with low biofouling. Likely, the particles, which have been transported by surface currents alone in the run without biofouling, were transitioned to different depths (but not to the bottom yet) in the run with low biofouling. Since a relatively strong outflow dominated in the subsurface layer in July-August, more particles were carried to the boundary than in the reference run.

The last series of experiments explored combinations of processes with either suppressed or unsuppressed transport. In the suppressed transport scenario, it is evident that removal processes played a dominant role, leading to a rapid decrease in the number of particles in the water column. The suppressed transport scenario closely resembled the strong

beaching scenarios, suggesting that beaching was the predominant removal process. Moreover, the rigid distinction between settled and beached particles might have led to an underestimation of beached particles due to the reasons described above. In the strong transport scenario, diffusion played a major role in spreading particles across the GoF. However, high accumulation areas were still seen close to the sources. As previously suggested, resuspension may have been insufficient to counterbalance settling due to biofouling and should be increased to reproduce realistic MP behavior.

In future developments, it might also be worthwhile to consider implementing a transitional zone where particles entrapped in sediments in shallow waters are also regarded as beached (e.g., as in Daily et al. 2021). This potential ambiguity could be mitigated through additional data analysis or post-processing techniques, such as labeling particles in the beach area as both settled and beached. Likewise, the inclusion of wind wave induced resuspension will be implemented.

Furthermore, it will be imperative to reassess the vertical motion and consider adding additional drivers for vertical mixing, including influences from wind and waves to the Lagrangian particle model. Also, it is important to acknowledge that a uniform time increment may not be suitable, given that the vertical grid steps are typically significantly smaller than their horizontal counterparts (Gräwe et al. 2012). This distinction becomes particularly pronounced in longer simulations, where the time step can be many hours. One potential solution might involve splitting the integration time step for vertical motion to ensure that particles do not cross multiple layers within a single time step. However, this approach may impact computational time.

Finally, future simulations should also consider atmospheric forcing. Presently, its effects can be seen indirectly in the current field - the variability in atmospheric forcing determines stratification, current fields, algae growth, and other factors that impact the four processes. Summer 2018, particularly until July, was particularly warm, with a high occurrence of winds from easterly directions (Hänsel et al. 2022; Hoy et al. 2020; Stoicescu et al. 2022; Wilcke et al. 2020). Such conditions likely encouraged the formation of the thin upper layer and more intense outflow of the upper layer towards the Baltic Proper (Elken et al. 2003; Liblik and Lips 2017; Stipa 2004). The described seasonal pattern in wind forcing is reflected in the time series of the particles at the boundary. The share of particles at the boundary increased until early August, after which it decreased (Figs. 8, 10, 12, 14 and 16). The latter exemplifies the importance of variability in atmospheric forcing in the pathways of MPs.

The results of this study will be used in the simulations with the realistic loads of MPs for the GoF. Based on the sensitivity runs, the most suitable settings for different processes can be selected considering available observations of MPs in the water column, sediments, and biota (Aigars et al. 2021; Chubarenko et al. 2022; Halbach et al. 2022; Mishra et al. 2022). These results will be presented in the follow-up paper by Mishra et al. (manuscript under preparation).

5 Summary and conclusions

We used a Lagrangian particle tracking model to simulate microplastic particle dynamics in the Gulf of Finland (GoF), Eastern Baltic Sea. A sensitivity analysis explored the impact of key processes—diffusion, beaching, resuspension, and biofouling—examining each process independently with varying strength and collectively with either suppressing or enhancing the transport.

The individual processes exhibited expected outcomes: beaching and biofouling acted as removal mechanisms, diminishing active particles in the water column and hindering transport from the GoF. In addition, the beaching of particles was enhanced due to the convergence of particles in the downwelling area. Conversely, resuspension countered particle removal by elevating them back into the water column for ongoing transport, while turbulent diffusion contributed to dispersion and flow out of the GoF. These insights guide the refinement of model parameters for realistic simulations. Once tuned, the model holds promise for identifying microplastic pathways and accumulation areas in the marine environment. Future research should include wind waves, address particle interactions with the seabed and beaches, and explore more robust parametrizations for vertical motion and beaching processes.

Appendix A

Model comparison

We ran two experiments to compare our model with the OpenDrift model. The first experiment was carried out in the Gulf of Finland using surface current data from same high-resolution GETM output as in the sensitivity scenarios (horizontal grid spacing of approximately 250 m and temporal resolution of 12 hours). The particles were initialized in a grid with a step of approximately 1 km in areas where the depth was at least 20 meters. This resulted in a total of 11682 particles (Fig. 17a).

In the second experiment, we used the surface current data from the European North-West shelf reanalysis product from the Copernicus Marine Service (Atlantic - European North West Shelf - Ocean Physics Reanalysis. E.U. Copernicus Marine Service Information (CMEMS). Marine Data
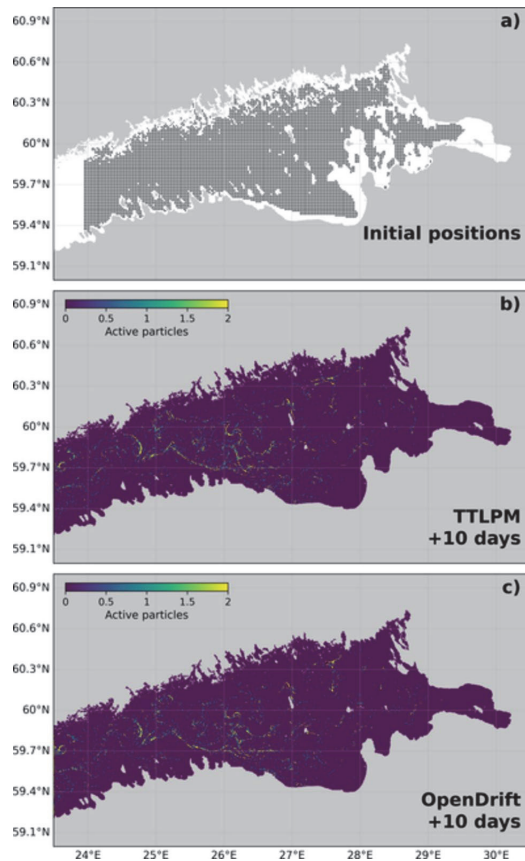
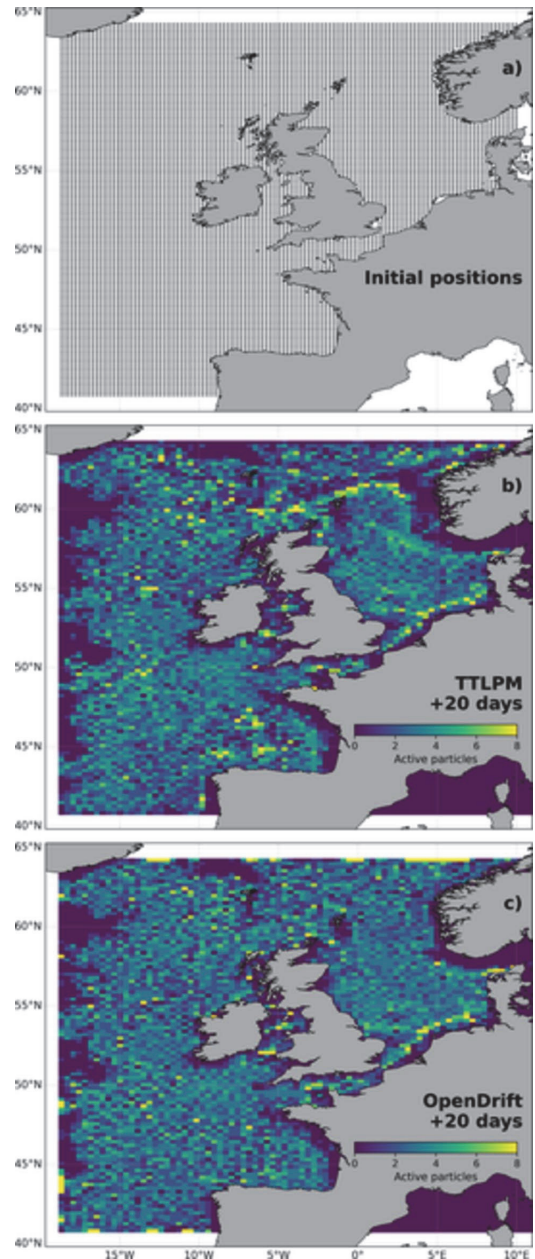**Fig. 17** Comparison of particle distributions in the Gulf of Finland using our model (referred to as TTLPM – TalTech Lagrangian Particle Model) and OpenDrift. Panel a shows the initial positions at the start of the simulation. Panels b and c show the particle distribution after 10 days for TTLPM and OpenDrift, respectively.

Store (MDS). DOI: https://doi.org//10.48670/moi-00059. Accessed on 01-Oct-2023). The horizontal resolution of the data is 7 km and the temporal resolution is 24 hours. A total of 15258 particles were released in a grid shown in Fig. 18a.

The particles were advected in the 2D current field with a time step of 1 hour by a second-order Runge-Kutta scheme in both experiments and models. No extra horizontal diffusion was applied to the particles and particles that hit the coastline were immediately removed from the simulation. The particle trajectories were calculated for 10 (20) days in the first (second) experiment and the final positions were mapped onto a uniform grid with a resolution of 500 (25000) meters. The b and c panels in Figures 17 and 18 show the number of particles in the grid cells at the final time moment.

Fig. 18 Comparison of particle distributions over the European North-West shelf using our model (referred to as TTLPM – TalTech Lagrangian Particle Model) and OpenDrift. Panel a shows the initial positions at the start of the simulation. Panels b and c show the particle distribution after 20 days for TTLPM and OpenDrift, respectively

Declarations

Conflict of interest The authors declare that the research was conducted in the absence of any commercial or financial relationships that could be construed as a potential conflict of interest.

References

Aigars J, Barone M, Suhareva N, Putna-Nimane I, Dimante-Deimantovica I (2021) Occurrence and spatial distribution of microplastics in the surface waters of the Baltic Sea and the Gulf of Riga. Mar Pollut Bull 172:112860. https://doi.org/10.1016/j.marpolbul.2021.112860

Alosairi Y, Al-Salem SM, Al Ragum A (2020) Three-dimensional numerical modelling of transport, fate and distribution of microplastics in the northwestern Arabian/Persian Gulf. Mar Pollut Bull 161:111723. https://doi.org/10.1016/j.marpolbul.2020.111723

Andrady AL (2011) Microplastics in the marine environment. Mar Pollut Bull 62(8):1596–1605. https://doi.org/10.1016/j.marpolbul.2011.05.030

Andrejev O, Soomere T, Sokolov A, Myrberg K (2011) The role of the spatial resolution of a three-dimensional hydrodynamic model for marine transport risk assessment. Oceanologia 53:309–334. https://doi.org/10.5697/oc.53-1-TI.309

Berglund S, Döös K, Campino AA, Nycander J (2021) The water mass transformation in the upper limb of the overturning circulation in the Southern Hemisphere. J Geophys Res: Oceans 126(8):e2021JC017330. https://doi.org/10.1029/2021JC017330

Bigdeli M, Mohammadian A, Pilechi A, Taheri M (2022) Lagrangian modeling of marine microplastics fate and transport: the state of the science. J Mar Sci Eng 10(4):481. https://doi.org/10.3390/jmse10040481

Blumberg AF, Mellor GL (1983) Diagnostic and prognostic numerical circulation studies of the South Atlantic Bight. J Geophys Res: Oceans 88(C8):4579–4592

Bruggeman J, Bolding K (2014) A general framework for aquatic biogeochemical models. Environ Model Softw 61:249–265. https://doi.org/10.1016/j.envsoft.2014.04.002

Burchard H, Bolding K (2001) Comparative analysis of Four Second-Moment Turbulence Closure models for the Oceanic mixed layer. J Phys Oceanogr 31(8):1943–1968.

Burchard H, Bolding K (2002) *Getm – a general estuarine transport model. Scientific documentation.* Technical Report EUR 20253 En. https://op.europa.eu/en/publication-detail/-/publication/5506bf19-e076-4d4b-8648-dedd06efbb38#

Canuto VM, Howard A, Cheng Y, Dubovikov MS (2001) Ocean Turbulence. Part I: one-point Closure Model—Momentum and Heat Vertical diffusivities. J Phys Oceanogr 31(6):1413–1426.

Caruso G (2019) Microplastics as vectors of contaminants. Mar Pollut Bull 146:921–924. https://doi.org/10.1016/j.marpolbul.2019.07.052

Chubarenko I, Esiukova E, Zobkov M, Isachenko I (2022) Microplastics distribution in bottom sediments of the Baltic Sea Proper. Mar Pollut Bull 179:113743. https://doi.org/10.1016/j.marpolbul.2022.113743

Cloux S, Allen-Perkins S, de Pablo H, Garaboa-Paz D, Montero P, Pérez Muñuzuri V (2022) Validation of a Lagrangian model for large-scale macroplastic tracer transport using mussel-peg in NW Spain (Ría De Arousa). Sci Total Environ 822:153338. https://doi.org/10.1016/j.scitotenv.2022.153338

Cole M, Lindeque P, Halsband C, Galloway TS (2011) Microplastics as contaminants in the marine environment: a review. Mar Pollut Bull 62(12):2588–2597. https://doi.org/10.1016/j.marpolbul.2011.09.025

Dagestad K-F, Röhrs J, Breivik Ø, Ådlandsvik B (2018) OpenDrift v1.0: a generic framework for trajectory modelling. Geosci Model Dev 11(4):1405–1420. https://doi.org/10.5194/gmd-11-1405-2018

Daily J, Onink V, Jongedijk CE, Laufkötter C, Hoffman MJ (2021) Incorporating terrain specific beaching within a lagrangian transport plastics model for Lake Erie. Microplastics Nanoplastics 1(1):19. https://doi.org/10.1186/s43591-021-00019-7

Delpeche–Ellmann NC, Soomere T (2013) Using Lagrangian models to assist in maritime management of Coastal and Marine protected areas. J Coastal Res 65(sp1):36–41. https://doi.org/10.2112/SI65-007.1

Dietrich WE (1982) Settling velocity of natural particles. Water Resour Res 18(6):1615–1626. https://doi.org/10.1029/WR018i006p01615

Döös K, Meier HEM, Döscher R (2004) The Baltic Haline Conveyor Belt or the overturning circulation and mixing in the Baltic. AMBIO: J Hum Environ 33(4):261–266. https://doi.org/10.1579/0044-7447-33.4.261

Döös K, Jönsson B, Kjellsson J (2017) Evaluation of oceanic and atmospheric trajectory schemes in the TRACMASS trajectory model v6.0. Geosci Model Dev 10(4):1733–1749. https://doi.org/10.5194/gmd-10-1733-2017

Elken J, Raudsepp U, Lips U (2003) On the estuarine transport reversal in deep layers of the Gulf of Finland. J Sea Res 49(4):267–274. https://doi.org/10.1016/S1385-1101(03)00018-2

Engqvist A, Döös K, Andrejev O (2006) Modeling water exchange and contaminant transport through a Baltic Coastal Region. AMBIO: J Hum Environ 35(8):435–447. https://doi.org/10.1579/0044-7447(2006)35[435:MWEACT]2.0.CO;2

Fischer M, Friedrichs G, Lachnit T (2014) Fluorescence-based quasi-continuous and in situ monitoring of biofilm formation Dynamics in Natural Marine environments. Appl Environ Microbiol 80(12):3721–3728. https://doi.org/10.1128/AEM.00298-14

Fischer R, Lobelle D, Kooi M, Koelmans A, Onink V, Laufkötter C, Amaral-Zettler L, Yool A, van Sebille E (2022) Modelling submerged biofouled microplastics and their vertical trajectories. Biogeosciences 19(8):2211–2234. https://doi.org/10.5194/bg-19-2211-2022

Frishfelds V, Murawski J, She J (2022) Transport of microplastics from the daugava estuary to the open sea. Front Mar Sci 9. https://doi.org/10.3389/fmars.2022.886775

GESAMP (2015). Sources, fate and effects of microplastics in the marine environment: a global assessment. In: Kershaw PJ (ed) (IMO/FAO/UNESCO-IOC/UNIDO/WMO/IAEA/UN/UNEP/UNDP Joint Group of Experts on the Scientific Aspects of Marine Environmental Protection). Rep Stud GESAMP No. 90, p 96

Gewert B, Ogonowski M, Barth A, MacLeod M (2017) Abundance and composition of near surface microplastics and plastic debris in the Stockholm Archipelago, Baltic Sea. Mar Pollut Bull 120(1–2):292–302. https://doi.org/10.1016/j.marpolbul.2017.04.062

Graca B, Szewc K, Zakrzewska D, Dołęga A, Szczerbowska-Boruchowska M (2017) Sources and fate of microplastics in marine and beach sediments of the Southern Baltic Sea—a preliminary study. Environ Sci Pollut Res 24(8):7650–7661. https://doi.org/10.1007/s11356-017-8419-5

Gräwe U, Deleersnijder E, Shah SHAM, Heemink AW (2012) Why the Euler scheme in particle tracking is not enough: the shallow-sea pycnocline test case. Ocean Dyn 62(4):501–514. https://doi.org/10.1007/s10236-012-0523-y

Gräwe U, Holtermann P, Klingbeil K, Burchard H (2015) Advantages of vertically adaptive coordinates in numerical models of stratified shelf seas. Ocean Model 92:56–68. https://doi.org/10.1016/j.ocemod.2015.05.008

Gröger M, Placke M, Meier HEM, Börgel F, Brunnabend S-E, Dutheil C, Gräwe U, Hieronymus M, Neumann T, Radtke H, Schimanke S, Su J, Väli G (2022) The Baltic Sea Model Intercomparison Project (BMIP) – a platform for model development, evaluation, and uncertainty assessment. Geosci Model Dev 15(22):8613–8638. https://doi.org/10.5194/gmd-15-8613-2022

Guingo M, Minier J (2008) A new model for the simulation of particle resuspension by turbulent flows based on a stochastic description of wall roughness and adhesion forces. J Aerosol Sci 39(11):957–973. https://doi.org/10.1016/j.jaerosci.2008.06.007

Halbach M, Vogel M, Tammen JK, Rüdel H, Koschorreck J, Scholz-Böttcher BM (2022) 30 years trends of microplastic pollution: Mass-quantitative analysis of archived mussel samples from the North and Baltic seas. Sci Total Environ 826:154179. https://doi.org/10.1016/j.scitotenv.2022.154179

Hänsel S, Hoy A, Brendel C, Maugeri M (2022) Record summers in Europe: variations in drought and heavy precipitation during 1901–2018. Int J Climatol 42(12):6235–6257. https://doi.org/10.1002/joc.7587

HELCOM (2018) State of the Baltic Sea–Second HELCOM holistic assessment 2011–2016. Baltic Sea Environ Proc 155:1–155

Hersbach H, Bell B, Berrisford P, Hirahara S, Horányi A, Muñoz-Sabater J, Nicolas J, Peubey C, Radu R, Schepers D, Simmons A, Soci C, Abdalla S, Abellan X, Balsamo G, Bechtold P, Biavati

G, Bidlot J, Bonavita M, Thépaut J-N (2020) The ERA5 global reanalysis. Q J R Meteorol Soc 146(730):1999–2049. https://doi.org/10.1002/qj.3803

Hofmeister R, Burchard H, Beckers JM (2010) Non-uniform adaptive vertical grids for 3D numerical ocean models. Ocean Model 33(1–2):70–86. https://doi.org/10.1016/j.ocemod.2009.12.003

Hoy A, Hänsel S, Maugeri M (2020) An endless summer: 2018 heat episodes in Europe in the context of secular temperature variability and change. Int J Climatol 40(15):6315–6336. https://doi.org/10.1002/joc.6582

Jonsson PR, Moksnes P-O, Corell H, Bonsdorff E, Nilsson Jacobi M (2020) Ecological coherence of Marine protected areas: new tools applied to the Baltic Sea network. Aquat Conserv: Mar Freshw Ecosyst 30(4):743–760. https://doi.org/10.1002/aqc.3286

Kaandorp MLA, Dijkstra HA, van Sebille E (2020) Closing the Mediterranean Marine floating Plastic Mass Budget: Inverse modeling of sources and sinks. Environ Sci Technol 54(19):11980–11989. https://doi.org/10.1021/acs.est.0c01984

Khatmullina L, Chubarenko I (2019) Transport of marine microplastic particles: why is it so difficult to predict? Anthropocene Coasts 2(1):293–305. https://doi.org/10.1139/anc-2018-0024

Klingbeil K, Lemarié F, Debreu L, Burchard H (2018) The numerics of hydrostatic structured-grid coastal ocean models: state of the art and future perspectives. Ocean Model 125:80–105. https://doi.org/10.1016/j.ocemod.2018.01.007

Kooi M, van Nes EH, Scheffer M, Koelmans AA (2017) Ups and downs in the ocean: effects of biofouling on vertical transport of microplastics. Environ Sci Technol 51(14):7963–7971. https://doi.org/10.1021/acs.est.6b04702

Kuhrts C, Fennel W, Seifert T (2004) Model studies of transport of sedimentary material in the western Baltic. J Mar Syst 52(1):167–190. https://doi.org/10.1016/j.jmarsys.2004.03.005

Laanemets J, Väli G, Zhurbas V, Elken J, Lips I, Lips U (2011) Simulation of mesoscale structures and nutrient transport during summer upwelling events in the Gulf of Finland in 2006. Boreal Environ Res 16(A):15–26

Lacerda ALDF, dos Rodrigues LS, van Sebille E, Rodrigues FL, Ribeiro L, Secchi ER, Kessler F, Proietti MC (2019) Plastics in sea surface waters around the Antarctic Peninsula. Sci Rep 9(1):3977. https://doi.org/10.1038/s41598-019-40311-4

Lange M, van Sebille E (2017) Parcels v0.9: prototyping a Lagrangian ocean analysis framework for the petascale age. Geosci Model Dev 10(11):4175–4186. https://doi.org/10.5194/gmd-10-4175-2017

Lehmann A, Myrberg K, Post P, Chubarenko I, Dailidiene I, Hinrichsen H-H, Hüssy K, Liblik T, Meier HEM, Lips U, Bukanova T (2022) Salinity dynamics of the Baltic Sea. Earth Sys Dyn 13(1):373–392. https://doi.org/10.5194/esd-13-373-2022

Liblik T, Lips U (2012) Variability of synoptic-scale quasi-stationary thermohaline stratification patterns in the Gulf of Finland in summer 2009. Ocean Sci 8(4):603–614. https://doi.org/10.5194/os-8-603-2012

Liblik T, Lips U (2017) Variability of pycnoclines in a three-layer, large estuary: the Gulf of Finland. Boreal Environ Res 22:27–47

Liblik T, Laanemets J, Raudsepp U, Elken J, Suhhova I (2013) Estuarine circulation reversals and related rapid changes in winter near-bottom oxygen conditions in the Gulf of Finland, Baltic Sea. Ocean Sci 9(5):917–930. https://doi.org/10.5194/os-9-917-2013

Liblik T, Väli G, Lips I, Lilover M-J, Kikas V, Laanemets J (2020) The winter stratification phenomenon and its consequences in the Gulf of Finland, Baltic Sea. Ocean Sci 16(6):1475–1490. https://doi.org/10.5194/os-16-1475-2020

Liblik T, Väli G, Salm K, Laanemets J, Lilover M-J, Lips U (2022) Quasi-steady circulation regimes in the Baltic Sea. Ocean Sci 18(3):857–879. https://doi.org/10.5194/os-18-857-2022

Lindeque PK, Cole M, Coppock RL, Lewis CN, Miller RZ, Watts AJR, Wilson-McNeal A, Wright SL, Galloway TS (2020) Are we underestimating microplastic abundance in the marine environment? A comparison of microplastic capture with nets of different mesh-size. Environ Pollut. https://doi.org/10.1016/j.envpol.2020.114721

Lips I, Lips U, Liblik T (2009) Consequences of coastal upwelling events on physical and chemical patterns in the central Gulf of Finland (Baltic Sea). Cont Shelf Res 29(15):1836–1847. https://doi.org/10.1016/j.csr.2009.06.010

Liubartseva S, Coppini G, Lecci R, Clementi E (2018) Tracking plastics in the Mediterranean: 2D lagrangian model. Mar Pollut Bull 129(1):151–162. https://doi.org/10.1016/j.marpolbul.2018.02.019

Lobelle D, Kooi M, Koelmans AA, Laufkötter C, Jongedijk CE, Kehl C, van Sebille E (2021) Global modeled sinking characteristics of Biofouled Microplastic. J Geophys Resh Oceans 126(4):e2020JC017098. https://doi.org/10.1029/2020JC017098

Markus Meier HE, Barghorn L, Börgel F, Gröger M, Naumov L, Radtke H (2023) Multidecadal climate variability dominated past trends in the water balance of the Baltic Sea watershed. Npj Clim Atmos Sci 6(1):58. https://doi.org/10.1038/s41612-023-00380-9

Martyanov S, Ryabchenko V (2016) Bottom sediment resuspension in the Easternmost Gulf of Finland in the Baltic Sea: a case study based on three–dimensional modeling. Cont Shelf Res 117:126–137. https://doi.org/10.1016/j.csr.2016.02.011

Martyanov SD, Isaev AV, Ryabchenko VA (2023) Model estimates of microplastic potential contamination pattern of the eastern Gulf of Finland in 2018. Oceanologia 65(1):86–99. https://doi.org/10.1016/j.oceano.2021.11.006

Miettunen E, Tuomi L, Myrberg K (2020) Water exchange between the inner and outer archipelago areas of the Finnish Archipelago Sea in the Baltic Sea. Ocean Dyn 70(11):1421–1437. https://doi.org/10.1007/s10236-020-01407-y

Mishra A, Buhhalko N, Lind K, Lips I, Liblik T, Väli G, Lips U (2022) Spatiotemporal variability of Microplastics in the Eastern Baltic Sea. Front Mar Sci 9:875984. https://doi.org/10.3389/fmars.2022.875984

Möhlenkamp P, Purser A, Thomsen L (2018) Plastic microbeads from cosmetic products: an experimental study of their hydrodynamic behaviour, vertical transport and resuspension in phytoplankton and sediment aggregates. Elem Sci Anth 6(1):61. https://doi.org/10.1525/elementa.317

Murawski J, She J, Frishfelds V (2022) Modeling drift and fate of microplastics in the Baltic Sea. Front Mar Sci 9(September):1–20. https://doi.org/10.3389/fmars.2022.886295

Neumann T, Schernewski G (2008) Eutrophication in the Baltic Sea and shifts in nitrogen fixation analyzed with a 3D ecosystem model. J Mar Syst 74(1–2):592–602. https://doi.org/10.1016/j.jmarsys.2008.05.003

Neumann T, Fennel W, Kremp C (2002) Experimental simulations with an ecosystem model of the Baltic Sea: a nutrient load reduction experiment. Glob Biogeochem Cycles 16(3):7. https://doi.org/10.1029/2001GB001450

Neumann T, Radtke H, Cahill B, Schmidt M, Rehder G (2022) Non-redfieldian carbon model for the Baltic Sea (ERGOM version 1.2) – implementation and budget estimates. Geosci Model Dev 15(22):8473–8540. https://doi.org/10.5194/gmd-15-8473-2022

Niemistö J, Lund-Hansen LC (2019) Instantaneous effects of Sediment Resuspension on Inorganic and Organic Benthic nutrient fluxes at a shallow water Coastal Site in the Gulf of Finland, Baltic Sea. Estuaries Coasts 42(8):2054–2071. https://doi.org/10.1007/s12237-019-00648-5

Onink V, Jongedijk CE, Hoffman MJ, van Sebille E, Laufkötter C (2021) Global simulations of marine plastic transport show

plastic trapping in coastal zones. Environ Res Lett 16(6):064053. https://doi.org/10.1088/1748-9326/abecbd

Onink V, Kaandorp MLA, van Sebille E, Laufkötter C (2022) Influence of particle size and fragmentation on Large-Scale Microplastic Transport in the Mediterranean Sea. Environ Sci Technol 56(22):15528–15540. https://doi.org/10.1021/acs.est.2c03363

Osinski RD, Enders K, Gräwe U, Klingbeil K, Radtke H (2020) Model uncertainties of a storm and their influence on microplastics and sediment transport in the Baltic Sea. Ocean Sci 16(6):1491–1507. https://doi.org/10.5194/os-16-1491-2020

Pärn O, Moy DM, Stips A (2023) Determining the distribution and accumulation patterns of floating litter in the Baltic Sea using modelling tools. Mar Pollut Bull 190:114864. https://doi.org/10.1016/j.marpolbul.2023.114864

Pilechi A, Mohammadian A, Murphy E (2022) A numerical framework for modeling fate and transport of microplastics in inland and coastal waters. Mar Pollut Bull 184:114119. https://doi.org/10.1016/j.marpolbul.2022.114119

Rasmus K, Lindfors A, Kiirikki M (2015) Long-term field measurements of turbidity and current speed in the gulf of finland leading to an estimate of natural resuspension of bottom sediment. Boreal Environment Publishing Board 6:735–747. http://hdl.handle.net/10138/228308

Redfield AC (1934) On the proportions of organic derivatives in sea water and their relation to the composition of plankton. James Johnstone memorial volume: 176–192. https://www.researchgate.net/profile/Yair-Suari/publication/344709447_ON_THE_PROPORTIONS_OF_ORGANIC_DERIVATIVES_IN_SEA_WATER_AND_THEIR_RELATION_TO_THE_COMPOSITION_OF_PLANKTON_This_is_the_text_fromTHE-PROPORTIONS-OF-ORGANIC-DERIVATIVES-IN-SEA-WATER-AND-THEIR-RELATION-TO-THE-COMPOSITION-OF-PLANKTON-This-is-the-text-from-Alfred-Charles-Redfield-paper.pdf

Rosas E, Martins F, Tosic M, Janeiro J, Mendonça F, Mills L (2022) Pathways and hot spots of floating and submerged Microplastics in Atlantic Iberian Marine Waters: a Modelling Approach. J Mar Sci Eng 10(11):1640. https://doi.org/10.3390/jmse10111640

Sainio E, Lehtiniemi M, Setälä O (2021) Microplastic ingestion by small coastal fish in the northern Baltic Sea, Finland. Mar Pollut Bull 172:112814. https://doi.org/10.1016/j.marpolbul.2021.112814

Salm K, Liblik T, Lips U (2023) Submesoscale variability in a mesoscale front captured by a glider mission in the Gulf of Finland, Baltic Sea. Front Mar Sci 10.https://doi.org/10.3389/fmars.2023.984246

Schernewski G, Radtke H, Robbe E, Haseler M, Hauk R, Meyer L, Piehl S, Riedel J, Labrenz M (2021) Emission, Transport, and deposition of visible plastics in an Estuary and the Baltic Sea—a monitoring and modeling Approach. Environ Manage 68(6):860–881. https://doi.org/10.1007/s00267-021-01534-2

Schönlau C, Karlsson TM, Rotander A, Nilsson H, Engwall M, van Bavel B, Kärrman A (2020) Microplastics in sea-surface waters surrounding Sweden sampled by manta trawl and in-situ pump. Mar Pollut Bull 153:111019. https://doi.org/10.1016/j.marpolbul.2020.111019

Shields A (1936) Anwendung der Aehnlichkeitsmechanik und der Turbulenzforschung auf die Geschiebebewegung. PhD Thesis Technical University Berlin

Smagorinsky J (1963) General circulation experiments with the primitive equations. Mon Weather Rev 91(3):99–164.

Stipa T (2004) Baroclinic adjustment in the Finnish coastal current. Tellus A: Dynamic Meteorol Oceanogr 56(1):79. https://doi.org/10.3402/tellusa.v56i1.14391

Stoicescu S-T, Laanemets J, Liblik T, Skudra M, Samlas O, Lips I, Lips U (2022) Causes of the extensive hypoxia in the Gulf of Riga

in 2018. Biogeosciences 19(11):2903–2920. https://doi.org/10.5194/bg-19-2903-2022

Suhhova I, Liblik T, Lilover M-J, Lips U (2018) A descriptive analysis of the linkage between the vertical stratification and current oscillations in the Gulf of Finland. Boreal Environ Res 23:83–103

Tsiaras K, Hatzonikolakis Y, Kalaroni S, Pollani A, Triantafyllou G (2021) Modeling the pathways and accumulation patterns of Micro- and macro-plastics in the Mediterranean. Front Mar Sci 8. https://doi.org/10.3389/fmars.2021.743117

Väli G, Zhurbas V, Lips U, Laanemets J (2017) Submesoscale structures related to upwelling events in the Gulf of Finland, Baltic Sea (numerical experiments). J Mar Syst 171:31–42. https://doi.org/10.1016/j.jmarsys.2016.06.010

Väli G, Zhurbas V, Lips U, Laanemets J (2018) Clustering of floating particles due to submesoscale dynamics: a simulation study for the Gulf of Finland, Baltic Sea. AGU Fall Meeting Abstracts, 2018, OS53D-1364. https://ui.adsabs.harvard.edu/abs/2018AGUFMOS53D1364V

Väli G, Meier HEM, Placke M, Dieterich C (2019) River runoff forcing for ocean modeling within the Baltic Sea Model Intercomparison Project. Meereswissenschaftliche Berichte 113. https://doi.org/10.12754/msr-2019-0113

Väli G, Meier HEM, Liblik T, Radtke H, Klingbeil K, Gräwe U, Lips U (2023) Submesoscale processes in the surface layer of the central Baltic Sea: a high-resolution modelling study. Oceanologia. https://doi.org/10.1016/j.oceano.2023.11.002

van Sebille E, Griffies SM, Abernathey R, Adams TP, Berloff P, Biastoch A, Blanke B, Chassignet EP, Cheng Y, Cotter CJ, Deleersnijder E, Döös K, Drake HF, Drijfhout S, Gary SF, Heemink AW, Kjellsson J, Koszalka IM, Lange M, Zika JD (2018) Lagrangian ocean analysis: fundamentals and practices. Ocean Model 121:49–75. https://doi.org/10.1016/j.ocemod.2017.11.008

Viikmäe B, Soomere T (2018) The persistence of spatial patterns of beaching of current-driven pollution in a changing wind climate: a case study for the Gulf of Finland. Boreal Environ Res 23(1–6):299–299–314

Waldschläger K, Schüttrumpf H (2019) Erosion behavior of different microplastic particles in comparison to natural sediments. Environ Sci Technol 53(22):13219–13227. https://doi.org/10.1021/acs.est.9b05394

Wilcke RAI, Kjellström E, Lin C, Matei D, Moberg A, Tyrlis E (2020) The extremely warm summer of 2018 in Sweden – set in a historical context. Earth Sys Dyn 11(4):1107–1121. https://doi.org/10.5194/esd-11-1107-2020

Wilcock PR (1988) Methods for estimating the critical shear stress of individual fractions in mixed-size sediment. Water Resour Res 24(7):1127–1135. https://doi.org/10.1029/WR024i007p01127

Wright SL, Thompson RC, Galloway TS (2013) The physical impacts of microplastics on marine organisms: a review. Environ Pollut 178:483–492. https://doi.org/10.1016/j.envpol.2013.02.031

Xia F, Yao Q, Zhang J, Wang D (2021) Effects of seasonal variation and resuspension on microplastics in river sediments. Environ Pollut 286:117403. https://doi.org/10.1016/j.envpol.2021.117403

Zhurbas V, Laanemets J, Vahtera E (2008) Modeling of the mesoscale structure of coupled upwelling/downwelling events and the related input of nutrients to the upper mixed layer in the Gulf of Finland, Baltic Sea. J Phys Res 113(C5):C05004. https://doi.org/10.1029/2007JC004280

Zhurbas V, Väli G, Golenko M, Paka V (2018) Variability of bottom friction velocity along the inflow water pathway in the Baltic Sea. J Mar Syst 184(December 2017):50–58. https://doi.org/10.1016/j.jmarsys.2018.04.008

Zhurbas V, Väli G, Kuzmina N (2019) Rotation of floating particles in submesoscale cyclonic and anticyclonic eddies: a model study for the southeastern Baltic Sea. Ocean Sci 15(6):1691–1705. https://doi.org/10.5194/os-15-1691-2019

Curriculum Vitae

Personal data

Name   Arun Mishra
Date of birth   08.05.1993
Place of birth India
Nationality   Indian

Contact information

E-mail   arun.mishra@taltech.ee

Education

2020–2025   Tallinn University of Technology, School of Science,
                Physical Sciences, Oceanography and Meteorology, PhD
2018–2020   Tallinn University of Technology, School of Engineering,
                Environmental Engineering and Management (Cum Laude), MSc
2011–2015   KIIT University, Bhubaneswar, India
                Electrical Engineering, BTech

Language competence

English   Fluent
Hindi   Fluent
Estonian   Basic

Professional Employment

2020–present   Tallinn University of Technology, School of Science, Department of
                Marine Systems,
                Junior Researcher

Scientific work

Publications according to ETIS

1.1   Siht, Enriko; Väli, Germo; Liblik, Taavi; Mishra, Arun; Buhhalko, Natalja; Lips, Urmas (2025). Modeling the pathways of microplastics in the Gulf of Finland, Baltic Sea − sensitivity of parametrizations. Ocean Dynamics 75, 9 (2025). DOI: 10.1007/s10236-024-01649-0.

1.1   Mishra, Arun; Siht, Enriko; Väli, Germo; Liblik, Taavi; Buhhalko, Natalja; Lips, Urmas (2025). Mapping microplastic pathways and accumulation zones in the Gulf of Finland, Baltic Sea − insights from modeling. Frontiers in Marine Science, 11, 1−17. DOI: 10.3389/fmars.2024.1524585.

1.1   Ayankunle, Ayankoya Yemi; Buhhalko, Natalja; Pachel, Karin; Lember, Erki; Kõrgmaa, Vallo; Mishra, Arun; Lind, Kati (2023). Estimating Microplastics related to Laundry Wash and Personal Care Products released to Wastewater in Major Estonian Cities: a comparison of calculated and measured microplastics. Journal of Environmental Health Science and Engineering, 21 (1), 225−237. DOI: 10.1007/s40201-023-00856-z.

1.1   Mishra, A.; Buhhalko, N.; Lind, K.; Lips, I.; Liblik, T.; Väli, G.; Lips, U. (2022). Spatiotemporal Variability of Microplastics in the Eastern Baltic Sea. Frontiers in Marine Science, 9. DOI: 10.3389/fmars.2022.875984.

1.1   She, J.; Buhhalko, N.; Lind, K.; Mishra, A.; Kikas, V.; Costa, E.; Gambardella, C.; Montarsolo, A.; Faimali, M.; Garaventa, F.; Lips, I. (2022). Uncertainty and consistency assessment in multiple microplastic observation datasets in the Baltic Sea. Frontiers in Marine Science, 9, #886357. DOI: 10.3389/fmars.2022.886357.

Elulookirjeldus

Isikuandmed

Nimi	Arun Mishra
Sünniaeg	08.05.1993
Sünnikoht	India
Kodakondsus	India

Kontaktandmed

E-post	arun.mishra@taltech.ee

Hariduskäik

2020–2025	Tallinna Tehnikaülikool, Loodusteaduskond, Füüsikalised loodusteadused, Okeanograafia ja meteoroloogia, PhD
2018–2020	Tallinna Tehnikaülikool, Inseneriteaduskond, Keskkonnatehnika ja juhtimise erialal (Cum Laude), MSc
2011–2015	KIIT University, Bhubaneswar, India Elektrotehnika, BTech

Keelteoskus

Inglise keel	Kõrgtase
Hindi keel	Emakeel
Eesti keel	Algtase

Teenistuskäik

2020–…	Tallinna Tehnikaülikool, Loodusteaduskond, TTÜ Meresüsteemide instituut, doktorant-nooremteadur

Teadustegevus

Publikatsioonid Eesti Teadusinfosüsteemi klassifikaatori järgi

1.1	Siht, Enriko; Väli, Germo; Liblik, Taavi; Mishra, Arun; Buhhalko, Natalja; Lips, Urmas (2025). Modeling the pathways of microplastics in the Gulf of Finland, Baltic Sea – sensitivity of parametrizations. Ocean Dynamics 75, 9 (2025). DOI: 10.1007/s10236-024-01649-0.
1.1	Mishra, Arun; Siht, Enriko; Väli, Germo; Liblik, Taavi; Buhhalko, Natalja; Lips, Urmas (2025). Mapping microplastic pathways and accumulation zones in the Gulf of Finland, Baltic Sea – insights from modeling. Frontiers in Marine Science, 11, 1–17. DOI: 10.3389/fmars.2024.1524585.
1.1	Ayankunle, Ayankoya Yemi; Buhhalko, Natalja; Pachel, Karin; Lember, Erki; Kõrgmaa, Vallo; Mishra, Arun; Lind, Kati (2023). Estimating Microplastics related to Laundry Wash and Personal Care Products released to Wastewater in Major Estonian Cities: a comparison of calculated and measured microplastics. Journal of Environmental Health Science and Engineering, 21 (1), 225–237. DOI: 10.1007/s40201-023-00856-z.

1.1 Mishra, A.; Buhhalko, N.; Lind, K.; Lips, I.; Liblik, T.; Väli, G.; Lips, U. (2022). Spatiotemporal Variability of Microplastics in the Eastern Baltic Sea. Frontiers in Marine Science, 9. DOI: 10.3389/fmars.2022.875984.

1.1 She, J.; Buhhalko, N.; Lind, K.; Mishra, A.; Kikas, V.; Costa, E.; Gambardella, C.; Montarsolo, A.; Faimali, M.; Garaventa, F.; Lips, I. (2022). Uncertainty and consistency assessment in multiple microplastic observation datasets in the Baltic Sea. Frontiers in Marine Science, 9, #886357. DOI: 10.3389/fmars.2022.886357.